
University of Strathclyde

Department of Pure and Applied Chemistry

# Nanoparticle-based Assays for the Detection of Protein Glycosylation in Biopharmaceutical Characterisation

By Craig Ward

A thesis submitted to the Department of Pure and Applied Chemistry, University of Strathclyde, in fulfilment of the requirements for the degree of Doctor of Philosophy

October 2019

This thesis is the result of the author's original research. It has been composed by the author and has not been previously submitted for examination which has led to the award of a degree. The copyright of this thesis belongs to the author under the terms of the United Kingdom Copyright Acts as qualified by University of Strathclyde Regulation 3.50. Due acknowledgement must always be made of the use of any material contained in, or derived from, this thesis.

Signed:

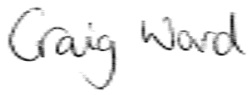

Date:

7th October 2019

# Acknowledgements

Firstly, thanks has to go to my two Strathclyde supervisors, Professor Duncan Graham, and Professor Karen Faulds. Your daily support has helped hugely throughout my PhD, and thank you for allowing me to go on plenty of holidays… I mean, conferences. Thank you also to my UCL supervisor, Professor Daniel Bracewell for allowing me to be part of the biochemical engineering CDT. I learned a lot.

I have to say a huge thank you to the Bionanotechnology group for your help and support every minute of every day. Special thanks goes to Vegas: Laura, Ryan, Rachel, Sian, Alex, and Fay for listening to my rants, helping me through the bad times, and celebrating the good times. Also thanks to the postdocs, Sam, Lauren, Kirsten, Hayleigh, Stacey, Lee, and Steve for their help throughout and for reading all of my reports and presentations! Thanks also to my girls, Sureyya, Kirsty, Jenny, Iona, Emma, and Amy, for always answering my plea for "Ark?" after difficult days, or even just Tuesdays. Those after work pints got me through this PhD.

Also thank you to my CDT cohort at UCL, especially Victoria and Leon, for all the laughs during my trips to London and for the brilliant "networking" Biochem Eng ski trips to The Alps!

Outside of work, I need to thank my fantastic friends, specifically my "Best Ones" Aoife, Jonny, Quinton, and Sergi for their support through the years, and keeping me sane when I was hating it! I also need to give a massive thanks to Emma and Ed for keeping me calm in the lead up to the viva with food, drinks, and bunnies.

Finally, and my biggest thanks, goes to my wonderful mum who has helped and supported me throughout the most difficult times, and helped me reach my goals. The one person in the world I can rely on for absolutely everything. I would not be where I am today without her encouragement.

# Abstract

In biopharmaceutical processing, the glycosylation of a therapeutic protein must be stringently monitored as this can affect the efficacy and safety of the final formulation. Current methods of analysis are time consuming, expensive, and require skilled personnel. Therefore, it would be advantageous to have rapid, cheap, and user-friendly assays to sensitively assess glycan composition. This research has made progress in the development of such assays.

The first objective was to create sensing beacons which could be easily detected when binding to a target glycan occurred. Gold nanoparticles were investigated for this role due to their ease of functionalisation and optical properties. These were conjugated with a Raman-active molecule to act as a beacon, and a carbohydrate-binding protein *via* a heterobifunctional ligand. The conjugation procedure was shown to be successful and versatile, allowing for the attachment of various lectins using two different linking molecules.

Next, a solution-based assay was investigated to characterise the sensing capabilities of the functionalised gold nanoparticles. This could allow for the development of a glycosylation evaluation kit whereby a library of nanoparticle conjugates could be mixed with protein samples and analysed to assess glycan composition. Originally, the drive was to use surface enhanced resonance Raman scattering (SERRS) as a sensitive method of analysis. However, this was shown to be less useful in this setting, but localised surface plasmon resonance measurements proved to be a simple and rapid avenue for glycan characterisation. Detection of mannose was shown to have a limit of detection of 29.2 nM using the lectin from *Galanthus nivalis*. This technique was also shown to be versatile using various lectins for the detection of different glycan targets, and could potentially be more sensitive.

A second route for glycan detection was investigated to provide a rapid and user-friendly method of analysis. Lateral flow assays were used to show the binding capabilities of the prepared nanoparticle conjugates, but had significant

disadvantages arising from the application of the target glycoprotein to the nitrocellulose surface as a spot rather than a line spanning the width of the strip. This led to an unsatisfactory assay sensitivity. To overcome this, a simpler and more sensitive format was investigated to create a high-throughput glycan analysis platform. For this to remain user-friendly, evaluation methods involved the use of a simple flatbed scanner to provide rapid colorimetric results, but this assay was also coupled with SERRS to investigate the capabilities of producing highly sensitive glycan detection. This paper-based analytical device still requires research, but has shown excellent potential for use as a valuable tool in biopharmaceutical glycan analysis.

Finally, the development of an enzyme-linked immunosorbent assay was investigated. This relied on the production of hydrogen peroxide by glucose oxidase when the target glycan was present. Hydrogen peroxide would then act as a reducing agent and induce the growth of gold nanoparticles in the presence of $Au^{3+}$ cations. Although still in the early stages of development, this assay produced interesting results with many issues still to consider, but showed that it could have the capability of becoming a sensitive method of glycan detection. The common use of enzyme-linked immunosorbent assays in biochemical detection means that a glycosylation analysis kit based on this assay format could be an attractive alternative to current industrial analysis methods.

# Abbreviations

| | |
|---|---|
| α-AG | α-acid glycoprotein |
| µPAD | Microfluidic paper-based analytical device |
| Ala | Alanine |
| Asn | Asparagine |
| BCA | Bicinchoninic acid |
| BSA | Bovine serum albumin |
| CALNN | Cysteine(C)-Alanine(A)-Leucine(L)-Asparagine(N)-Asparagine(N) |
| CHO | Chinese hamster ovary |
| Con A | *Concanavalin* A |
| CRD | Carbohydrate recognition domain |
| $CT(PEG)_{12}$ | Carboxy-(polyethylene glycol)$_{12}$-thiol |
| DLS | Dynamic light scattering |
| DNA | Deoxyribonucleic acid |
| EDC | 1-ethyl-3-(3-dimethylaminopropyl)carbodiimide |
| ELISA | Enzyme-linked immunosorbent assay |
| EMA | European Medicines Agency |
| ER | Endoplasmic reticulum |
| ESI-MS | Electrospray ionisation – mass spectrometry |
| FDA | Food and Drug Administration |
| Fuc | Fucose |

| | |
|---|---|
| Gal | Galactose |
| GalNAc | N-Acetylgalactosamine |
| GCase | Glucocerebrosidase |
| GC-MS | Gas chromatography – mass spectrometry |
| Glc | Glucose |
| GlcNAc | N-Acetylglucosamine |
| GNA | *Galanthus nivalis* agglutinin |
| GOx | Glucose oxidase |
| HRP | Horseradish peroxidase |
| IgG | Immunoglobulin G |
| LFA | Lateral flow assay |
| LOD | Limit of detection |
| LSPR | Localised surface plasmon resonance |
| MAL | *Maackia amurensis* lectin |
| MALDI-MS | Matrix-assisted laser desorption/ionisation – mass spectrometry |
| Man | Mannose |
| MGITC | Malachite green isothiocyanate |
| mRNA | Messenger ribonucleic acid |
| MS | Mass spectrometry |
| NA | Numerical aperture |
| Neu5Ac | N-Acetylneuraminic acid |
| PB | Phosphate buffer |

| | |
|---|---|
| PBS | Phosphate buffered saline |
| PEG | Polyethylene glycol |
| Pro | Proline |
| PSA | Prostate specific antigen |
| PTM | Post translational modification |
| PVA | Polyvinyl alcohol |
| RGB | Red Green Blue |
| RIA | Radioactive immunoassay |
| RNA | Ribonucleic acid |
| RNase A | Ribonuclease A |
| RNase B | Ribonuclease B |
| RRM | Raman reporter molecule |
| SA | Sialic acid |
| SAM | Self-assembled monolayer |
| Ser | Serine |
| SERRS | Surface enhanced resonance Raman scattering |
| SERS | Surface enhanced Raman scattering |
| SNA | *Sambucus nigra* agglutinin |
| sNHS | N-hydroxysulfosuccinimide |
| TBE | Tris-borate-EDTA |
| TERS | Tip enhanced Raman scattering |
| Thr | Threonine |
| TMB | 3,3’,5,5’-tetramethylbenzidine |

| | |
|---|---|
| tRNA | Transfer ribonucleic acid |
| Trp | Tryptophan |
| UEA | *Ulex Europaeus I* agglutinin |
| USD | Ultra scale down |
| UV-vis | Ultraviolet-visible |
| WGA | Wheat germ agglutinin |

# Contents

# 1. Introduction

On 28th October 1982, the first recombinant human insulin drug, Humulin® (Eli Lilly), was approved by the US Food and Drug Administration (FDA).[1,2] This marked the emergence of biopharmaceuticals, medicinal products derived from, or manufactured in, biological sources, which then flourished and became the fastest growing sector of the biopharmaceutical industry. This highly competitive sector made $99 billion (US) sales in 2009,[2] which grew to almost $100 billion (US) in 2010.[3] Nowadays, there are more than 130 therapeutic proteins approved for use by the FDA.[1]

The majority of biopharmaceuticals are glycoproteins,[2] proteins with carbohydrate structures, also known as glycans, covalently attached to amino acid side chains on the surface. The glycan attachments are usually a result of post-translational modifications (PTMs), called glycosylation, that take place *in vitro* during the protein synthesis in the cell harvesting process. These glycoproteins are much more complex than small molecule pharmaceuticals, which presents new challenges in characterisation and quality control during bioprocessing.

At present, many therapeutic protein patents are due to expire.[2] This will allow for generic versions of these drugs to be produced. In the case of small molecule drugs, abbreviated regulatory pathways are available to gain approval for these generics. This means that pharmaceutical companies only need to prove that the generic is pharmaceutically equivalent by having the same active ingredient, purity, strength, dosage form, and administration route. As these drugs do not need to go through the same level of evaluation, it is less costly, and therefore the generics can be sold at a substantially cheaper price.[3]

This process, however, is not as simple in the case of biopharmaceuticals due to their size and complexity. Biosimilars, generic versions of therapeutic proteins, are now being considered, and with them various analytical challenges are met. Abbreviated regulatory pathways for generic biopharmaceuticals are not as well established as for

small molecule drugs, and existing analytical techniques used for small molecule drugs may be more limited when dealing with therapeutic proteins.[3]

The FDA have highlighted three properties of therapeutic proteins that it deems important for the behaviour of biopharmaceuticals to be understood, but which cannot currently be measured sufficiently. These are PTMs, 3D structures, and protein aggregation.[3,4] PTMs, with glycosylation being the most prominent,[2] are vastly important in that they can affect the structure, efficacy and safety of the proteins.[2,3,5] It is therefore necessary that the glycosylation states of the proteins are monitored closely, especially as these can be altered *in vitro* by changes in the manufacturing process.[3–5]

In order to analyse glycosylation of therapeutic proteins, sophisticated instruments and skilled analysts are required, and the process is normally time consuming.[3] Since analytical methods typically used for small molecule drugs are very limited in their capabilities to measure the structural differences between large and complex proteins, the analysis process can be slowed down significantly in this case. The FDA has stated that they are hindered by their inability to accurately evaluate structural differences of therapeutic proteins, which could be a result of alterations to the manufacturing process. Therefore, they may require results from both animal and human studies before approving a manufacturing change.[4] This in turn could potentially hamper the approval of innovative process improvements, and also affect the manufacturers ability to react to sudden raw material changes.[4] Therefore, an improvement in the analysis methods used for biosimilars, and biopharmaceuticals in general, could greatly improve bioprocessing of therapeutic proteins.

## 1.1 Biomolecules

### 1.1.1 Proteins

Proteins are organic macromolecular structures containing one or more polymeric chains of amino acids, known as polypeptides. These are complex biomolecules which have a wide variety of functions. An amino acid is a molecule with a carboxylic acid

group at one end, and an amino group at the α-carbon. The general structure of an amino acid is shown below in Figure 1.1.

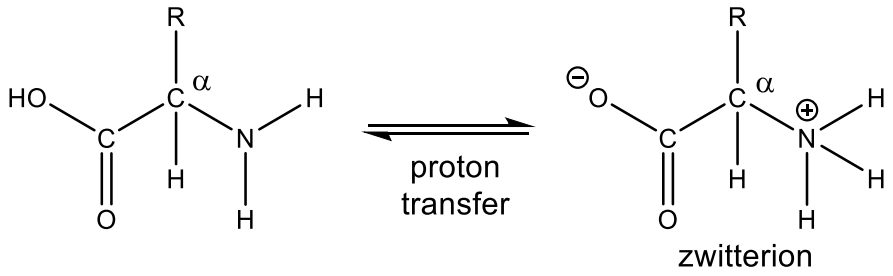


*Figure 1.1: General amino acid and zwitterion structures, showing the proton transfer between the carboxylic acid and amine groups.*

Within amino acids the carboxylic acid group can donate a proton, and the amine group can accept a proton. The amino acid can therefore become zwitterionic, carrying both a positive and negative charge. There are 20 different natural amino acids in total, the simplest being glycine where R = H. Amino acids are polymerised through condensation reactions in various combinations within a cell to form numerous diverse protein structures.

#### *1.1.1.1 Protein Synthesis*

In 1902, Archibald Garrod first hypothesised the direct relationship between deoxyribonucleic acid (DNA) and proteins.[6] As a result of this hypothesis, scientists believed at the time that protein synthesis took place within the nucleus. However, subsequent experiments by Haemmerling[7] disproved this. Haemmerling removed the nucleus from Acetabularia cells and observed that proteins continued to be produced. This suggested that the nucleus was not the primary protein-producing organelle. Scientists were initially unable to explain this as no DNA exists outside of the cell nucleus. However, earlier research by Brachet *et al*[8] showed that there was a second type of nucleic acid known as ribonucleic acid (RNA), which was the missing link between DNA and proteins. Brenner *et al*[9] then deduced that messenger RNA (mRNA) was able to transfer genetic information from the nucleus in to the cytoplasmic ribosomes to be translated in to protein structures.

There are two major processes involved in the synthesis of a protein: transcription, followed by translation.[10] Transcription is the synthesis of RNA from DNA. DNA and RNA have similar structures. DNA is comprised of two complementary strands, each consisting of sequences of deoxyribose sugars, nucleotides, and phosphate groups. Hydrogen bonding exists between complementary nucleotides, adenine to thymine and guanine to cytosine, to give DNA the double helix structure. RNA differs in structure in that it is single stranded and consists of sequences of ribose sugars, nucleotide bases and phosphate groups. They also differ in that the nucleotide base uracil is present instead of thymine.[10] There are different types of RNA, with each having different functions. One type is mRNA. This is coded from the DNA through RNA polymerase which creates a complementary strand to the DNA template. (Figure 1.2)

Translation is the synthesis of a polypeptide chain directed by RNA. In order for a polypeptide chain to be synthesised, the amino acids must firstly be synthesised and arranged in order. This requires information from the DNA, which is carried by mRNA. The mRNA uses triplets of nucleotide bases to code for each amino acid. These triplets are known as codons. The mRNA carries transcribed information from the DNA to ribosomes on the rough endoplasmic reticulum where the protein synthesis takes place.

Here the mRNA is translated, aided by a second type of RNA, known as transfer RNA (tRNA). The tRNA is typically 80 nucleotides in length and single stranded. This single strand folds on itself to form a hydrogen bond stabilised three-dimensional structure, consisting of four regions of complementary base paired regions and three loops. On one of these loops there is a triplet nucleotide base sequence known as an anticodon. This anticodon is specific to one of the amino acids, which is covalently attached to the 3’ end of the tRNA structure. The tRNA anticodon is complementary to an mRNA codon and allows for the construction of an amino acid sequence as directed by the mRNA strand. (Figure 1.2) The interaction of the codons and anticodons bring the amino acids in to close proximity, allowing for a bond to form between them through condensation, enabling the formation of a polypeptide chain.

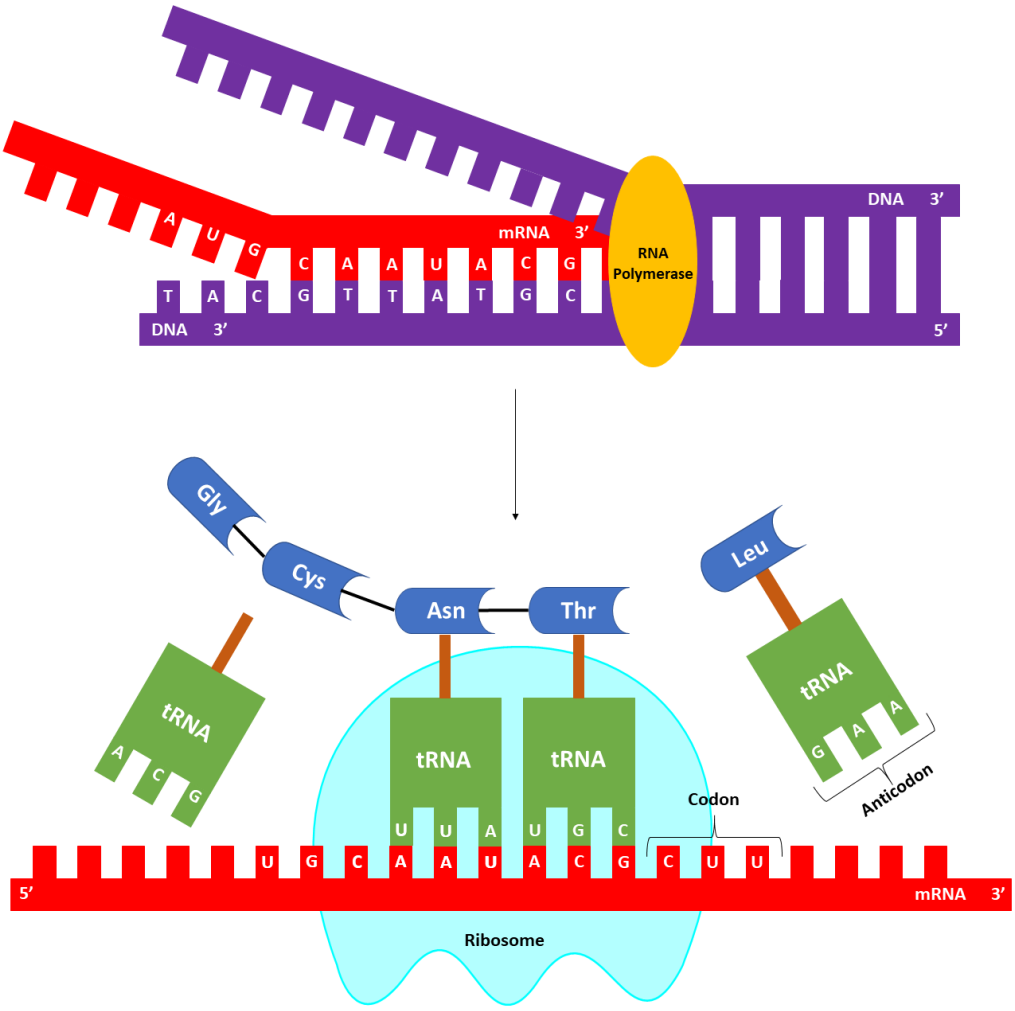


*Figure 1.2: Transcription process where mRNA is produced by RNA polymerase using DNA as a template, followed by the process of translation where mRNA codons are translated by tRNA anticodons to synthesise a polypeptide chain.*

### *1.1.1.2 Protein Structure*

The structure of a protein as a whole is very complex, so in order to simplify this the structure is split up in to different levels: primary, secondary, tertiary, and quaternary.[11] The primary structure of a protein is the basic sequence of amino acids in a chain, viewed as linear. As mentioned previously, the individual amino acids undergo a condensation reaction to form polypeptide chains, which in turn make up the primary protein structure. As there are 20 natural amino acids, which act as the

protein building blocks, the primary structures can be vastly varied, meaning that there can be a great diversity in protein function. (Figure 1.3)

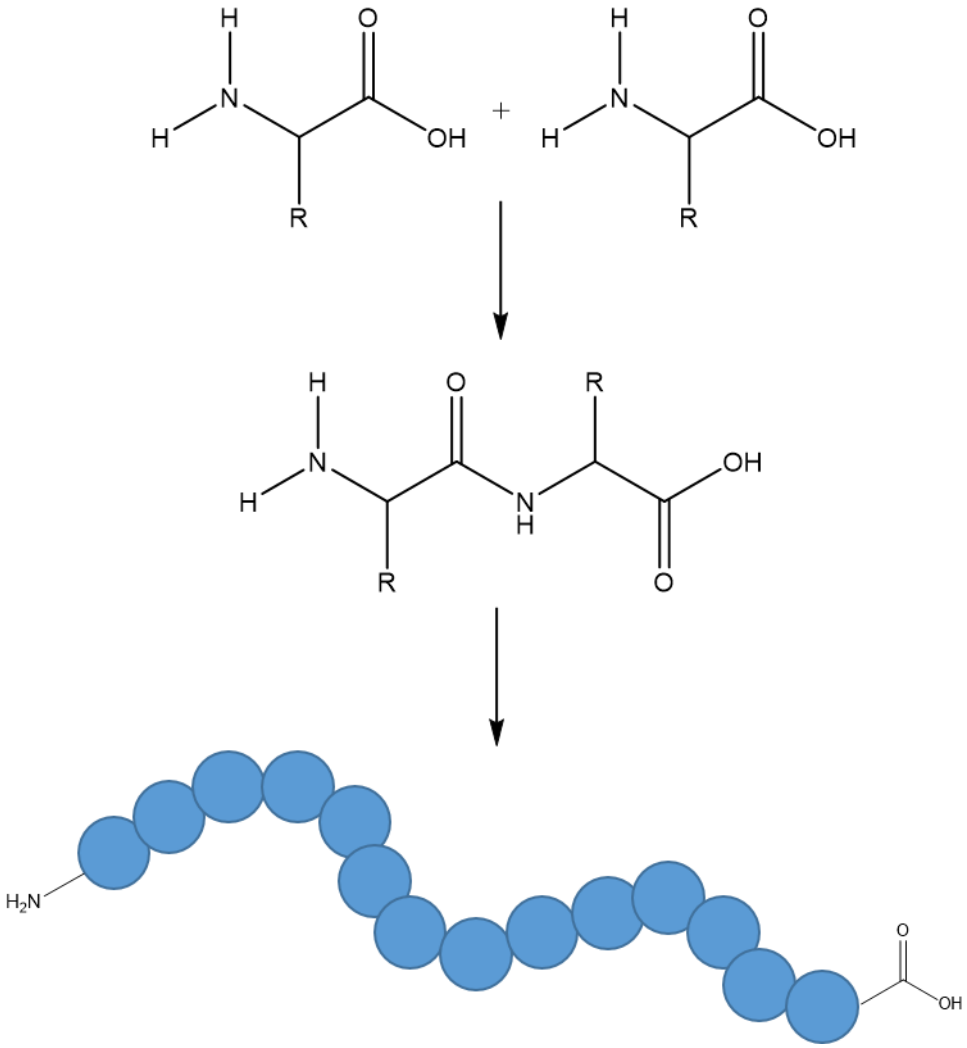


*Figure 1.3: Condensation reaction between amino acids to form the polypeptide chain which makes up protein primary structure.*

The secondary structure describes the local conformations of the amino acids in the protein chain.[11] These conformations are stabilised by different intramolecular interactions: hydrogen bonding between the carboxy oxygens and the amido hydrogens of different amino acid residues, and electrostatic interactions between different amino acid R groups. Although hydrogen bonding is a weak interaction, the sum of the bonding energies in the secondary structure can be relatively strong, making this the dominant force in stabilising these structures.

There are two common secondary structure conformations.[11] The first common secondary structure is the α-helix. In an α-helix the polypeptide chain adopts a helical shape around an imaginary axis. Normally this has 3.6 amino acids per turn at an angle of about 100° between amino acid residues, with all R-groups pointing outwards. This is stabilised by hydrogen bonding between a carboxyl oxygen and an amino hydrogen 4 amino acids further along the chain. (Figure 1.4)

The second common secondary structure is the β-strand. This is where the polypeptide chain is extended, with no hydrogen bonding between neighbouring amino acids. Hydrogen bonding does, however, take place between different β-strands, which form an overall structure of a β-sheet. The R groups of the amino acid residues can point above and below the plane of the sheet, which then means that ionic bonds may also be present between strands. In schematic representations, the β-sheets of proteins are normally shown as broad arrows. (Figure 1.4)

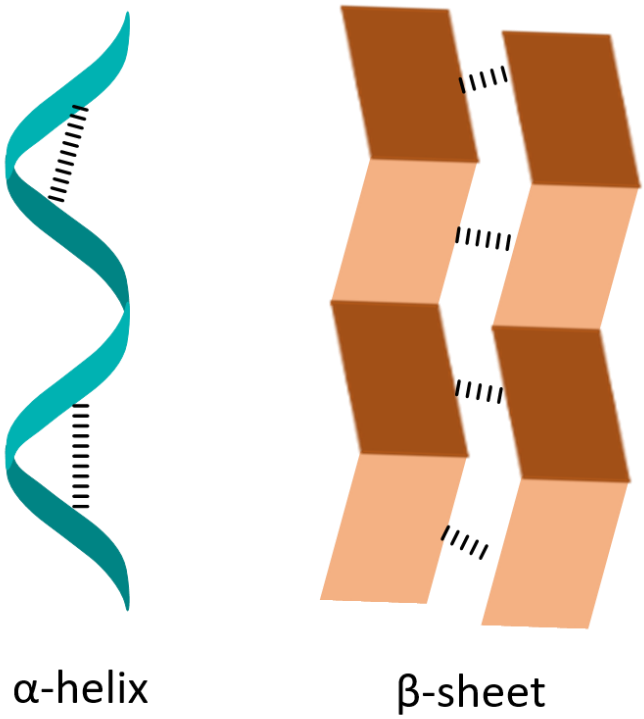


*Figure 1.4: The two most common types of protein secondary structure, the α-helix, and β-sheets.*

Proteins contain other secondary structures, which are not as instantly recognisable. One such structure is a turn. In a polypeptide chain a 180° turn is important, especially

between different strands of β-sheets. These turns usually contain 3-4 amino acid residues.[11] Often the turns contain glycine residues, as these are the smallest, and also tryptophan residues, as these can undergo CH-π interactions with neighbouring amino acids to stabilise the turn.[11]

One other secondary structure is a coil. The coils may be described as 'random' or 'unordered' but each amino acid still has a defined position in the protein structure. Their function is to give the protein added flexibility and also to allow for any conformational changes.[11]

Following on from secondary structures within the protein, there are tertiary and quaternary structures also. The tertiary structure describes how the components of protein secondary structures are arranged to make up the overall protein conformation. (Figure 1.5) This overall structure is brought about by interactions between the amino acids that are far apart in the polypeptide chain but are brought in to close proximity by protein folding. Much like secondary structures, tertiary structure is stabilised by hydrogen bonding, as well as various other stabilising forces. Certain pockets are created within the protein as a result of hydrophobic interactions. Ionic interactions are present between charged R groups. Van der Waals forces are present throughout the structure, and disulfide bonds can be present between cysteine residues.[11]

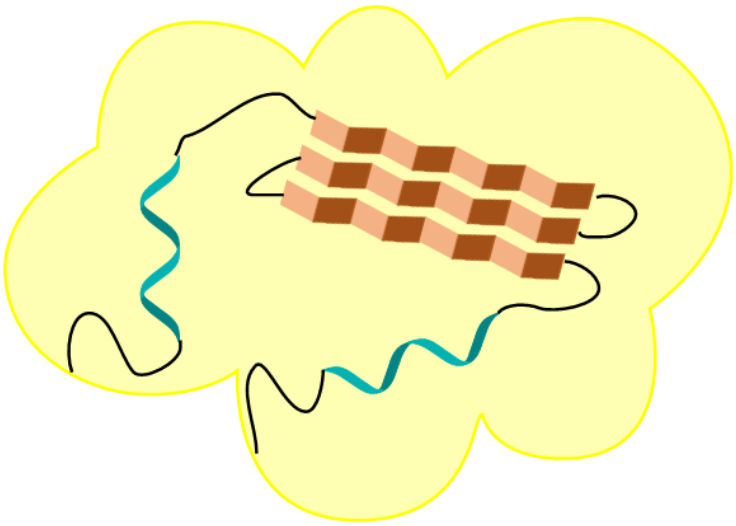

*Figure 1.5: A cartoon of protein tertiary structure, where the overall conformation is formed by the arrangements of the secondary structures in the polypeptide chain.*

Finally, the quaternary structure describes how two or more polypeptide chains come together to form one single functional protein with multiple subunits, each of which can be identical or different. Again, various interactions can stabilise these overall conformations, such as hydrogen bonding, disulfide bridges, ionic bonding and hydrophobic interactions.

### 1.1.2 Post-translational Modifications

During the process of protein synthesis in the cell, there are a series of additional structural changes that can occur through various modifications to the amino acids in the protein chain. These are typically a result of enzymatic processes, which can include cross-linking or cleavage reactions. These modifications can lead to changes to local or higher-order structures and are known as PTMs.[12] These PTMs may or may not affect the overall protein function, but they further increase the diversity of possible structures. The five most common types of PTM are glycosylation, phosphorylation, acylation, alkylation and oxidation.[11–13] Whilst the combination of amino acids in the protein polypeptide chain can create a variety of protein structures, each of these PTMs introduces a much greater source of diversity.

### 1.1.3 Glycosylation

Glycosylation is one of the most common PTMs, but is also accepted as the most structurally diverse.[14,15] This involves the enzymatic process of covalently attaching an oligosaccharide, also known as a glycan, to an amino acid residue in the protein polypeptide chain. As the position and composition of these oligosaccharides can vary greatly, this introduces further diversity to the proteome. There are five main types of glycosylation: N-glycosylation, O-glycosylation, C-glycosylation, glypiation and phosphoglycosylation. N-linked glycosylation applies to the glycan binding to the amine group of an asparagine (Asn) residue in the polypeptide chain. O-linked glycosylation involves the binding of monosaccharides to the hydroxyl groups of serine (Ser) or threonine (Thr) residues. C-linked glycosylation is the attachment of

mannose to the indole ring of a tryptophan (Trp). Glypiation is the linkage of a protein to a phospholipid by a glycan core; an oligosaccharide chain. Phosphoglycosylation is the use of a phosphodiester to bind a glycan to a Ser residue. Of these five types, the most common are N-linked and O-linked glycosylation.

The complexity that glycosylation introduces to protein structures is particularly large, not only due to the five different types of glycosylation, but also due to the variability between the possible structures of these modifications. Taking N-linked glycosylation as an example, there are three main types.[16] (Figure 1.6) These glycans are preformed before addition to the protein at the primary amine group of an Asn residue when it is in the sequence Asn – X –Ser/Thr, where X can be any amino acid except for proline (Pro). This occurs in the endoplasmic reticulum (ER) before further modification in the Golgi apparatus. The majority of the N-linked glycans have the same inner core sequence of sugars consisting of two *N*-acetylglucosamines (GlcNAc) and a mannose (Man) arranged linearly with two further Man groups branching from the first Man.[11] The simplest form of N-glycan is of the high-mannose type, which consists of branches made purely from Man chains. However, in the Golgi the Man groups can be trimmed from the glycan structure and replaced with other carbohydrate groups, such as galactose (Gal) or a sialic acid (SA) such as N-Acetylneuraminic acid (Neu5Ac), to create what is known as a complex N-glycan, which introduces significant variability to the glycans and in turn diversifies the overall protein structure. It is also possible to have a combination of these two N-glycan types, with one branch being a complex oligosaccharide, and the other being similar to a high-Man glycan. This is known as a hybrid N-glycan.[11,13–15]

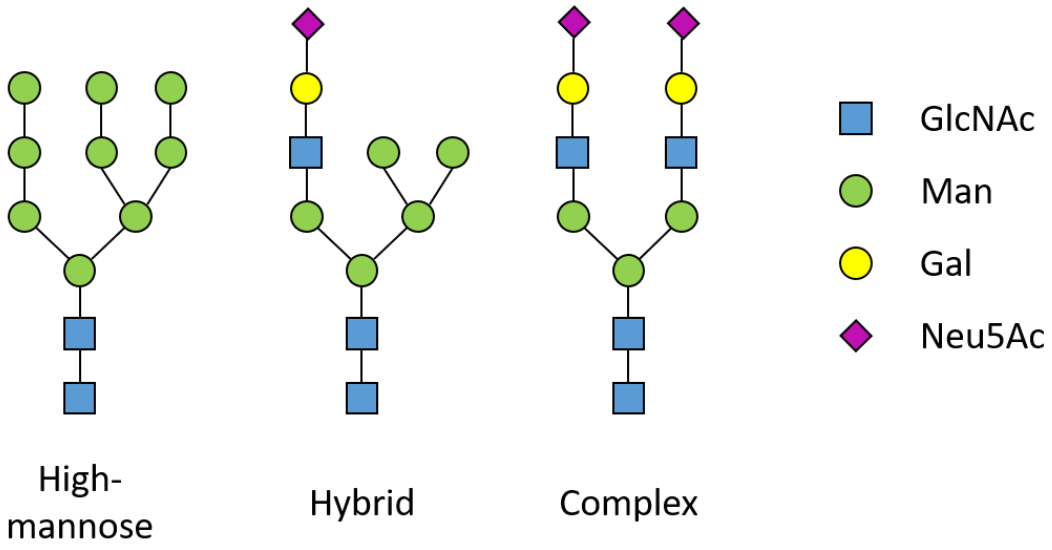


*Figure 1.6: Three major types of N-glycans, all of which contain the same core pentasaccharide structure consisting of two N-acetylglucosamine, and three mannose residues.*

O-linked glycans differ from N-glycans in that they are enzymatically built up in a step-wise fashion from monosaccharide units rather than being preformed before addition to the protein. This makes these much more complex than N-glycans, although they are less common. These modifications are initiated in the cell Golgi by attachment of a monosaccharide to the hydroxyl group of a Ser/Thr residue in the amino acid chain. Unlike N-glycans which only attach in the presence of a specific amino acid sequence, there is no specific known sequence for attachment of O-glycans.[2] However, there is evidence to suggest that regions rich in Ser/Thr, Pro and alanine (Ala) are preferable for O-glycan attachment.[17] Also, unlike N-glycans, there are different possible core sequences of oligosaccharides. These diverse glycans can be initiated from the attachment of GlcNAc, Man, fucose (Fuc) or *N*-acetylgalactosamine (GalNAc) with further monosaccharides sequentially added, adding to the variability of these complex glycan structures.[17]

Glycosylation is a highly important PTM in that it is known to have an effect on the protein's overall structure, which in turn can have an effect on its efficacy and safety as a biopharmaceutical drug.[2,3,5] For example, the activity and half-life of erythropoietin, used to stimulate red blood cell production, is affected by its glycosylation sites. If it is lacking in sialic acid residues then its *in vivo* activity is

drastically reduced, and if it contains less branched glycans then it has a much lower half-life in the body.[16] There is also a newer engineered version of erythropoietin that has two extra N-glycans added to the protein structure, which has led to it having a much longer half-life than the original erythropoietin protein.[16] In the treatment of Gaucher's disease, which is caused by mutation of the genes that encode for the lysosomal enzyme glucocerebrosidase (GCase), enzyme replacement therapy is required. This involves administering exogenously prepared GCase that has a very specific glycan pattern. The efficacy of the enzyme is critically dependent on it having terminal Man residues on its N-glycans, which allows it to target the Man receptors on macrophage cell surfaces.[2] This required that the enzyme was deglycosylated prior to administering to a patient to cleave any other terminal carbohydrate residues to leave only the three core Man residues. However, a new, safe and cost effective method has now been developed which allows for GCase to be produced with oligomannose type glycans, which simplifies the bioprocessing of these enzymes.[18] These are just two examples of biopharmaceuticals where having the correct glycosylation pattern is essential for the efficacy of the drug, and highlights the importance of full characterisation of these complex PTMs.

### 1.1.4 Lectins

One type of protein which is of particular interest in this project is lectins. These were first discovered in nature towards the end of the 19$^{th}$ century, and were known as hemagglutinins due to their ability to agglutinate red blood cells. Stillmark was the first to describe such a biomolecule when he isolated the highly toxic hemagglutinin ricin from castor tree seeds during his doctoral studies.[19] This was further studied by Hellin at the same university, who described another toxic hemagglutinin, abrin.[20] Subsequent immunological studies by Ehrlich at the Royal Institute of Experimental Therapy in Frankfurt using ricin and abrin showed that there was a specific antibody response to these hemagglutinins in mice, allowing him to establish many of the fundamental principles of immunology.[19,20]

In 1919, Sumner isolated concanavalin A (Con A) from jack bean, which was the first time a pure hemagglutinin had been obtained.[19] In 1936, however, Sumner and Howell first described the carbohydrate specificity of Con A when they noticed that the hemagglutinin activity was inhibited by the presence of sucrose.[21] They were the first to suggest that the hemagglutination by Con A was due to the protein binding to surface carbohydrates on red blood cells.[19] By the 1940s, different hemagglutinins were shown to only agglutinate certain blood groups over others, which led to a major application of this class of proteins in blood typing. This specific agglutinating activity prompted Boyd and Shapleigh to propose the name lectins, which is taken from the Latin word, *legere*, meaning to pick out or choose.[22] Interest in lectins grew and many had been identified by the 1970s, mainly in plants, but few had been isolated and purified until the development of affinity chromatography. This allowed scientists to finally purify and characterise lectins.[19]

Lectins are now defined as carbohydrate binding proteins that do not have an immune origin, such as antibodies, and are not catalytic, like enzymes.[23] It is understood nowadays that carbohydrate recognition by lectins is important in protein trafficking, cell adhesion, inflammation and immune responses, and cancer.[23,24] However, their properties are being harnessed as recognition molecules. It has been shown that lectins can be used in detecting over-expression of sialic acid and fucose on cells, which is a biomarker for cancer,[25,26] as well as differentiating between different IgG glycoforms, which can play a role in various diseases such as rheumatoid arthritis and Crohn's disease.[27] In a bioprocessing setting, lectins have also been shown as useful for glycoprotein analysis. They have been used in lectin affinity columns to isolate glycosylated proteins from unglycosylated proteins[28] and also used as aggregating agents to probe the glycosylation states of proteins tethered to gold nanoparticles (Au NPs).[29] Whilst these studies provided alternative methods for investigating the glycans present on proteins, mass spectrometry (MS) measurements remain the gold standard for glycan analysis. However, they prove to be interesting and useful tools which could hold the key to faster and potentially cheaper methods of analysis.

Lectins have the same hierarchy of structure as other proteins, but they differ in that they possess carbohydrate recognition domains (CRDs), which allow them to target and bind to specific carbohydrate moieties. These CRDs are specific amino acid sequences that allow for multivalent interactions between the polypeptide chain and the carbohydrate molecule.[30,31] As an example, the high density of hydroxyl groups on carbohydrates allow for multivalent hydrogen bonding interactions with amino acid groups in the lectin structure. The directionality of these hydroxyl groups also means some carbohydrates can be amphiphilic. This allows for further stabilisation and specificity through hydrophobic interactions by orienting the carbohydrate to align complementary regions.[32]

Some lectins require the presence of $Ca^{2+}$ and $Mn^{2+}$ cations in order for their CRDs to have the correct conformation and to allow for lectin activity. These cations aid the orientation of important lectin functional groups for coordination to the carbohydrate ligand.[32] This is the case for Con A, which is specific for glucose (Glc) and Man. (Figure 1.7)

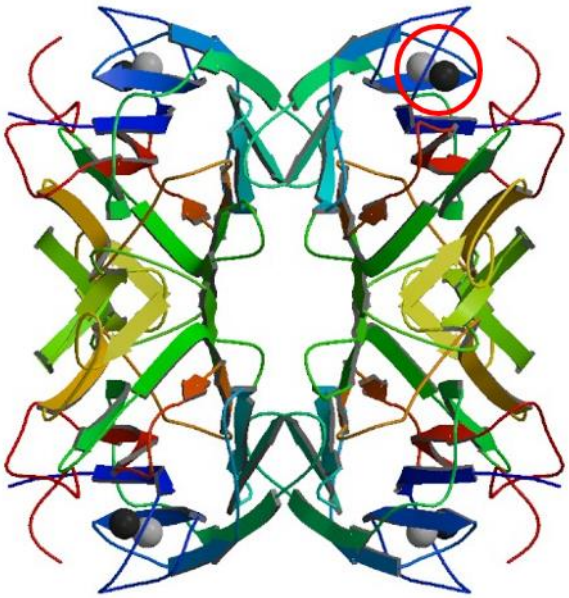

*Figure 1.7: Structure of concanavalin A, showing the $Ca^{2+}$ and $Mn^{2+}$ cations present (circled) which are necessary for carbohydrate recognition. (Protein data bank - 3CNA)*

The CRD in this lectin, however, does not form any hydrogen bonds with one of the oxygens present on these carbohydrates, which accounts for its inability to

distinguish between these two moieties.[30] In contrast to this, *galanthus nivalis* agglutinin (GNA) from snowdrops is specific purely for Man residues. (Figure 1.8) This is due to the hydrogen bond formed by its CRD to the O2 of the pyranose ring in mannose, which is missing in Con A.[30]

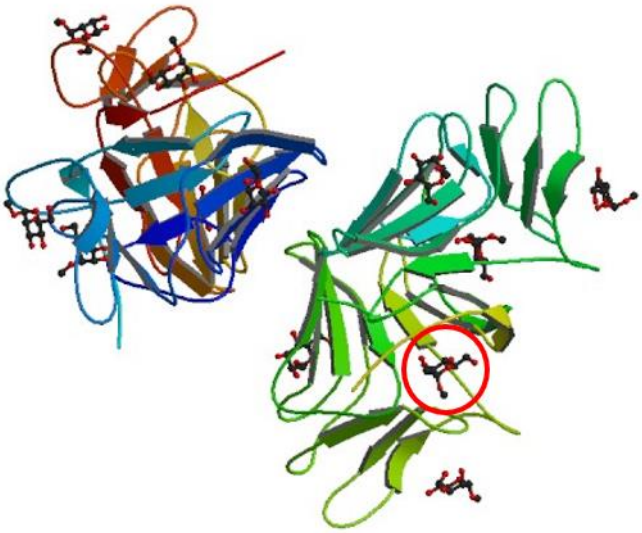

*Figure 1.8: Structure of the mannose-specific galanthus nivalis agglutinin, showing the mannose residues (circled). (Protein data bank - 1MSA)*

## 1.2 Bioprocessing

### 1.2.1 From Cell to Drug

A long and complex process is used in the manufacture of biopharmaceuticals: from cell growth, harvest and disruption to gain the therapeutic proteins, to the purification and isolation of the protein of interest. This process is split in to two streams: upstream and downstream. (Figure 1.9)

The upstream process involves the cell or bacteria growth, often from mammalian cells such as Chinese hamster ovary (CHO) cells or bacteria like *E.coli*.[33] These cells may have been transfected with specific DNA plasmids to amplify the production of the protein of interest *via* the transcription and translation process described previously.[34] The bioprocessing steps begin with the preparation and sterilisation of appropriate medium containing the necessary nutrients such as a carbon source,

often glucose, and a nitrogen source, often ammonia. This is then fed to a bioreactor where cell seeds are added. The fermentation process allows the cells to grow and multiply until they are harvested to be processed.

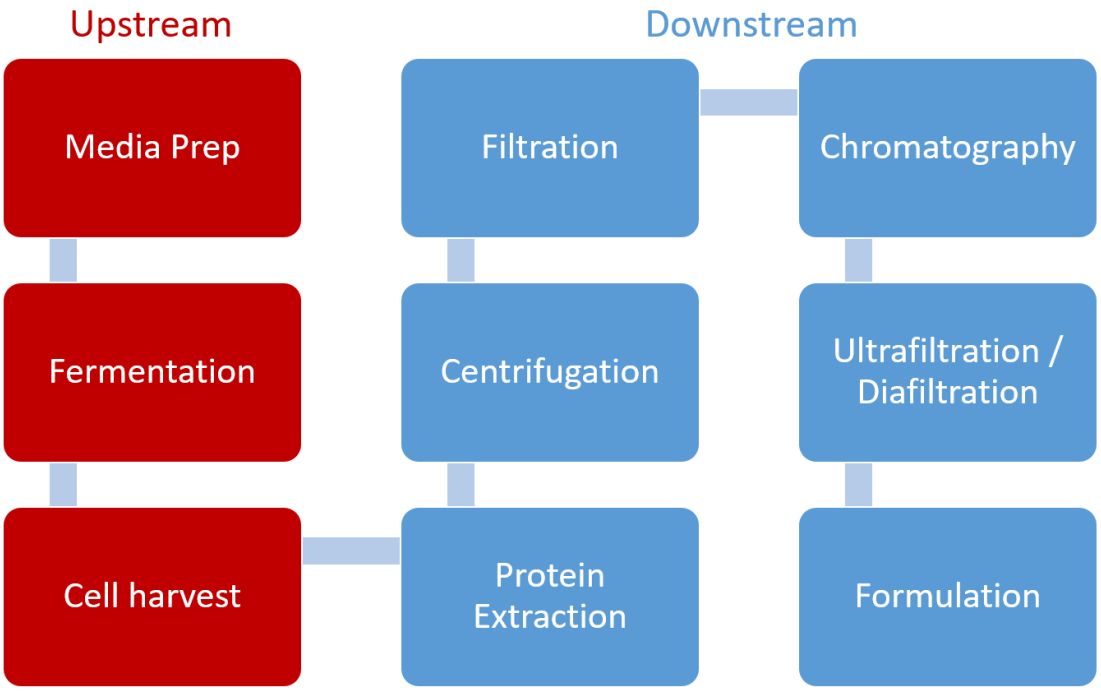


*Figure 1.9: Simplified scheme of the harvest and purification process in biopharmaceutical manufacture, showing the general upstream and downstream steps.*

The downstream process contains a variety of steps that are dependent on the cells and target proteins used. The first step is to extract the protein of interest from the harvested cells. This may be through homogenisation, which disrupts the cells to release the protein, but this method leaves cell debris along with DNA that can cause the resulting broth to be more viscous, making isolation and purification difficult. During the transfection process, however, it is possible to transfect an additional plasmid, which engineers the cell to produce periplasmic nuclease. This then has access to the DNA following homogenisation and causes it to hydrolyse in to more manageable smaller molecules.[35] Another method of protein extraction, especially used for proteins in the periplasmic space in *E.coli*, is the use of chemicals and/or heat, which can draw the proteins out of the bacteria without disrupting the inner cytosol, reducing the volume of DNA release.[36]

Following on from the homogenisation or buffer extraction it is important to remove any debris or unwanted matter from the broth. This is commonly carried out by centrifugation and filtration steps. The centrifugation steps are useful for removing large heavy contaminant particles to clarify the broth. Next, a series of filtration steps with microporous membranes can be used to separate out any larger proteins or biomolecules based on their molecular weight. This will leave a broth containing the target protein and other similar sized molecules.

In order to finally purify the broth to obtain the target protein of interest, a series of chromatography steps are often used. The types of column used depend on the properties of the target protein and any other known contaminants. Often the first step is to use affinity chromatography as an initial capture step to bind the protein of interest, whilst impurities in the broth flow through. The target protein can then be eluted separately to be further purified by other columns. Common stationary phases include anionic exchange and cationic exchange resins, or hydrophobic interaction steps. Finally, the chromatographic steps are followed by ultrafiltration to concentrate the product, and diafiltration to exchange the target protein in to the desired final formulation buffer.

The various steps can be altered in response to the target product. In some instances, however, it will be necessary for a manufacturer to reassess their processes in response to a new protein or change in raw materials or equipment. It is obvious then that the costs of new testing at plant scale would be unreasonable. Lab based evaluations are therefore carried out, which are comparable to plant scale processes. These ultra scale down (USD) techniques can be applied to centrifugation, filtration and chromatographic steps allowing for parameters such as shear stresses, buffer compositions, pH and stationary phase resins to be assessed in terms of their effect on the target protein and the processing efficiency.[37,38] Also assessed at small scale are any PTMs present on the final product, such as glycosylation. Upon scale up the change in cell growth and harvest conditions may cause a change in the oligosaccharide patterns on the protein chains, and therefore affect the efficacy and

safety of the final product.[39] This therefore means that extensive comparability studies must be carried out before full scale-up to biopharmaceutical production.

The guidelines set out by the European Medicines Agency (EMA) have stated that any change to the manufacturing process and/or raw materials must be characterised to ascertain whether or not the heterogeneity of the product PTMs are maintained.[40] This indicates that the manufacturing process may have an effect on the glycosylation profile of the therapeutic protein. It has been shown that changes to upstream processes in cell culture and harvest can have various effects on the final glycosylation profile.[41,42] However, there is little data to show that there are changes made through downstream processing. At this stage, the proteins are put under various stresses such as shear forces in centrifugation, or pH adjustments. It would therefore be reasonable to expect that this could have an effect on the glycosylation profile of the proteins. Work by Hoare *et al*,[43] however, showed in their USD studies of the effect of centrifugation following cell harvest on the protein PTMs that the fermentation process could greatly affect the PTM profile, and therefore should be kept consistent to avoid introducing additional heterogeneity. However, they did also find in their study that shear forces introduced by centrifugation did not alter the protein PTMs, including the glycan profiles, but could affect the quaternary structure of the proteins or antibodies being processed. The influence of glycosylation on the efficacy of the final product, however, is too great to ignore through processing, so must be characterised in every stage of the process, especially following manufacturing and raw material changes. Fast and reliable assessments are therefore essential in order to continually validate the production process to ensure the safety of the final product.

### 1.2.2 Current Therapeutic Protein Glycosylation Analysis Methods

The EMA has set out standards for testing of therapeutic proteins to ensure that they are safe for use in biopharmaceuticals. In comparison to the testing of small molecule

drugs, this is a much more thorough process due to the heterogeneous nature of complex biomolecules. These standards are set out in their document "Specifications: Test Procedures and Acceptance Criteria for Biotechnological/Biological Products" (ICH Topic Q6B, 1999).[40] This document states that, due to the fact that proteins are produced by living organisms, structural heterogeneity is to be expected and, therefore, the final product may be a mixture of different forms of the same protein as a result of various PTMs. A review by Greer[44] summarised the main structural characteristics that must be defined for biopharmaceutical products, as set out in ICH Topic Q6B mentioned previously.[40] This highlighted the need to understand the amino acid sequence and composition in the primary structure as well as the terminal amino acid sequence. The characteristics of the peptide map must be known, along with the position of sulfhydryl groups and disulfide bridges. Finally, it was highlighted that the carbohydrate structures must be well understood in glycoproteins.[44] It is therefore the manufacturer's responsibility to define the heterogeneity of the target product and prove that there is consistency in the heterogeneity between batches with preclinical and clinical studies. This heterogeneity, however, can be introduced during manufacture and/or storage of the product. It is therefore paramount that the product be thoroughly characterised throughout the manufacturing process.

The most common method of characterising biomolecular structures is by MS.[45,46] This technique has proven itself to be sensitive and versatile in detecting and quantifying changes in the primary and higher order structures of proteins. There is, however, no one spectrometer that can fully characterise a therapeutic protein product, which therefore often requires the use of multiple instruments. Whilst there are strong advantages of using MS, this throws up a major disadvantage from the high costs involved.[46] Although significant advances have been made in MS technology, which has improved the analysis of protein structures, for a full structural characterisation it is important to not only use modern soft ionisation MS techniques, but also techniques such as gas chromatography MS (GC-MS) in order to define branches and linkages in protein structure as well as distinguishing between same mass sugar isomers.[45]

The development of electrospray ionisation MS (ESI-MS) and matrix assisted laser desorption/ionisation MS (MALDI-MS) methods has made elucidation of glycoprotein structure easier. These techniques are important for initial protein analysis in molecular weight determination. ESI-MS can determine masses of proteins up to 150 kDa, but MALDI-MS is the more sensitive of the two techniques and can detect much larger biomolecules up to 500 kDa.[46] These methods, however, are very gentle and can result in little or no fragmentation. Therefore, they often require tandem MS instruments to allow for the mass of the parent ion to be detected by the first analyser, before collisions induced dissociation of the molecular ions produce fragments to be analysed by the second analyser.[45] These methods are often also combined with quadrupole orthogonal acceleration time of flight component to increase sensitivity further.[45] However, digestion steps may also be required for more in-depth analysis of the glycans present on the protein.[46]

As mentioned previously, the MS instruments along with their additional modifications are expensive, and the analyses are time consuming. This is especially true with the additional digestion steps required to fully elucidate the glycan structures. In the biopharmaceutical industry, where competition is high to bring therapeutic proteins to the market quickly and cost effectively, it would therefore be advantageous for techniques to be developed that could rapidly assess the glycosylation states of therapeutic proteins at various stages in the manufacturing process.

## 1.3 Nanotechnology

Officially, for a substance to be described as ‘nano’ it must have at least one dimension within the range of 1-100 nm.[47] This allows for different nanoparticle geometries. Spherical nanoparticles have all three dimensions within this range, nanorods and nanofibres have two, and platelets only one.[48] Each can have different properties that open up a wide variety of uses.

Although this technology may appear to be relatively new, Au and Ag NPs have actually been used for hundreds of years. The most well-known piece of evidence for this is the Lycargus cup, a Roman artefact thought to be from the 4$^{th}$ century CE. This cup has colour changing properties in different lights. When light is shone from above, the cup is a green colour, but when the light is shone from within the cup, it turns a bright red.[49] This is due to the fact that the glass contains colloidal Au and Ag, with diameters of around 70 nm, which appear green in scattered light, and red in transmitted light.

In more recent times, nanotechnology has grown with a long list of applications. Particular focus has been placed on biomedical applications[31,47,50,51], catalysis,[31,52–54] optical and electrochemical sensors,[50,54,55] and as polymer fillers.[56,57] The wide variety of research being conducted makes apparent just how useful nanotechnology is in current research and in future applications.

### 1.3.1 Localised Surface Plasmon Resonance

Metal NPs, in particular, have received significant attention due to their optical properties. Au and Ag NPs, for example, are known for being optically 'bright' and thus can be detected in solutions by the naked eye at very low concentrations.[58] This is a result of the metallic nanoparticles having free conductive electrons on their surface that can collectively oscillate upon irradiation by an electromagnetic field, such as a light source.[59,60] The electron cloud alters in position in relation to the metal nuclei, but due to the coulombic attraction between the nuclei and the electrons this results in the oscillation of the electron cloud. (Figure 1.10) This collective oscillation of electrons on each individual nanoparticle is known as the localised surface plasmon resonance (LSPR).

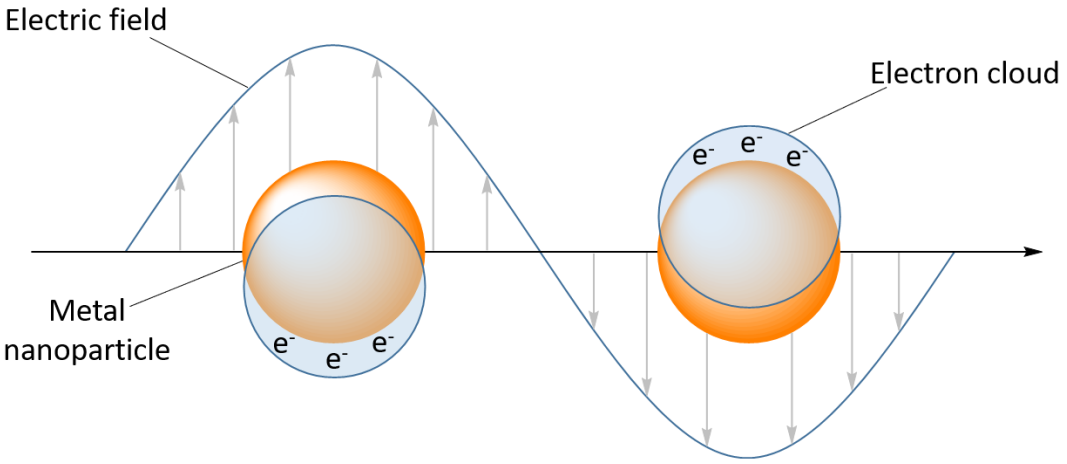


*Figure 1.10: Illustration of the localised surface plasmon resonance of a metal nanoparticle.*

The oscillating electrons will scatter electromagnetic radiation at the same frequency as the electron oscillation. This allows the LSPR to be seen in the ultraviolet-visible (UV-vis) extinction spectrum of the metal nanoparticles where it presents itself as a characteristic peak. The peak position can change in relation to the size, shape and homogeneity of the nanoparticles, but also in response to the refractive index of the surrounding medium.[59,61,62] This can be explained by a theory that was proposed by Gustav Mie in 1908.[59,62,63] Mie proposed that as the size of the particles increases, there is a shift of the absorption and scattering to longer wavelengths. This has been shown to be true in particles that are in the range of 5-100 nm. The effect of size alone on the LSPR can be illustrated by the fact that Au NPs in solution change from a dark ruby red colour at diameters of around 5 nm to a light blue/violet colour at larger diameters of around 100 nm.

### 1.3.2 Nanoparticle Biosensing

The LSPR phenomenon of metallic nanoparticles has been harnessed to provide powerful techniques in biological and chemical sensing.[64–66] DNA functionalised nanoparticles have been used as biosensors that target complementary DNA sequences, inducing aggregation of nanoparticles upon DNA hybridisation.[67,68] This hybridisation brings particles closer together, causing the LSPR absorbance band to shift to longer wavelengths due to the coupling of LSPRs of neighbouring

nanoparticles. Shifts in the LSPR have also been used in detection of interactions between proteins, and also between proteins and DNA.[69] Similar measurements have also been used to probe interactions between carbohydrates and lectins.[65,70] Metallic nanoparticles have become useful tools in biosensing, and the LSPR phenomenon has paved the way for surface enhancement techniques. One such analytical technique that has become increasingly useful with the use of metallic nanoparticles is Raman spectroscopy, where the coupling of the nanoparticles LSPRs upon aggregation has led to surface enhanced Raman scattering (SERS), which has allowed for analysis with much higher sensitivity.

## 1.4 Raman Spectroscopy

Raman scattering was first observed experimentally in 1928 by Raman and Krishnan,[71] although the theory was first proposed in 1923 by Smekal.[60,72,73] It is a widely used technique that has advantages in that vibrational and rotational information can be obtained in a variety of physical states, such as solids, liquids, vapours, and also in a variety of solvents.[60]

### 1.4.1 Raman Scattering

Photons from a light source, such as a laser, will interact with the electrons of an analyte of interest. These photons can be absorbed, scattered, or can have no interaction. If the energy of the incident photon matches the energy difference between the ground and excited state, then the molecule absorbs the photon and is promoted to an excited state. During this interaction of the electrons with the incident photon, the electron clouds surrounding the molecule are distorted. This interaction induces a polarisation of the electron cloud, which in turn causes a photon to be scattered.[60] Scattering, however, can also occur in the absence of absorption, where the energy of the incident photon is not equal to the energy difference between the ground and excited state. In this case, the polarisation of the electron cloud results in the formation of a short-lived excited state, known as a 'virtual state,'

which then scatters upon relaxation. The vast majority of scattered photons have a wavelength equal to that of the incident photon. This elastic scattering phenomenon is known as Rayleigh scattering. In some cases, however, the energy of the incident photon can be different from the scattered photon. During inelastic scattering, light can gain or lose energy as it relaxes from the virtual state, and thus the molecule returns to a different vibrational state. This is known as Raman scattering.

There are two types of Raman scattering: Stokes and anti-Stokes scattering. When energy is transferred from the incident photon to the molecule, this is known as Stokes scattering. The scattered photon, therefore, has an energy one vibrational unit lower than the incident photon. This is the strongest form of Raman scattering at room temperature. When the scattered photon has greater energy than the incident photon, this is known as anti-Stokes scattering. This occurs when energy is transferred from the nuclei to the scattered photon due to thermal energy, since some molecules would already exist in an excited vibrational state.[60] (Figure 1.11)

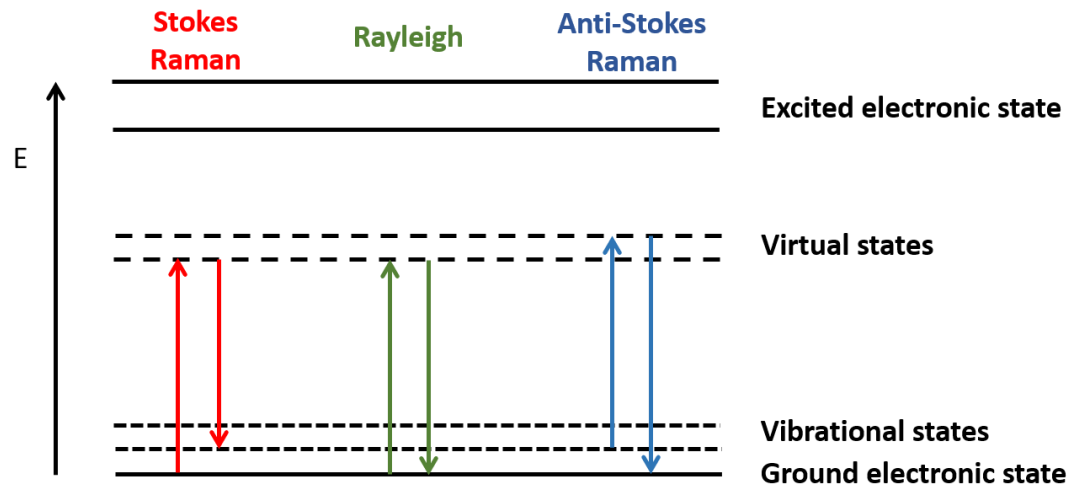


*Figure 1.11: Jablonski diagram illustrating the differences between Rayleigh, Stokes, and anti-Stokes scattering.*

Raman spectroscopy does, however, have a disadvantage in that it is a very weak process when compared to Rayleigh scattering as only one in $10^6$-$10^8$ scattered photons are Raman scattered, with the intensity of Raman scattering being described by Equation 1.

$$I = KI_L \propto^2 v^4 \qquad \text{Equation 1}$$

Where the Raman intensity is given by *I*. *K* is a constant, $I_L$ is the laser power, $\alpha$ is the polarizability, and *v* is the laser frequency. This relationship allows for tuning of the instrumentation to produce more intense spectra. Since the intensity is directly proportional to the laser frequency to the fourth power, shorter excitation wavelengths can be used to increase the intensity of the Raman signal.

The lack of Raman scattered photons, however, is the primary reason why it is not as commonly used as other analytical techniques. Recently, however, significant advances in technology have reduced the downfalls of Raman spectroscopy and simplified the equipment required, bringing it more in to the foreground in analytical chemistry.[60]

### 1.4.2 Resonance Raman Scattering

Initially in Raman spectroscopy, coloured compounds were avoided in analysis due to the fact that the visible radiation used to excite the coloured molecules was often absorbed by the sample. This absorption process could cause strong fluorescence, which prevented Raman scattering from being detected. It was later discovered, however, that when the frequency of the incident laser is close to the frequency of an electronic transition, enhancement of the Raman scattering was observed, often in the order of $10^3$ or $10^4$. These scattering enhancements have also been seen in the order of $10^6$.[60]

During this process, the electrons from the chromophore of an analyte molecule are promoted to an electronic excited state. In the absorption process, the nuclei reach equilibrium positions with electrons in the excited state. However, in the resonant scattering process, the time that the electrons occupy the excited state is significantly shorter, and therefore prevent the nuclei from reaching equilibrium positions.[60] This is known as resonance Raman scattering. (Figure 1.12) This resonance effect has made Raman spectroscopy a much more sensitive analytical tool. Also, since it is only

the chromophore that experiences the resonance effect, this process is therefore selective for the chromophore in the analyte molecule.

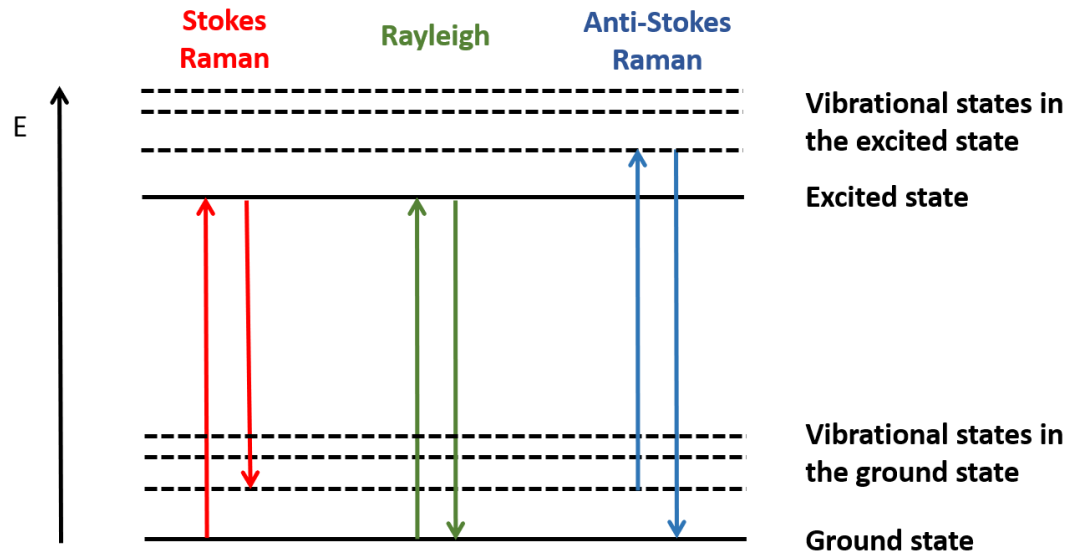


*Figure 1.12: Jablonski diagram showing the resonance Raman scattering process.*

Another advantage of this effect is that it does not require an excitation laser wavelength that corresponds exactly with the energy difference between the ground and excited state, as enhancement can also be obtained with a laser that has an excitation frequency which is close to that of the electronic transition.[60] However, whilst this phenomenon has meant that more molecules can be analysed with Raman spectroscopy, fluorescence is still a problem, which can make observing the Raman spectra difficult.

### 1.4.3 Surface Enhanced Raman Scattering

Raman spectroscopy can be used effectively with solid samples as strong scattering can be obtained, but with samples in solution, Raman can be considered a relatively insensitive technique. As mentioned previously, one of the key limitations of Raman scattering is that it is very weak. However, techniques have been developed to provide a marked enhancement of the Raman spectra when adsorbed on to a roughened metal surface. This technique is known as SERS, and can give an enhancement of up to around $10^6$ over Raman scattering alone.[60]

SERS was first reported by Fleischmann *et al*.[74] This study observed an increase in the Raman scattering from pyridine molecules, which had been adsorbed on to the surface of a roughened silver electrode. They attributed this to an increased number of pyridine molecules on the electrode surface due to an increase in the surface area. However, later studies by Jeanmarie and Van Duyne[75] and Creighton and Albrecht[76] showed that, since the enhancement obtained was of the order of $10^6$, much greater than could be obtained from surface roughening, this effect was in fact due to a specific surface enhancement from the silver electrode.

As mentioned previously, on a metal surface there exists free conductive electrons that oscillate upon interaction of light, known as the LSPR. (Figure 1.10) When this surface is roughened, the plasmons can further oscillate, which increases the scattering efficiency, which in turn enhances the Raman scattering and therefore the Raman signal. Two different theories are currently used to explain this phenomenon.

Firstly, the electromagnetic enhancement is generally believed to be the strongest contribution to the enhancement of the Raman signal.[60] This is due to the molecule that is adsorbed on to, or in close proximity to, the metal surface experiencing an increased local electric field due to the LSPR. The interaction between the electrons of the adsorbed molecule and the LSPR causes a greater polarisation of the electrons around the adsorbed molecule, resulting in a significant enhancement of the Raman scattering.[60,77] This principle allows for the use of nanoparticle aggregation to generate further surface enhancement of the Raman signals. This technique takes advantage of an increase of the localisation of the electromagnetic field between nanoparticles, sometimes referred to as 'hot spots,' providing significant increases in the SERS intensity.

The second theory used to explain this phenomenon is chemical enhancement. This is also referred to as charge transfer, due to the formation of a bond between the analyte and the metal surface. The new molecular species, consisting of the analyte and a few of the metal surface atoms, allows for a transfer of charge from the metal surface to the analyte, increasing the polarisability of the analyte molecule. It is proposed that the formation of the metal-analyte bond creates new electronic states,

which are resonant intermediates in Raman scattering, and therefore enhance the Raman signals. This suggests that instead of the incident photon being absorbed or scattered by the metal surface, it is absorbed in to the metal and transferred to the analyte. The Raman excitation then occurs and is transferred back to the metal before being re-radiated.[60,78]

### 1.4.4 Surface Enhanced Resonance Raman Scattering

It is possible to combine the effects of SERS with the use of an analyte molecule with a resonant chromophore. This is known as surface enhanced resonance Raman scattering (SERRS). This shows significant enhancement over SERS and resonance Raman spectroscopy alone, with enhancements of up to $10^{14}$ in the Raman spectrum being observed.[60] It also overcomes the issues with fluorescence in resonance Raman spectroscopy, since the adsorption of a chromophore containing analyte on to a SERS active substrate results in almost complete quenching of any fluorescence.[60]

Further advantage of SERRS include that it lowers issues with contaminants in the analyte due to the resonant component of the chromophore. It also means that lower laser powers and shorter accumulation times can be used due to the enhancement effects, which is advantageous when working with analytes that are sensitive to photodecomposition.[60] These favourable features have made SERRS a much more widely used technique, which can significantly increase the sensitivity of Raman spectroscopic measurements.

## 1.5 Advances in Glycan Detection Assays

In order to overcome the disadvantages of current glycosylation analysis methods, research has been carried out to provide new means of assessing this vital biopharmaceutical characteristic. The diversity of this research shows its importance and significant advancements have been made towards alternative detection assays.

An interesting development in glycoprotein detection is the use of molecular imprinting. This has been carried out on Au surfaces to selectively bind specific glycoproteins, monitored by changes to the SPR.[79,80] A glycoprotein template is bound by boronic acid groups at basic pH and a polymer layer is formed surrounding the protein. The template is then removed by changing to acidic pH leaving a specifically shaped cavity with sugar-binding properties. This same technique has also been applied to nanoparticles and has shown to be able to selectively bind to a specific glycoprotein target in complex mixtures.[81] These are significant advances with a promising future in biomedical assays. However, for specific structural component analysis of glycans, further research is required to improve the specificity for individual carbohydrates.

Raman spectroscopy has also been investigated to assess the glycosylation status of glycoproteins. Brewster *et al*[82] utilised this powerful technique alongside multivariate data analysis to distinguish the glycoprotein ribonuclease B (RNase B) from its non-glycosylated counterpart, ribonuclease A (RNase A) and could even quantify their presence in mixtures. Further to this, Ashton *et al*[83] used chemometric techniques to identify variations in the Raman spectra of proteins caused by structural changes induced by glycosylation. This could also not only distinguish between glycosylated and non-glycosylated transferrin, but could also be used for quantification in mixtures. This research in to the use of Raman was a considerable step forward for this technique which has a history of use in protein characterisation due to its non-destructive nature.[84] Raman spectroscopy could therefore be an attractive analysis method. The only real disadvantage to this technique is the requirement for chemometric data analysis techniques. Otherwise, this could provide a wealth of protein structural information rapidly and non-destructively.

Whilst Raman scattering has been very useful in biopharmaceutical analytics, it is an inherently weak technique due to the fact that only 1 in $10^6$ photons are Raman scattered.[60] Therefore, enhancement techniques could be used in order to improve the sensitivity of glycan detection. Cowcher *et al*[85] used tip-enhanced Raman scattering (TERS) and showed that this could not only differentiate between the

native and glycosylated forms of bovine pancreatic RNase B, but also made steps towards structural characterisation. This technique is still in its infancy, but has excellent potential for sensitively obtaining structural information.

Fluorescence measurements are commonly used in biochemical assays, and have been applied to the detection of protein glycosylation characterisation through lectin microarrays. This has allowed the high-throughput detection of immobilised glycoproteins using fluorescently labelled lectins.[86] Similar techniques have also led to therapeutic protein glycan analysis which utilised a broad range of lectins to build a picture of the overall glycan structure.[87] These assays provide rapid and cheap analysis methods with good sensitivity. However, if SERS measurements could be used in these formats, the sensitivity could be improved further, and the possibility for multiplexing could significantly reduce the number of samples required for full analysis.

The biopharmaceutical industry would benefit from new analysis methods which give clear, rapid, and sensitive results regarding glycan structure. The wealth of research in this area, and the advancements made towards rapid and sensitive assays for glycan characterisation is promising. Further research in this field could eventually produce viable assays for therapeutic protein characterisation, reducing time, cost and the need for highly trained analysts.

# 2. Research Aims

The overall aim of this project was to investigate new methods of assessing the glycosylation characteristics of biopharmaceutical proteins. The current methods are time consuming and expensive, so alternatives which are rapid, cheap, and have high-throughput capabilities would be advantageous. The overall concept of this detection involved the use of carbohydrate-binding proteins to selectively seek out specific glycan components. When these were tethered to Au NPs, this allowed for the capability of sensing *via* SERRS and LSPR measurements.

This research investigated the use of these functionalised NPs in selective and sensitive protein glycosylation detection. Methods were selected for their ease-of-use and applicability to industrial settings. Three main routes were considered. Firstly, to develop a simple solution-based assay whereby glycan detection could be tracked and quantified *via* shifts in the LSPR peak position. The versatility of this method was also investigated to broaden the scope of the detection capabilities, for a more detailed analysis of the glycan structural components.

A paper-based assay was also investigated to provide a cheap, and rapid alternative to current glycan analysis methods. This involved the evaluation of common lateral flow assays, as well as the consideration of alternative assay formats to increase both throughput and sensitivity. This method was coupled with two different analysis methods. Firstly, a user-friendly colorimetric evaluation utilising a simple flatbed scanner. Secondly, the assay was coupled with SERRS measurements to provide a sensitive detection platform.

Finally, due to the commonplace use and commercial availability of enzyme-linked immunosorbent assays (ELISAs) this assay format was investigated for use in glycan detection. These are often available as pre-prepared kits and can allow for rapid and sensitive detection of analytes. Research was therefore started on the development of such an assay relying on the induced growth of Au NP seeds as a sensitive detection method.

# 3. Functional Gold Nanoparticles for Glycosylation Detection

## 3.1 Introduction

Metallic nanoparticles have been used widely in biochemical detection mechanisms due to their optical properties. These structures can be readily functionalised to produce beacons for the selective detection of biomolecular targets, and coupled with techniques such as SERS can produce highly sensitive assays. The ease of functionalisation for an array of targets makes them attractive for use in detection assays.

In the characterisation of glycoproteins, the use of metallic NPs have been investigated using a variety of techniques. Sanchez-Pomales *et al*[29] coated Au NPs with biopharmaceutical glycoproteins and aggregated them using lectins. The changes observed in the LSPR peak following aggregation allowed for sensitive detection of the high-Man glycan on RNase B, with a limit of detection of 1 µg/mL, which could also be applied to biopharmaceutical samples. This assay showed the possibility for LSPR measurements in protein characterisation. Since their assay relied on NP aggregation, they could have incorporated a Raman reporter molecule (RRM) to produce a SERS assay for glycan quantification, which could have improved the sensitivity of their assay. One drawback to this assay format, however, was the need for sample preparation. They had to attach the glycoprotein to the NP surface before inducing aggregation with a lectin. Whilst this produced a sensitive assay, removal of sample preparation steps would increase its viability in industrial settings.

Similar approaches were used to show the potential of functionalised NPs to quantify protein-carbohydrate interactions using LSPR measurements. Tsutsumi *et al*[88] used LSPR measurements of peptide-carbohydrate coated Au NPs to detect lectins by quantifying changes in the peak position. Van Duyne[65] showed that there were LSPR shifts when Man-functionalised NPs bound to Con A. Craig *et al*[70] also showed that

LSPR measurements could identify the aggregation of glycol-NPs in the presence of Con A, and used SERS measurements to produce a sensitive assay.

It would be advantageous if pre-functionalised NPs could be used in simple LSPR measurements for biopharmaceutical glycoprotein analysis. In past research, functionalised NPs have been used to detect specific glycan components. Chen *et al*[89] used sialidase-coated NPs to detect and map glycosylation on single cells by binding to SA. NPs have also been functionalised with lectins for the detection of cancer cells. Wang *et al*[90] used lectin-coated NPs to bind to HeLa cells, and used extinction measurements to show that binding was successful. Craig *et al*[25] also used lectin-coated NPs. They showed that NPs functionalised with WGA would bind to overexpressed SA on cancer cells, which could be mapped through SERS measurements.

Au NPs have excellent potential to be used in the characterisation of biopharmaceutical glycosylation. They can be readily functionalised with targeting biomolecules, such as lectins, which can selectively bind to glycan structures. Their versatility in measurement options makes them attractive avenues for rapid diagnostic tests. LSPR measurements can be made through extinction spectroscopy to show shifts in the characteristic Au NP peak position to confirm binding, and the optical properties of metallic NPs lend themselves well to SERS measurements which have the potential for sensitive detection. Therefore, lectin-coated Au NPs were used here to selectively bind to glycans, elucidating information about the structural components.

## 3.2 Results and Discussion

### 3.2.1 Gold Nanoparticle Synthesis

A method for producing citrate-capped Au NPs was first reported by Turkevich in 1951,[91] which was later refined by Frens in 1973[92] to produce monodisperse colloids. Lee and Meisel also utilised a similar method in their research.[93] A modified Lee-Meisel method was used to synthesise Au NPs in this work. This can be applied to the

reduction of Au or silver salts using sodium citrate to produce spherical particles. The initial step involves the partial reduction of the metal ions by the citrate to metal atoms which flocculate to form small seed particles. The remaining Au cations are attracted to and held in the electronic double layer of the seed particles. Finally, the remaining Au cations are reduced on to the seed particle surfaces causing growth controlled by the capping citrate groups.[94] This introduces stability to the NPs by providing a negatively charged surface layer which prevents aggregation by electrostatic repulsion. The Au NPs were characterised using extinction spectroscopy, dynamic light scattering (DLS), and zeta potential measurements. The extinction spectroscopy results are shown in Figure 3.1.

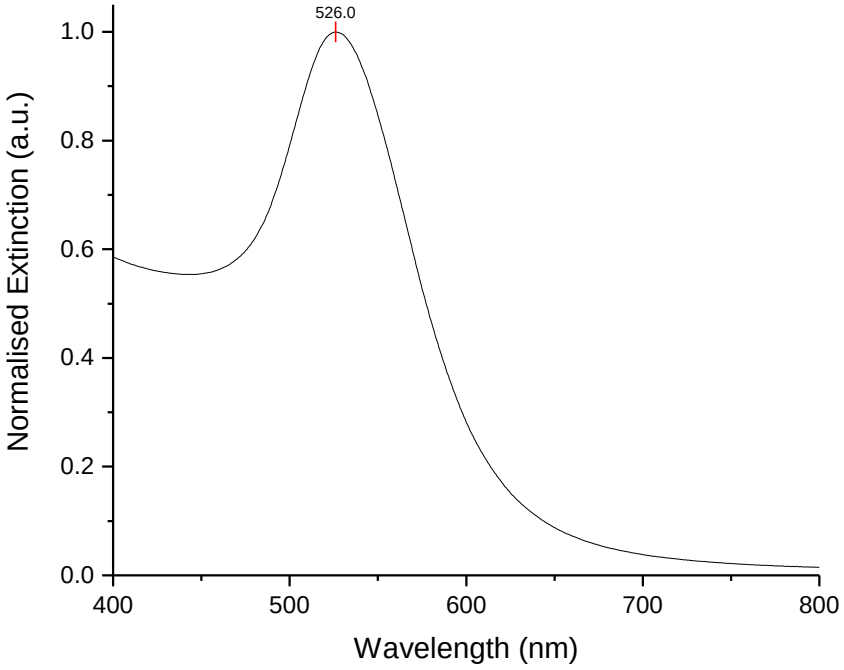


*Figure 3.1: Extinction spectrum of gold nanoparticles prepared via the modified Lee-Meisel method. Spectrum has been normalised to one.*

As shown in Figure 3.1, the Au NPs had an LSPR peak with a $\lambda_{max}$ at 526 nm, which is characteristic of nanoparticles of this size.[95] DLS measurements showed the Au NPs to be 41 ± 1 nm in diameter. The particles also had a zeta potential of -40.6 ± 1.27 mV indicating that the particles were stable, with the negative charge arising from the negatively charged citrate layer that caps the nanoparticles. The closer the zeta potential value is to zero, the greater the nanoparticle instability,[96] and high degrees

of stability have been reported for NPs that have a zeta potential lower than -25 mV.[97] Finally, using the extinction spectrum and size data the NP concentration was calculated to be 0.13 nM using the Beer-Lambert Law.[95] (molar extinction coefficient = $9.26 \times 10^9$ $M^{-1}cm^{-1}$)

The characterisation showed that the Au NP synthesis method was successful, so work was carried out on providing the NPs with functionality using Raman reporter molecules and linking molecules.

## 3.2.2 Nanoparticle Functionalisation and Bioconjugation

The Au NPs are stabilised through the electrostatic interaction between the charged groups of trisodium citrate (Figure 3.2) and the NP surface. The overall negative charge provided by the citrate group provides stability by creating repulsive forces between the NPs and preventing aggregation.

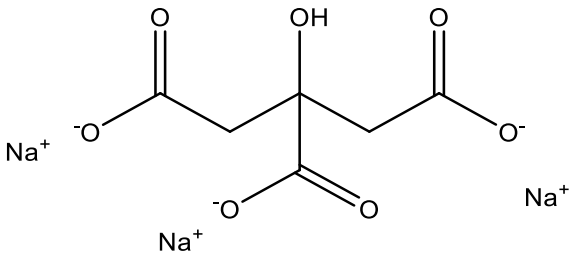


*Figure 3.2: Structure of trisodium citrate showing negatively charged groups which interact with the gold nanoparticle surface and provide an overall negative charge.*

The interaction between the NPs and the citrate is relatively weak in comparison to other surface modification processes involving chemisorption. The use of salt solutions, for example, can disrupt the electrostatic forces between the NPs and induce uncontrolled and irreversible aggregation causing them to precipitate out of solution.[98] Capping the NPs *via* alternative chemisorption methods, however, can provide the necessary protection to withstand such conditions.

Thiol group-containing molecules are most widely used for chemisorption on to Au NP surfaces, due to the high affinity of the Au-S interaction.[99] The specific mechanism of this reaction has been a cause for discussion, but it is commonly agreed to be like

a strong covalent interaction, due to the very similar electronegativities of the Au and sulfur.[100] Thiolated ligands with terminal functional groups are therefore commonly used to replace electrostatic capping agents on Au surfaces, forming self-assembled monolayers (SAMs) to provide stability to the NP and functionality for further modification.[100,101] In turn, modification of these available terminal functional groups can provide opportunities for NPs to target a variety of biomarkers in biological detection assays.

Thiolated-polyethylene glycol (PEG) with a terminal carboxylic acid or amine are commonly used heterobifunctional linkers.[102,103] One example is carboxy-$(PEG)_{12}$-thiol ($CT(PEG)_{12}$) (Figure 3.3) which contains a thiol for binding to the NP surface, a PEG spacer, and a carboxylic acid which can be further modified with targeting biomolecules.[104,105]

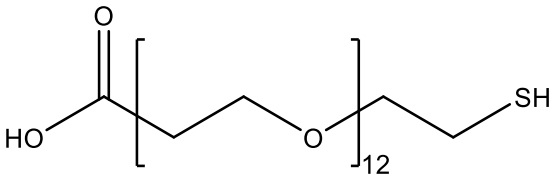


*Figure 3.3: Carboxy-polyethylene glycol-thiol ($CT(PEG)_{12}$), which contains a thiol for chemisorption to the nanoparticle surface, and a carboxylic acid for further modification.*

The variable length of PEG linkers, and their resulting flexibility, in combination with their polarity makes them viable choices for NP surface coverage. These linkers can fold and interact intermolecularly to form stable monolayers around a nanoparticle whilst containing a functional carboxylic acid terminus.

Another example of a functional linker is the pentapeptide molecule, CALNN.[106–108] (Figure 3.4) This molecule makes use of three main properties to form stable monolayers surrounding a NP surface. Firstly, the cysteine (C) at the amine terminus has a thiol-containing side chain which is used for binding to the metal surface, which may be further stabilised by the presence of the amine. Secondly, this is followed by alanine (A) and leucine (L) which contain aliphatic side chains. This segment is therefore hydrophobic so forms a dense monolayer of protection, excluding water. The fact that the leucine group has a longer side chain helps account for the curvature

of the NP and further stabilises the monolayer. Finally, this is followed by two asparagine (N) groups which have polar side chains, allowing the coated NPs to be soluble and stable in aqueous solutions.[107] The final asparagine is also the carboxylic acid terminus, which can be modified with biomolecules to provide the NPs with detection capabilities.

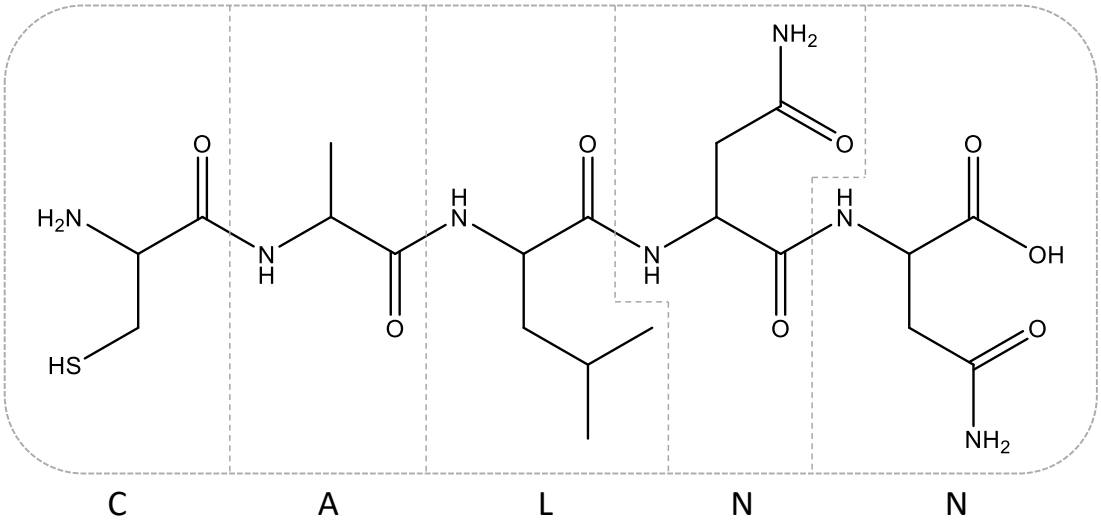


*Figure 3.4: The structure of the pentapeptide CALNN, showing each of the individual amino acid components: Cysteine (C); Alanine (A); Leucine (L); Asparagine (N).*

Both PEG and CALNN are suitable linkers for NP conjugation experiments. Initially, CALNN was used in the successful functionalisation of Au NPs to GNA. However, when expanding this research to include other lectins, PEG was used as an alternative to maintain nanoparticle stability. (Section 3.2.4)

Overall, the functionalisation process involved two main steps. (Figure 3.5) Firstly the RRM was added to the Au NPs to allow for attachment to the surface. Next, the linker-lectin ligand which was prepared separately using carbodiimide-crosslinking chemistry was added to the NPs, allowing for a stable mixed-monolayer to form around the NPs. Centrifugation was then used to remove unbound ligands, leaving a solution of SERRS-active lectin-functionalised NPs. This process required that studies were first performed to select the optimal RRM and linker concentrations for stable NP production.

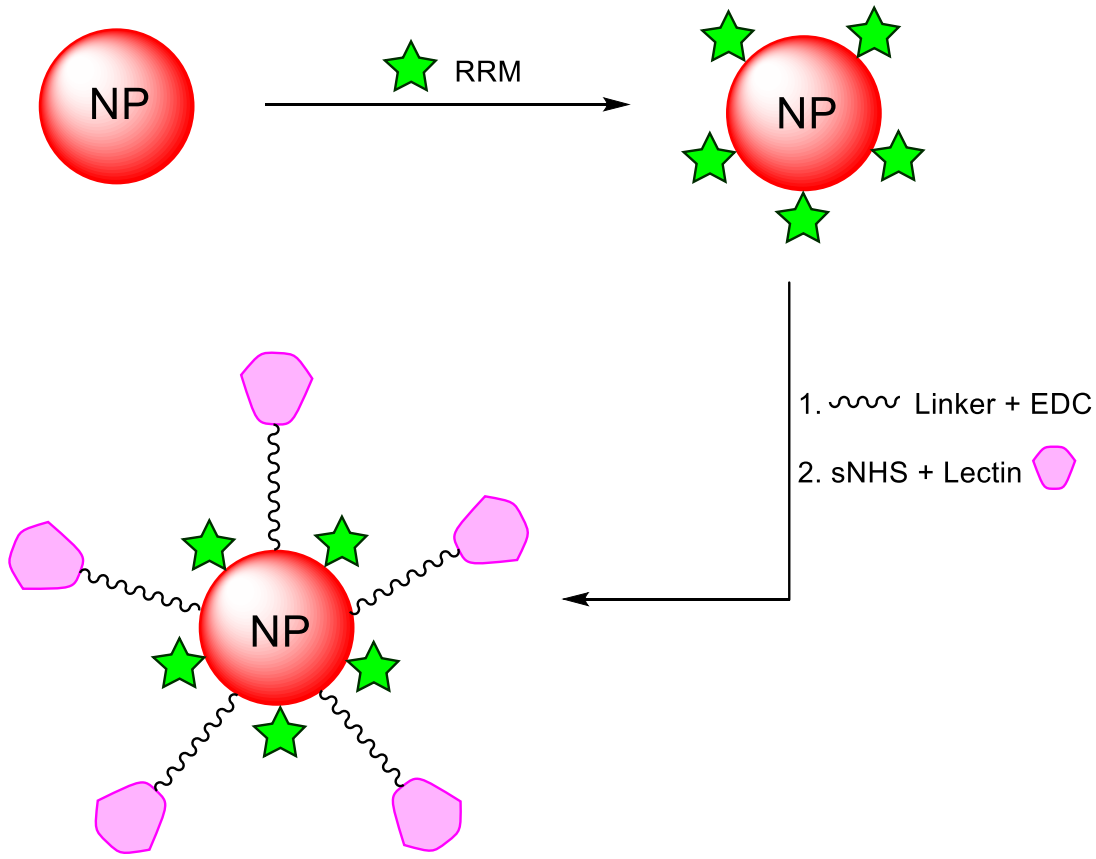


*Figure 3.5: General step-wise process of preparing functionalised gold nanoparticles. The Raman-active beacon was added first to allow for attachment to the gold surface before addition of the pre-prepared linker-lectin ligand which then forms a mixed monolayer around the nanoparticle.*

### *3.2.2.1 Producing Stable and Functional SERRS-Active Nanoparticles*

The Au NPs were functionalised with a RRM to provide a unique Raman fingerprint spectrum that can indicate detection of the target analyte. Its signal intensity could then be correlated to the concentration of target detected. In this research, malachite green isothiocyanate (MGITC) was used. (Figure 3.6) This was chosen as it contained an isothiocyanate group allowing for strong adsorption on to the Au NP surface and scatters strongly to provide a characteristic, recognisable SERS signal.

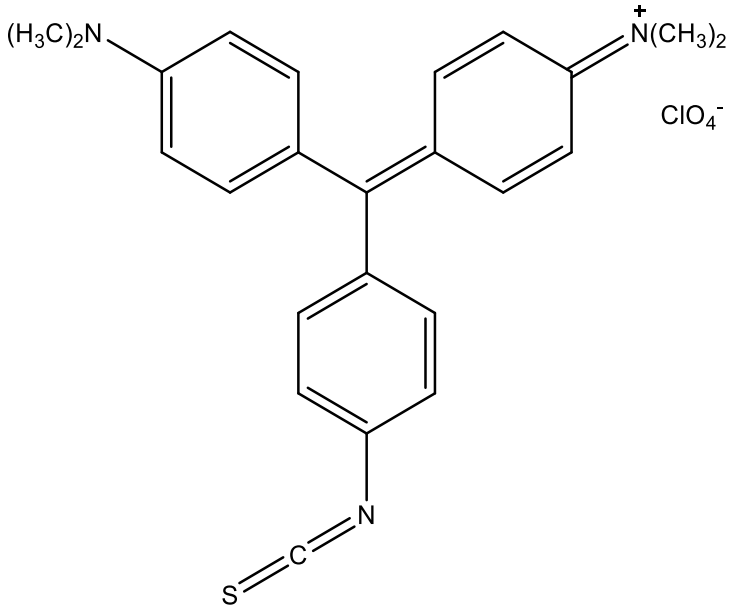


*Figure 3.6: The structure of malachite green isothiocyanate (MGITC) used to provide a unique SERS fingerprint to indicate analyte detection.*

MGITC exhibits a strong absorption band at 625 nm, making it an ideal candidate for SERRS measurements using available laser wavelengths at 633 nm and 638 nm.[109] Selecting a laser line close to the MGITC absorbance maxima increased the intensity of the scattering due to the resonance enhancement of the dye signal.

It was also important that the Au NPs were stable, so that any aggregation to induce an increased SERRS response was due to specific detection and not an uncontrolled aggregation process. Salt solution can be used to assess the stability of Au NPs by disruption of the electrostatic forces between the NPs.[98] Uncoated NPs will aggregate in an uncontrolled manner, whereas NPs coated in a protective layer would remain stable. The pentapeptide linker CALNN was used to provide this protection, but still retain functionality for further modification. An optimum coating concentration of CALNN on the Au NPs therefore had to be determined.

Firstly, 1 mL NP stock solution was coated with various final concentrations of CALNN (0.75, 1.00, 1.25, 1.50, 1.75, and 2.00 µM) by mixing different volumes of 1.87 mM CALNN with 1 mL stock Au NPs. To test their stability, 100 µL NaCl stock solution (120 mM) was mixed with 275 µL Au@CALNN and then studied using extinction

spectroscopy in order to determine which CALNN coating concentration provided the greatest protection from aggregation. (Figure 3.7)

For bare Au NPs (Figure 3.6(A)), the extinction spectrum showed a marked difference following the addition of salt. The dampening of the extinction showed that the concentration of free NPs in solution had reduced, and the increased signal at higher wavelengths is characteristic of the formation of aggregates. In this condition, the Au NPs were only coated electrostatically with citrate, which can easily be disrupted with salt ions, causing the particles to aggregate. However, following coating of the Au NPs with CALNN, the extinction spectra (Figure 3.6(B)) indicated that the colloid remained stable at all coating concentrations following salt addition. The CALNN coatings around the NP surfaces at all concentrations tested were sufficient enough to protect them from the salt in the surrounding solution.

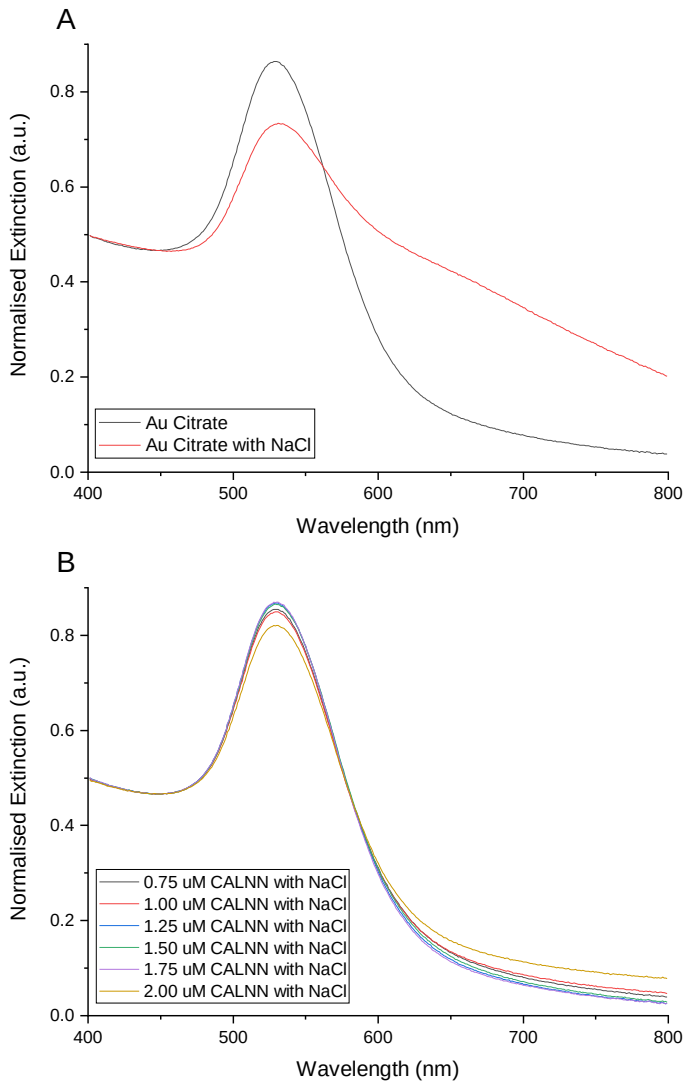


*Figure 3.7: (A) Extinction spectra of gold NPs before (black) and after NaCl addition (red), showing the aggregation taking place; (B) Extinction spectra of CALNN coated gold nanoparticles following the addition of NaCl solution. No observable NP aggregation was recorded at any of the CALNN coating concentrations, highlighting the stability of the colloid due to the CALNN coating. Extinction spectra normalised to 448 nm for clarity and ease of comparison.*

Good NP stability and protection from uncontrolled aggregation due to the presence of salt was observed for all the CALNN coating concentration tested. Therefore, it was decided to carry forward the two lowest concentrations used (0.75 µM and 1.00 µM) since any higher would be in excess.

Following selection of the CALNN linker concentration for coverage of the Au NPs surface, the concentration of the RRM, MGITC, had to be determined. Varying volumes of MGITC solution (1 µM) were briefly mixed with the Au NPs to give

different final concentrations (10, 20, 30, 40, and 50 nM) followed by the addition of the fixed final concentrations of CALNN. (0.75 µM - Figure 3.8; and 1.00 µM - Figure 3.9) These were mixed for 3 h, centrifuged, and resuspended in $dH_2O$ to remove any excess unbound ligands. The SERRS responses of the coated Au-MGITC-CALNN NPs were then measured with a laser excitation of 638 nm. This wavelength was close to the absorbance band of MGITC, ensuring that SERRS was achieved instead of SERS. Salt was also added to see if the SERRS signal would increase to simulate an on-off change once detection had taken place.

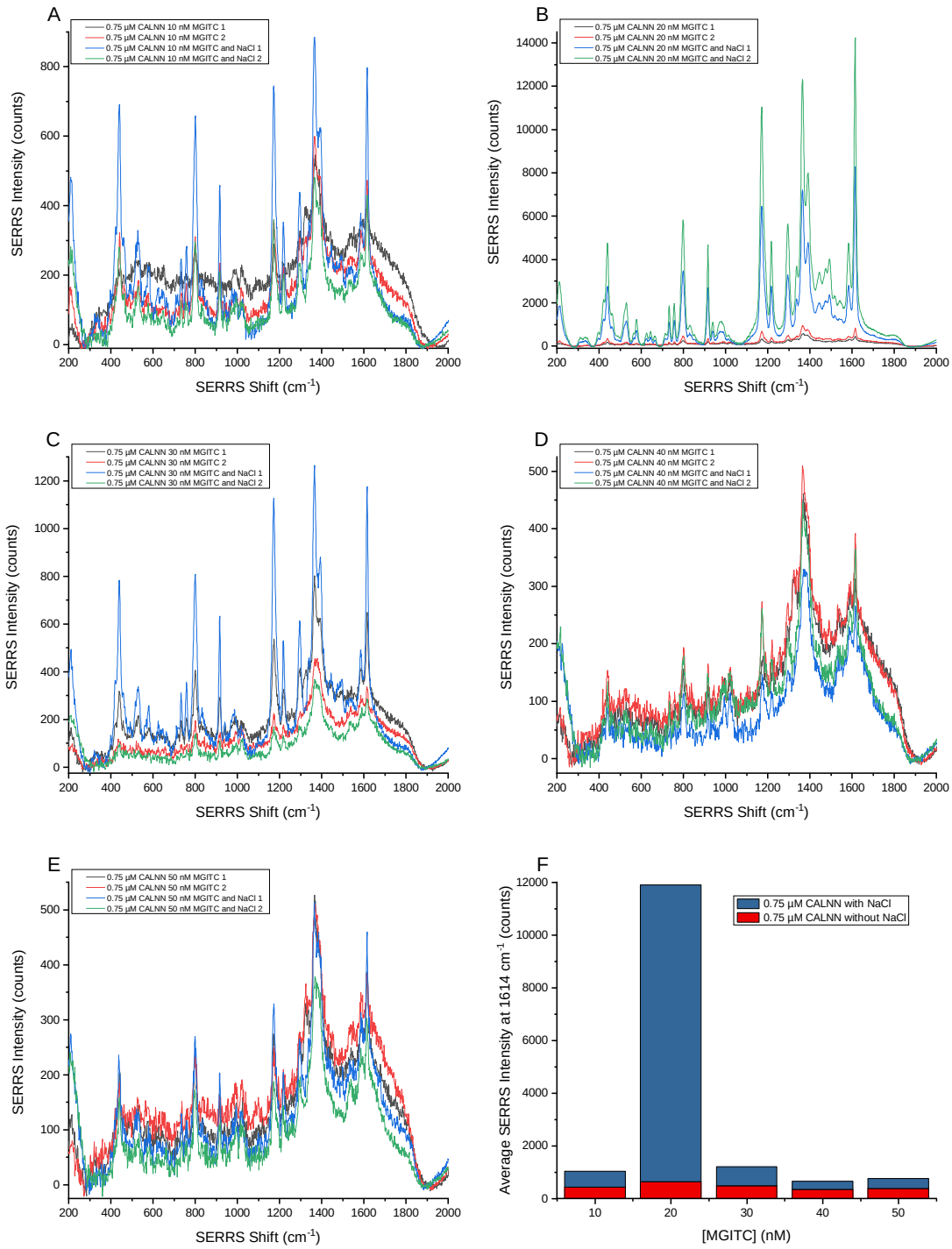


*Figure 3.8: SERRS spectra of gold nanoparticles coated with 0.75 µM CALNN and (A) 10 nM MGITC; (B) 20 nM MGITC; (C) 30 nM MGITC, (D) 40 nM MGITC; (E) 50 nM MGITC. (F) The average SERRS intensities from each set of experiments was plotted to show the changes following addition of NaCl. Two samples were analysed for each condition. Each spectrum shown is a single replicate, recorded with a 638 nm laser excitation, 40 mW laser power, and 1 s acquisition. All spectra were baseline corrected using Matlab. The black and red lines are from the conjugates in $dH_2O$. The blue and green lines are from samples after addition of 120 mM NaCl stock solution.*

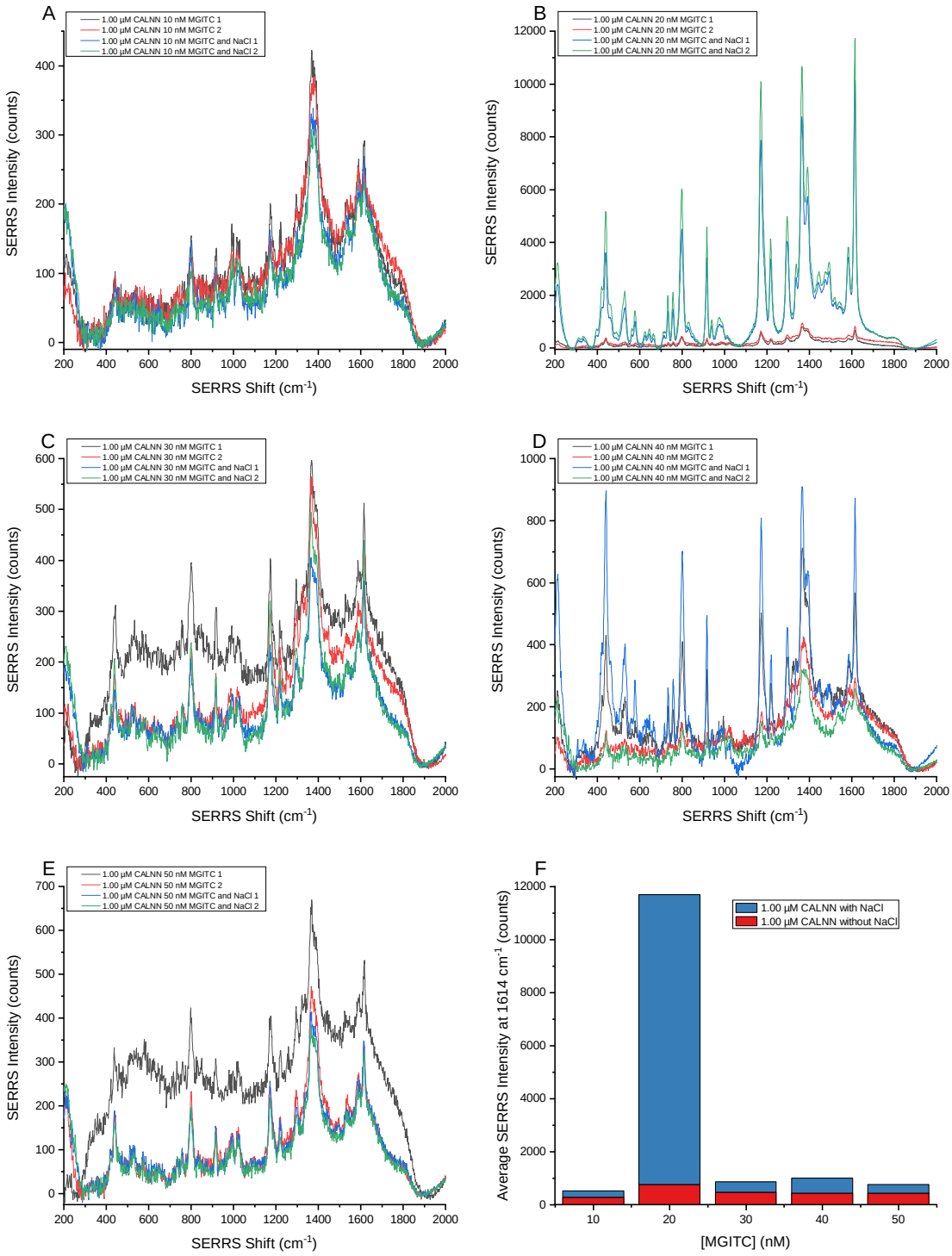


*Figure 3.9: SERRS spectra of gold nanoparticlescoated with 1.00 µM CALNN and (A) 10 nM MGITC; (B) 20 nM MGITC; (C) 30 nM MGITC, (D) 40 nM MGITC; (E) 50 nM MGITC. (F) The average SERRS intensities from each set of experiments was plotted to show the changes following addition of NaCl. Two samples were analysed for each condition. Each spectrum shown is a single replicate, recorded with a 638 nm laser excitation, 40 mW laser power, and 1 s acquisition. All spectra were baseline corrected using Matlab. The black and red lines are from the conjugates in $dH_2O$. The blue and green lines are from samples after addition of 120 mM NaCl stock solution.*

In both sets of experiments, no overall increase in the SERRS spectra were observed with the addition of salt, except in the samples with 20 nM MGITC. (Figure 3.8(B) and Figure 3.9(B)) In both of these samples, there was a low SERRS signal observed from the functionalised Au NPs alone, but with the addition of salt there was a large increase of the SERRS intensity. This simulated the expected response when a target analyte was present, and appeared to be the optimum concentration of MGITC for use in future assays. In comparing the two sets of data, the samples with 1.00 µM CALNN and 20 nM MGITC gave the most consistent SERRS intensities before and after salt addition, whereas when looking at other concentrations of MGITC there was no overall trend before or after addition of NaCl.

Due to the consistency of the signals achieved from the sample containing 1.00 µM CALNN and 20 nM MGITC, these conditions were used in further functionalisation with a lectin using carbodiimide crosslinking chemistry.

### *3.2.2.2 Lectin-functionalisation via Carbodiimide Crosslinking*

To conjugate sugar-binding proteins on to the nanoparticles, carbodiimide crosslinking chemistry was used. The CALNN ligand and the lectin were prepared for conjugation prior to the addition of the MGITC functionalised Au NPs, as this allowed for a simple final conjugation of the terminal CALNN thiol to the Au metal surface. The crosslinking reaction was performed using 1-ethyl-3-(3-dimethylaminopropyl) carbodiimide (EDC) and N-hydroxysulfosuccinimide (sNHS). (Figure 3.10)

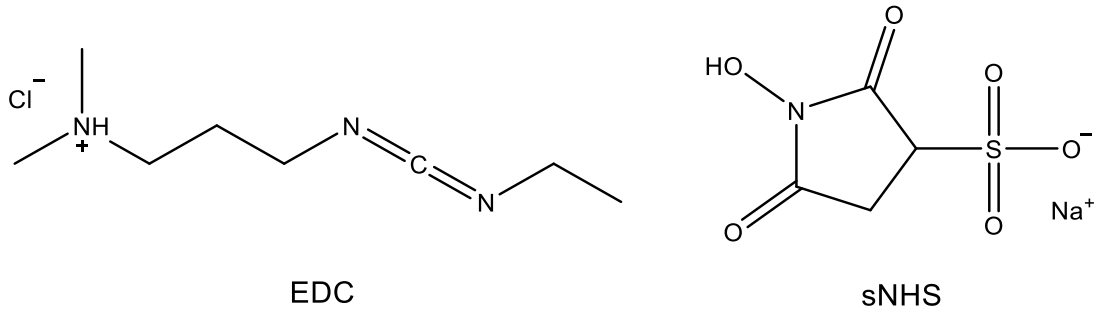


*Figure 3.10: Full structures of EDC and sNHS used in carbodiimide coupling reactions to conjugate lectins to gold nanoparticles.*

EDC is often used alone to react with a carboxylic acid group to form an O-acylisourea intermediate. This group is easily displaced by primary amines through nucleophilic attack, which can allow for proteins to bind to terminal carboxylic acids. However, the O-acylisourea group is not a stable intermediate, and readily hydrolyses in aqueous conditions to re-form the carboxylic acid if it does not first react with a primary amine, resulting in poor efficiency in the coupling reaction. Therefore, sNHS is often used to stabilise this intermediate and form a reactive sNHS ester.[110] This then allows for a much more efficient coupling process, so that complete ligands can be synthesised consisting of a thiol-terminated linker and a lectin which can subsequently be attached to SERRS-active MGITC coated Au NPs. (Figure 3.11) The use of sNHS rather than N-hydroxysuccinimide also aids solubility and stability since it is a sodium salt.

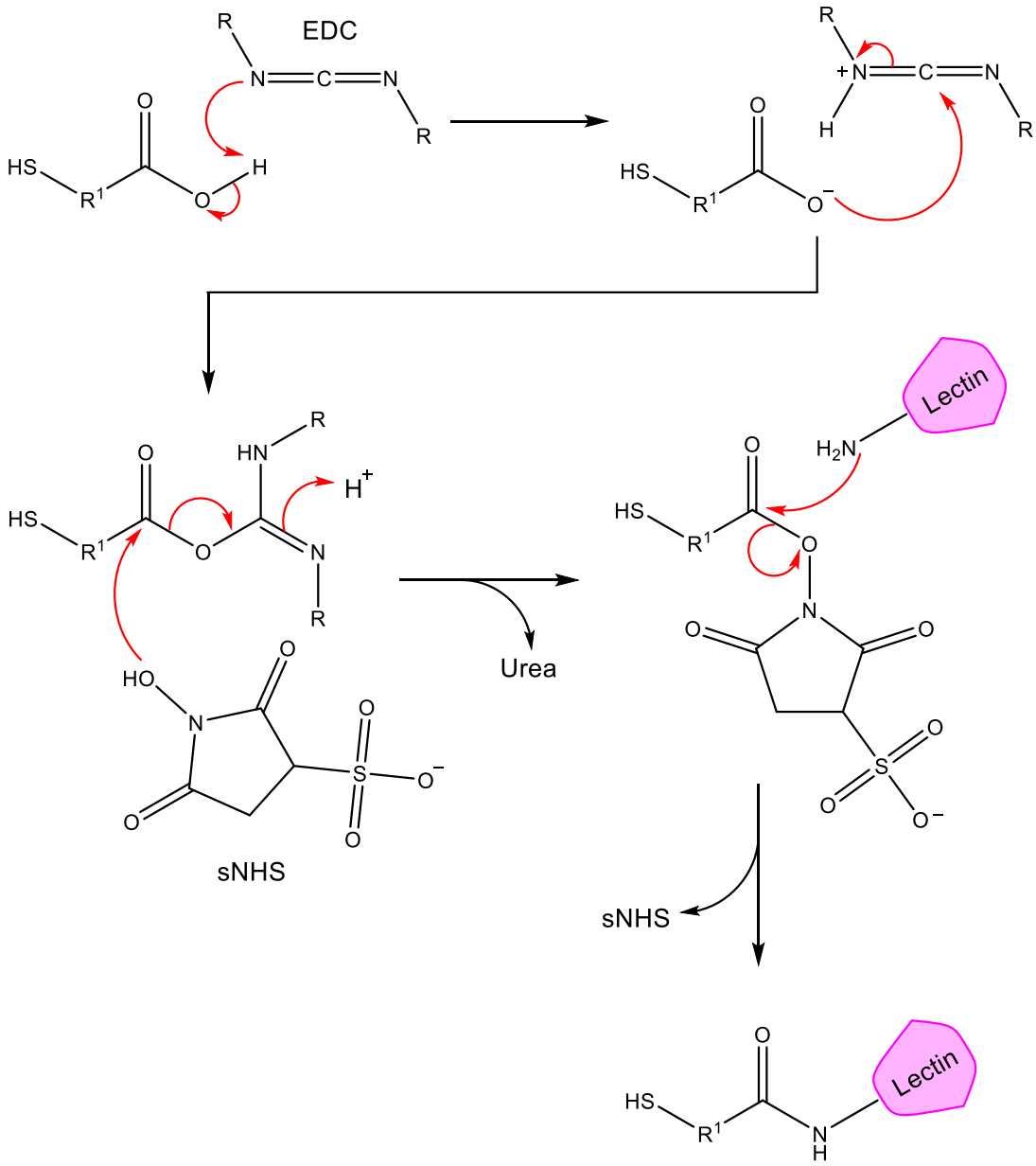


*Figure 3.11: Reaction scheme showing the use of EDC-sNHS coupling to bind a terminal carboxylic acid group of a thiolated linker (eg. CALNN) to a primary amine of a lectin.*

Initial studies used the Man-binding GNA as the lectin. Briefly CALNN was pre-mixed with EDC and GNA was mixed with sNHS. The solutions were combined and mixed overnight to complete coupling. EDC, sNHS, and GNA were kept in excess of CALNN to ensure all linkers were attached to GNA. Following preparation of the CALNN-GNA ligand, it was mixed with MGITC functionalised Au NPs for 3 h and then separated from any excess unbound ligand *via* centrifugation. MGITC was added first to allow for attachment to the NP surface before mixed-monolayer formation. The Au@GNA

NP conjugates were then characterised using extinction spectroscopy, DLS, gel electrophoresis, and SERRS measurements.

The LSPR peak of the Au@GNA NP conjugates was measured and compared to that of the unfunctionalised Au NPs. (Figure 3.12) The LSPR of the Au@GNA conjugates had the same characteristic peak shape as the unfunctionalised NPs, but the $\lambda_{max}$ had red-shifted 4 nm, from 526 nm to 530 nm. This shift was caused by a change in the dielectric medium surrounding the particle, such as when the surface is functionalised or coated.[59,61–63] Therefore, this shift indicated that the attachment of the pentapeptide ligand was successful.

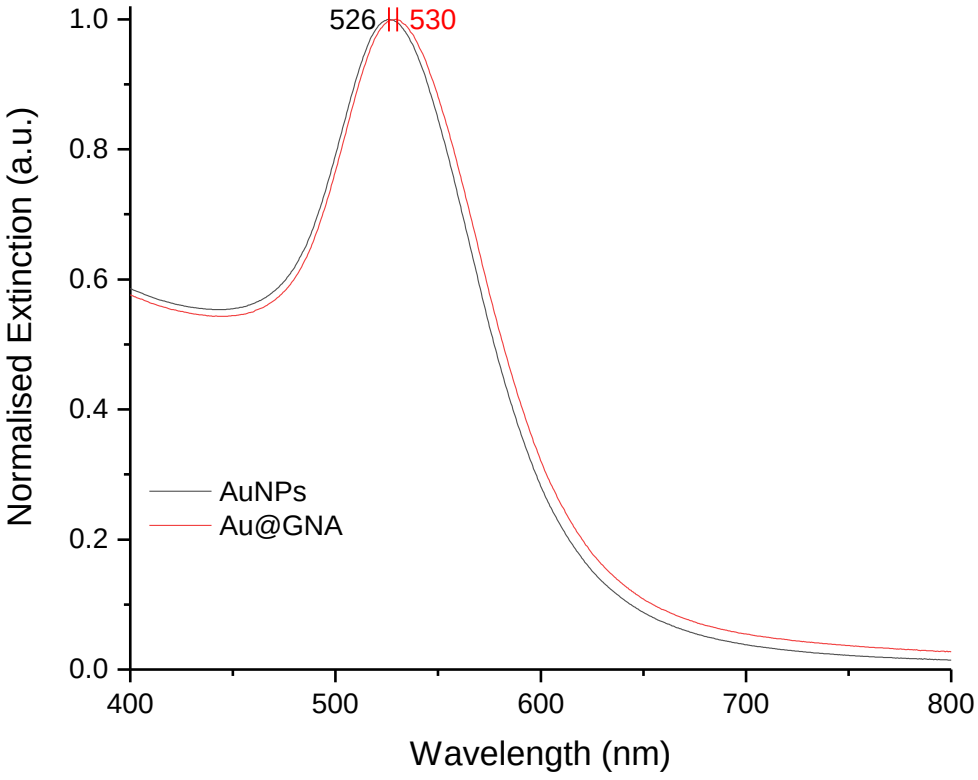


*Figure 3.12: Extinction spectra of the lectin-functionalised nanoparticles (Au@GNA) (black) in comparison to the unfunctionalised citrate-capped nanoparticles (red) showing the shift in the LSPR peak upon conjugation. Spectra were normalised to one for clarity and ease of comparison.*

To confirm this conjugation, DLS and zeta potential measurements were used, as well as gel electrophoresis. DLS confirmed an increase in the hydrodynamic radius of the particles due to the conjugation process, showing an increase from 41 ± 1 nm to 46 ± 1 nm. The zeta potential of the citrate-capped Au NPs was -40.6 ± 1.27 mV, which

lowered to -30.0 ± 2.65 mV when the NP was coated in MGITC and the CALNN-GNA ligand indicating that attachment was successful. Gel electrophoresis measurements were made with samples from each stage in the conjugation process. (Figure 3.13) The first sample was citrate-capped Au NPs which had not been subjected to any conjugation steps. The second had been functionalised with MGITC. The third had been functionalised with both MGITC and CALNN. Finally, the last sample had completed the entire conjugation process with GNA. These results showed that the unfunctionalised Au NPs aggregated within the well (dark purple colour) due to being unprotected from the tris-borate-EDTA (TBE) buffer and the applied charge. The MGITC functionalised NPs mostly aggregated, again due to incomplete surface coverage. For the CALNN coated NPs, however, no aggregation was observed and they travelled through the gel. The NPs which had been conjugated with the pre-prepared CALNN-GNA ligand were also stable and travelled through the well. However, the distance travelled by these NPs was less than those just coated by CALNN. This confirmed the successful conjugation of the lectin to the Au NPs, due to their increased size hindering their movement through the gel.

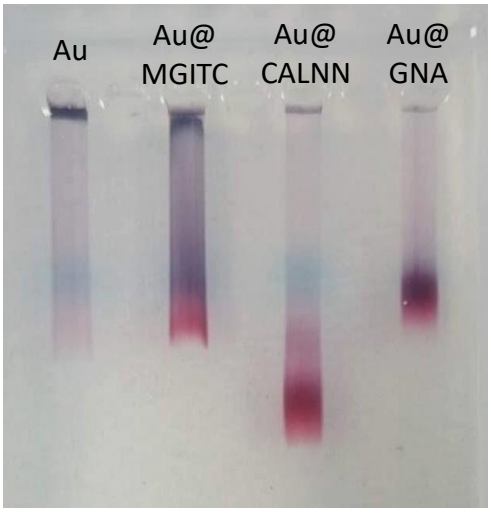


*Figure 3.13: Gel electrophoresis of samples from each stage in the conjugation process, highlighting the aggregation of the gold nanoparticles, and the malachite green isothiocyanate functionalised nanoparticles due to the lack of protection from the gel matrix. The CALNN and lectin coated particles remained stable and travelled through the gel, with the lectin-coated particles travelling a shorter distance due to an increased diameter, suggesting that the conjugation was successful.*

The final stage in the characterisation of the GNA-conjugated NPs was to measure the SERRS response. (Figure 3.14) In the conjugation process, the MGITC was added first to the Au NPs before the CALNN-GNA ligand. This was to ensure that the Raman reporter had direct access to the NP surface to anchor itself in place. It is possible that the addition of the CALNN linker can displace the MGITC due to its ability to form a more thermodynamically stable monolayer around the NP surface. Therefore, it is important to confirm that the MGITC is still present in each purified conjugated nanoparticle through SERRS measurements. The SERRS measurement taken from these conjugates showed that the characteristic MGITC peaks could still be obtained, and therefore could be used in assays to detect the presence of Man-containing glycoproteins.

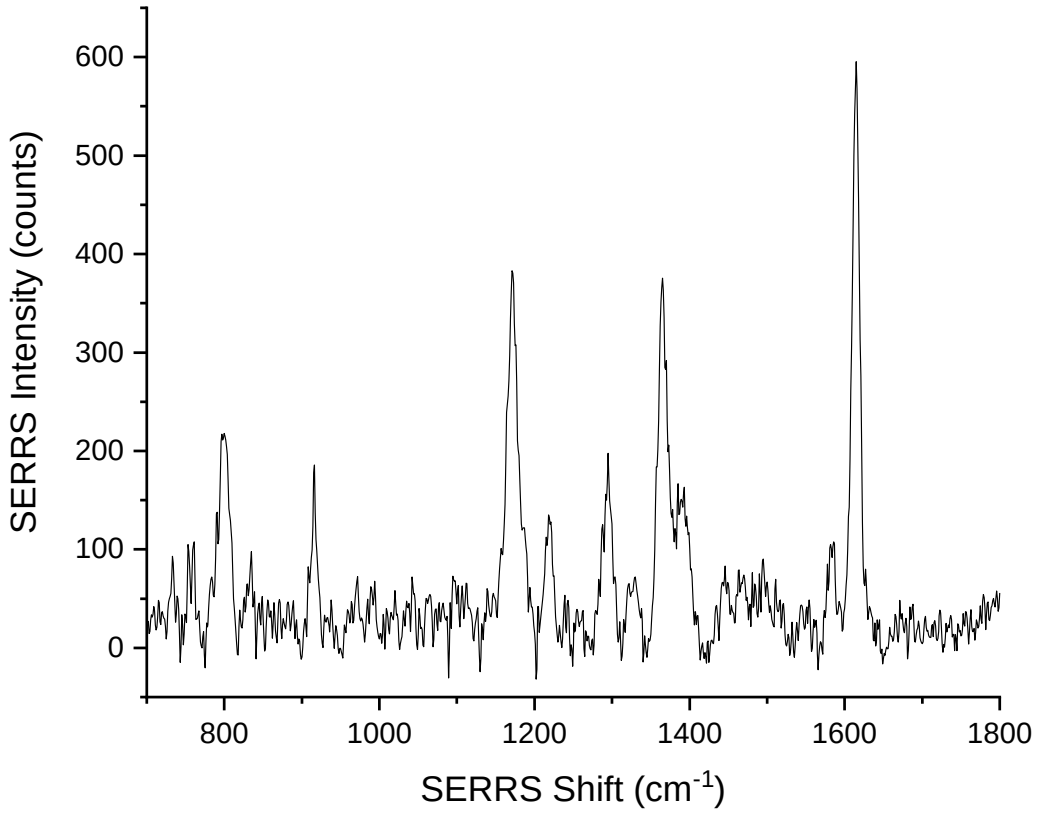


*Figure 3.14: SERRS spectrum obtained from the nanoparticles functionalised with malachite green isothiocyanate and galanthus nivalis agglutinin. The spectrum shown is a single replicate, recorded with a 638 nm laser excitation, 40 mW laser power, and 1 s acquisition. The spectrum was baseline corrected using Matlab.*

The obtained SERRS signals were lower in these measurements than previously, which could be due to the addition of GNA to the end of the CALNN linker displacing the attached MGITC molecules. Regardless, the SERRS measurement taken from these conjugates showed that the characteristic MGITC peaks could still be obtained, and therefore could be used in assays to detect the presence of Man-containing glycoproteins.

## 3.2.3 Glycosylation Detection in Solution

### *3.2.3.1 LSPR Detection experiments*

#### 3.2.3.1.1 Initial Glycoprotein Detection Experiments

Initial studies on glycan detection using lectin-functionalised Au NPs were carried out using RNase A and RNase B as glycoprotein standards. These two proteins are identical in structure, except that RNase B is a glycosylated form, containing one high-Man glycan.[111] RNase A was therefore used as a negative control in detection procedures.

Solutions of RNase B, ranging in concentration from 81 nM to 1.63 µM, were added to the Au@GNA NP conjugates HEPES buffer (10 mM, pH 7.4) and monitored with extinction spectroscopy immediately, and after 10 min. The RNase A was assessed as a negative control at 1.63 µM, also at the same time intervals. The extinction measurements were used in this way to track any changes in the medium surrounding the NP conjugates[59,62,63] *via* binding to the high-Man glycan of RNase B.

Firstly, the Au@GNA conjugates were analysed alone without the presence of RNase A or B, to show that no change to the colloid occurred during the analysis time frame. (Figure 3.15(A)) This also served to obtain an initial LSPR peak position, allowing for the observation of any shifts taking place upon successful detection. Next, increasing concentrations of RNase B were added in the same way and the extinction spectrum recorded. (Figure 3.15(B-F)) The extinction spectrum showed that addition of the glycoprotein RNase B induced a red-shift in the LSPR peak, indicating that the Au@GNA NPs were binding to the high-Man glycan. With increasing concentrations

of RNase B, a more pronounced shift was observed, showing that more of the Au@GNA NPs were involved in interactions with the oligosaccharide structures on the RNase B surface. The concentrations of RNase B added and the associated LSPR shifts are detailed in Table 3.1. For comparison, 1.63 μM RNase A was also added to the Au@GNA NP conjugates. Since there are no glycans present on RNase A, no shift in the LSPR peak was expected. However, as shown in Figure 3.15(G), there was an initial LSPR peak shift of 3 nm, which then after 10 min, reverted back to a 1 nm shift from the unbound NP measured LSPR peak. Although this is small in comparison to the shift observed when RNase B was present, this still indicated that some non-specific interactions were taking place between the Au@GNA and RNase A.

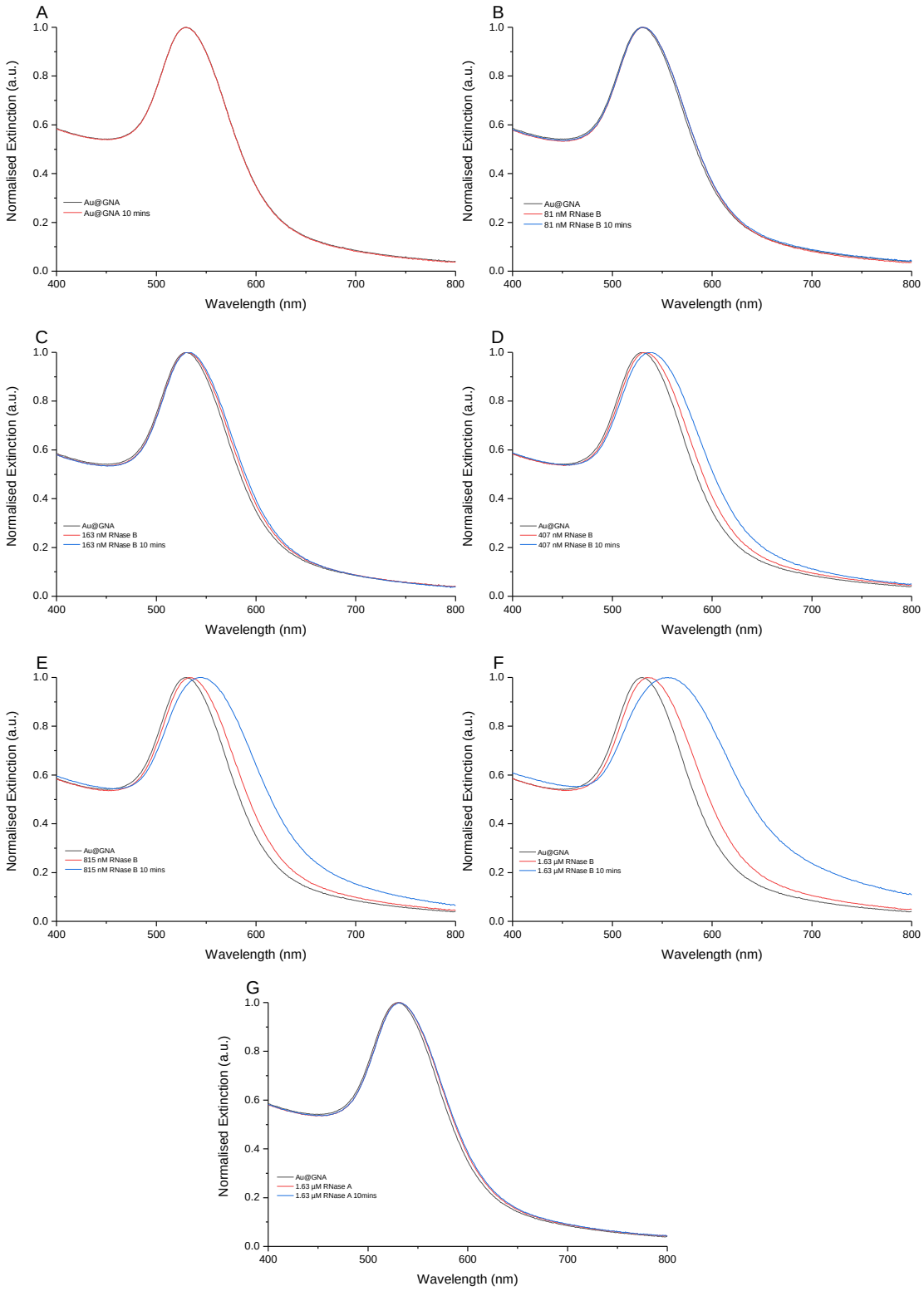


*Figure 3.15: Extinction spectra showing responses of Au@GNA to glycosylated and unglycosylated ribonuclease B and A, respectively. (A) Au@GNA initially and after 10 min without any ribonuclease present, showing no change in LSPR peak at 530 nm; Following addition of ribonuclease B and after 10 min at concentrations of (B) 81 nM; (C) 163 nM; (D) 407 nM; (E) 815 nM; (F) 1.63 µM; (G) Following*

*addition of 1.63 µM ribonuclease A and after 10 min. Spectra were normalised to one for clarity and ease of comparison.*

*Table 3.1: LSPR peak shifts of Au@GNA nanoparticle conjugates once bound to various concentrations of ribonuclease B and ribonuclease A after mixing for 10 min. $\Delta\lambda_{max}$ shows the deviation of the LSPR from its original position before addition of ribonuclease.*

| Sample | $\lambda_{max}$ 10 mins / nm | $\Delta\lambda_{max}$ / nm |
|---|---|---|
| Au@GNA | 530 | 0 |
| Au@GNA and 81 nM RNase B | 531 | 1 |
| Au@GNA and 163 nM RNase B | 533 | 3 |
| Au@GNA and 407 nM RNase B | 539 | 9 |
| Au@GNA and 815 nM RNase B | 543 | 13 |
| Au@GNA and 1.63 µM RNase B | 556 | 26 |
| Au@GNA and 1.63 µM RNase A | 531 | 1 |

These initial experimental results were encouraging. They demonstrated that the conjugates could potentially bind selectively to a specific glycan on a protein surface, and that concentration dependent responses could be obtained. However, the interaction observed with the negative control, RNase A, indicated there may have been some non-specific binding of the conjugates occurring.

#### 3.2.3.1.2 Timed Glycosylation Detection Experiments

In order to further evaluate the detection of RNase B, and to investigate the interactions with RNase A, timed experiments were used following a similar procedure. The same concentrations of RNase A and RNase B were used, with extinction spectra taken immediately following mixing with Au@GNA, and then every 12 min for 1 h. (Figure 3.16)

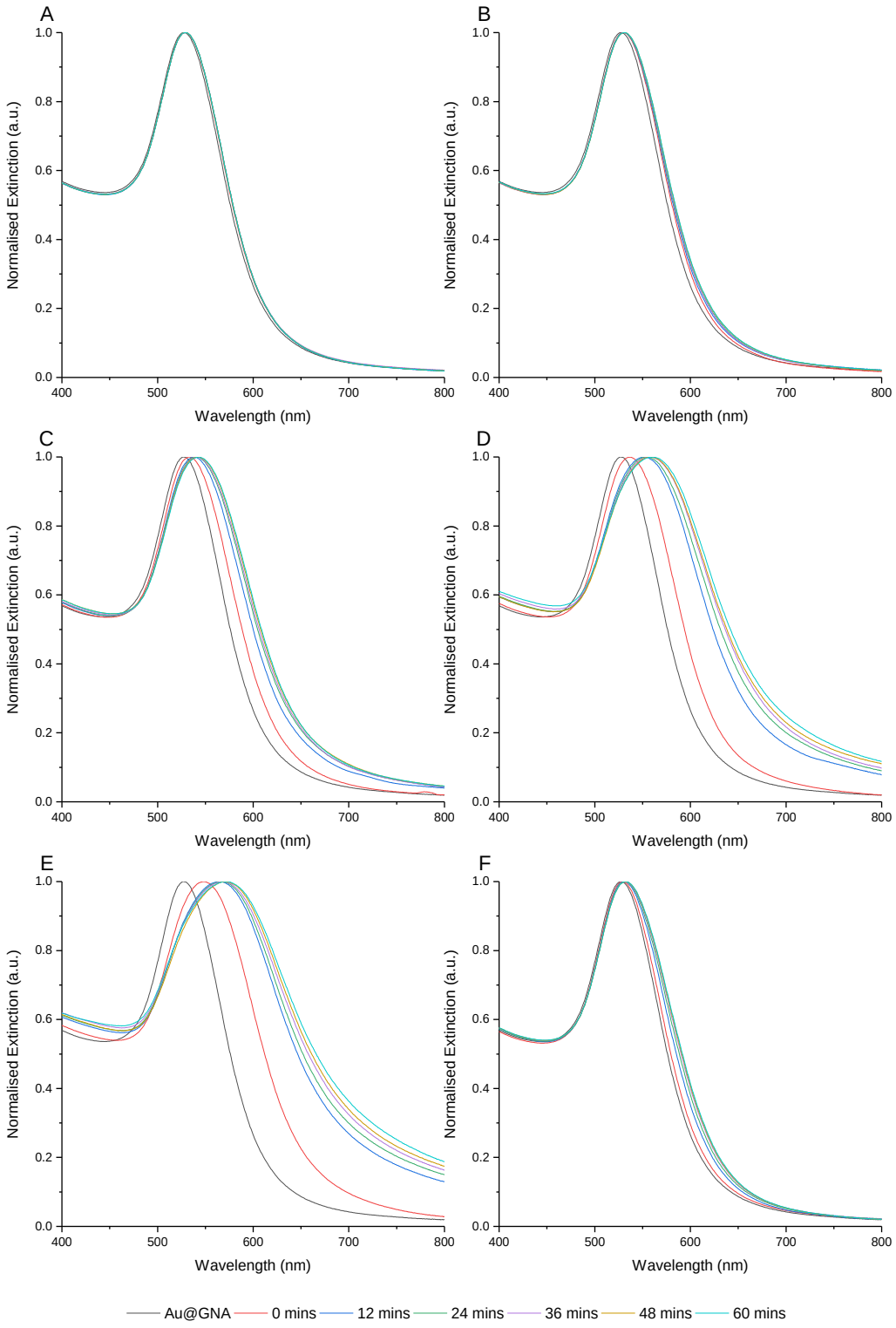


*Figure 3.16: Extinction spectra taken from samples of Au@GNA and various concentrations of ribonuclease A and B. Spectra were taken immediately following mixing, and every 12 min for 1 h. (A) 81 nM ribonuclease B; (B) 163 nM ribonuclease B; (C) 407 nM ribonuclease B; (D) 815 nM ribonuclease B; (E) 1.63 µM ribonuclease B; (F) 1.63 µM ribonuclease A. Spectra were normalised to one for clarity and ease of comparison.*

Using extinction spectroscopy to monitor the LSPR peak is convenient in that it gives a visual change to the spectra upon detection. It is clear to see that with increasing concentration of glycoprotein present, there is a greater red-shift of the peak, as was expected from the previous experiment. In addition, especially with increasing concentrations of RNase B, the spectral broadening was an indicator of NP heterogeneity in terms of size and shape.[112] This fits with the theory that the Au@GNA conjugates were binding to the RNase B glycans, effectively altering the overall size and shape of the NP, which would continue to increase as more glycoprotein was bound. (Figure 3.17)

The timed experiments also showed that the greatest shifts were observed soon after mixing of the Au@GNA conjugates and the glycoprotein. After 12 min the shift of the LSPR peak was less obvious and would increase more slowly. (Figure 3.17) This would indicate that most of the conjugates were binding to RNase B quickly, invoking the large initial LSPR shift, and binding would slow as the RNase B glycans were taken.

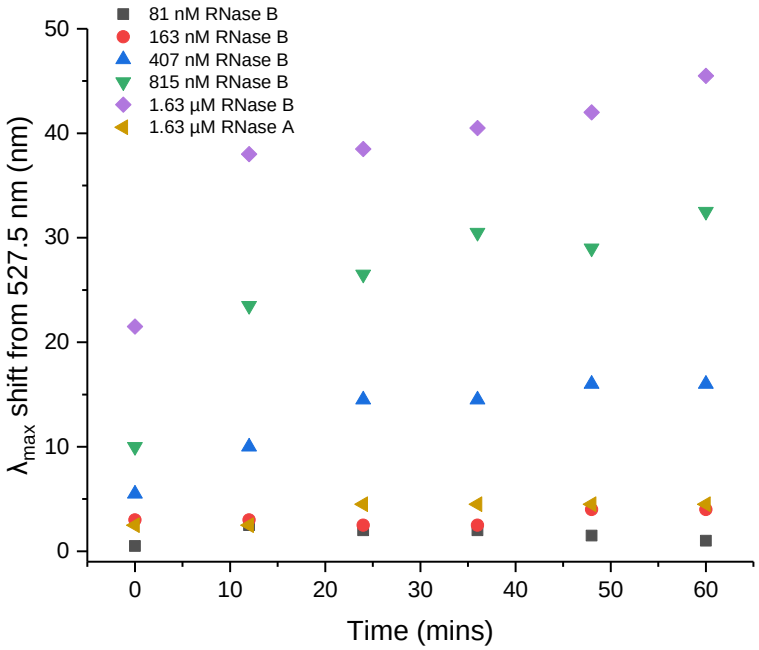


*Figure 3.17: Shift in the Au@GNA conjugates' LSPR peak from the original $\lambda_{max}$ of 527.5 nm over a period of 60 min at each concentration of glycoprotein.*

Important to note, however, is the shifts observed in the sample containing RNase A. This should not have induced any change in the extinction spectrum of Au@GNA

since it should not have any glycans on its surface.[111] The shift observed, in fact, surpassed that of samples containing 81 nM and 163 nM RNase B. This suggested that either the Au@GNA conjugates were binding non-specifically, or that the RNase A contained glycosylated impurities. Therefore, an alternative negative control was investigated.

Bovine serum albumin (BSA) is a protein often used in biochemical assays as a blocking agent due to its relative inactivity and small size.[113] In immunochemical and biosensing reactions, BSA can be used to adsorb on to surfaces *via* physicochemical interactions and minimise non-specific binding of biomolecules to these unoccupied sites. BSA's inactivity, along with the fact that it is not a glycoprotein, made it an ideal candidate for a negative control in place of RNase A.[114]

Au@GNA was mixed with BSA in the same way as RNase A and the extinction spectrum was measured after 1 h. (Figure 3.18) The results showed that there was no significant shift in the extinction spectrum of Au@GNA mixed with BSA (Figure 3.17(B)), compared with the 4.5 nm shift observed when RNase A was added (Figure 3.17(A)). From this comparison it was concluded that the RNase A may have contained some glycosylated impurities. As such, BSA was used in future experiments as a negative control.

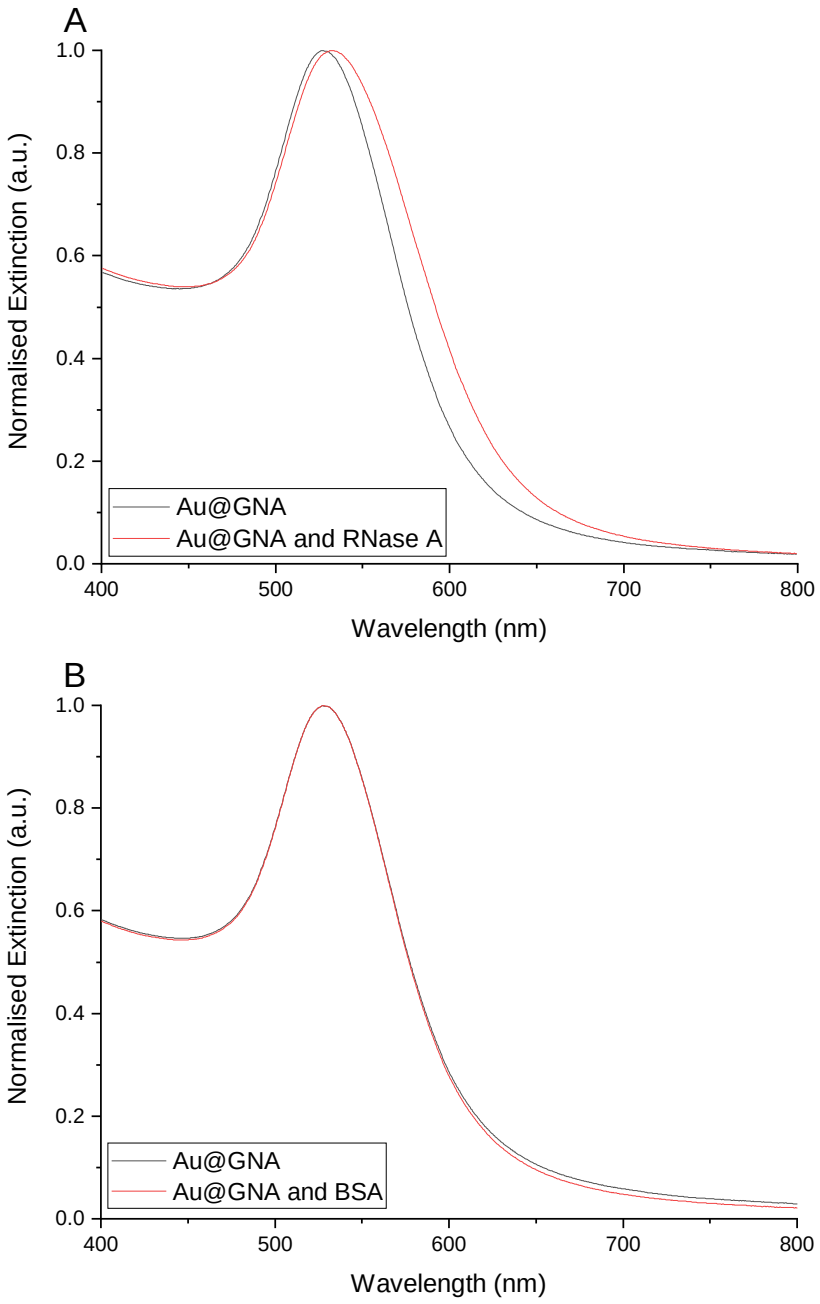


*Figure 3.18: Comparison of (A) ribonuclease A and (B) bovine serum albumin as negative controls in glycosylation detection experiments at a concentration of 1.63 µM.*

Using BSA as a negative control, the LSPR peaks of the Au@GNA conjugates were then monitored again in the presence of RNase B at concentrations ranging from 40 nM to 815 nM. The relationship between the shift in $\lambda_{max}$ of Au@GNA conjugates and the RNase B concentration after 12 min were then plotted and a theoretical limit of detection (LOD) for the assay calculated. (Figure 3.19)

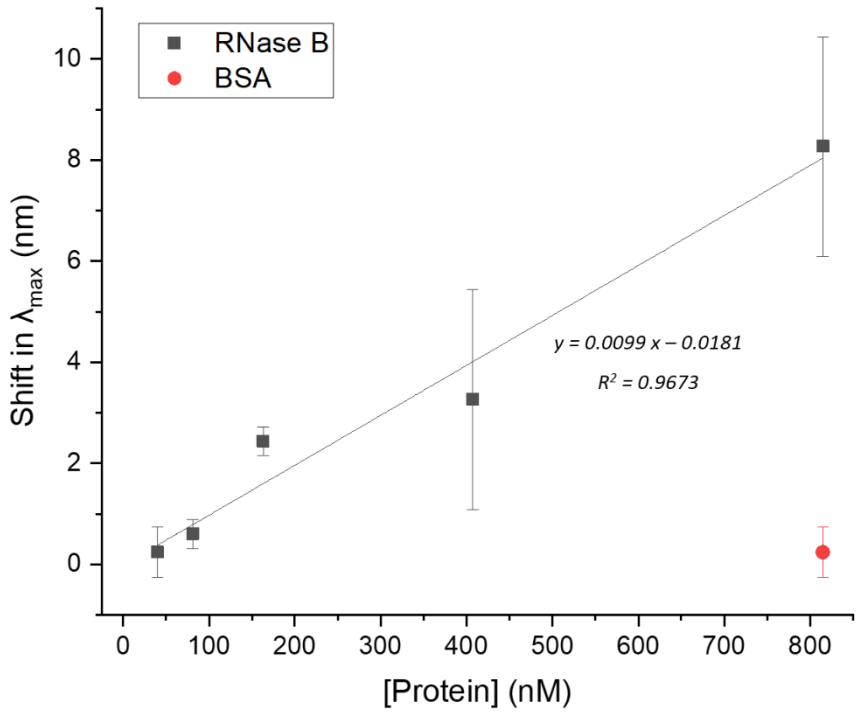


*Figure 3.19: Linear response from monitoring LSPR peak shifts of Au@GNA conjugates when mixed with ribonuclease B for 12 min, when compared to the original LSPR peak at 527.5 nm. A negative control, BSA, was also used and its corresponding shift in $\lambda_{max}$ is shown on the plot. The equation of the line is also shown. Error bars are the standard deviation of the measurements taken.*

Figure 3.18 showed good linearity within the assay and a theoretical LOD of 29.2 nM for RNase B was calculated by taking 3 × standard deviation of the blank sample divided by the gradient of the line. This equates to 29.2 pmol in a sample. Commercial glycoprotein detection assays can detect glycoproteins in gel experiments at 1.67 pmol per sample. This assay isn't far from this limit but has the benefit of potentially being applicable to specific glycan components rather than a glycoprotein as a whole.

There are, however, limitations to this method of detection. Firstly, the instrumentation has a minimum possible wavelength step size of 0.1 nm. Although this could generate large quantities of data, it sacrifices speed of analysis, which could mean that the crucial LSPR peak position could be prone to error if the timings of experiments are not exact. In these experiments, a 0.5 nm step size was used in order to provide sufficient information with reasonable speed. However, this means that calculating a limit of detection perhaps is not particularly accurate, since the standard deviation of the blank sample is limited by the capabilities of the instrument.

Also worthy of note is the high standard deviation of the higher concentration samples. The detection of LSPR shifts are not sensitive, again due to instrumental limitations, so any variations can be seen as large deviations. Therefore, in order to improve the LOD of these experiments, a better linear relationship between the shift in $\lambda_{max}$ and the glycoprotein concentration would be required.

A final point to note, in comparing Figure 3.17 with Figure 3.19, there is a clear difference in the LSPR shifts observed when the experiment was repeated. This could be a lack of reproducibility in the experiment when new conjugates are prepared. There could be batch to batch variability when conjugates are prepared, resulting in different sensitivities of the assays, which would be an issue when used as a glycan detection method.

#### *3.2.3.2 SERRS Glycosylation Detection in Solution*

The glycan detection experiments *via* extinction spectroscopy indicated that there was a change to the surface of the NP occurring through shifts in the LSPR peak, and a subsequent change in the heterogeneity of the size and shape of the NPs. Following this work, SERRS was then applied to determine if these changes were a result of NP clusters being formed. If so, the plasmonic coupling of proximal Au NPs would provide an increase in the scattering efficiency of the NPs, and in turn an increase in the SERRS intensity from the MGITC bound to the Au surface would be observed.[60,77]

The Au@GNA conjugates were mixed with RNase A and B for 1 h and then interrogated with a 638 nm excitation laser to evaluate the SERRS response. (Figure 3.20) Although the key characteristic peaks of MGITC were observed, the SERRS signal intensity did not follow a linear relationship with respect to the glycoprotein concentration. If controlled aggregation were being induced from the addition of RNase B, a marked increase in the SERRS intensity would be observed.[60,77] Therefore, from these SERRS measurements, it was deduced that no significant aggregation was taking place.

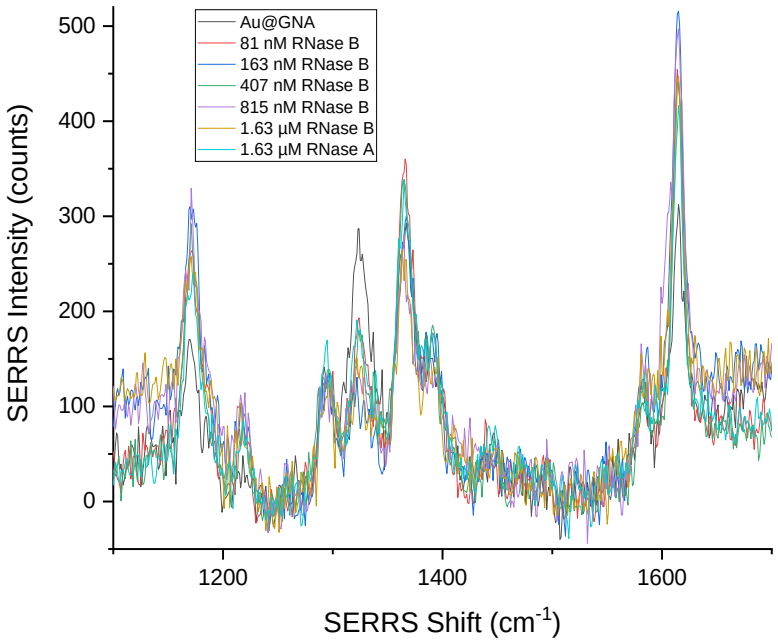


*Figure 3.20: SERS response from Au@GNA following addition, and 1 h of mixing, of different concentrations of RNaseB and RNase A. Single spectra for each glycoprotein concentration added were collected using a 638 nm laser excitation, 40 mW laser power, 1 s acquisition. The spectra were baseline corrected using Matlab.*

RNase B has a single high-Man glycan,[82,111] to which GNA binds in solution. However, the lone glycan makes binding of multiple NPs to terminal Man residues difficult. The proximity of the terminal carbohydrate moieties creates too much steric hinderance to allow multiple NPs to come in to close proximity through binding to different Man residues, and in turn induce an increased SERRS response. This highlighted a significant flaw in the SERRS solution assay design. If a glycoprotein contained only a single glycan, then a solution assay would not be suitable for SERRS measurements, so alternatives must be investigated. One such design could be to use a surface, on which the SERRS-active functionalised NPs could be selectively immobilised to allow for plasmonic coupling, resulting in concentration-dependent SERRS responses.

### 3.2.4 Lectin Variation for Further Solution Studies

In order to increase the diversity of the assay, different lectins were investigated to determine if it would be possible to detect different carbohydrate moieties on

glycoproteins. For these studies, wheat germ agglutinin (WGA) from *triticum vulgaris* was used in the detection of GlcNAc, which is the other carbohydrate component forming the constant inner core of an N-glycan. Con A was also investigated as an alternative lectin in the detection of Man groups.

Often the N-glycan core sequence can be fucosylated, which can have significant effects on the action of a biopharmaceutical in the body. As an example, it is important to monitor the level of fucosylation in a therapeutic antibody which is designed to induce antibody dependent, cell-mediated cytotoxicity, since this carbohydrate moiety can greatly influence the action of the therapeutic.[115] The lack of Fuc can increase a therapeutic antibody's cytotoxic capabilities, which could be particularly useful in cancer treatments.[115–117] Therefore, this glycan component is of interest, so agglutinin from *Ulex Europaeus I* (UEA) was used in efforts to detect this carbohydrate.

Another carbohydrate of interest is SA. This carbohydrate is known for influencing the *in vivo* activity of erythropoietin if the presence of this moiety is lacking.[16] Therefore, bioprocessing is optimised to produce highly sialylated erythropoietin to maximise its efficacy in the body.[117] It is also known that a lack of SA can reduce the half-life of a therapeutic protein, thus reducing its efficiency.[118] Since SA can have different conformations in a glycan structure, two lectins were investigated in the detection of this carbohydrate: *Maackia amurensis II* (MAL) and *sambucus nigra* (SNA). MAL binds to SA with an α2-6 linkage with Gal, whereas SNA binds to SA with an α2-3 linkage with Gal.[87]

#### *3.2.4.1 N-Acetyl Glucosamine Detection*

##### 3.2.4.1.1 Functionalisation with Wheat Germ Agglutinin

The functionalisation of Au NPs with WGA was not as simple as previous experiments involving GNA. When CALNN was used in the conjugation process as before the NPs would aggregate. It is unclear what caused this, but to circumvent this problem, $CT(PEG)_{12}$ (from here referred to as PEG) was used. (Figure 3.3) This was chosen due

to it containing a thiol group for conjugation to the Au NP surface, a flexible polar backbone to aid NP coverage and provide solubility, and a terminal carboxylic acid group for further modification. The same procedure was used as with CALNN for the preparation of the PEG-lectin ligand involving EDC-sNHS coupling. The WGA was used at two concentrations, 4 µM and 8 µM. The Au@WGA conjugates were purified by centrifugation and the extinction spectra were measured. (Figure 3.21)

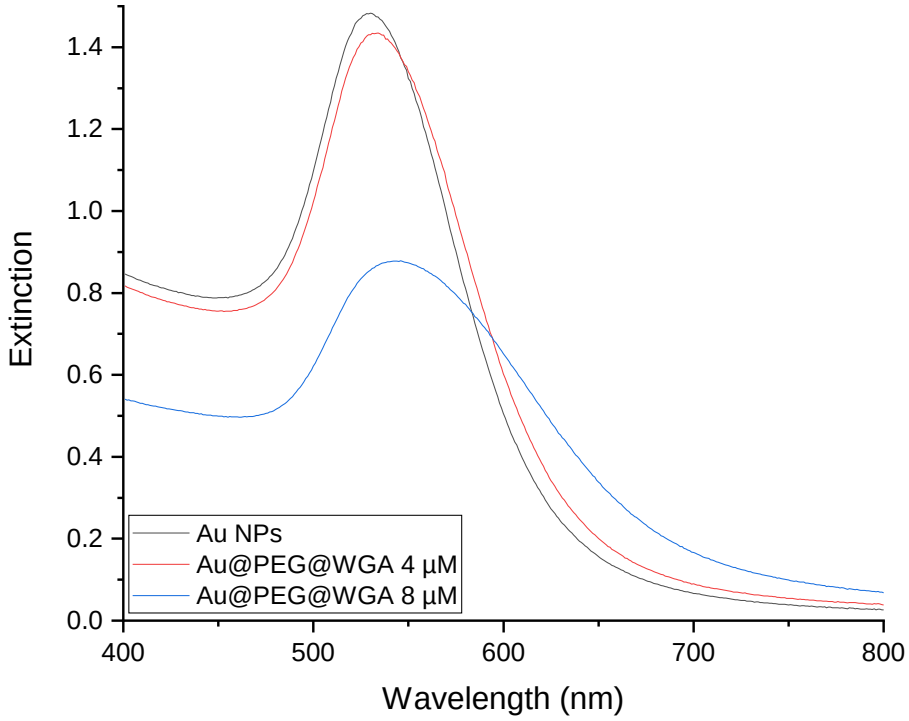


*Figure 3.21: Extinction spectra of the gold nanoparticles functionalised with a PEG-WGA linker with 4 µM WGA (red line) and at 8 µM WGA (blue line) in comparison to the unfunctionalised stock solution. (black line)*

The experiment involving 8 µM WGA caused the NPs to become unstable, as viewed by the dampening and broadening of the LSPR peak. The 4 µM WGA sample remained monodispersed in size, and there was an LSPR red-shift of 4 nm indicating a change to the surface composition. Due to the instability of the conjugation using 8 µM WGA, the lower concentration of 4 µM was used to detect the GlcNAc in the high-Man N-glycan of RNase B.

#### 3.2.4.1.2 LSPR Detection of N-Acetyl Glucosamine

As mentioned previously, all N-linked glycans have the same core structure containing two GlcNAc residues convalently linked to three Man residues. Therefore, the Au@WGA conjugates were used to detect these core GlcNAc structures. The same procedure was used as with the detection of Man on RNase B by Au@GNA NPs with extinction spectra taken every 12 min following mixing of the glycoprotein and the NP conjugates. (Figure 3.22)

The shifts in $\lambda_{max}$ were again plotted over time to easily view to the changes in the LSPR peak as the Au@WGA conjugates were incubated with RNase B. (Figure 3.22(F)) Similar to the reaction of Au@GNA with RNase B, the greatest LSPR shift took place within the first 12 min of incubation, after which the LSPR changes were minimal. Again, this shows that the majority of the interactions between he WGA and the core GlcNAc residues took place immediately following mixing, after which binding was slow due to the lower concentration of free RNase B. It is worthy to note, however, the fluctuation in the LSPR peak position in the sample containing Au@WGA and 815 nM RNase B after 24 min. (Figure 3.22(F)) This could be due to the reaction still equilibrating over time, where some previously bound RNase B dissociated from the Au@WGA conjugates before being taken up again shortly after.

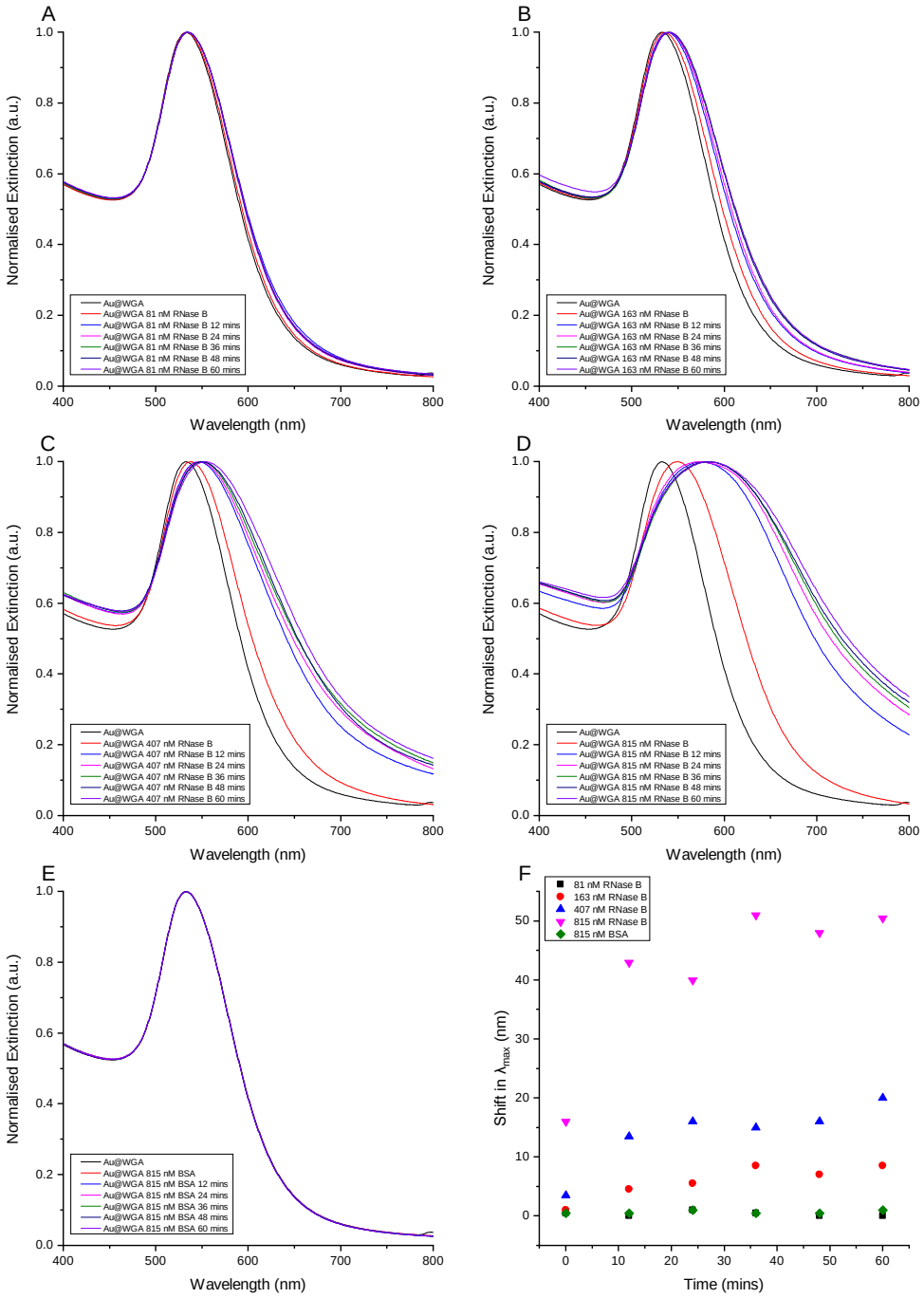


*Figure 3.22: Extinction spectra taken from samples of Au@WGA and various concentrations of ribonuclease B, and BSA as a negative control. Spectra were taken immediately following mixing, and every 12 min for 1 h. (A) 81 nM ribonuclease B; (B) 163 nM ribonuclease B; (C) 407 nM ribonuclease B; (D) 815 nM ribonuclease B; (E) 815 nM BSA; (F) Shifts in $\lambda_{max}$ observed over the experimental time frame. Spectra were normalised to one for clarity and ease of comparison.*

The shift in the LSPR peak position was plotted as a function of protein concentration using the values obtained from the reaction after 12 min of mixing. (Figure 3.23) This seemed to follow a similar linear trend as was observed with the Au@GNA conjugates detecting the Man groups on RNase B. (Figure 3.19) There was also no shift observed in the sample containing Au@WGA and BSA. Therefore, it could be deduced that the interactions between the Au@WGA and RNase B was due to the specific detection of the core GlcNAc groups of the surface N-glycan.

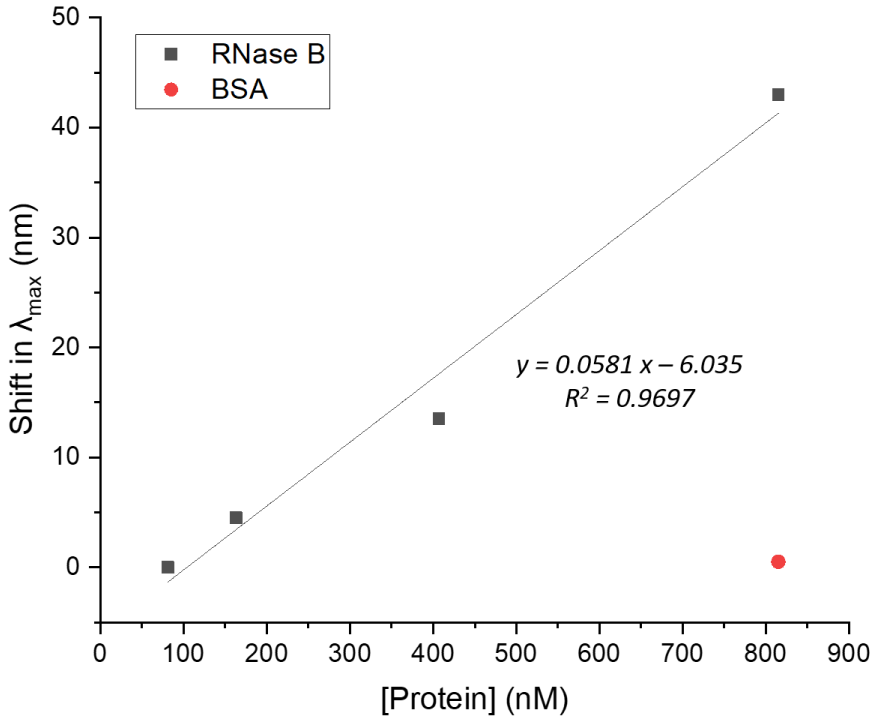


*Figure 3.23: Comparison of the shifts in $\lambda_{max}$ from the Au@WGA LSPR at 530 nm when mixed with RNase B for 12 min, indicating successful detection of N-acetyl glucosamine. A linear relationship is proposed with the equation of the line shown. BSA was used as a negative control, showing a lack in LSPR shift.*

The LSPR shifts observed when Au@WGA was mixed with RNase B showed that specific glycan detection was taking place. This showed that the use of lectins-functionalised NPs could be used to detect not only terminal glycan components, but could also be used to specifically bind to inner core saccharides. Detection of such glycan residues shows that conjugated NP systems have the potential for glycan profiling in biopharmaceutical protein manufacturing processes.

### *3.2.4.2 Mannose Detection*

#### 3.2.4.2.1 Functionalisation with *Concanavalin A*

Although GNA had already been used in the detection of the high-Man glycan on RNase B, Con A was also investigated. Con A is very well characterised[19] and is often using in lectin assays.[29,70,119] In lectin microarrays, Con A has been shown to exhibit much greater sensitivity in Man detection over GNA.[87,120] Therefore Au NPs were functionalised with Con A and used in the detection of Man on RNase B.

Like WGA, functionalisation was attempted using CALNN and PEG. The functionalisation process was carried out in the same manner as GNA where the ligand was synthesised with the lectin in excess (8 µM for PEG, 6 µM for CALNN) of linker, EDC, and sNHS, and also at a concentration equal to that of sNHS. (4 µM for PEG, 3 µM for CALNN) However, this resulted in NP aggregation. (Figure 3.24) The samples changed from red to blue/purple. Extinction measurements showed the dampening and broadening of the LSPR peaks, confirming the instability of the NPs.

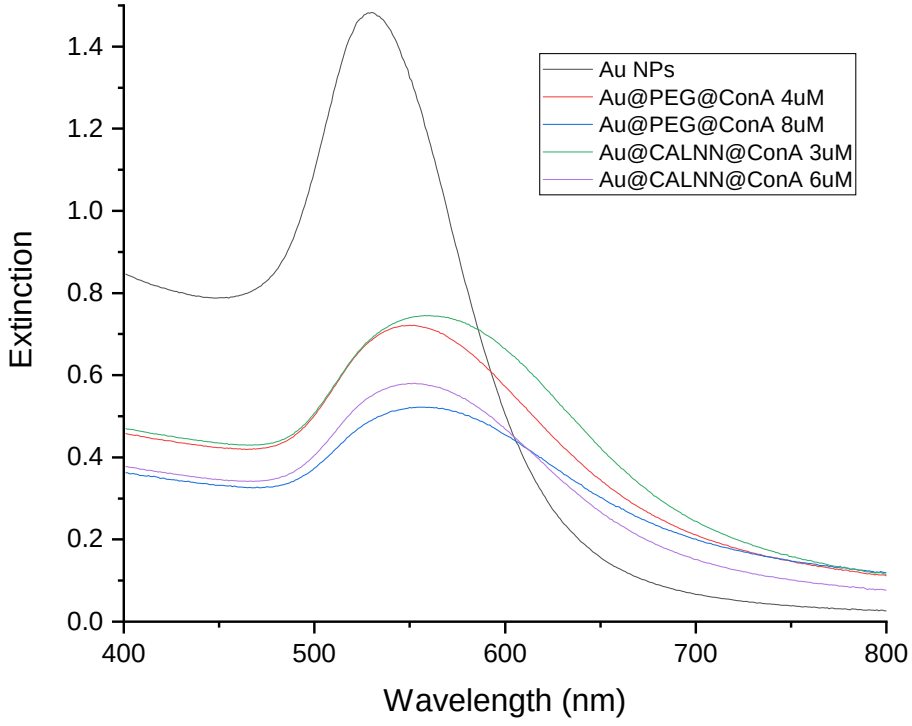


*Figure 3.24: Attempted gold nanoparticle functionalisation with Con A using PEG and CALNN as linkers.*

Following the success of the WGA conjugation, PEG was used as the linker instead of CALNN, but the functionalisation procedure was altered to contain lower concentrations of Con A. Although the concentration of Con A was now lower than that of the sNHS and in some cases lower than the PEG concentration, it was assumed that in the presence of water the sNHS ester would hydrolyse to re-form the carboxylic acid terminus of the PEG linker. When attached to the particle, this would provide protection of the NP surface from the surrounding medium, whilst tethering Con A with less steric hinderance.

The samples appeared much more stable following the conjugation procedure, retaining their red colour. Extinction spectroscopy was used to confirm the NP stability and successful tethering of the Con A to the NP surface. (Figure 3.25) This showed that samples containing 1 µM, 2 µM, and 3 µM Con A began to lose their stability, shown by the decrease in LSPR intensity, and the broadening of the peak. Therefore, these samples were discarded.

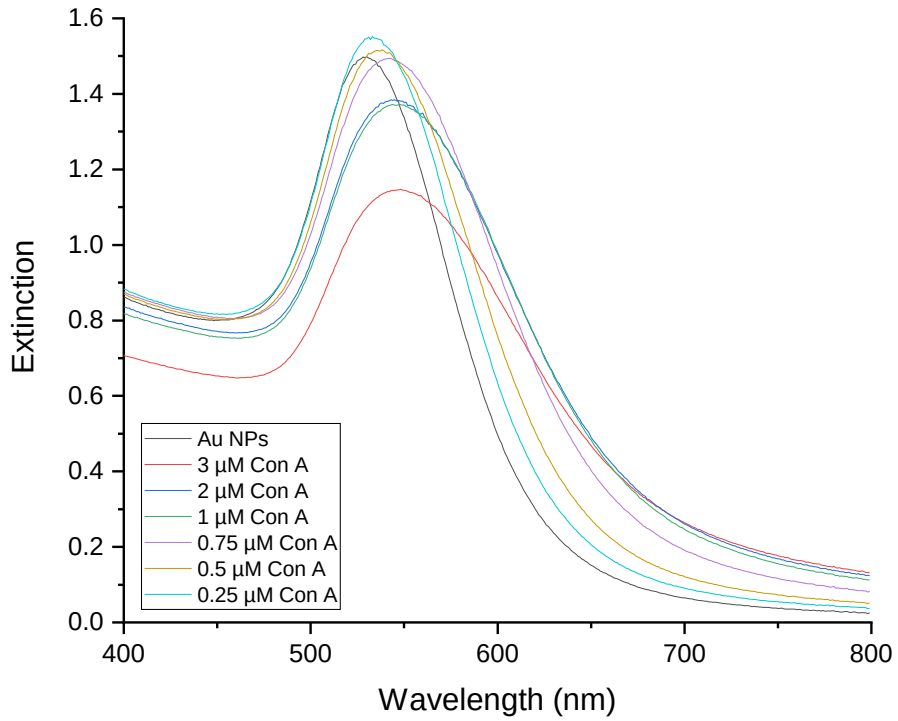


*Figure 3.25: Extinction measurements of gold nanoparticles functionalised with PEG-Con A linkers at lower concentrations.*

Samples containing 0.25 µM, 0.5 µM, and 0.75 µM Con A, however, exhibited intense LSPR peaks with minimal broadening. The LSPR peak position also red-shifted due to a change in the NP surface composition, indicating that binding was successful. All of these samples were then used in the detection of the high-Man glycan on RNase B.

#### 3.2.4.2.2 LSPR Detection of Mannose

The Au@Con A NPs were then used in the LSPR assay for glycan detection using the same procedure are before. The conjugates were mixed with varying concentrations of RNase B and the extinction was measured every 12 min over a period of 1 h. (Figure 3.26)

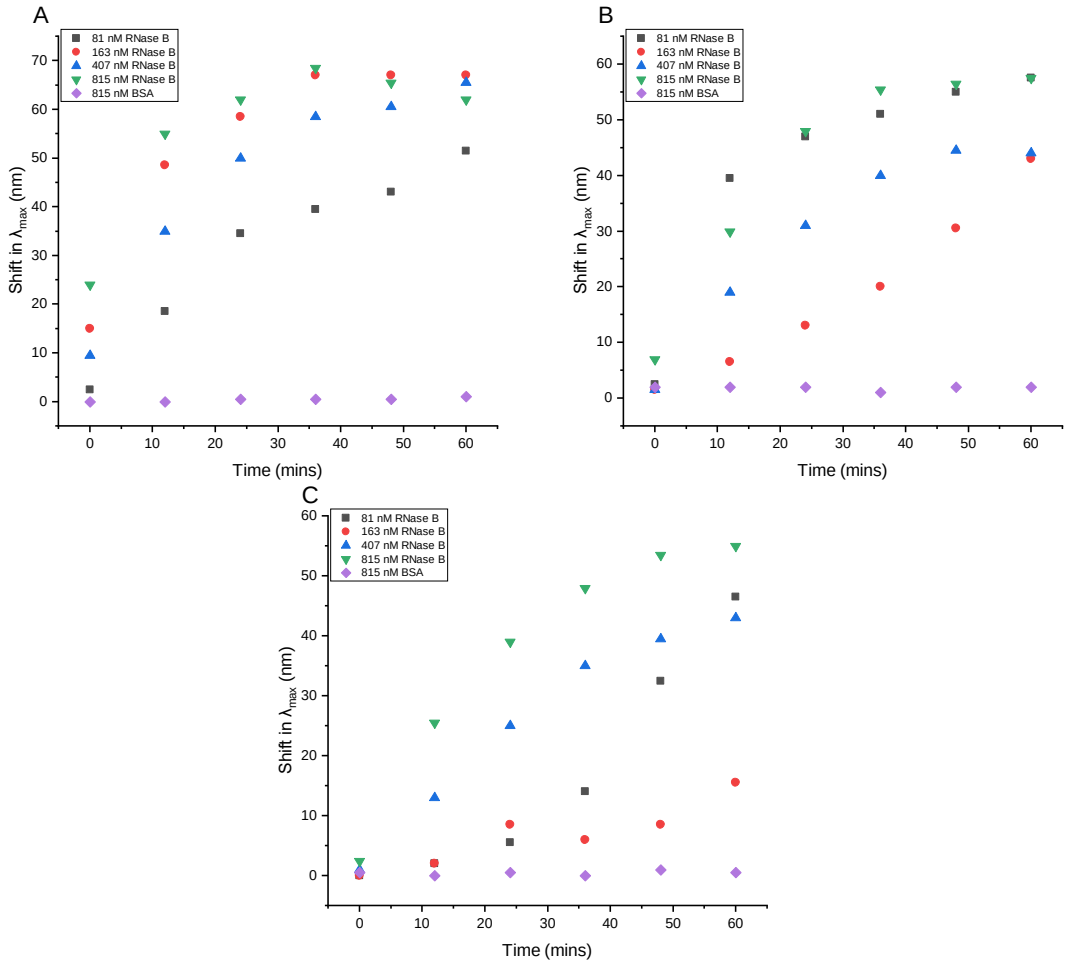


*Figure 3.26: Shift in the LSPR peak positions for each of the Au@Con A conjugates at varying concentrations of RNase B. BSA was used as a negative control. (A) 0.25 µM Con A; (B) 0.50 µM Con A; (C) 0.75 µM Con A.*

Firstly, these results showed that a positive result was obtained. The Au@Con A NPs were each able to selectively detect the high-Man glycan on RNase B as shown by the significant LSPR peak shifts upon mixing with the glycoprotein. In contrast, no significant changes were observed when BSA was used as the negative control. This once again shows that the lectin binding is specific to the presence of Man in the RNase B glycan.

There were, however, discrepancies in the samples containing 81 nM and 163 nM RNase B. These did not follow the same trend as the other samples in terms of degree of LSPR shift compared to glycoprotein concentration. Often the shifts associated with these samples were much greater than expected, indicating that the binding of the Au@Con A conjugates was taking place much more rapidly than the samples containing higher RNase B concentrations. Whilst the specific reason for this is unknown, it could be down to the lower concentrations of Con A on the NP surface being less hindered in its binding to the glycan. Therefore at lower glycoprotein concentrations there is less competition for binding, resulting in faster uptake by the lectin. At higher glycoprotein concentration, there could be increased competition for binding to the lectin, resulting in more hindered binding. The shift in LSPR peak would then appear at a slower rate. However, the lack of a trend in the LSPR peak shifts at these concentrations makes defining a cause difficult.

Overall, the binding of NPs conjugated to Con A through a PEG linker were shown to be specific for the Man residues in the RNase B glycan, as shown by the significant shifts in the positive controls, and the maintained LSPR peak position in the negative controls. The lectin concentrations used here was much lower than the concentrations used with GNA, yet the LSPR shifts were much more pronounced with Con A. this could be a result of the greater spacing between the lectin units on the NP surface, but could equally be a result of the more favourable binding of Con A to Man over GNA as shown in previous published material.[87,120] The successful binding of Con A to Man on RNase B gave further diversity to the build-up of a viable and simple solution assay for glycan detection. Again, due to the single RNase B glycan, SERRS detection in solution was not possible.

#### *3.2.4.3 Fucose and Sialic Acid Detection*

##### 3.2.4.3.1 Functionalisation with *Ulex Europaeus I, Maackia Amurensis II,* and *Sambucus Nigra* Lectins

High-Man glycans are the most common of the N-glycans found in glycoproteins. However, complex and hybrid glycans exist which contain particularly important carbohydrates contributing to biopharmaceutical protein function. Therefore, it was important to diversify the Au NP conjugates further to allow for full glycan characterisation. In addition, the presence of other forms of glycosylation such as the more complex O-glycans, would require a broader repertoire of functional NPs for a fully working assay.

As mentioned previously, Fuc and SA were of particular interest, so two glycoproteins were chosen which contained these chosen carbohydrates. The first is α-acid glycoprotein (α-AG) which contains five surface glycans in three possible conformations: bi-, tri-, and tetra-antennary.[121] (Figure 3.27 (Top)) This was chosen due to its terminal SA residues, and was used with MAL and SNA. The second is horseradish peroxidase (HRP) which contains eight or nine identical hybrid glycans.[81] (Figure 3.27 (Bottom)) This short glycan contains a Fuc moiety attached to a core GlcNA. It had already been shown that Au@WGA could detect core GlcNAc residues, so this glycoprotein was used to assess the specific detection capabilities of UEA conjugated NPs.

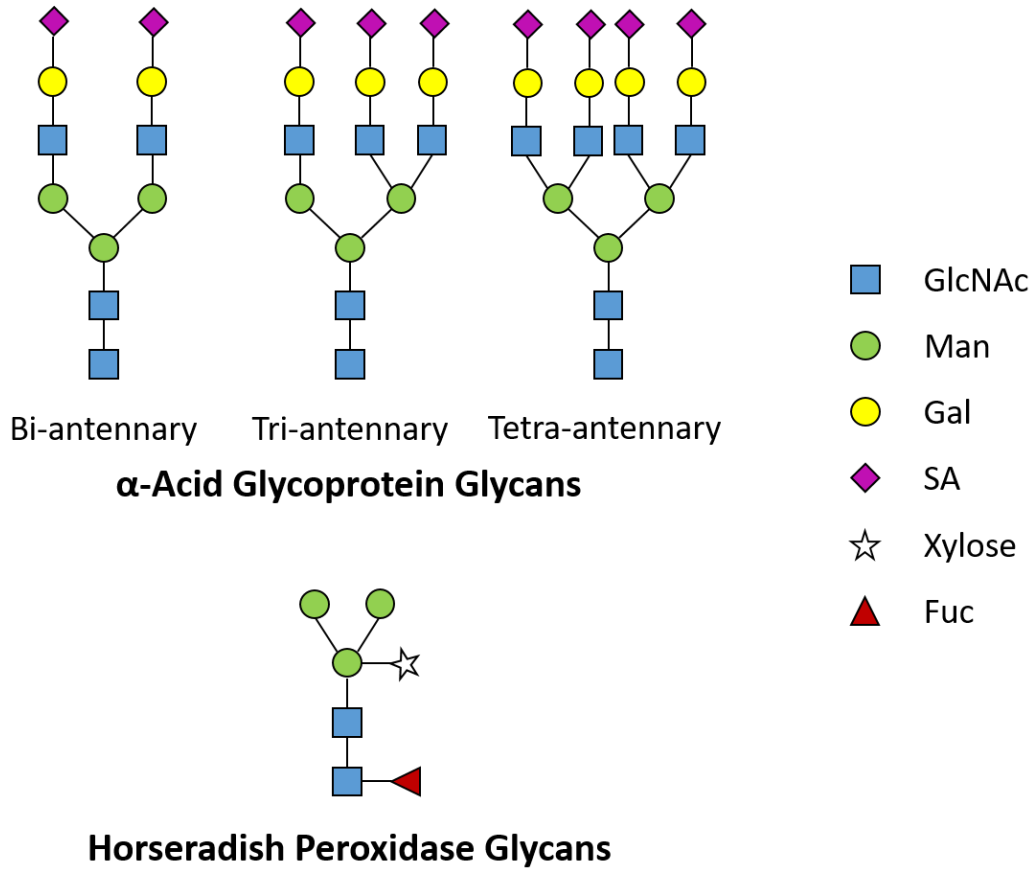


*Figure 3.27: Glycan structures present on the two glycoproteins chosen for this study. (Top) The bi-, tri- and tetra-antennary sialic acid-containing glycans of α-acid glycoprotein; (Bottom) The fucose-containing glycan present on the surface of horseradish peroxidase.*

MAL and SNA are large proteins, with molecular masses of 130 and 140 kDa, respectively. These are comparable to the size of Con A which has a mass of 104 kDa. Con A made the NPs unstable at concentrations above 1 µM, as shown previously. Therefore, these two SA-binding lectins were attached to Au NPs at low concentrations: 0.50, 0.75, and 1.00 µM.

The Fuc-binding lectin, UEA, has a molecular mass of 63 kDa. Since this was much smaller than the SA-binding lectins it was treated like WGA (36 kDa) and was attached to the NPs at concentrations of 1, 2, 3, and 4 µM. Following the conjugation procedure, the extinction spectra of the NP solutions were measured to assess any shifts in the LSPR peak position (Figure 3.28) which are detailed in Table 3.2.

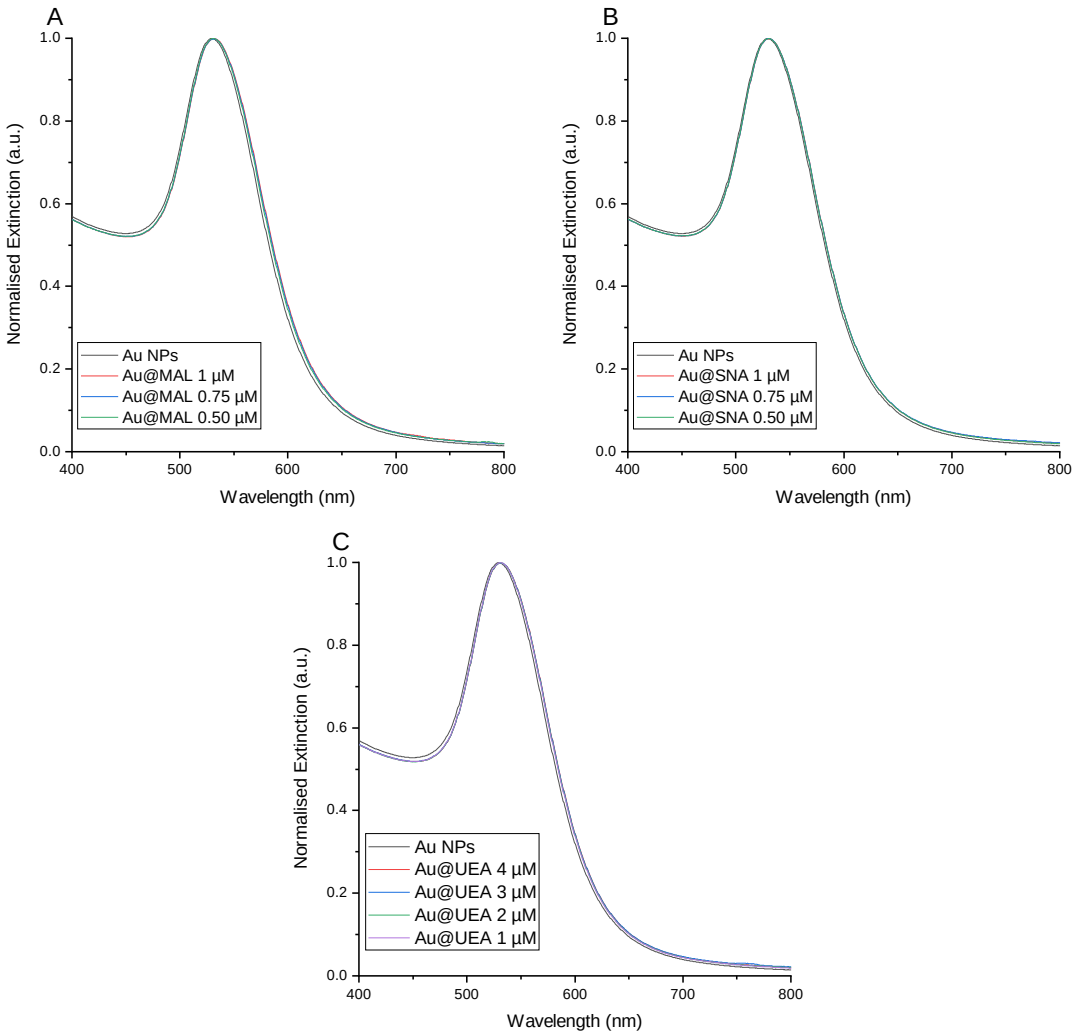


*Figure 3.28: Extinciton spectra of Au NPs following conjugation to sialic acid and fucose-binding lectins: (A) MAL; (B) SNA; (C) UEA.*

*Table 3.2: Shifts in the LSPR peak position following lectin conjugation from the original LSPR position of the citrate-capped gold nanoparticles at 529.5 nm.*

| [MAL] / µM | $\Delta\lambda_{max}$ / nm | [SNA] / µM | $\Delta\lambda_{max}$ / nm | [UEA] / µM | $\Delta\lambda_{max}$ / nm |
|---|---|---|---|---|---|
| 0.50 | 2.0 | 0.50 | 1.0 | 1.00 | 1.0 |
| 0.75 | 2.0 | 0.75 | 1.5 | 2.00 | 1.5 |
| 1.00 | 1.0 | 1.00 | 1.0 | 3.00 | 1.5 |
| | | | | 4.00 | 1.0 |

In comparison to previous Au NP conjugation procedures, the shifts observed with these lectins were small. This could be due to the use of low lectin concentrations, so the shifts are mainly observed from the attachment of CALNN molecules. To confirm that the lectins had been attached to the NPs, gel electrophoresis was used. (Figure 3.29) This was used on the principle that NPs which were not sufficiently coated would aggregate, and that the more layers attached to the NPs, the slower they would travel through the gel matrix due to the increase in size.

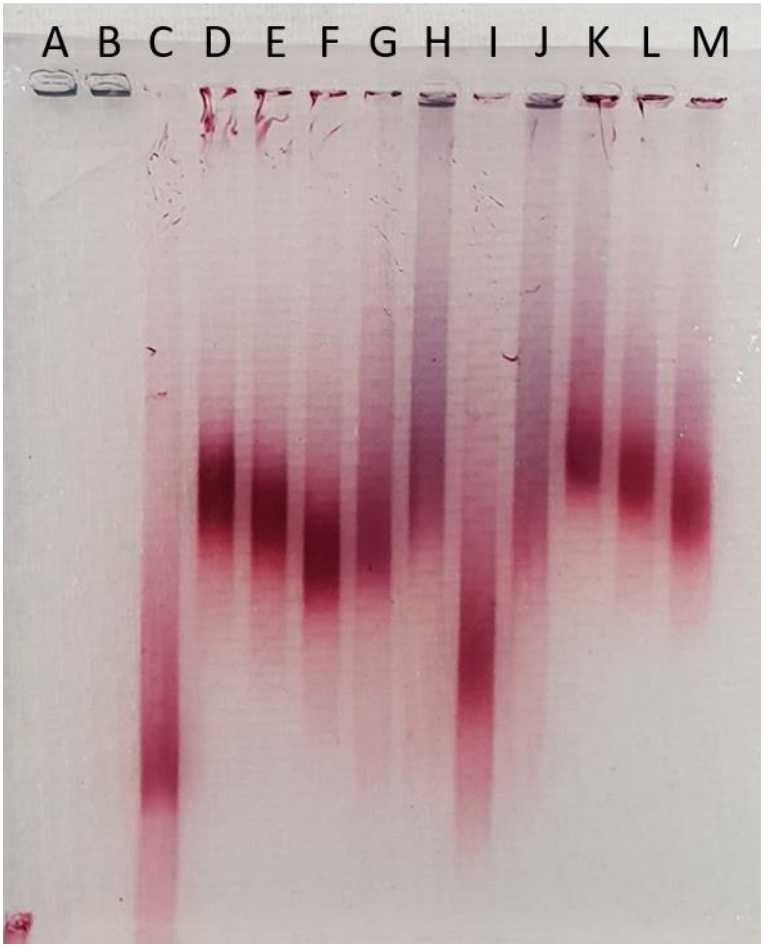


*Figure 3.29: Gel electrophoresis of lectin-functionalised gold nanoparticles: (A) Citrate-capped gold nanoparticles; (B) Au@MGITC; (C) Au@CALNN; (D) Au@MAL, 1 µM; (E) Au@MAL, 0.75 µM; (F) Au@MAL, 0.50 µM; (G) Au@UEA, 4 µM; (H) Au@ UEA, 3 µM; (I) Au@UEA, 2 µM; (J) Au@UEA, 1 µM; (K) Au@SNA, 1 µM; (L) Au@SNA, 0.75 µM; (M) Au@SNA, 0.5 µM.*

The gel showed that the unfunctionalised Au NPs and those functionalised with MGITC aggregated in the well due to not having sufficient protection from the buffer salt. (Figure 3.29 (A + B)) The CALNN-coated NPs were shown to be fully coated and

travelled through the gel matrix. (Figure 3.29(C)) Once the lectins were attached the distance travelled was significantly reduced, indicating successful conjugation. (Figure 3.29(D-M)) Looking at the samples containing MAL (Figure 3.29(D – F)) the distance travelled by the conjugates slightly increases with decreasing lectin concentration. This shows that increasing the lectin concentrations produces slight increases in overall size of the conjugate, so it travels through the gel at a slower rate. A similar trend was observed with the SNA conjugates. (Figure 3.29(K – M)) Lower SNA concentrations resulted in faster movement through the gel. The greater mass of the lectin also resulted in a slightly slower rate of movement in comparison to the MAL conjugates. The results for the UEA conjugates were less consistent. (Figure 3.29(G – J)) The samples containing 3 µM (H) and 1 µM (J) showed signs of instability, presented as the purple aggregates in the wells, as well as the continuous purple streak down the gel. The 2 µM sample (I) seemed stable, but travelled far down the gel, but less than that of the CALNN-coated NPs. This would suggest successful conjugation. The 4 µM UEA sample (G) also seemed stable and travelled a much shorter difference due to its greater size.

The extinction spectroscopy measurements indicated that all samples had excellent stability in solution, and the gel electrophoresis results confirmed successful attachment of the lectins. The gel results also indicated that two of the UEA conjugates were not stable in the presence of the buffer salts so full coverage may not have been achieved. Using these results, the SNA and MAL conjugates were selected at 1.0 µM lectin concentration, and the UEA conjugates were selected with 4 µM lectin. These were then carried forward for glycan detection by LSPR measurements.

#### 3.2.4.3.2 LSPR Detection of Fucose

Au@UEA conjugates with 4 µM lectin were selected for Fuc detection within the HRP glycans. Fuc often appears in the core residues of an N-glycan, as is the case in HRP. Following the success of the detection of GlcNAc with WGA it was expected that the Au@UEA conjugates would be able to selectively bind to the core Fuc component.

The same procedure was followed as in previous experiments, whereby the Au@UEA conjugates were mixed with various concentrations of HRP and the extinction was measured over the course of 1 h. (Figure 3.30)

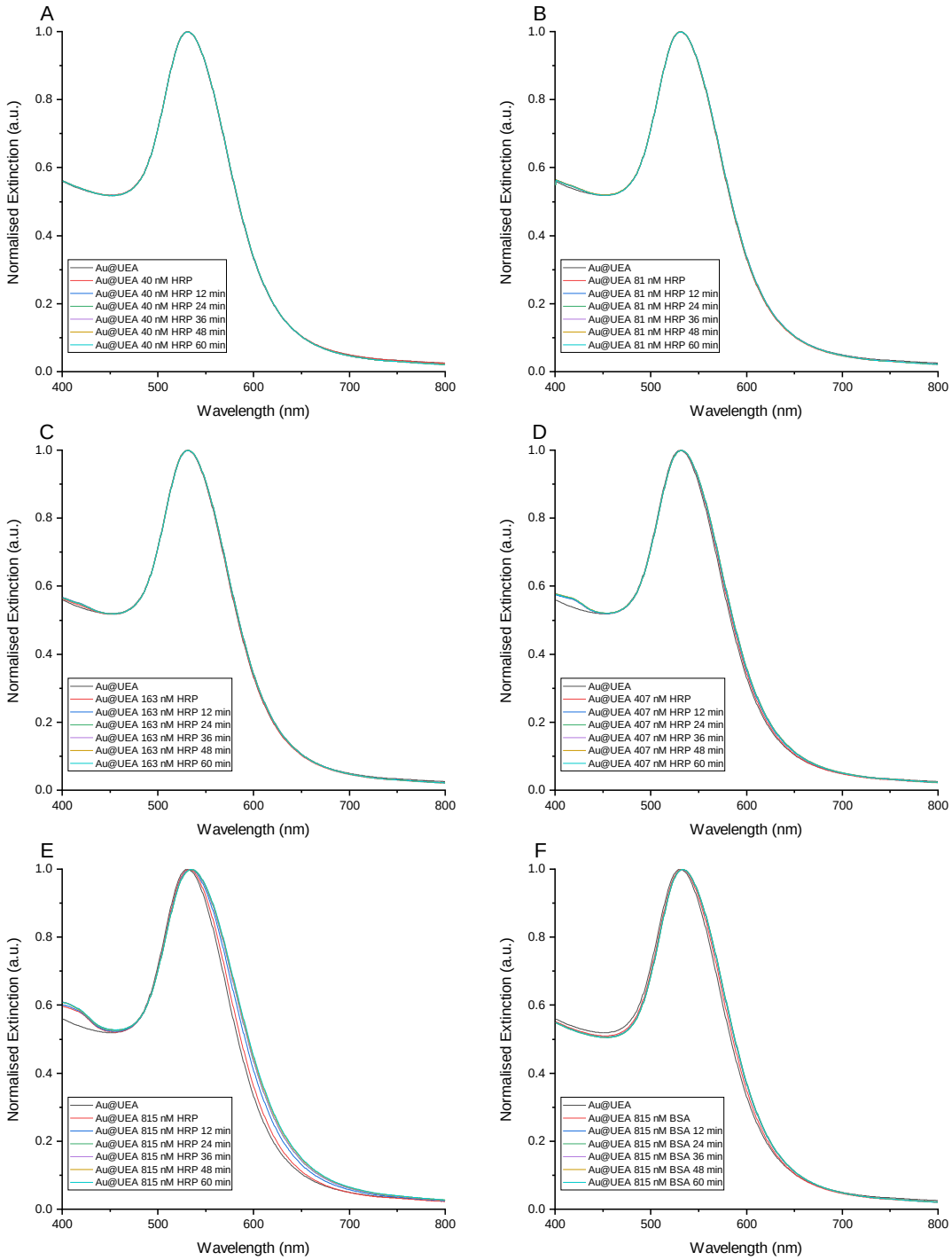


*Figure 3.30: Extinction spectra taken from samples of Au@UEA and various concentrations of HRP. BSA was used as a negative control. Spectra were taken immediately following mixing, and every 12 min*

*for 1 h. (A) 40 nM HRP; (B) 81 nM HRP; (C) 163 nM HRP; (D) 407 nM HRP; (E) 815 nM HRP; (F) 815 nM BSA. Spectra were normalised to one for clarity and ease of comparison.*

The presence of HRP in solution led to an observed absorption band from approximately 400 – 450 nm, which was not observed in the BSA sample. However, the shifts in LSPR peak positions were much less significant than in previous experiments. There were no overall shifts observed in the samples containing 40 nM and 81 nM HRP. (Figure 3.30(A + B)) The samples containing 163 nM and 407 nM HRP exhibited a small peak shift of 1.5 nm. (Figure 3.30(C + D) In the 815 nM HRP sample, there was a slightly more pronounced shift of 4 nm. (Figure 3.30(E)) This would suggest that some detection was taking place, but that this was not as sensitive as the detection of Man or GlcNAc. This could be due to increased steric hinderance since the Fuc moiety is attached to the core GlcNAc which in turn is attached to the protein polypeptide chain.

UEA, like Con A and WGA, requires counter ions for activity. Here, the Au@UEA conjugates were resuspended in HEPES buffer (10 mM, pH 7.2) which contained 0.1 mM $Ca^{2+}$, $Mn^{2+}$, and $Zn^{2+}$ as recommended by the manufacturer. This was fixed for this experiment, but if this was altered it would perhaps affect the binding efficiency and improve the sensitivity of the assay.

The sample containing Au@UEA and 815 nM BSA (Figure 3.30(F)) also exhibited a shift in the LSPR peak. This had not been observed in previous experiments, since BSA should not contain any glycans. However, following 1 h of mixing there was a shift of 2.5 nm in the LSPR peak which would indicate that some interaction was taking place in solution, causing a change in the refractive index of the medium surrounding the NP. This shift was slightly less than that observed with the HRP sample, but still indicated that some nonspecific binding could be taking place.

Whilst there were some observed changes in the LSPR peak position at higher HRP concentrations, it was not sensitive in comparison to previous experiments. It was also not very specific, since some changes were observed in the sample containing BSA, as well as the Fuc-containing HRP samples. Therefore, whilst some Fuc detection

may be taking place, it could not be said that this was a successful specific glycan detection event.

#### 3.2.4.3.3 LSPR Detection of Sialic Acid

MAL and SNA were tethered to Au NPs at a concentration of 1 μM for the detection of SA. For this, α-AG was used as a positive control, since it possessed five glycosylation sites with bi-, tri-, and tetra-antennary SA-containing glycans. Au@MAL (Figure 3.31) and Au@SNA (Figure 3.32) were mixed with varying concentrations of α-AG and the extinction was measured to monitor the position of the LSPR peak.

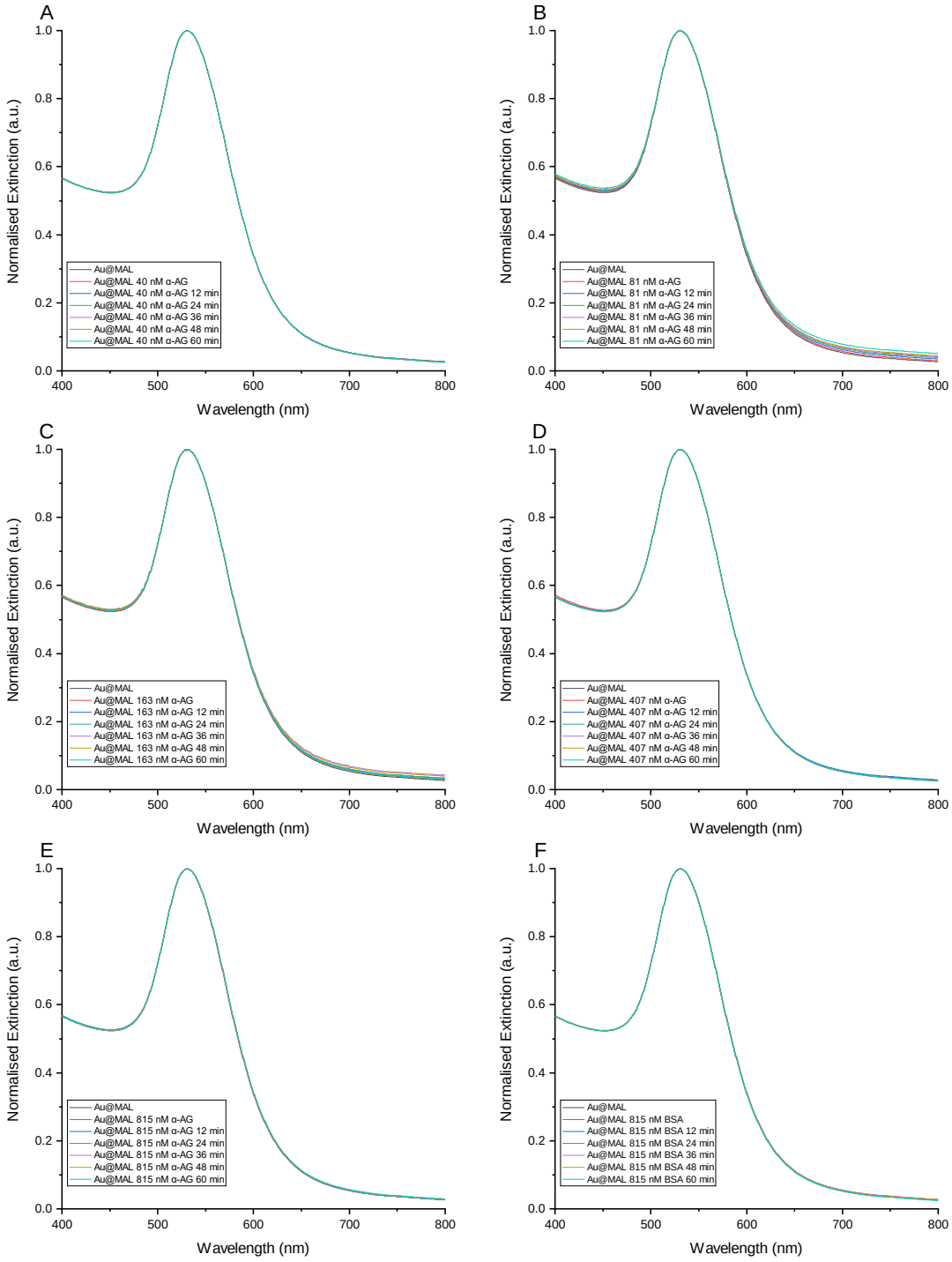


*Figure 3.31: Extinction spectra taken from samples of Au@MAL and various concentrations of α-AG. BSA was used as a negative control. Spectra were taken immediately following mixing, and every 12 min for 1 h. (A) 40 nM α-AG; (B) 81 nM α-AG; (C) 163 nM α-AG; (D) 407 nM α-AG; (E) 815 nM α-AG; (F) 815 nM BSA. Spectra were normalised to one for clarity and ease of comparison.*

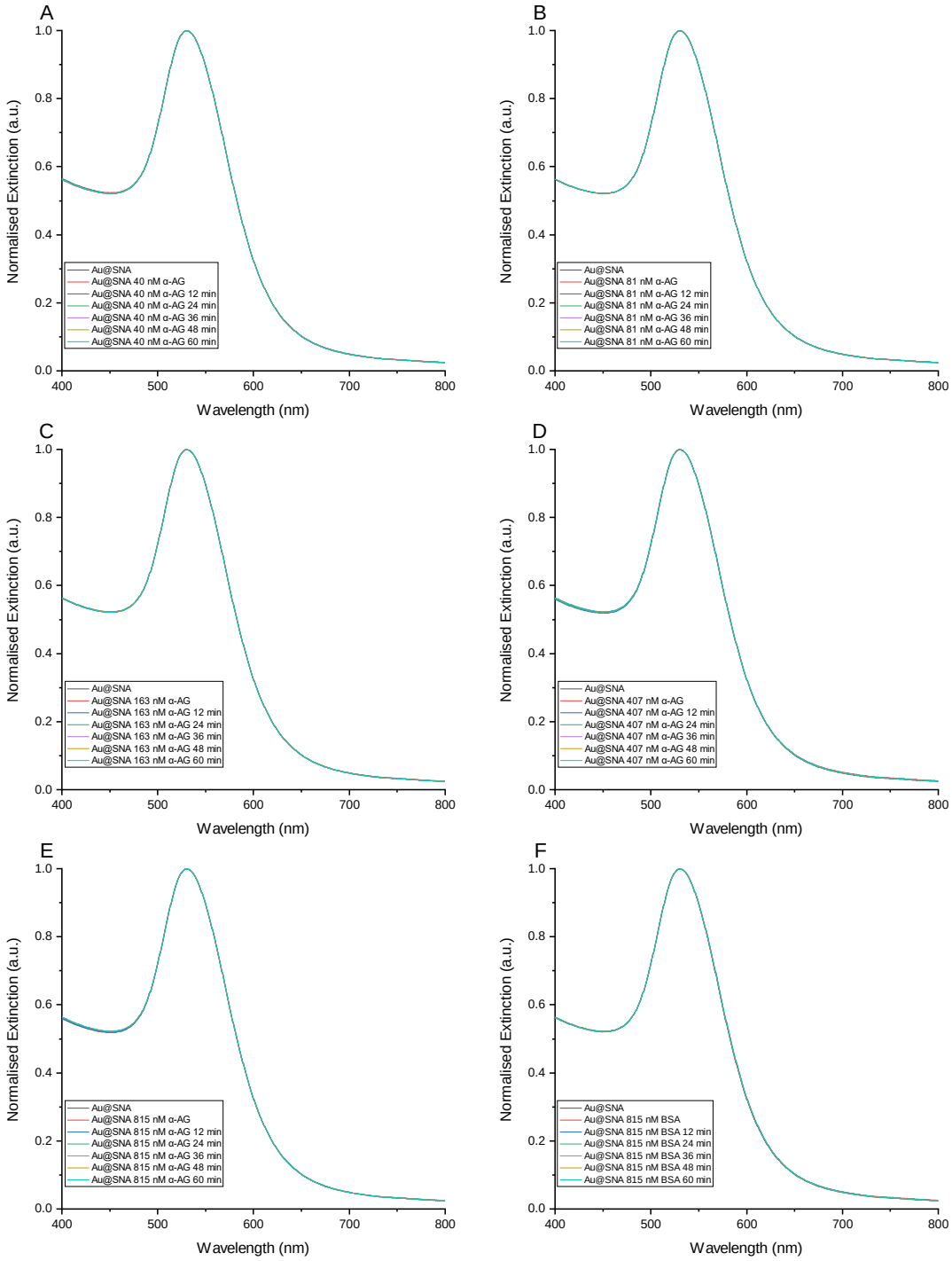


*Figure 3.32: Extinction spectra taken from samples of Au@SNA and various concentrations of α-AG. BSA was used as a negative control. Spectra were taken immediately following mixing, and every 12 min for 1 h. (A) 40 nM α-AG; (B) 81 nM α-AG; (C) 163 nM α-AG; (D) 407 nM α-AG; (E) 815 nM α-AG; (F) 815 nM BSA. Spectra were normalised to one for clarity and ease of comparison.*

In both sets of the experiments, there was no significant shift in the LSPR peak position. This means that there was no change in the refractive index of the medium surrounding the Au NP conjugates, indicating that no binding took place between the lectins and the SA on the α-AG surface. Unlike Con A, WGA, and UEA, the SA-specific lectins don't require counter ions to facilitate their binding. Therefore, the reason for the lack of binding could be a number of reasons. In terms of attachment to the NP, the conjugations were shown to be successful through gel electrophoresis (Figure 3.29) so it would be expected that the lectins would facilitate the binding of the NPs. However, the EDC-sNHS coupling method used may pose problems due to its lack of conjugation site selectivity. This method facilitates binding of the carboxylic acid of the linker to a primary amine on the lectin. Therefore, any free primary amine could be used in the attachment, which could potentially obscure the CRD of the lectin and prevent it from binding to the glycans on the α-AG surface.

Both lectins have been used in fluorescent microarrays in literature.[87,120] They have been demonstrated to have glycan sensing capabilities, albeit not as sensitive as some other lectins. It could be this lack of sensitivity which presents issues in this assay. There was no indication that any binding took place at all in these experiments.

## 3.3 Concluding Remarks

The preparation of stable, monodispersed Au NPs was successfully carried out using the Turkevich-Frens method. These were subsequently functionalised with a RRM, MGITC, and a Man-binding lectin, GNA, *via* a bi-functional linker molecule, CALNN. The conjugation principles were also shown to be transferable to include the use of an alternative linker, PEG, and a variety of lectins. This facile method of NP functionalisation could therefore lend itself well to the detection and characterisation of protein glycosylation.

Initial experiments using RNase B as a glycoprotein highlighted flaws in the assay design. It was hoped that glycan detection in solution would induce controlled aggregation of the NP conjugates, resulting in a quantifiable increase in the intensity

of the SERRS spectrum. However, since RNase B only has one glycan site, this aggregation could not take place. However, whilst SERRS may not have been a good technique for solution detection of all glycoproteins, it was shown that detection could be observed in the extinction spectra of the NP conjugates. When the functional NPs were mixed with the glycoprotein, a shift was observed in the position of the LSPR peak, due to the change in the dielectric field surrounding the NP. This indicated that binding was taking place between the attached lectin and the RNase B high-Man glycan.

Further investigation showed that this shift in the LSPR peak was proportional to the concentration of glycoprotein present, and in the case of Au@GNA and RNase B gave a linear response with a possible LOD of 29.2 nM, which corresponded to 29.2 pmol RNase B in solution. Commercially glycoprotein quantification assays have a limit of detection of 1.67 pmol in gel experiments. However, this is in reference to the quantification of the glycoprotein as a whole but is not selective for specific carbohydrate moieties in the glycan structure. These initial experiments, whilst not as sensitive as commercial assays, raised the potential for a selective assay which could quantify glycoproteins with specific carbohydrates present, whilst still maintaining sensitive LODs.

Research was then carried out to diversify the range of carbohydrate detection capabilities. Firstly, WGA was used for the detection of GlcNAc. These moieties are found within the core sequence of N-glycans, so are directly next to the polypeptide chain of the glycoprotein. This therefore presented a challenge for the NP conjugates to overcome steric hindrance and bind to these inner residues. However, the NP conjugates were shown to selectively bind these core carbohydrates, producing pronounced shifts in the LSPR peak position.

Con A was then investigated as an alternative for Man detection. This was due to the fact that it is widely used in the study of lectin-carbohydrate interactions and has been shown to be very sensitive in detection of Man-containing structures. Even though this lectin was used at very low concentrations on the NP surface, they were able to produce significant shifts in the LSPR peak position in the presence of RNase

B. Whilst this shows the potential for the creation of a highly sensitive glycan characterisation assay, the results were not consistent across the NP conjugates, specifically with large shifts observed with low concentrations of RNase B present. Whilst the accuracy of the assay depends on the consistency of results, it highlighted that the concentration of RNase B present could be pushed to lower levels, with detection still taking place. The fact that no binding was observed in the sample containing BSA showed that this detection was specific for the presence of Man.

Finally, the detection of other carbohydrates of interest were tested. These were Fuc and SA, due to the influence they can have on the efficacy of biopharmaceutical proteins. For the detection of Fuc, UEA was selected. This was used to detect the core Fuc present in HRP glycans. Following the success of WGA in detecting core N-glycan components, it was hoped that UEA would have similar results with HRP. However, this was not observed in the results. Whilst small shifts in the LSPR peak position were observed at higher glycoprotein concentrations, these were not sensitive measurements. This could indicate that this lectin is not as sensitive as those previously used, which could lead to an assay with lower detection. Further issues included the presence of a small, but significant, shift in the LSPR peak in the BSA sample. Since this protein should contain no glycan this highlighted that there may be a lack of specificity of the lectin and some other binding interactions could be taking place.

In the detection of SA, MAL and SNA were selected due to their specificities of different conformations of SA. However, neither was shown to be successful in the binding of the SA-containing glycans of α-AG. These lectins have been successfully used in microarrays described in literature, showing that they would be viable selections for this purpose. However, they were shown to be successful at lower sensitivities in comparison to other lectins, so it may be that the glycoprotein concentrations used here were too low to elicit a response.

The solution LSPR assays shown here have the potential for incorporation in to industrial settings for glycan characterisation. With further research, this could be built up in to a library of Au NP conjugates with various lectins which, when mixed

with a glycoprotein sample, could show rapid and sensitive changes to the LSPR peak position, selectively indicating the presence of specific carbohydrate moieties. This could be used in microplate readers for high throughput testing, giving valuable information of glycan composition which could help identify issues in the biopharmaceutical purification process.

# 4. Paper-based Assays as a Platform for Glycosylation Detection

## 4.1 Introduction

There are a multitude of different methods of detecting either small molecules, or large biomolecules, including MS and ELISAs. These methods can be highly sensitive and specific, with incredibly reproducible results. However, they are often complex, requiring highly trained personnel and expensive instrumentation, and can be time consuming.[46] Therefore, alternative analytical methods, such as paper-based assays have become attractive tools due to their speed and versatility, whilst remaining cheap. They are user-friendly, and highly portable, which, along with giving colorimetric results visible to the naked eye, have contributed to their growth as a diagnostic aid.[122] They can be used as a platform for immunoassays,[123] and in combination with nanomaterials to achieve a colorimetric response to various target analytes.[123–125] Lateral flow assays (LFAs) have also been used with SERS detection which has added advantages. SERS LFAs can be used to visualise binding of NPs functionalised with a RRM at low concentrations which do not produce a colorimetric response,[126] and have also shown the capability of multiplexed analysis.[127]

In 1976, the first LFA for home use was developed to detect human gonadotropin[122] and the approach is now widely used as a point-of-care diagnostic tool. This highlights their ease of use in that they can be used without extensive training by anyone with reliable results. Since then, these assays have been adapted in to various 2D and 3D conformations,[128] and their uses have grown to include a variety applications. In healthcare this has included the detection of biomarkers for pneumonia,[126] hepatitis B,[125] and nucleic acids specific for the herpes virus[127] and HIV.[129] Paper-based assays have also been used in environmental,[130–132] food safety,[130] and defence applications[133] highlighting their versatility and adaptability.

These paper-based devices are normally made using a nitrocellulose membrane.[122,134] This provides a support platform for the reaction between the

target analyte and sensing materials to take place. Nitrocellulose is often chosen due to its polar nature, which allows it to interact with proteins and other biomolecules electrostatically.[122] The nitrate ester of nitrocellulose contains a strong dipole which can bind to the polar peptide bonds of proteins. (Figure 4.1) This binding is aided further by hydrogen bonding and hydrophobic interactions.[122] Biomolecular targets can then be simply placed on the membrane and allowed to bind to be used in sensing applications.

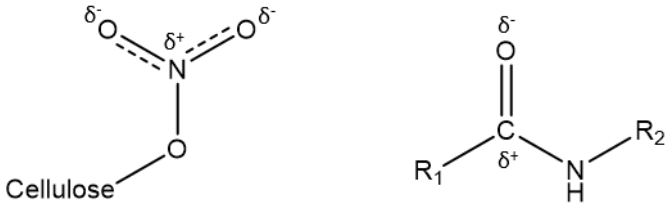


*Figure 4.1: Structures of nitrocellulose ester and peptide dipoles, which allow for electrostatic binding of target biomolecules to a membrane.*

Any remaining unbound active sites on the membrane can be blocked using an inert biomolecule such as BSA, or a polymer such as polyvinyl alcohol. (PVA)[113,114,135] The sensing moieties can then flow along the membranes *via* capillary action and bind to the targets, often giving an easily identified colorimetric response.[122]

Paper-based LFAs were investigated as they provided an attractive alternative to the solution assays. They are cheap and easy-to-use detection methods with a wide array of applications.[122,134,136] LFAs have also been used in quantitative SERS assays using DNA hybridisation[127] and immunoassay formats.[123,125] Typically, commercial LFAs use functionalised Au NPs to detect a target to give a user-friendly colorimetric result, which has meant that it can be used in home-testing kits for rapid responses. Literature searches suggest that these simple diagnostic tests have not been investigated in the detection of glycosylation, which could be an attractive rapid analysis method in biopharmaceutical production, where maintaining glycosylation profiles are vastly important.

## 4.2 Results and Discussion

### 4.2.1 Lateral Flow Assays

#### *4.2.1.1 Lateral Flow Assay Design*

The proposed design for the glycosylation detection LFA was simple, consisting of three regions. (Figure 4.2) The first region was a conjugate pad where functionalised Au NPs are introduced to the membrane. The second region was the nitrocellulose membrane. Here, the target glycoprotein was spotted and allowed to dry. This allowed the protein to bind to the membrane. The last region was the absorbent pad. Excess running buffer and Au NPs are wicked away from the nitrocellulose on to this pad.

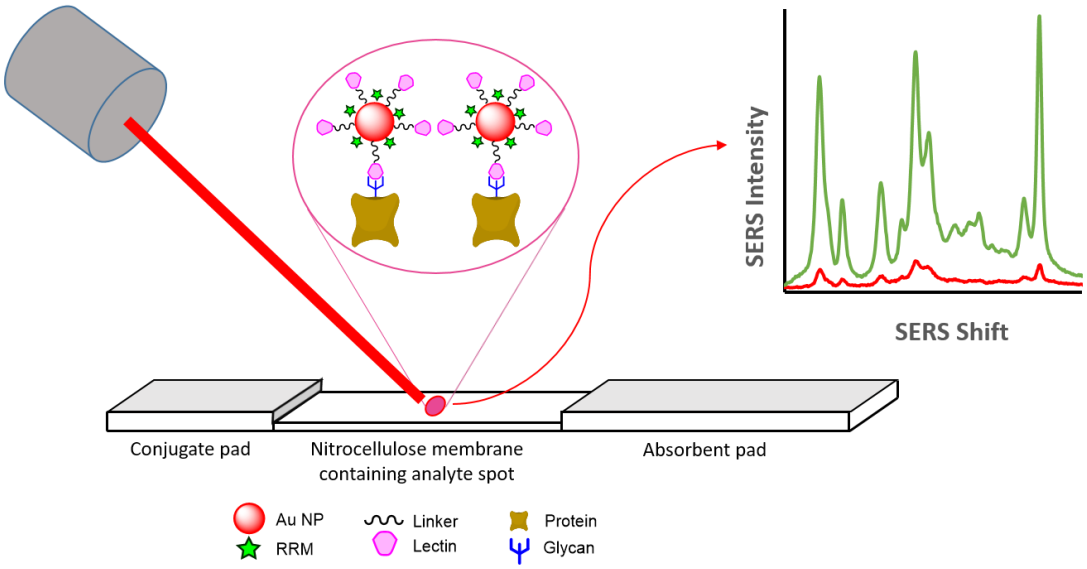


*Figure 4.2: An example of a lateral flow assay device, and how it was designed for glycosylation detection. The conjugate pad is placed in to a solution containing functionalised nanoparticles which flow on to the nitrocellulose membrane and bind to the attached analyte. A pink spot is produced, from which a SERS response can be measured. The absorbent pad allows any excess buffer and unbound nanoparticles to be wicked away.*

Performing the LFA was also simple. Once the glycoprotein target was dried on to the surface, the strip was placed vertically with the conjugate pad in to a well containing functionalised Au NPs in running buffer. The NPs travelled along the nitrocellulose membrane by capillary action and over the target spot. The conjugates bound to the

glycans on the protein surface to produce a colorimetric response. It was hypothesised that this spot could be used in quantitative SERRS experiments, with higher glycoprotein concentrations producing more intense SERRS spectra. (Figure 4.2)

#### *4.2.1.2 Running of Lateral Flow Assay Strips*

In order to run the LFAs, first the protein target was spotted on to the nitrocellulose and allowed to dry at RT for 15 min. The conjugate pad was then placed in to a well with the strip vertical in to running buffer containing Au@GNA conjugates. The conjugates were concentrated using centrifugation to 1.88 nM and suspended in running buffer which consisted of 10 mM phosphate buffer (PB), 1 % BSA, and 0.05 % Tween 20. The role of the BSA was to block unoccupied sites on the LFA strip, so that the Au@GNA conjugates would not bind non-specifically to the nitrocellulose.[113] Tween 20 is a detergent which helps to disrupt intermolecular interactions, preventing non-specific binding by only allowing interactions to take place if there is specific binding energy, such as when the GNA finds its target glycan.[137] The Au@GNA conjugates would travel along the strip by capillary action and over the protein spot. This provided a colorimetric response to show whether or not binding was taking place.

Three strips were used initially to test the specificity of the Au@GNA to the high-Man glycan on RNase B. (Figure 4.3) To the first LFA, 73.3 µM RNase A was spotted on to the nitrocellulose strip and placed in running buffer with Au@GNA. (Figure 4.3(A)) No colorimetric response was observed, indicating that no binding was taking place as should be expected in the absence of a glycan. The second LFA used RNase B as the analyte protein, but with Au@CALNN as the conjugate in the buffer, and no lectin present. (Figure 4.3(B)) This was used to ensure that if any binding to the glycoprotein took place that it was through the interaction between the GNA and the Man residues, and not through interactions with any unfunctionalised CALNN linkers. Finally, a LFA was run using Au@GNA with 73.3 µM RNase B as the target protein.

(Figure 4.3(C)) This provided colorimetric confirmation that binding was taking place between the Au@GNA conjugates and the high-Man glycan on RNase B.

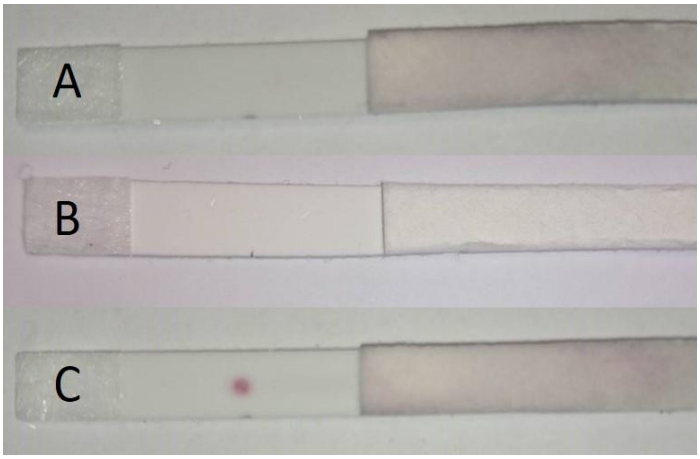


*Figure 4.3: Lateral flow assays showing specific binding of Au@GNA to the high-mannose glycan on ribonuclease B. (A) Au@GNA with a spot of ribonuclease A; (B) Au@CALNN with a spot of ribonuclease B; (C) Au@GNA with a spot of ribonuclease B.*

This confirmed that the binding of Au@GNA to RNase B was a specific interaction between the CRD of GNA and the terminal Man residues of the glycan on the protein surface. Therefore, the next logical development was to evaluate the sensitivity of LFAs in this assay, to see how low the concentration could be detected using colorimetric methods.

#### *4.2.1.3 Analysis and Quantification of Lateral Flow Assays*

The initial proof-of-principle experiments indicated that glycan detection was possible using LFAs. To develop this further, the responses gained were analysed using both colorimetric analysis and SERRS measurements to verify if quantitative results could be obtained.

Strips were prepared using the same method, with different concentrations of target protein. (Figure 4.4) RNase A was again used as a negative control at a concentration of 73.3 µM. (Figure 4.4(A)) Here a grey streak appeared following the point of contact with RNase A. Normally for positive results a pink spot would be expected, and for negative results no spot should be seen at all. However, this had given a response

which seemed to suggest that contact with the protein produced some instability in the Au@GNA conjugates causing them to aggregate as they travelled along the strip. RNase B was then used at concentrations of 73.3 µM, 7.33 µM and 0.73 µM as positive controls. (Figure 4.4(B-D)) Here it was clear to see by a difference in intensity of the spot with the naked eye, especially with change from 73.3 µM to 7.33 µM RNase B. However, no spot could be seen in the strip with 0.73 µM RNase B.

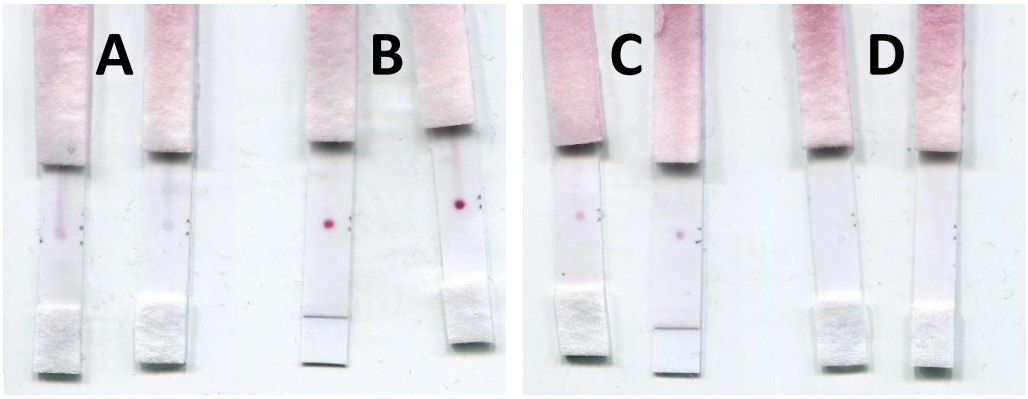


*Figure 4.4: Colorimetric responses of lateral flow assays for mannose detection with Au@GNA and different concentrations of target proteins. (A) 73.3 µM RNase A; (B) 73.3 µM RNase B; (C) 7.33 µM RNase B; (D) 0.73 µM RNase B.*

The strips were placed in to a flatbed scanner to be visualised. ImageJ software was then used to analyse the image and produce values for the red, green, and blue pixels used in each spot. (RGB values) Since white light is shown when all three channels are at their maximum value (255), the obtained results were normalised by subtracting the value given from the maximum value and presented in Table 4.1. Due to the red/pink colour of the Au NPs the green channel is shown to be most sensitive. This gives the possibility of quantifying colorimetric responses but cannot detect beyond visual signals. Using this method, there was still no signal from the 0.73 µM RNase B strip. However, there was a marked difference in the responses from the higher concentrations of RNase B, which were higher than the response gained from the RNase A strips. These observations showed that quantifiable responses were possible using LFAs for the detection of glycoproteins but may be hindered by their lack of sensitivity.

*Table 4.1: Normalised responses of the red, green, and blue channels from image analysis using ImageJ of scanned strips. Results from strip D have been omitted due to undefined analyte spot.*

| LFA | [Protein] / µM | Mean Red / a.u. | Mean Green / a.u. | Mean Blue / a.u. |
|---|---|---|---|---|
| A | 73.3 µM RNase A | 41.3 | 48.3 | 33.1 |
| B | 73.3 µM RNase B | 92.0 | 184.2 | 140.1 |
| C | 7.33 µM RNase B | 38.2 | 73.3 | 48.6 |

The lack of sensitivity in LFAs continues to be one of their greatest disadvantages, as well as being difficult to quantify responses further than just a positive or negative result. In many cases, they are used as mostly to gain qualitative information.[122] However, research has been carried out to overcome this using various methods, such as electrochemical responses,[122,124,136] enzymatic processes,[123] and SERS,[126,127] all of which increase the sensitivity. Wang *et al*[127] used SERS to significantly increase the measurable response from LFAs using DNA hybridisation in the detection of dual targets. This yielded limits of detection of 43 fM for Kaposi's sarcoma-associated herpes virus, and 74 fM for bacillary angiomatosis which could be detected simultaneously. In comparison to previously reported values using standard Au NP aggregation-based detection methods, the SERS-based LFAs were found to be approximately 10 000 times more sensitive. Blanco-Covián *et al*[126] also used SERS in combination with their LFAs in the detection of pneumolysin. Their research compared the use of SERS with colorimetric evaluations of point-of-care LFAs. They found that the use of SERS lowered the limit of detection to 1 pg/mL, 1000 times lower than the colorimetric method. There is therefore a place for SERS in diagnostic LFAs in improving not only the sensitivity, but also allowing for the quantification of responses which go beyond the reach of colorimetric methods.

The spots containing MGITC functionalised Au@GNA bound to RNase B were tested using SERRS to assess the viability of this method in future quantifiable assays. The areas where the analyte proteins were applied to the strips were mapped using a 633 nm laser excitation, which was in resonance with the MGITC reporter,[138] with 100 µm steps. (Figure 4.5) Using WiRE software, a look-up table was applied which

generated a signal intensity heat map for the 1614 $cm^{-1}$ peak which corresponds to the phenyl C-C stretching of the MGITC.[139,140] The heat maps showed that there was no discernible signal from RNase A (Figure 4.5(A), but a very clear signal from RNase B (Figure 4.5(B)), again confirming that the functionalised NPs were selectively binding to the Man residues on RNase B.

The nitrocellulose membrane surrounding the analyte spot was also mapped. This showed a slight signal from the MGITC phenyl C-C stretching at 1614 $cm^{-1}$ although at a very low intensity. (Figure 4.5(C)) This indicated that there may have been some residual Au@GNA conjugates in the nitrocellulose surrounding the spot. However, on the spot there was a significant enhancement of the SERRS spectra over the off-spot response, showing that the Au@GNA conjugates were brought in to close proximity with one another by binding to the RNase B, creating "hot spots" of increased electron density. The signal heat map generated by the SERRS responses also shows the highest signal responses towards the centre of the spot, with the intensity dampening towards the outer limits as would be expected. On solid supports it is common to see a "coffee ring" effect which results in dense array of analyte molecules at the borders of an evaporating droplet, which can be used to an advantage in SERS detection.[141] However, here this is not seen, which indicates that the glycoproteins have electrostatically bound to the nitrocellulose membrane to create a more uniform distribution of the target. This positive and uniform SERRS result for glycan detection gives rise to the possibility for quantification of carbohydrate residues, and thus detailed glycan characterisation.

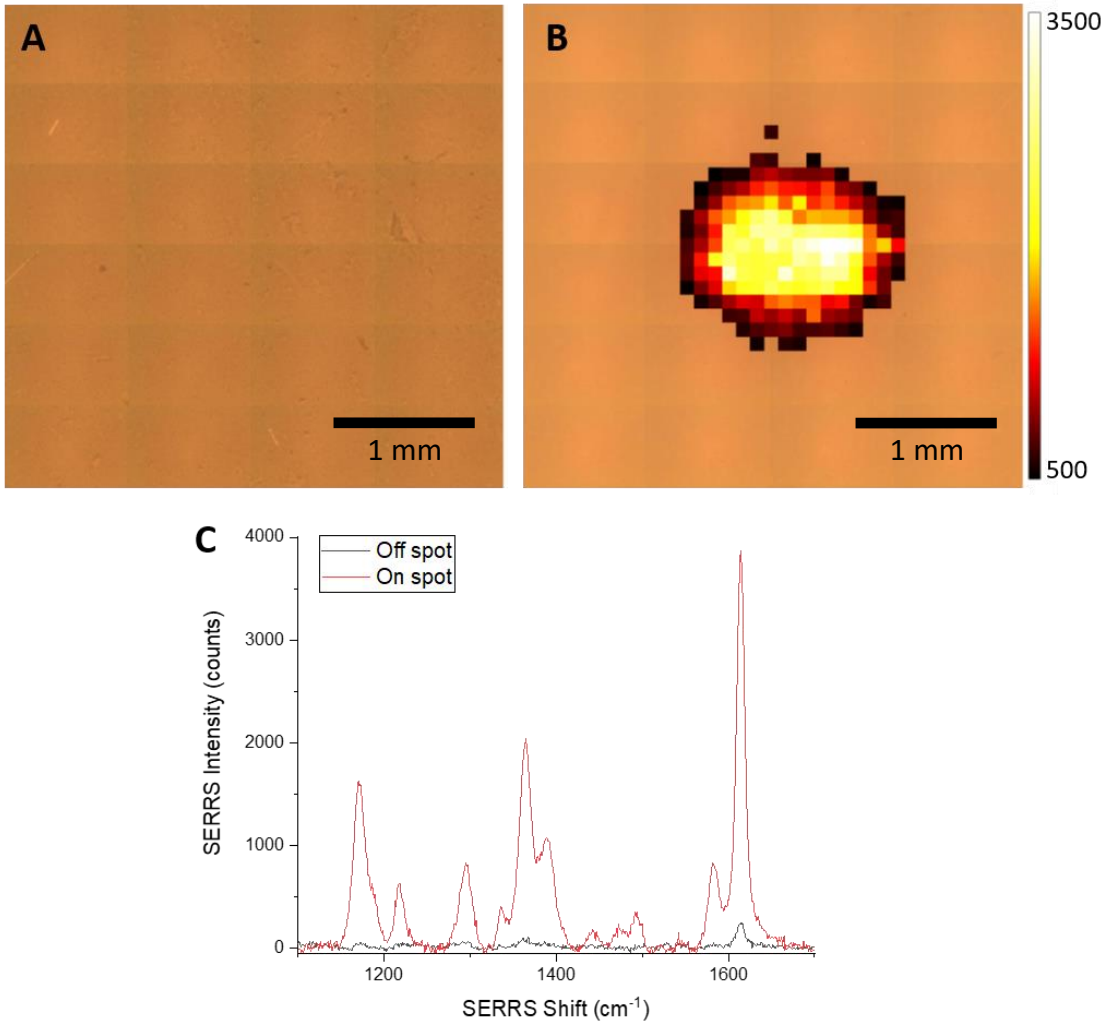


*Figure 4.5: Signal intensity maps of the analyte spots showing (A) the lack of binding of Au@GNA to ribonuclease A, and (B) the conclusive binding to ribonuclease B. (C) The SERRS signals from off-spot and on-spot from Au@GNA and ribonuclease B. (633 nm laser, 100 µm step size, single 6 s acquisitions, 10 % laser power, 0.8 mW)*

#### *4.2.1.4 Issues with Lateral Flow Assay Strips*

The LFAs confirmed that the Au@GNA conjugates were selectively binding to RNase B over RNase A. However, they also had some issues. Firstly, the LFAs lack sensitivity. Colorimetrically, they were not able to detect low concentrations of RNase B. (Figure 4.4, Table 4.1) In standard LFAs, the analytes are normally presented as lines traversing the whole width of the strip. This essentially creates a barrier through which the NPs must travel. The NPs therefore always come in to contact with the

analyte, allowing for binding to take place, and providing a sensitive assay format. With the equipment available, a spot was created on the strip. This, however, allowed the NPs in the running buffer to travel around the spot. The analyte proteins provided some resistance to the flow, and so the running buffer initially flowed around the spots before eventually running over the spot. This creates a significant loss in sensitivity, since the visible spot is only being created by the minority of NP conjugates. Looking at the absorbent pads in Figure 4.4, they have a clear pink colour, showing that many NPs are bypassing the analyte completely and travelling to the end of the strip.

Secondly, the LFAs didn't seem to be entirely reproducible. In Figure 4.4(B), a streak is visible on the nitrocellulose following successful detection of RNase B. This could be due to flow issues again. The flow was no longer unidirectional, and a line appeared on the strips beyond the spot where the two separate flow paths around the analyte spots meet. However, this was not consistent with Figure 4.3(C), where no streak was observed on the strip. The reason for this could be that the flow in both strip is not reproducible, so therefore detection could be variable.

Further to this, comparing Figure 4.3(A) and Figure 4.4(A), the results gained from the RNase A strips were also not consistent. Whilst it was expected that no binding should take place, as was demonstrated in Figure 4.3(A), there was some visual interaction in Figure 4.4(A). It has already been discussed that the presence of RNase A did cause changes to the LSPR peak of Au@GNA, indicating it contained glycosylated impurities. This, combined with the flow issues with these LFAs, could be a cause for the inconsistencies with the colorimetric responses from the RNase A.

However, LFA strips were useful in that they provided confirmatory evidence that the Au@GNA conjugates were able to specifically bind to the Man residues in the single glycan present on the surface of RNase B. Therefore, the assay could provide colorimetric responses, which when combined with RGB measurements could be used as a quantifiable tool. It was also shown that SERRS measurements were possible from the nitrocellulose surface to visualise the presence of NPs once detection had taken place. This indicated that SERRS could be another viable method

in quantifying responses from these assays, with literature showing that this could be used even when the detection was not visible to the naked eye.[126,127] However, the disadvantages with the LFAs meant that they would not be viable for this application in this format. The lack of sensitivity and reproducibility due to the analyte application and resulting conjugate flow required changes to be made to improve the assay design and achieved results.

### 4.2.2 Nitrocellulose Spot Tests

The nitrocellulose LFA was able to provide a support to detect the glycan on RNase B, but the conjugate flow was creating the greatest issues with sensitivity and reproducibility. Therefore, an alternative format of paper-based assay was investigated.

Whitesides *et al*[142] were the first to describe the method of patterning hydrophobic barriers on paper to create channels for use in bioassays, and from there they moved to demonstrate the versatility of this technique by creating 3D paper-based patterned structures.[143]

This has since been investigated further so that a variety of 3D microfluidic paper-based analytical devices (µPADs) in many formats are available in different applications. The Mace group at Tufts University have developed a freely available software tool, AutoPAD, which can be used to design a variety of µPADs.[144] They have created both 2D and 3D formats for different diagnostic applications. A sandwich immunoassay 3D µPAD was developed and used in the detection of human chorionic gonadotropin, and compared to conventional LFA pregnancy tests.[145] They showed that their modular assay format could be easily adapted, and the microfluidic channels created were particularly useful for small sample volumes. (Figure 4.6)

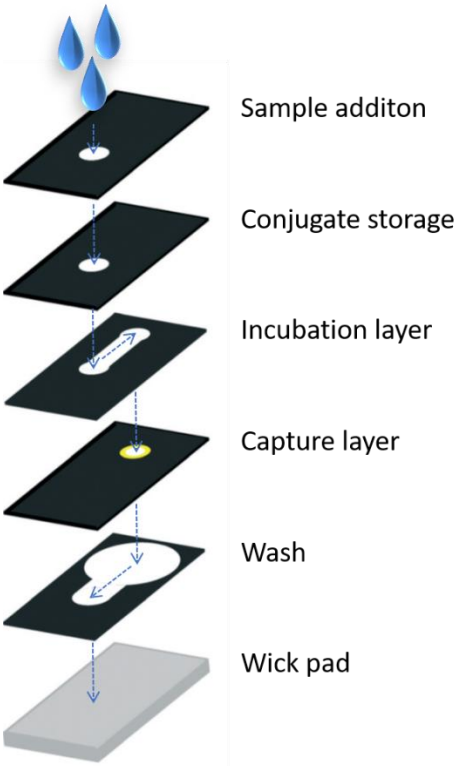


*Figure 4.6: 3D microfluidic paper-based analytical device designed for sandwich immunoassays. Adapted from Ref [145] with permission from The Royal Society of Chemistry.*

This assay format was used with functionalised Au NPs. The sample with the human chorionic gonadotropin target was added in buffer to the sample addition layer where it flowed vertically through the Au NPs in the conjugate storage layer. The NPs and target then flowed laterally through the incubation layer, where they were able to bind together before flowing in to the capture layer. Here, antibodies specific to the target were stored, and a colorimetric response was given as the target bound to the capture antibodies. The buffer and excess NPs would enter the wash layer and be removed in to the wick pad below. The modular nature of the 3D µPAD permits the removal of the top layers to expose the capture layer, allowing for a qualitative colorimetric response to be obtained, or a quantitative response through RGB value measurement.[145] The versatility, portability, and potentially high throughput nature of these devices gives them great potential for use in a wide range of detection assays.

### 4.2.2.1 *Fabrication and Negative Control Studies*

In the detection of glycoproteins, the direct binding of the lectin-functionalised NPs removes the need for a sandwich assay. Therefore, a simpler assay format can be used. The use of a wax printer to create channels gives the µPADs versatility in that various 2D and 3D formats can be designed. A 96-well plate format was used here (Figure 4.7) so that many sites could be printed quickly, allowing for higher throughput studies. The yellow ring around the white channel aided in visualising the Au NPs.

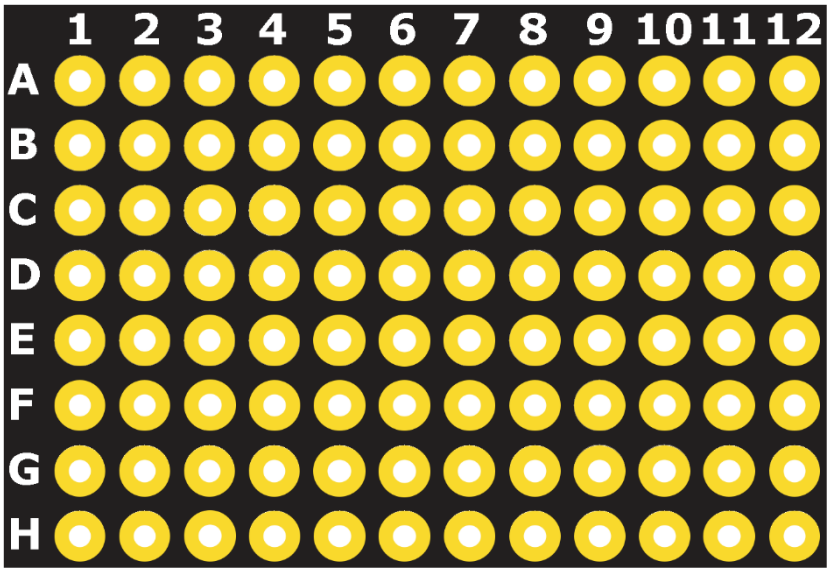


*Figure 4.7: 2D design used for the microfluidic paper-based analytical device in glycoprotein detection.*

The 96-well plate design was printed directly on to the nitrocellulose membrane and melted through the paper in an oven at 85 °C for 1 min to create the channels. The analyte samples were then applied directly on to the spots and dried in an oven at 60 °C for 10 min. At this temperature the wax would not melt but the sample buffer would evaporate to leave the protein bound to the nitrocellulose surface. The nitrocellulose and a wick pad were sprayed with an adhesive and bound together using a laminator to remove air bubbles. The device was then ready to use.

In the solution-based studies, it was noticed that RNase A appeared to bind to the Au@GNA conjugates which presented as a shift in the $\lambda_{max}$ in the UV-vis spectra. This was tested again in the initial studies of the new 2D µPADs. (Figure 4.8) The

concentrations of the analyte samples were varied with two different negative controls used. The first row used BSA as the negative control, and the second row used RNase A.

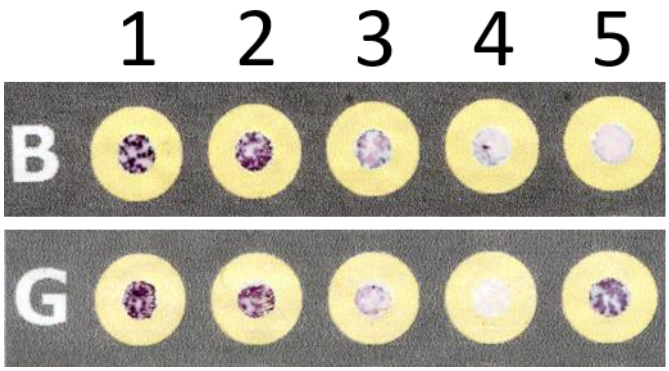


*Figure 4.8: Initial studies using the 2D microfluidic paper-based analytical devices with Au@GNA and RNase B. The top row used BSA as a negative control, and the bottom row used RNase A. The samples used are as follows: (1) 24.4 µM RNase B; (2) 2.44 µM RNase B; (3) 0.24 µM RNase B; (4) Blank; (5) 24.4 µM negative control.*

These initial assays showed a general visual colour gradient with the change in concentration of RNase B, which could be detected more efficiently with the naked eye than the LFAs. The greatest difference, however, came with the binding of the Au@GNA conjugates to RNase A. As mentioned previously, this protein should not contain any glycans, so should not be detected by lectins.[111] The strong signal observed in comparison to BSA suggests that there may be some RNase B present as a contaminant. BSA was then used as a negative control in all subsequent studies. These initial experiments with the 2D µPADs gave promising results with the highly visual response and the colour gradient which was observable to the naked eye.

#### *4.2.2.2 Buffer Tween Study*

As with the LFAs, Tween 20© was used to disrupt any non-specific interactions between the Au NP conjugates and the nitrocellulose. This then means that binding will only take place when there is a specific affinity between species, such as that between a lectin and a glycan. However, if too little is used then non-specific

interactions could take place, and conversely if too much is used, then even specific binding could be disrupted.[137]

The assay was run using the same procedure with Au@GNA, and with BSA as a negative control. (Figure 4.9) The concentrations of glycoprotein was also varied over a greater scale (Table 4.2) to see how the Tween 20 affected binding at lower concentrations. Initially the concentrations of Tween 20 used were 0.01 %, 0.05 %, and 0.10 %, but the addition of 0.10 % Tween 20 to the concentrated Au@GNA conjugates caused the particles to aggregate. Therefore, only the 0.01 % and 0.05 % Tween 20 buffer conditions were tested.

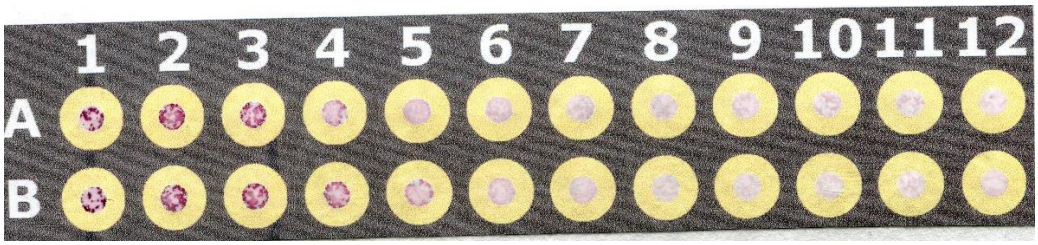


*Figure 4.9: Comparison of Tween 20 concentrations in running buffer with Au@GNA conjugates. Top row contains 0.01 % Tween 20, bottom row contains 0.05 % Tween 20.*

*Table 4.2: Samples and concentrations used in Tween 20 study with Au@GNA.*

| Column | Sample | Concentration / nM |
|---|---|---|
| 1 | RNase B | 10 000 |
| 2 | RNase B | 5 000 |
| 3 | RNase B | 2 500 |
| 4 | RNase B | 1 000 |
| 5 | RNase B | 500 |
| 6 | RNase B | 250 |
| 7 | RNase B | 100 |
| 8 | RNase B | 50 |
| 9 | RNase B | 25 |
| 10 | RNase B | 10 |
| 11 | Blank | 0 |
| 12 | BSA | 10 000 |

The assays were scanned using a flatbed scanner, and the RGB values were calculated using ImageJ software. This allowed for a value to be attached to the visual response of the Au NP conjugates. These values then showed that there was a correlation between the visual response received and the concentration of glycoprotein present. (Figure 4.10)

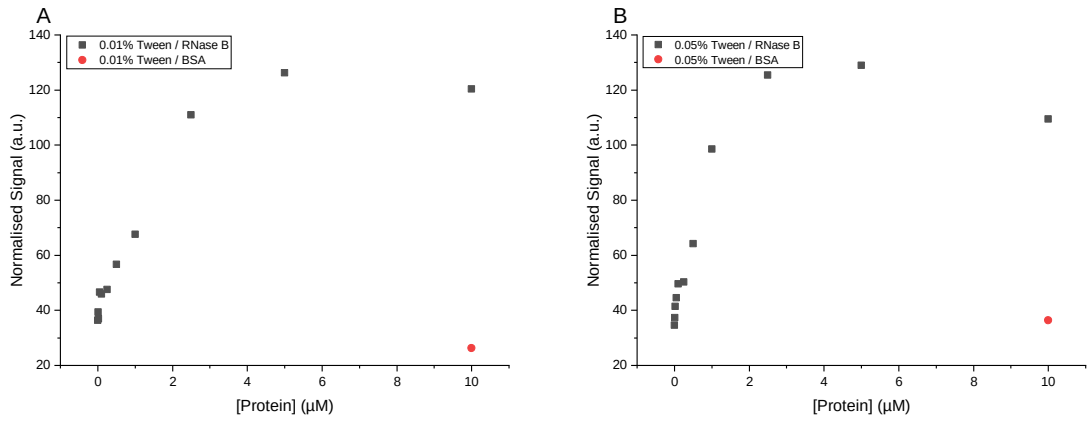


*Figure 4.10: Signals received from the green channels of the RGB values for the Tween 20 study: (A) 0.01 % Tween 20; (B) 0.05 % Tween 20.*

In both data sets, the signal obtained from the test spots increased with greater concentrations of glycoprotein, due to the higher proportion of functionalised NPs binding to the Man residues on the single RNase B glycan. The signal seemed to plateau around 5 µM, after which there was a slight decrease in signal. At this point the concentration of glycoprotein may have been too high so that the NPs were aggregating in defined areas rather than over the whole spot. This can be observed by eye at the higher concentration spots. There is a marbling effect over the spot where the NPs aggregated. (Figure 4.9) This localised aggregation could affect the results from the RGB values since the colour is not spread over the space of the entire spot.

The RGB values obtained also showed that the response from the negative control, BSA, was low. The response was also comparable to the values obtained from the blank sample, showing that the Au@GNA binding was specific to the presence of a glycan, and not an interaction with the nitrocellulose membrane. Comparing both

data sets, it seemed that the Au@GNA samples containing 0.05 % Tween 20 had a slightly steeper gradient in the signals obtained from 0 – 2 µM RNase B.

SERRS measurements were also taken from the spots to determine whether this could also be used to quantify the concentration of RNase B present. (Figure 4.11) These were taken by splitting the spots in to 4 quadrants and taking 6 spectra per quadrant at 6 s per acquisition with a 633 nm laser excitation. These spectra were then pre-processed using WiRE software and averaged using Matlab. The intensity of the 1614 $cm^{-1}$ peak from MGITC phenyl C-C stretching was used to track the response with respect to the sample concentration.

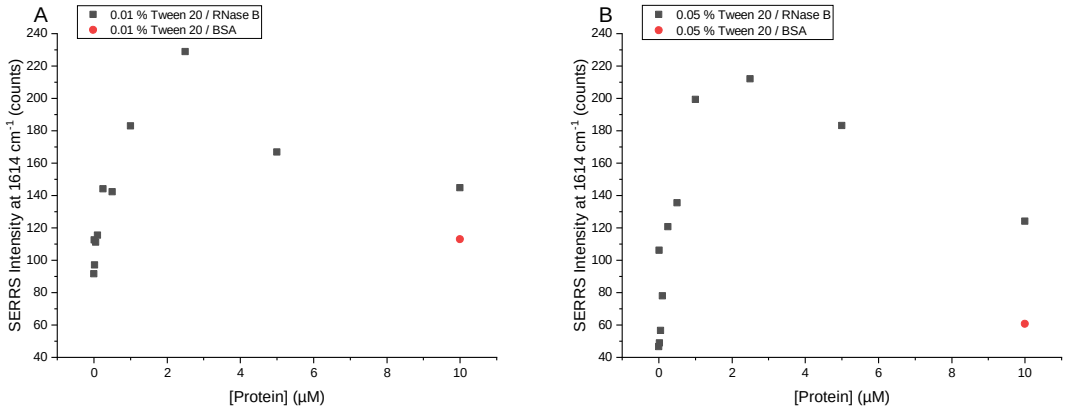


*Figure 4.11: SERRS responses taken from the 1614 $cm^{-1}$ peak of MGITC averaged over the sample spots: (A) 0.01 % Tween 20; (B) 0.05 % Tween 20. Spectra were averaged from 24 acquisitions of 6 s duration, using a 0.8 mW 633 nm laser.*

A general gradient was again observed with the SERRS signal increasing with the increase of RNase B present. In these data sets, however, the signal achieves a maximum slightly earlier at around 2 µM RNase B. The signal then decreases sharply. Again, this is due to the localised aggregation of the Au@GNA NPs, meaning that the average SERRS spectra obtained over the whole spot is much lower. The aggregates would also cause the signals gained to be much less reproducible.

It is important to note from this data the signals obtained from the negative controls. The BSA signal is much higher in the 0.01 % Tween 20 experiments, in comparison to the 0.05 % Tween 20 experiments. Therefore, the Au@GNA may be interacting non-specifically with nitrocellulose membrane when less detergent is present to disrupt

these interactions. This wouldn't necessarily be observed visually, but the presence of functionalised NPs in the membrane could be picked up by SERRS. This is also shown by the fact that there is a smaller gradient of signal increase at lower concentrations of RNase B. (Figure 4.12)

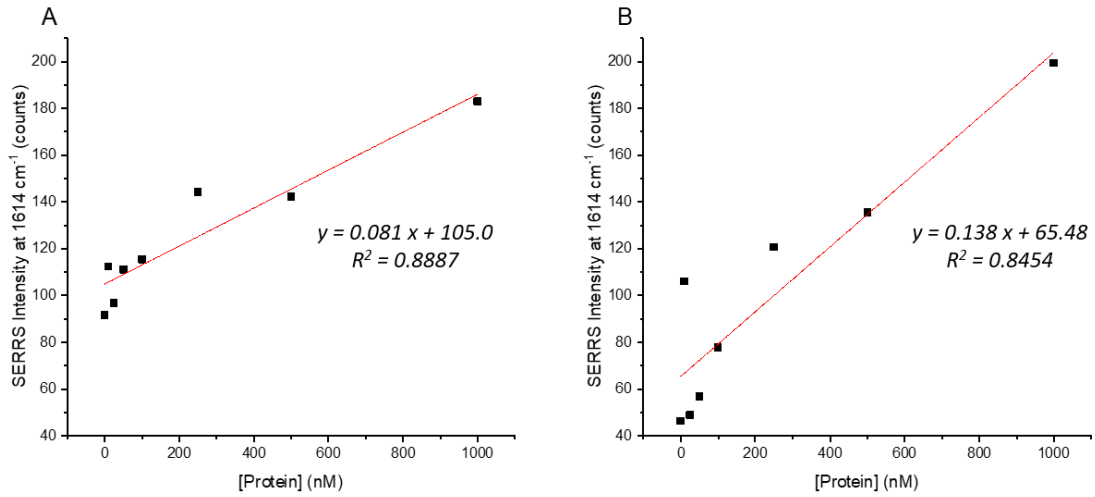


*Figure 4.12: SERRS signals from the MGITC 1614 $cm^{-1}$ peak obtained from 0 - 1 µM RNase B sample spots, showing the greater gradient from conjugates containing 0.05 % Tween 20: (A) 0.01 % Tween 20; (B) 0.05 % Tween 20.*

The signal obtained from the blank signal in the 0.01 % Tween 20 data set (Figure 4.12(A)) was around double the intensity of the signal obtained in the 0.05 % Tween 20 data set. (Figure 4.12(B)) This gives a clear indication that the Au@GNA conjugates are interacting electrostatically with the nitrocellulose membrane when a lower Tween 20 concentration is used. The signal gradient over this concentration range is consequently much lower, which would hinder the sensitivity of the assays. Due to this, 0.05 % Tween 20 was used in future assays to ensure that all interactions were specifically between lectins and glycans.

### *4.2.2.3 Issues with Assay Fabrication Method*

The previous studies were encouraging. They had shown that in general that these 2D µPADs had potential to be used in glycoprotein detection. They were not particularly useful, however, at higher glycoprotein concentrations due to localised aggregation of the nanoparticles which affected both the RGB and SERRS signals

obtained since both techniques take average results from over the entire spot. Therefore, the next experiments focussed on lower concentrations RNase B, below 1 µM. (Table 4.3) The Au@GNA conjugates contained 0.05 % Tween 20 to ensure the interactions were specifically between the GNA and the high-Man glycan. At a glance, the assay seemed to give a good visual response, with a noticeable colour gradient corresponding to the change in RNase B concentration. (Figure 4.13)

*Table 4.3: Sample concentrations used in detection of RNase B with Au@GNA.*

| Column | Sample | Concentration / nM |
|---|---|---|
| 1 | RNase B | 1000 |
| 2 | RNase B | 750 |
| 3 | RNase B | 500 |
| 4 | RNase B | 250 |
| 5 | RNase B | 100 |
| 6 | RNase B | 50 |
| 7 | RNase B | 25 |
| 8 | RNase B | 10 |
| 9 | RNase B | 5 |
| 10 | RNase B | 2.5 |
| 11 | Blank | 0 |
| 12 | BSA | 1000 |

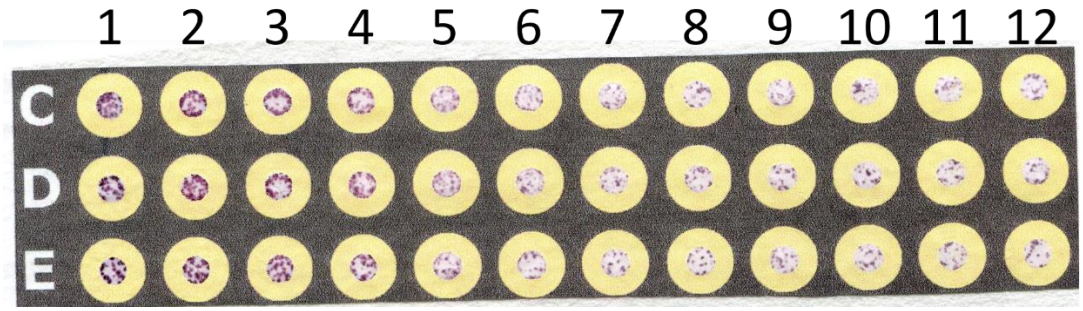


*Figure 4.13: Paper-based assay detecting Man on the surface of RNase B using Au@GNA carried out in triplicate. Rows C, D, and E are replicates of the same experiment.*

The 2D µPAD was scanned and the RGB values were calculated, again using ImageJ. This gave a generally linear response with respect to the glycoprotein concentration. (Figure 4.14) The signal obtained from the BSA sample was also very low, comparable with the blank sample. This indicated that the assay was adept at selectively detecting the high-Man glycan on RNase B.

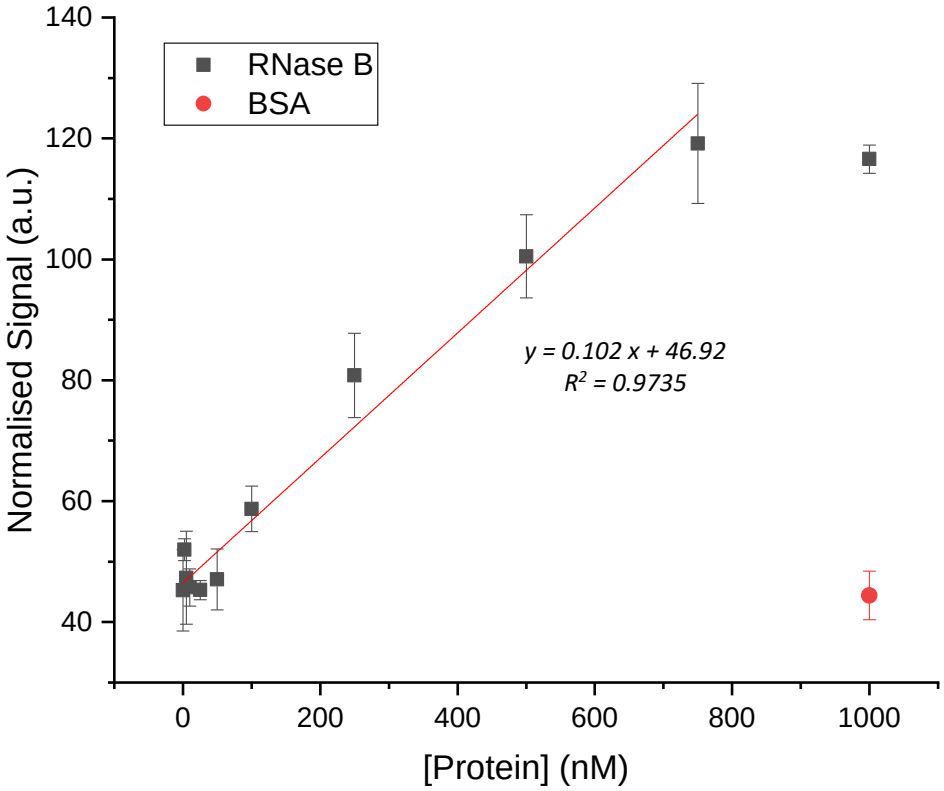


*Figure 4.14: Signals obtained from the green channel of the RGB values taken from the RNase B detection assay showing the linear correlation to the RNase B concentration.*

Although the visual response was strong, there was still significant localised aggregation, as shown by the marble-like appearance of the sample spots. This was not as prominent in previous experiments (compare with Figure 4.9) where localised-aggregation was much less at RNase B concentrations within this experimental range. The RGB values showed an overall linear correlation between the green channel signal and the concentration of RNase B up to 750 nM. This showed that a concentration dependent detection assay using these devices was possible. Plotting a trend line in this linear range allows for a limit of detection to be calculated by taking 3 × standard deviation of the blank response and dividing by the gradient of the linear

trend line. This gave a limit of detection of 197.2 nM, equating to 2.96 µg/mL. A proof of concept study for the detection of prostate specific antigen through the binding of SNA to the α2-6 SA residue on the surface glycan produced a LOD of 2 µg/mL using RGB values.[146] The 2D µPAD developed was comparable to this detection limit.

The response from the 1 µM RNase B sample had a lower signal than the 750 nM RNase B sample. This was a direct consequence of the greater degree of localised aggregation, which causes the overall average signal of the entire spot to be reduced. This was concerning since the assays were not consistent when conducted at different times. This meant that there was a factor which was not reproducible and was hindering the success of the assay. The fact that the same Au@GNA conjugates had been used indicated that perhaps there was an issue with the assay fabrication.

SERRS was used also to analyse the sample spots, with the 1614 $cm^{-1}$ MGITC peak used again to track the response. (Figure 4.15) As before, there was a general trend that the SERRS signal would increase with higher concentrations of glycoprotein, but this was not deemed reproducible.

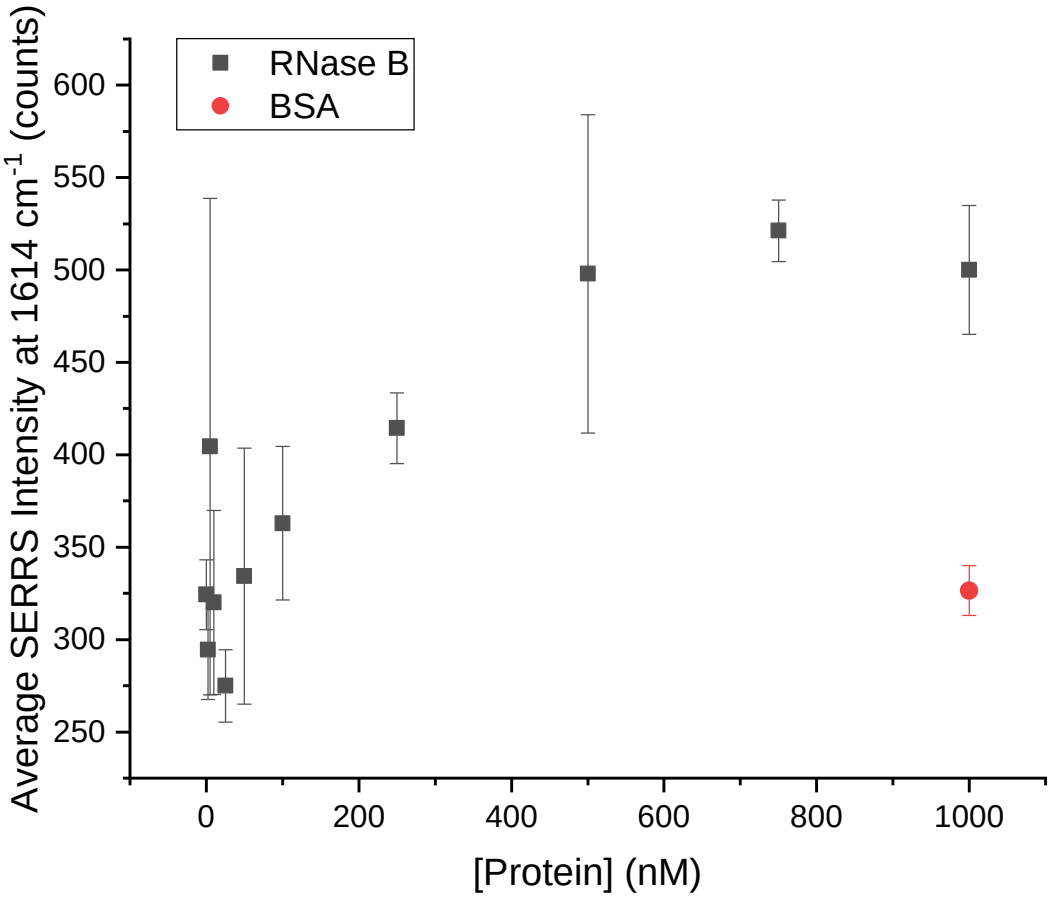


*Figure 4.15: SERRS responses taken from the 1614 $cm^{-1}$ peak of MGITC averaged over the sample spots. 3 replicates of 24 point spectra of 6 s duration were averaged, using a 0.8 mW 633 nm laser.*

Unlike previous assays, the signal from the BSA negative control was considerably higher than the lower concentration samples. It has been shown previously through solution and paper-based assays that the Au@GNA conjugates should not be binding to this sample. The addition of Tween 20 should also interfere with any electrostatic interactions with the nitrocellulose membrane. The higher signal obtained therefore points to another issue. Also, there is a noticeably large variability in the SERRS signals obtained between samples. This suggests that the assays are not reproducible over different sample runs. A general trend is observed in that the SERRS signal increases with RNase B concentration, but there is a great degree of variability. The same conjugates were used, so this strengthened the case that an issue with the fabrication process was increasing the variability and thus decreasing the effectiveness of the assay.

In the assembly of the 2D µPAD, the nitrocellulose membrane and the wick pad were both sprayed with an adhesive before being passed through a laminator to ensure that both layers were in complete contact. This ensures that the running buffer will continuously travel through the membrane. Work by Lewis *et al*[147]showed that using a spray adhesive did not affect the flow behaviour of these devices, and could actually increase their reproducibility. This is understandable, since the nitrocellulose is then in direct contact with the wick pad and reduces the chance of air bubbles between the layers. However, their research used dye solutions to illustrate the flow through the nitrocellulose. The use of colloidal nanoparticles could therefore interact differently with the adhesive. It was hypothesised that this could be the source of the reproducibility issues with these assays and would also explain the localised aggregation of the nanoparticles which could be clearly observed in all previous experiments.

Many µPAD designs use adhesive tape between layers which leave the channels free of interference.[136,143,148–150] This design could provide a way of running the assay without compromising the stability of the nanoparticles.

#### *4.2.2.4 Effects of Changes to Fabrication and Analysis Parameters*

##### 4.2.2.4.1 Using Adhesive Sheets

Adhesive sheets were prepared using a Graphtec CE6000-40 Plus cutting plotter. This allowed for a design corresponding to the spots printed on the nitrocellulose to be made creating clear channels from the nitrocellulose membrane to the wick pad. After the adhesive sheet was applied it was put through a laminator to remove any air bubbles. Then following drying of the samples, it was attached to the wick pad and placed in the laminator again to ensure complete adhesion of the two layers.

The assay was attempted using the adhesive sheets. (Figure 4.16) Here two lectins were compared initially, GNA and Con A. Since both lectins detect Man, RNase B was still used as the positive control at various concentrations. (Table 4.4)

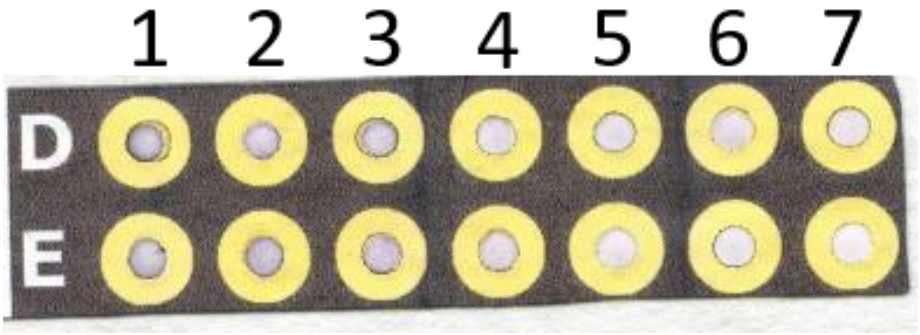


*Figure 4.16: Assays for the detection of Man on RNase B using two conjugates. Top row used Au@GNA. Bottom row used Au@Con A.*

*Table 4.4: Sample concentrations used in Man detection assays with Au@GNA and Au@Con A.*

| Column | Sample | Concentration / nM |
|---|---|---|
| 1 | RNase B | 500 |
| 2 | RNase B | 250 |
| 3 | RNase B | 100 |
| 4 | RNase B | 50 |
| 5 | RNase B | 25 |
| 6 | Blank | 0 |
| 7 | BSA | 500 |

When an adhesive sheet was used, the nitrocellulose membrane was not held directly in contact with the wick pad as it was with the adhesive spray. The NP conjugates therefore had a longer residence time on the nitrocellulose surface. As such, they had a grey appearance due to the drying of the nitrocellulose once they had finished flowing through. In comparison to earlier assays, the colour was more consistent across the spot, and there was no localised aggregation. The assays were scanned as before and RGB values were obtained. (Figure 4.17)

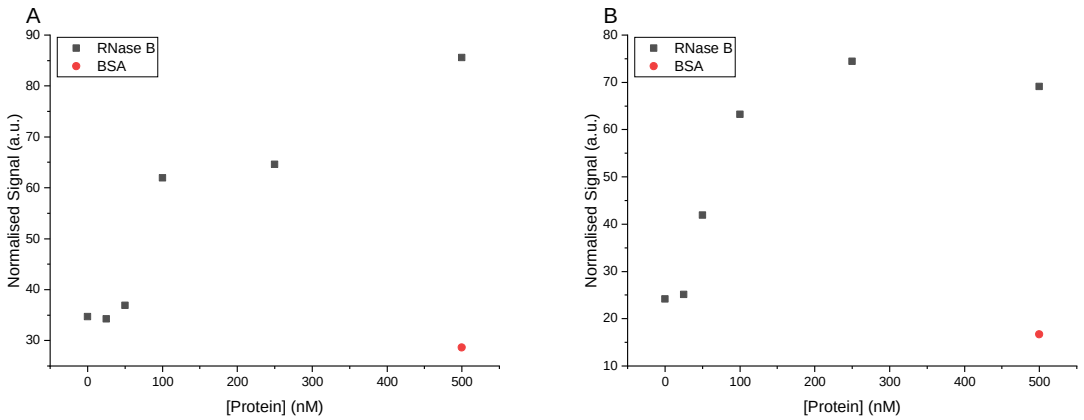


*Figure 4.17: Signals obtained from the green channel of the RGB values from the assays detecting Man on RNase B with (A) Au@GNA and (B) Au@Con A.*

In both cases a general increase in signal with the increase of RNase B concentration was observed as would be expected. The BSA negative control also gave the lowest signals, showing that the interactions were specific to the presence of the high-Man glycan on RNase B.

Comparing the two different lectins, there was a difference in the shapes of the two plots. When Au@GNA was used (Figure 4.17(A)) there was a relatively steady increase in the signal with the increase in RNase B concentration. However, when Au@Con A was used (Figure 4.17(B)) the increase in signal follows a much steeper gradient, and seemingly reaches a plateau. This suggests that Con A binds to Man more readily that GNA. This is supported by earlier findings (Section 3.2.4.2.2) in which Au@Con A had greater shifts in its $\lambda_{max}$ in solution assays when detecting the high-Man glycan of RNase B.

The use of the adhesive sheets instead of the adhesive spray seemed to be more effective in creating a more consistent signal over the entire spot, rather than allowing localised aggregation to take place. It was hoped that this would also make quantification using SERRS simpler also.

#### 4.2.2.4.2 A Change of Objective

SERRS measurements were taken of the sample spots with Au@GNA. This was carried out as all previous measurements. A montage of the spot was created with a 5 × objective, after which the spot was split in to 4 quadrants, and 6 point spectra were taken from each quadrant for a total of 6 s each, again using the 5 × objective. The spectra were then averaged and the 1614 $cm^{-1}$ MGITC peak was used to correlate with the RNase B concentration.

The localised aggregation of the NP conjugates in previous experiments where an adhesive spray had been used in the fabrication process was thought to be the reason for the lack of reproducibility in the SERRS responses. Therefore, it was hoped that the use of adhesive sheets would eliminate the problem. Initially, the 500 nM RNase B spot, the blank spot, and the 500 nM BSA negative control spot were tested first. (Figure 4.18)

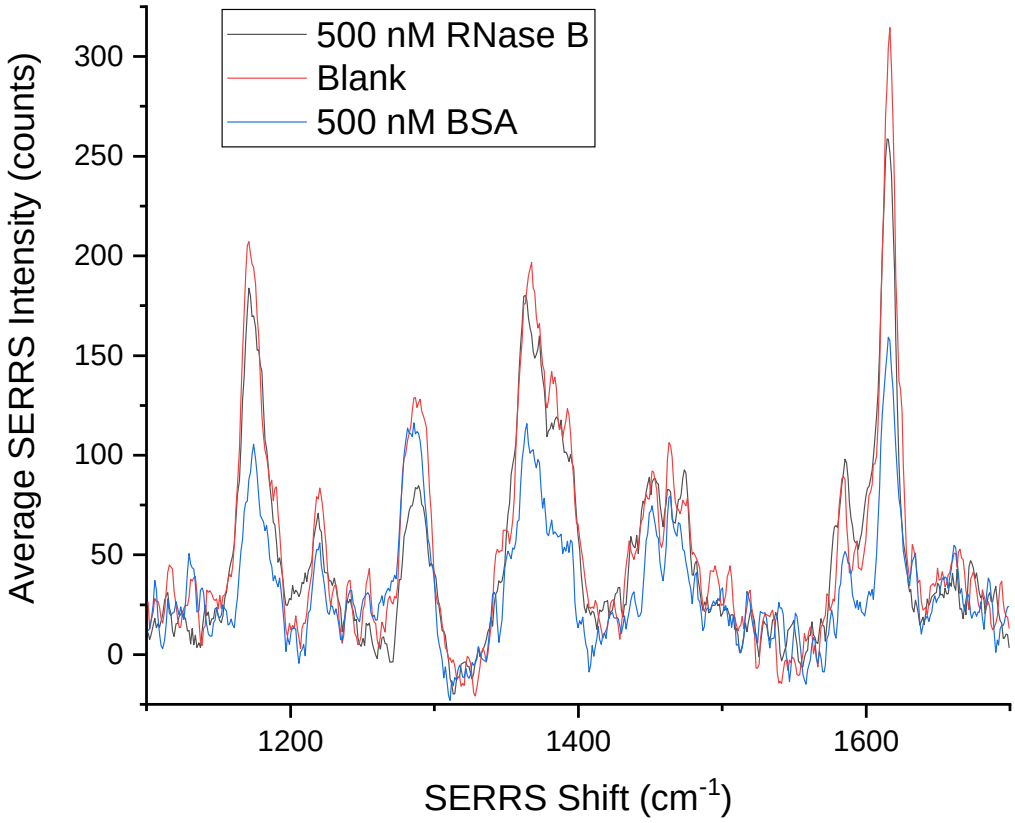


*Figure 4.18: SERRS responses from the 500 nM RNase B positive control spot (black line), the blank spot (red line), and the 500 nM BSA negative control spot (blue line), averaged from 24 spectra of 6 s duration, using a 0.8 mW 633 nm laser and a 5 × objective.*

These results showed that the blank signal was higher, which would suggest that more NPs were binding to this spot, allowing for plasmonic coupling and increasing the scattering efficiency of the MGITC tethered to the NP surface. This was not expected, and upon visual inspection of the assay (Figure 4.16) it was clear to see without instrumentation that more NPs were bound to the surface of the 500 nM RNase B sample spot, and the RGB analysis confirmed that there was a much greater response from the positive control samples. (Figure 4.17) Therefore, this highlighted that there was a further problem with the SERRS analysis of the 2D µPAD.

The instrumentation was looked at to see what could be causing the issues. As mentioned previously, a 5 × objective was used to create a montage of the spot, so that the entire area could be visualised and points for interrogation could be selected. The same 5 × objective was then used to collect the SERRS spectra. The reason for this was that this was the procedure used for the previous LFAs. However, two significant differences were not taken in to consideration, Firstly, the nitrocellulose membranes in the LFAs were thicker than in the 2D µPADs. Secondly, and arguably more importantly, the direction of flow is different in the two assay formats. In LFAs the flow takes the Au NP conjugates laterally across the target and the excess is wicked to the absorbent pad at the side. In the 2D µPADs the Au NP conjugates flow vertically through the target spots and the excess NPs are collected in the wick pad bellow. Therefore, the objective used could have a large effect on the results obtained.

The 5 × objective has a numerical aperture of 0.12, whereas the 50 × objective has a numerical aperture of 0.75. This means that the 50 × objective has a much wider collection angle, and a shorter working distance. Consequently, the longitudinal focussing spot size is shorter with this objective.[151] Therefore, the long focussing spot of the 5 × objective means it could potentially be picking up the Au NP conjugates in the wick pad as well as the nitrocellulose membrane on the surface. In the LFAs this would not be as much of a problem due to the increased thickness of the membrane, and the fact the excess NPs flow away from the target spot. This could explain the lack of reproducibility between sample runs when using the 5 × objective. The 50 ×

objective was then used to assess if the shorter longitudinal focussing spot size would allow for more precise and accurate SERRS signal collection from the NPs in the nitrocellulose membrane surface and avoiding interference from NPs in the absorbent pad below.

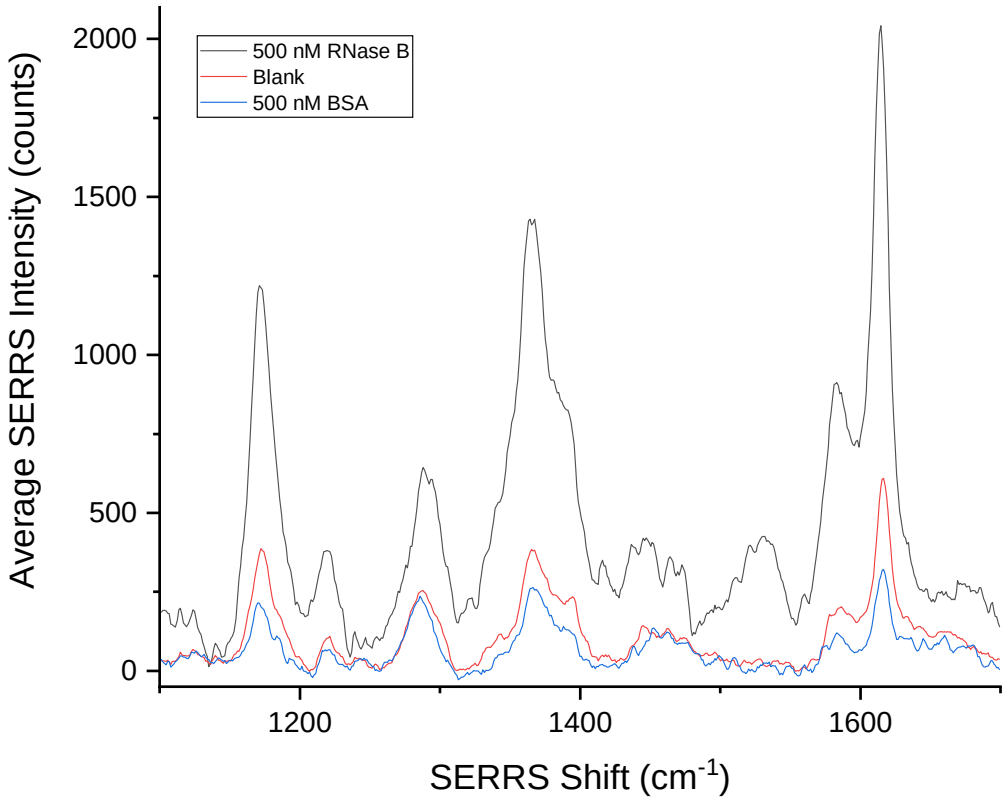


*Figure 4.19: SERRS responses using the 50 × objective from the 500 nM RNase B positive control spot (black line), the blank spot (red line), and the 500 nM BSA negative control spot (blue line), averaged from 24 spectra of 6 s duration, using a 0.8 mW 633 nm laser.*

Changing to the 50 × objective had a significant effect on the results of the SERRS analysis. The blank and negative control signals were low in comparison to the 500 nM RNase B positive control. The SERRS signals were now being collected primarily from the nitrocellulose membrane on the surface, thus increasing the accuracy of the assay. The fact that signals were observed in the blank and negative control samples suggested that some signal may still be observed from the unbound NPs in the lower wick pad layer. These could also be an indication that further wash steps are required, as the NPs may be weakly bound to the nitrocellulose membrane, but this could result in loss of signals by also removing the NPs bound to the

glycoproteins. Following the change of objective, SERRS measurements were carried out on the rest of the assay spots. (Figure 4.20)

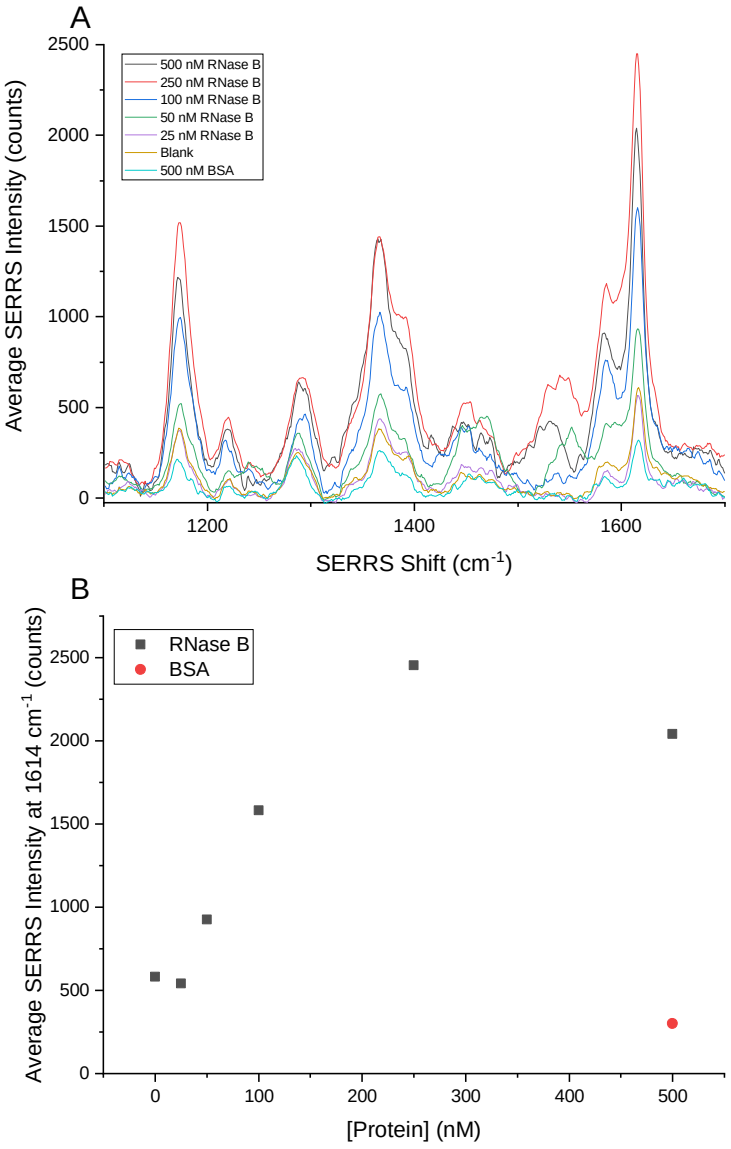


*Figure 4.20: (A) SERRS spectra observed using the 50 × objective from the sample spots on the 2D µPAD. (B) The signal intensities from the 1614 $cm^{-1}$ MGITC peak., averaged from 24 spectra of 6 s duration, using a 0.8 mW 633 nm laser.*

Using the 50 × objective not only improved the accuracy of the SERRS measurements, but also hugely increased the difference in signal between concentration points, which would increase the overall sensitivity of the assay. The negative control had the lowest signal, and there was a large increase in SERRS signal intensity with increasing concentration up to 250 nM RNase B. The 25 nM signal was lower than the

blank sample. This could be down to experimental error, or potentially could be below the LOD of the assay. The lower signal of the 500 nM RNase B sample could be due to the target concentration being too high, and potentially causing some localised aggregation of the NPs.

## 4.3 Concluding Remarks

The fact that RNase B only had one glycosylation site highlighted an issue with the development of a SERRS solution assay. As previously discussed, the functionalised NPs would not aggregate and come in close enough proximity to induce an increase in the SERRS spectrum upon detection of a glycan. Therefore paper-based assays were investigated to provide a support for the target glycoproteins, upon which assemblies of functionalised NPs could be formed allowing for a SERRS signal to be measured.

Initially LFAs were investigated due to their ease-of-use and versatility in both their applications and their analysis methods. This assay format showed promising results as colorimetric responses were easily obtained, indicating detection of RNase B was possible. It also showed that the functionalised NPs could discriminate between a glycoprotein and the unglycosylated BSA.

The LFAs were analysed using two different methods: RGB values, and SERRS measurements. The RGB measurements were carried out by scanning the LFA strips using a conventional flatbed scanner, and using ImageJ to analyse the sample spots. This simple method was able to show differences between two different RNase B concentrations. SERRS measurements were also used to show the potential use of this technique for quantitative analysis of glycoprotein concentration. A heat map was generated, based on the intensity of the 1614 $cm^{-1}$ MGITC phenyl C-C stretching peak, around the sample spot. This was able to show that the SERRS-active Au@GNA NPs could be detected specifically at the glycoprotein sample site, and could discriminate between a positive and negative sample.

The LFA strips, however, had some limitations. They lacked sensitivity due to the spot target on the nitrocellulose surface. This did not create a barrier which the NPs had to cross as they flowed towards the absorbent pad. The NPs travelled around the spot and did not efficiently bind to the target glycan. This loss of sensitivity meant that these assays could not detect a sample of 0.73 μM RNase B. A line of analyte could not be applied to the membrane since the correct instrumentation was not accessible. This limitation meant that an alternative paper-based format was investigated.

To overcome the lack of sensitivity due to the flow issues of LFAs, a 96-well plate design was used, in which the flow was vertical rather than lateral. These designs were printed on to a nitrocellulose membrane using a wax printer, and then the wax was melted through in an oven to create channels with hydrophobic barriers through the membrane. The target samples were spotted and dried in to these channels to bind them electrostatically to the nitrocellulose membrane. The prepared assay could then be attached to a wick pad to allow the vertical flow to take place. The target NPs were then spotted on top and allowed to flow directly through the target glycoproteins. This ensured that the NPs were unable to flow around the target, so that maximum binding could take place upon detection of a glycan.

This assay approach was effective as it promoted glycan detection, but had some limitations in their fabrication. Initially, an adhesive spray was used to bind the nitrocellulose membrane to the wick pad. The NPs flowed quickly through the membrane and give colorimetric responses, which through RGB measurements were shown to correlate well to the concentration of the glycoprotein present. These measurements, however, were not particularly sensitive, and an LOD of 197.2 nM was achieved. The SERRS measurements also varied greatly between samples, so was not very reproducible. This was due to the samples producing localised sites of aggregation on their surface. Since both analysis methods required average observations over the whole sample spot, these sites of aggregated NPs affected the results. This was determined to be due to the adhesive spray used to bind the

nitrocellulose membrane to the wick pad. The nature of spraying the adhesive on to the two layers created instability in the NPs, meaning that they lacked reproducibility.

Adhesive sheets were investigated to ensure that the channels were kept clear. This helped avoid localised aggregation, and increased residence time of the NPs on the membrane, ensuring that glycan detection could take place. An assay was performed and a colorimetric response was observed. The RGB values showed an overall linear trend between the concentration of RNase B and the signal from the green channel. However, when SERRS measurements were collected the data highlighted that there was an issue with the signal collection. The difference in the assay format from the LFAs indicated that the SERRS microscope objectives had to be taken in to consideration. The 5 × objective had a longer longitudinal focussing spot size, which meant that unbound Au@GNA NPs from the wick pad below were being included in the measurements. Changing to a 50 × objective not only eliminated this problem, but also increased the sensitivity of the response received, with a much greater difference in signals between concentrations tested observed.

There is still much work to be carried out with these 2D µPADs. They have shown that they can be used for detection of glycoproteins using a simple RGB measurement, but could also be used along with SERRS to increase sensitivity. The format of these assays lends themselves well to different applications, and also are simple to produce and assemble so could be used in different environments.

In order to improve these assays, further research could include the use of temporary adhesive sheets which would allow the nitrocellulose membrane to be peeled back from the wick pad for analysis,[150] to ensure more accurate analysis of the NPs bound to the surface. Also, the Raman reporter molecule could be investigated to improve the assays sensitivity. This could be increasing the concentration of MGITC on the NP surface, or by investigating other resonant dyes such as Alexa Fluor 633® or cyanine 5.[152]

Whilst the 2D µPADs require extensive optimisation, this research has shown that these devices have the potential for use in glycosylation detection. They can be simply and cheaply printed and assembled, and can produce rapid results that are

both colorimetric and qualitative by simple RGB measurements. Such a simple test could be attractive for rapid glycan characterisation during biopharmaceutical manufacture, easily performed by any employee with little training requirements. The design of the assay in a 96-well plate-style format gives the possibility for high-throughput analysis where different NP conjugates could be used in the detection of various glycan structures, building a picture of the glycan composition. These assays are also versatile in that they can be coupled with SERRS to produce sensitive measurements at low analyte concentrations. Further advancements in the 2D µPAD technology and broadening of the assay scope to include other lectins could provide a highly useful and adaptable glycan assessment tool for biopharmaceutical production.

# 5. Towards an Enzyme-mediated Nanoparticle Growth Platform for Glycosylation Detection

## 5.1 Introduction

Radioactive immunoassays (RIAs) were first reported in the 1960s by Rosalyn Yalow,[153] and in the following decade new analyte detection methods using this technique were published rapidly. This resulted in a Nobel Prize for Medicine being awarded to Yalow in 1977 for "the development of the RIA for peptide hormones."[154] However, there was a need to overcome the use of radioactive materials due to the health implications with handling such materials. This inspired the progression of immunoassay techniques, so that new formats utilising enzymes instead of radioactive labels were developed and introduced in to clinical use in the 1970s and 1980s.[154] At this point the number of articles on enzyme-based immunoassays surpassed that of RIAs and continued to grow. Nowadays, ELISAs have become heavily relied on in analytical and clinical investigations.

ELISAs have four distinct advantages as a diagnostic technique.[155] First of all, they are versatile. Many different ELISA formats are available for a variety of antigen targets including proteins, vitamins and drugs.[156] Secondly, they are rapid and user-friendly, with countless ELISA kits available for purchase.[155] Thirdly, they are highly sensitive due to the amplification of the analyte signal from the enzyme catalyst.[155] As an example, commercial ELISAs for the detection of cardiac troponin I following myocardial infarctions have been shown to detect this biomarker at picogram per millilitre levels.[157] Finally, they are easily quantifiable as they give colorimetric results which can be analysed by simple absorption measurements with a spectrophotometer.[155]

Enzyme-based assays have also been applied to the detection and analysis of glycoproteins.[135,158–160] These assays have been developed to try and provide sensitive glycan analysis methods which are cheaper, more user-friendly, and more freely accessible than conventional routes of glycan characterisation, such as MS.[135]

It was also shown in these studies that glycan cleavage was not required,[135] which allowed for intact glycoprotein analysis using different lectins to determine the presence of diverse glycan structures.[135,158–160] Thompson *et al*[135] focussed on the optimisation of enzyme-linked lectin assays, and showed that the choice of blocking agent was important to maximise possible glycoprotein binding, and in turn, increase the sensitivity. Fotinopoulou *et al*[160] highlighted the use of lectins in sensitive immunoglobulin G (IgG) glycan detection assays using both ELISAs and SPR measurements. They found that both assays had comparative results, with some lectins being more favourable for use in SPR, and others being more favourable in the ELISA. However, both methods were able to detect changes in the IgG glycan profile which arose from a difference in production method.[160] They also compared their findings with monosaccharide content measurements of the IgG glycans using high-pressure anion exchange chromatography and found that their results were agreeable with these results. Interestingly, these results indicated that the chromatographic method was not able to detect the changes in sialic acid content due to their low levels, but that the lectin assays were able to adequately sense these minute changes.[160] This supports the idea that the glycan recognition properties of lectins can be harnessed for use in glycosylation screening procedures in biopharmaceutical production.

Most ELISA formats utilise colorimetric detection methods, due to their simplicity. Often, 3,3',5,5'-tetramethylbenzidine (TMB) is used in the presence of an enzyme, like HRP to generate a colorimetric response.[155] HRP facilitates the oxidation of TMB by $H_2O_2$ which forms a blue charge transfer complex with an absorbance maximum at 650 nm. This can then be further oxidised in the presence of a strong inorganic acid to yield a yellow diamine product, terminating the reaction. This yellow diamine has an absorbance maximum at 450 nm.[161] Absorbance values can be taken using a basic spectrophotometer and used to sensitively determine an analyte concentration.

However, recently there has been some investigation into the use of plasmonic NPs to obtain a quantitative signal upon detection of a target analyte.[162] The size, shape, surface interactions, dielectric environments of a NP as well as their interactions with

one another can have an effect on the oscillations of the LSPR, and in turn induce a spectral change in the extinction, and often present as a colorimetric change. Researchers have harnessed this to create sensitive plasmonic assays for various targets.[162]

Au NPs are synthesised by reducing ionic Au to Au metal by means of a reducing agent. As mentioned previously, this can be carried out using sodium citrate with heat.[91,92] Other synthesis methods make use of stronger reducing agents such as sodium borohydride for room temperature preparations in both organic[163] and aqueous solvents.[164] However, it has been shown that $H_2O_2$ can be used as a reducing agent to mediate the growth of Au NPs, with the growth rate being dependent on the concentration of reducing agent.[162,165,166] De la Rica and Stevens[165] showed that the presence of catalase decomposed $H_2O_2$ and inhibited the reduction of $HAuCl_4$ to Au NPs, forming ill-defined aggregated particles. This presented a blue colorimetric response, which was then used in a sensitive plasmonic sandwich ELISA for the detection of prostate specific antigen (PSA), a biomarker for prostate cancer, and the HIV-1 capsid antigen p24. Liu *et al*[166] used a different approach in the detection of PSA using an ELISA where they induced the production of $H_2O_2$ when PSA was present, which in turn promoted the growth of 5 nm Au NP seeds. A schematic of their ELISA is shown in Figure 5.1. They tethered their detection antibody (blue) to glucose oxidase, (GOx) which they then used to functionalise an NHS-activated magnetic bead. This maximised the enzyme concentration when PSA was present, which was then used to generate the production of $H_2O_2$ by the reduction of Glc to D-glucono-1,5-lactone which subsequently hydrolyses to gluconic acid.

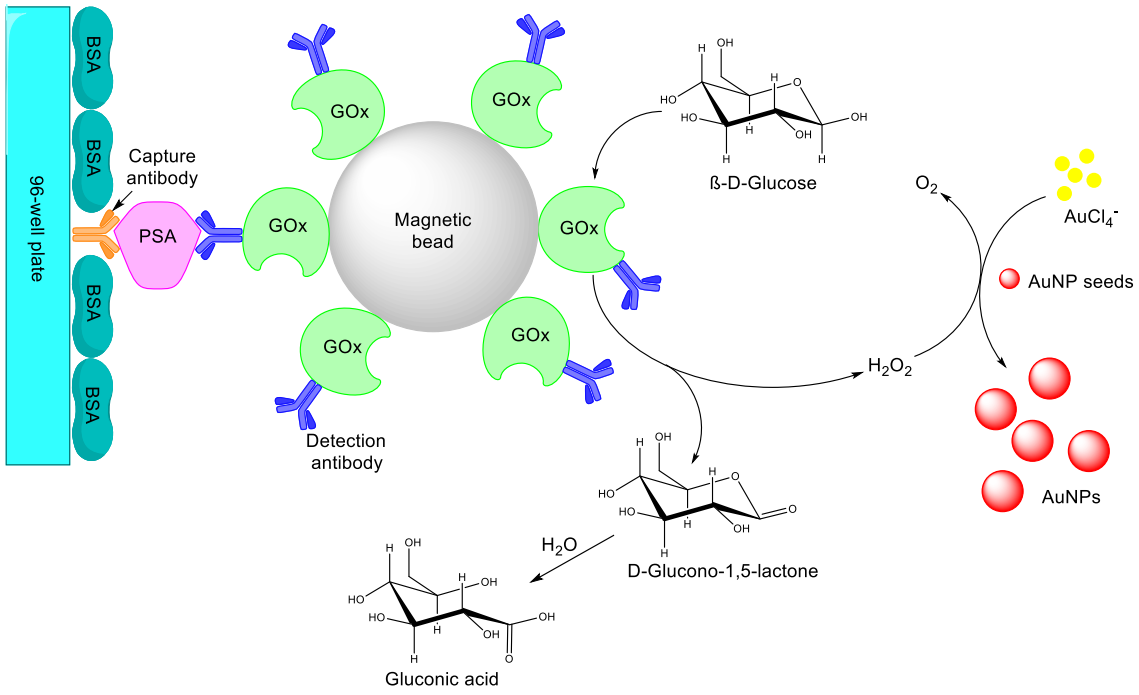


*Figure 5.1: ELISA format used by Liu et al[166] in the detection of PSA where they utilised the $H_2O_2$-mediated growth of gold nanoparticles.*

The extinction coefficient of 5 nm Au seeds is low ($9.696 \times 10^6$ $M^{-1}$ $cm^{-1}$) which means that when diluted the colloid appears colourless.[166] However, once the particles begin to grow as the $H_2O_2$ reduces the gold salt on to the particle surface, the extinction coefficient of the NPs increases. The solution begins to exhibit a red colour, and there is a marked increase in the LSPR peak intensity. Using this method, they were able to detect the presence of PSA down to aM concentrations, showing that a plasmonic assay based on NP growth could be highly sensitive to changes in the concentration of a biomolecular target.

## 5.2 Proposed Assay Design for Glycosylation Detection

In this project, a similar approach was proposed to that reported by Liu *et al*[166] in that GOx would generate the production of $H_2O_2$ when a target glycoprotein was present. This in turn would promote the growth of Au NP seeds by converting Glc to gluconic acid and $H_2O_2$. This would be facilitated through binding of the GOx to a lectin by a biotin-streptavidin interaction. (Figure 5.2)

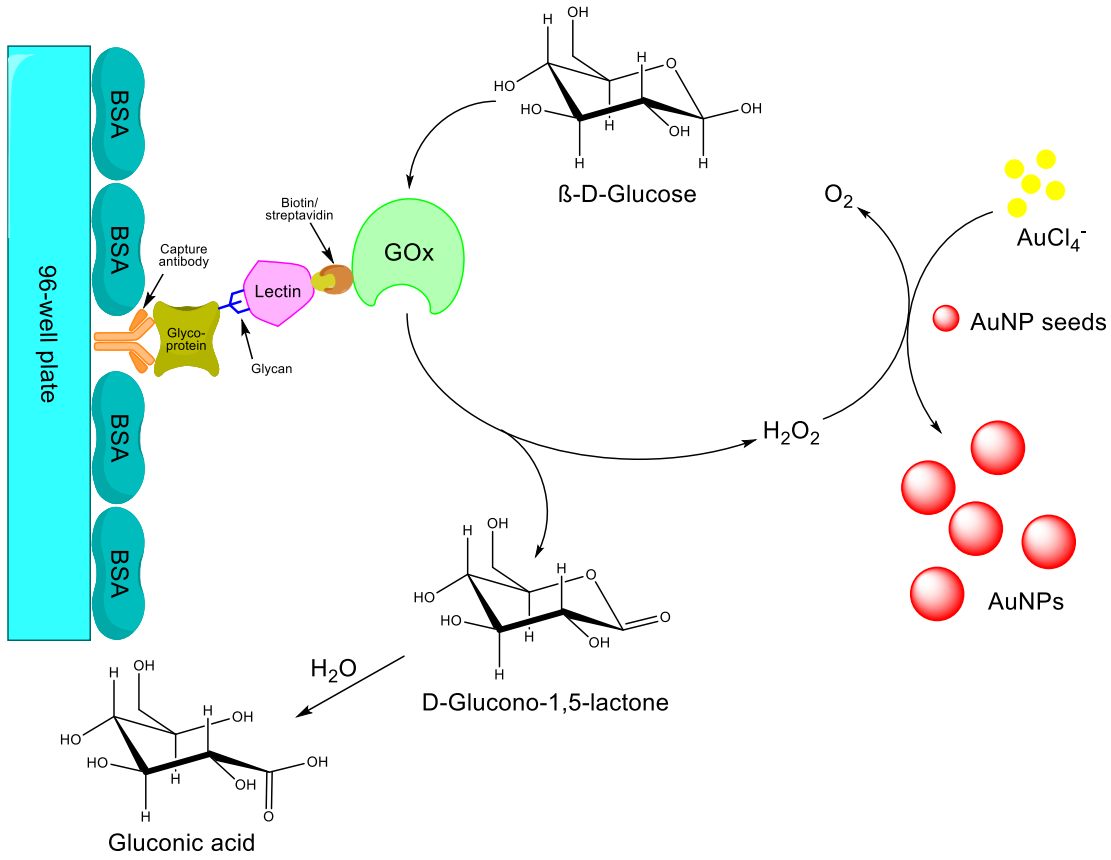


*Figure 5.2: Proposed assay design whereby the presence of a glycoprotein would be detected by a biotinylated lectin which would be bound by a streptavidin-conjugated glucose oxidase. This in turn would mediate the growth of gold nanoparticle seeds.*

In the research by de la Rica and Stevens[165] NP growth could be initiated just through the presence of $HAuCl_4$ and $H_2O_2$ alone. However, whilst the differences in intensity on the LSPR peak in the UV-Vis spectra were clearly visible with increasing concentration of $H_2O_2$, the relative intensities were low. This indicated that the NP growth was slow, and consequently resulted in small increases in the extinction coefficient over a period of 15 min. When Liu *et al*[166] used Au NP seeds, they provided an existing nucleation site upon which the $Au^{3+}$ ions could be reduced to $Au^0$. This resulted in a much faster growth over a period of 20 min, meaning the LSPR peak intensity was much more sensitive to the changes in $H_2O_2$ concentration. Therefore, Au NP seeds were also used in this assay design.

## 5.3 Nanoparticle Seed Growth

### 5.3.1 Seed Size Selection

The first step in creating a NP growth-mediated assay for glycan detection was determining optimal starting seed diameter. This would involve seeds that would be highly sensitive to the concentration of $H_2O_2$ present in solution and grow in relation to this. The change in extinction coefficient would present itself as an increase in the intensity of the extinction spectrum. This is due to the Beer-Lambert law. (Equation 2)

$$A = \varepsilon l c \qquad \text{Equation 2}$$

Whereby the absorbance (*A*) is directly proportional to the extinction coefficient, ($\varepsilon$) path length, (*l*) and concentration. (*c*) Since the path length is set at 1 cm by the spectrometer used, and the concentration of the Au NP seeds are kept constant, any changes in the extinction spectrum is due to a change in the extinction coefficient, which increases as the NPs grow in diameter.

Two seeded growth methods were used. Nanoparticle seeds 5 nm in diameter were synthesised using a method described by Ieong *et al*[164] and a method set out by Ghosh *et al*[167] was used in the controlled synthesis of 10 nm and 15 nm seeds. The seeds were diluted so that the extinction was between 0.05 and 0.10. (Figure 5.3) This would ensure that any changes in the spectrum with the growth of the nanoparticles were clearly observed. The corresponding concentrations of each diluted NP seed sample are shown in Table 5.1.

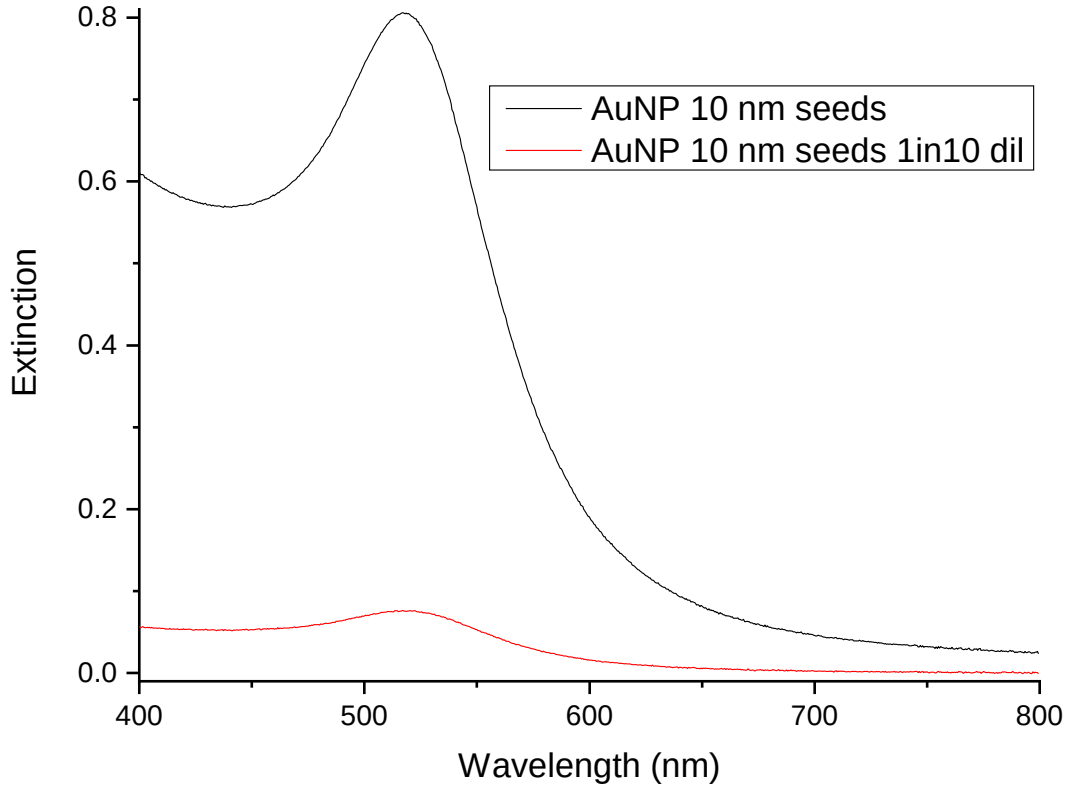


*Figure 5.3: Extinction spectra of 10 nm gold nanoparticle seeds undiluted (black) and diluted (red) so that extinction was between 0.05 and 0.10.*

*Table 5.1: Diluted extinction maxima and nanoparticle concentrations for each seed size.*

| Seed diameter / nm | Extinction | Concentration / nM |
|---|---|---|
| 5 | 0.065 | 6.67 |
| 10 | 0.076 | 0.84 |
| 15 | 0.065 | 0.13 |

The nanoparticle seeds were then placed in a 96-well plate and mixed with 0.6 mM $HAuCl_4$ and various concentrations of $H_2O_2$. The samples were allowed to mix for 20 min and then were analysed with extinction spectroscopy. This resulted in a change in colour of the samples from colourless to red (Figure 5.4(A)) arising from the increased scattering efficiency of the larger NPs. As the NPs grew the increase in their extinction coefficient led to an increase in the intensity of the extinction spectra. (Figure 5.4(B)) This was a direct consequence of the increase in concentration of

$H_2O_2$, which increased the rate of reduction of $HAuCl_4$ on to the surface of the Au NP seeds.

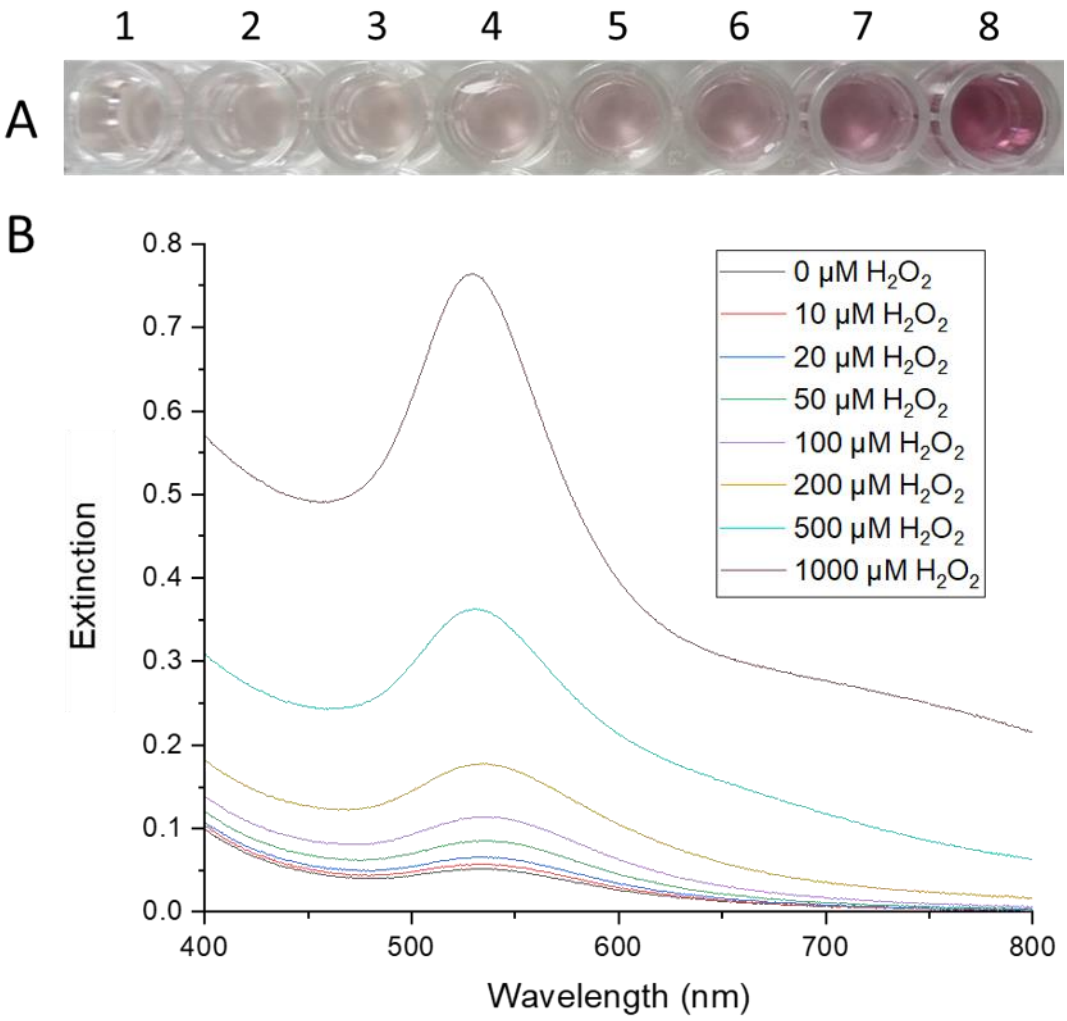


*Figure 5.4: (A) Colorimetric response from 5 nm gold nanoparticles mixed with 0.6 mM $HAuCl_4$ and varying concentrations of $H_2O_2$. (1) Blank, (2) 10 μM, (3) 20 μM, (4) 50 μM, (5) 100 μM, (6) 200 μM, (7) 500 μM, (8) 1000 μM; (B) Extinction spectra of 10 nm Au NP solutions following growth in presence of $H_2O_2$.*

This growth of the Au NPs in presence of $H_2O_2$ was tested using different seed sizes; 5 nm, 10 nm, and 15 nm. This would allow for an initial seed size to be selected which was most sensitive to the concentration of reducing agent present in the final assay when $H_2O_2$ is produced by the presence of GOx. In turn, this would result in an assay with greater sensitivity to the presence of a glycoprotein.

As previously, the NPs were exposed to the same reaction conditions, where they were mixed with various concentrations of $H_2O_2$ in the presence of 0.6 mM $HAuCl_4$

for 20 min. The maximum extinction from each sample was then plotted against concentration of reducing agent. (Figure 5.5)

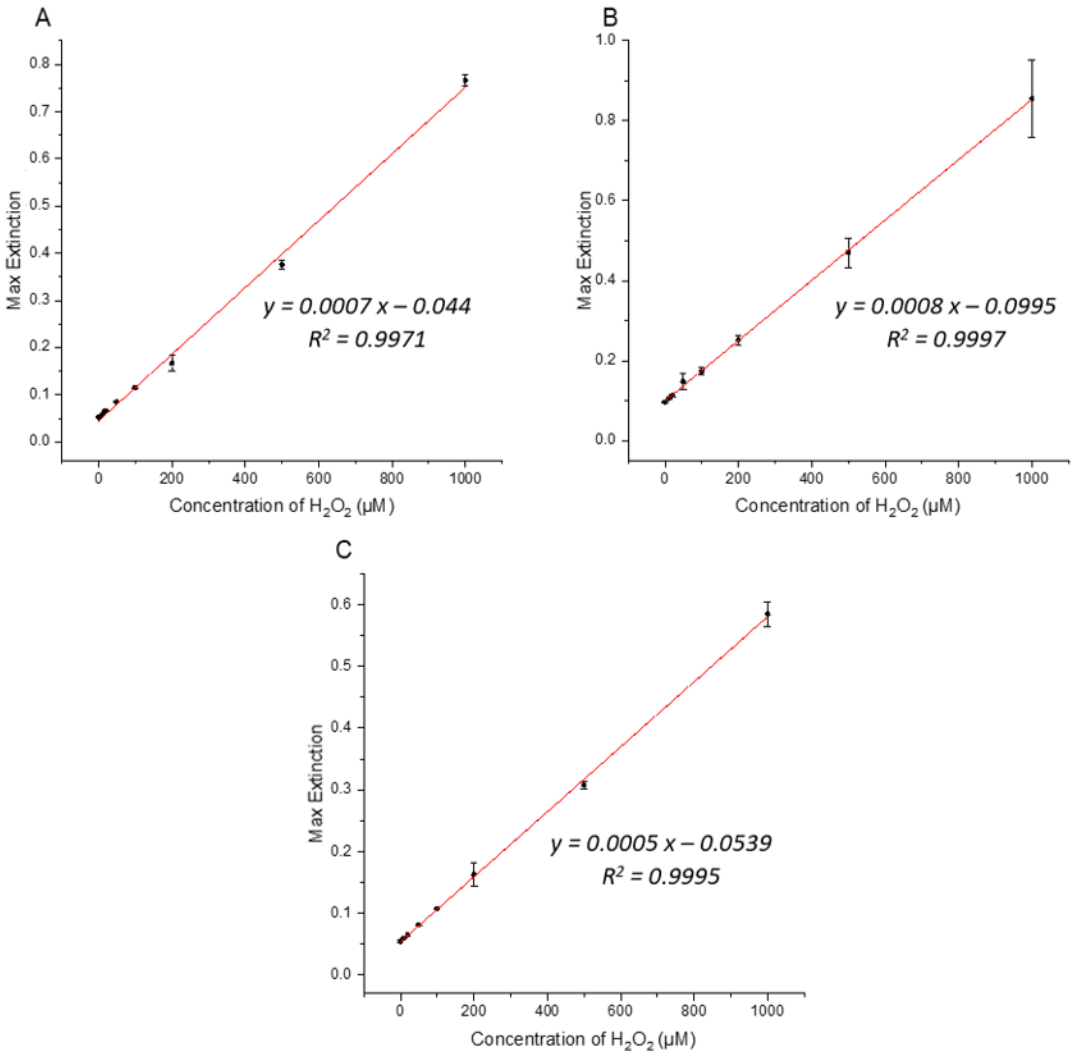


*Figure 5.5: Maximum extinctions after mixing increasing concentrations of $H_2O_2$ with (A) 5 nm, (B) 10 nm, and (C) 15 nm gold nanoparticle seeds with 0.6 mM $HAuCl_4$ for 20 minutes.*

In each experiment, the growth of the Au NP seeds produced an increase in the maximum extinction that was linear with respect to the concentration of reducing agent and was highly reproducible. This gave good indication that NP growth would be a sensitive probe for glycoprotein detection in the final assay format. The linear response observed allowed for a LOD to be determined for each Au NP seed size by taking the standard deviation of the blank sample and dividing it by the gradient of the linear response. For the 5nm, 10nm, and 15nm seeds, this yielded detection limits of 4.89 μM, 6.08 μM, and 8.71 μM $H_2O_2$, respectively. It was clear then that the 5 nm

seeds provided the most sensitive response to the changes in reducing agent concentration. This could be due to the smaller NPs having a lower extinction coefficient, so any changes in size lead to a greater response in the extinction spectrum. The smaller NPs also have a greater surface area upon which the $HAuCl_4$ can be reduced by the $H_2O_2$, which will also lead to enhanced NP growth and result in changes to the NP extinction.

This linear response to the concentration of $H_2O_2$, however, was not expected. In the research carried out by Liu *et al*[166] the linear range under these conditions was only viewed between 10 µM and 100 µM $H_2O_2$, after which a plateau was observed where maximum growth was reached within 20 min. However, here the linear growth range was observed between 10 µM and 1000 µM $H_2O_2$ and there was no decrease in the rate of increase in the extinction. The only difference between the two experiments is that these researchers used 8.3 nM Au NP seeds, whereas here 6.67 nM was used. It could be that the increased concentration of the Au NP seeds provided more sites for reduction of $Au^{3+}$ and subsequently the terminal particle size was reached with lower concentrations of $H_2O_2$. These experiments show a clear role of the $H_2O_2$ in inducing NP growth. In a study by Wang *et al*,[168] it was shown that the molar ratio of NP seeds to $HAuCl_4$ was important for a seeded growth method using $H_2O_2$ reduction to give specific NP sizes. Therefore all components could have influence on the reaction rates. Here, however, the NP seed and HAuCl4 concentrations have been kept constant to assess the effect of $H_2O_2$ on NP growth as this is the variable in the final assay format.

### 5.3.2 Nanoparticle Growth Kinetics Experiments

In order to better understand the growth of the Au NP seeds in the presence of $H_2O_2$ and $HAuCl_4$, kinetics experiments were set up. This involved monitoring the growth of the NP seeds over a longer period of time. The Au NP seeds were mixed with a solution of 0.6 mM $HAuCL_4$ and varying concentrations of $H_2O_2$ as before, and the extinction was measured every 20 min overnight. (Figure 5.6)

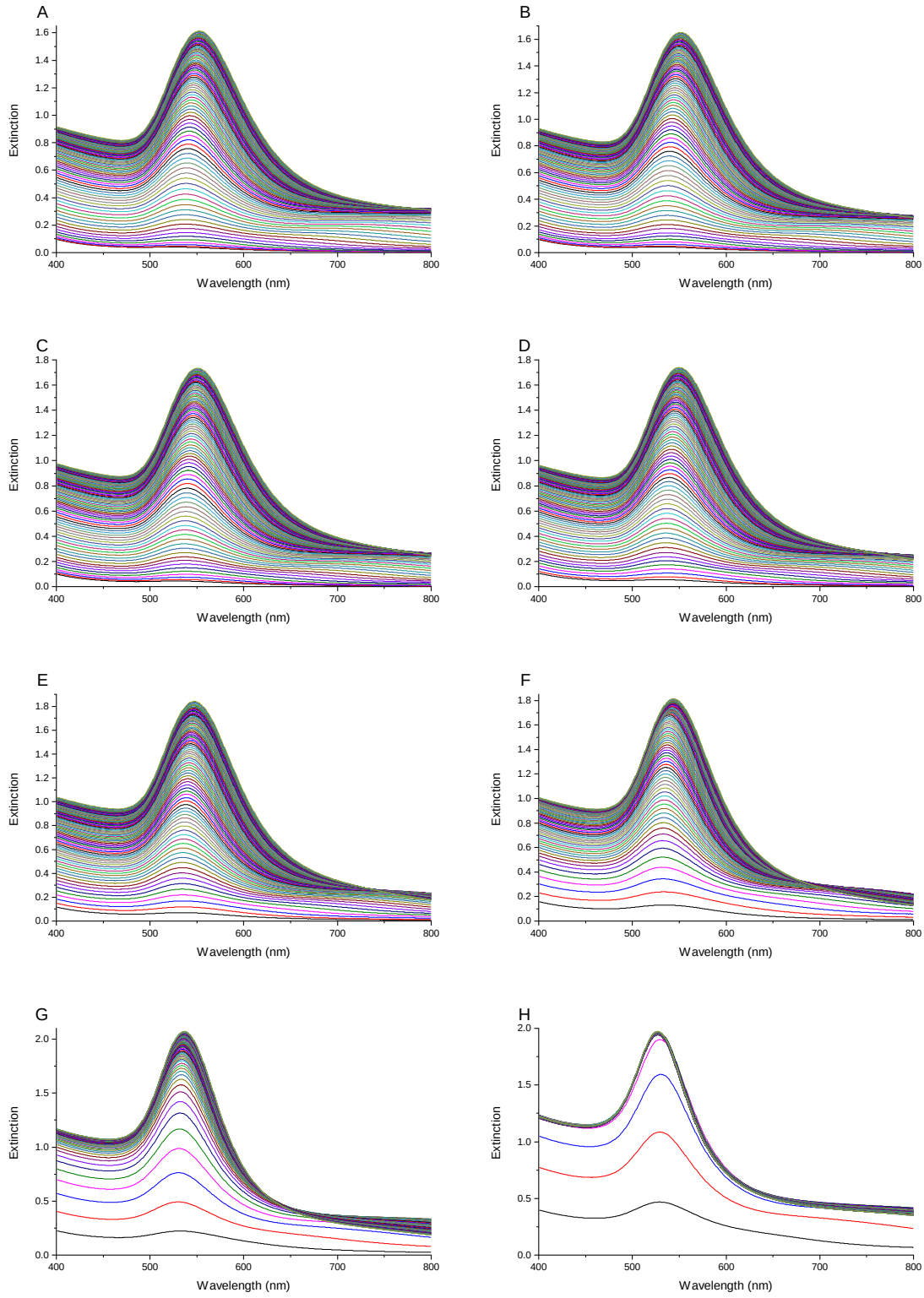


*Figure 5.6: Extinction of gold nanoparticle seeds measured every 20 min overnight in the presence of 0.6 mM $HAuCl_4$ and varying concentrations of $H_2O_2$. (A) Blank; (B) 10 µM $H_2O_2$; (C) 20 µM $H_2O_2$; (D) 50 µM $H_2O_2$; (E) 100 µM $H_2O_2$; (F) 200 µM $H_2O_2$; (G) 500 µM $H_2O_2$; (H) 1000 µM $H_2O_2$.*

The extinction spectra alone gave some interesting insights into the NP growth. At first glance, there didn't seem to be any significant difference between the data sets for the lower reducing agent concentrations, (Figure 5.6 (A-E)) whereas the higher reducing agent concentrations (Figure 5.6 (F-H)) showed a greater rate in the extinction increase, showing that the growth rate was faster when more $H_2O_2$ was present.

An interesting result, however, was that of the blank control sample (Figure 5.6(A)) where no $H_2O_2$ was present. Here the Au NP seeds still continued to grow, indicating that even in the absence of a reducing agent, the $Au^{3+}$ will still be reduced to $Au^0$ on to a crystal surface and result in the overall growth of the NP. It was clear, though, that the presence of $H_2O_2$ did increase the growth rate.

There were also differences in the final LSPR position at the end of the experiment. (Table 5.2) The 5 nm NP seeds had a $\lambda_{max}$ of 519.5 nm and a red-shift was observed with increasing NP size. However, the $\lambda_{max}$ shifted to 551.5 nm in the sample without $H_2O_2$, to 527.0 nm in the sample containing 1000 µM $H_2O_2$ during the course of the experiment. Along with this, the LSPR peak was narrower at higher $H_2O_2$ concentrations in comparison with the lower concentrations where the peak broadened as the NPs grew. This indicates that the faster growth with the higher $H_2O_2$ concentrations results in more monodisperse NPs, whereas the slower growth result in greater polydispersity. This polydispersity then presents as a broad peak with a red-shifted LSPR peak.

*Table 5.2: LSPR peak positions following nanoparticle seed growth with varying concentrations of $H_2O_2$.*

| **$[H_2O_2]$ / µM** | **$\lambda_{max}$ / nm** |
|---|---|
| 0 | 551.5 |
| 10 | 550.5 |
| 20 | 550.5 |
| 50 | 549.0 |
| 100 | 547.0 |
| 200 | 544.0 |
| 500 | 536.5 |
| 1000 | 527.0 |

The maximum extinction reached throughout the course of the experiment also increased as more $H_2O_2$ was used. This ranged from around 1.6 at the lower $H_2O_2$ concentrations, to around 2.0 at higher $H_2O_2$ concentrations. Figure 5.6 (H) also showed that the extinction reached a maximum very early in the experimental period. This suggested that the growth had stopped, which was confirmed, when the extinction was observed as a function of time. (Figure 5.7)

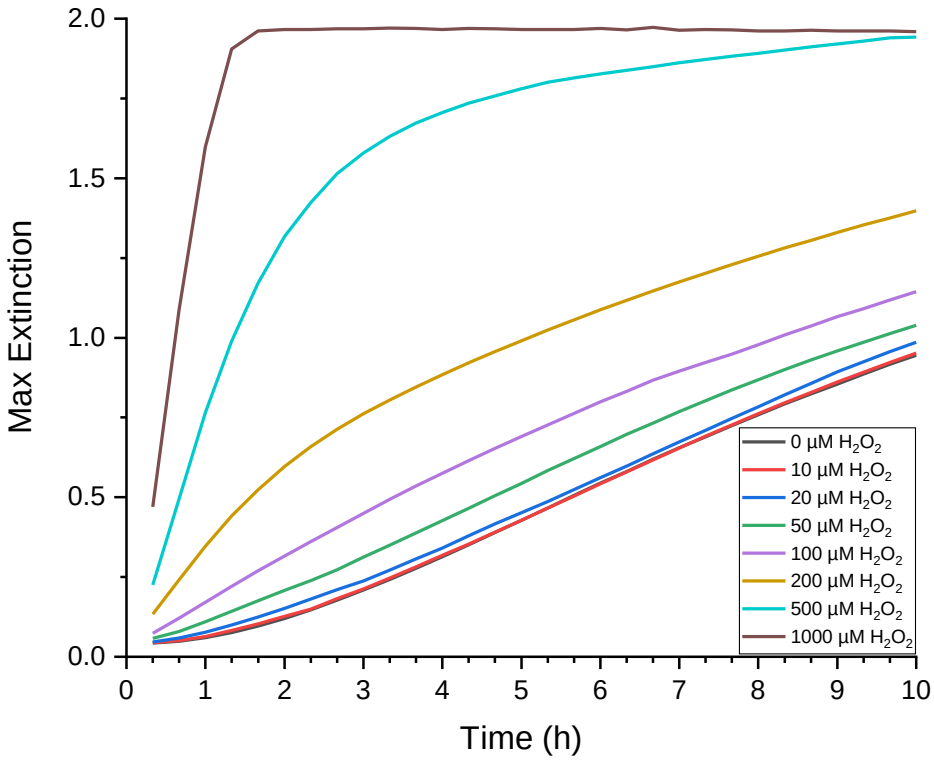


*Figure 5.7: Changes in maximum extinction with gold nanoparticle seed growth in the presence of varying concentrations of $H_2O_2$.*

Following around 100 min of reaction, the Au NPs had reached their maximum size in the presence of 1000 μM $H_2O_2$. This was due to the $HAuCl_4$ in solution being fully consumed during the course of the reaction. However, it took the sample containing 500 μM $H_2O_2$ 10 h to reach this size, and during the course of the experiment none of the other samples with lower reducing agent concentrations grew to their maximum size. Previously the Au NP seeds were allowed to grow for 20 min before their extinction was measured. However, the overnight growth results indicated that a longer growth period could be advantageous. If the NP seeds were left for 80 min

there would be a greater difference between the extinction intensities at different $H_2O_2$ concentrations, which could lead to a more sensitive experiment. (Figure 5.8)

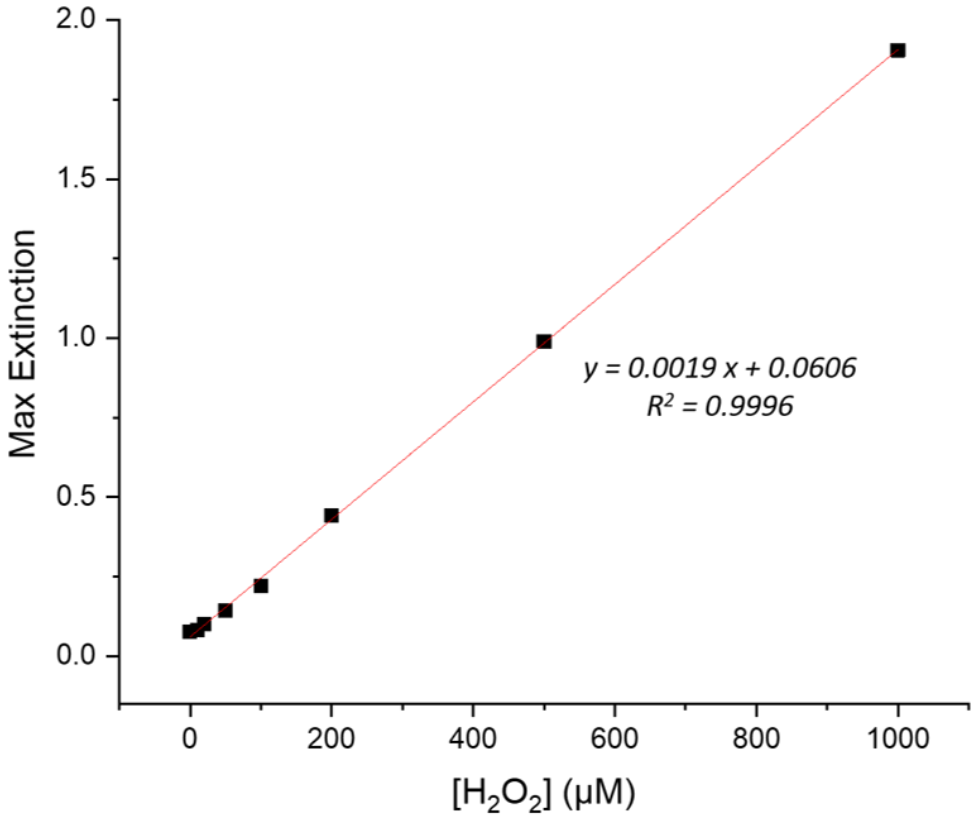


*Figure 5.8: Maximum extinction of gold nanoparticle seeds following incubation with varying concentrations of $H_2O_2$ and 0.6 mM $HAuCl_4$ for 80 minutes.*

As shown in Figure 4.8, when the Au NP extinctions were plotted following 80 min of growth the trend was still linear, since the maximum NP seed size had not been reached. However, the gradient of the line was more than 2.5 × that of the experiment following 20 min of growth. Therefore, extending the experimental time frame could allow for a greater differentiation between the response of the NP seeds to the reducing agent concentration, and therefore provide a more sensitive final assay.

## 5.4 Nanoparticle Growth Generated by Glucose Oxidase

### 5.4.1 Initial Glucose Oxidase Experiments

The next step in building the proposed assay for the detection of protein glycosylation was to use GOx to generate the $H_2O_2$ required for the reduction of $Au^{3+}$ to $Au^0$. GOx is an enzyme that catalyses the oxidation of Glc to D-glucono-1,5-lactone which spontaneously hydrolyses to gluconic acid and $H_2O_2$.[169] Therefore, attaching this enzyme to a glycan recognition molecule would ensure that $H_2O_2$ production would be representative of glycoprotein concentration, leading to a quantitative assay. As shown previously, Liu *et al*[166] followed this approach in their detection of PSA. The same research group also used this approach to produce a clinically relevant glucose detection assay for use in screening for diabetes.[170] Yan *et al*[171] also used GOx in the sensitive detection of thrombin, whereby the analyte presence allowed for $H_2O_2$ production, which caused Au seeds to grow on the surface of iron (III) oxide magnetic NPs. This resulted in a shift in the LSPR peak, and consequently a change in the colour of the solution.

Here, in order to generate sufficient $H_2O_2$ for $Au^{3+}$ reduction and in an attempt to maximise GOx concentration with each glycan present, a streptavidin-GOx polymer was used. This consisted of a polymer of 20 GOx enzymes functionalised with streptavidin at a ratio of 5:1, the presence of which would allow for binding to a biotinylated lectin in the final assay. Therefore, for every glycan detected there would be at least 5 GOx present for $H_2O_2$ production.

To confirm the reduction of Glc by the GOx polymer, TMB and HRP were used to provide a colorimetric response to the presence of $H_2O_2$. GOx is active over a pH range of 4 - 7,[172] with maximum oxidation of Glc taking place between pH 5.0 and 6.0.[173] Therefore, three sets of samples were prepared containing 1.67 mM Glc, 0.1 % v/v Tween 20, and 1 % BSA in pH 5.0 citrate-phosphate buffer with varying concentrations of GOx polymer. (3.33 µg/mL, 0.33 µg/mL, and 0.03 µg/mL) These were incubated with ELISA kit TMB and HRP for 1 h. (Figure 5.9)

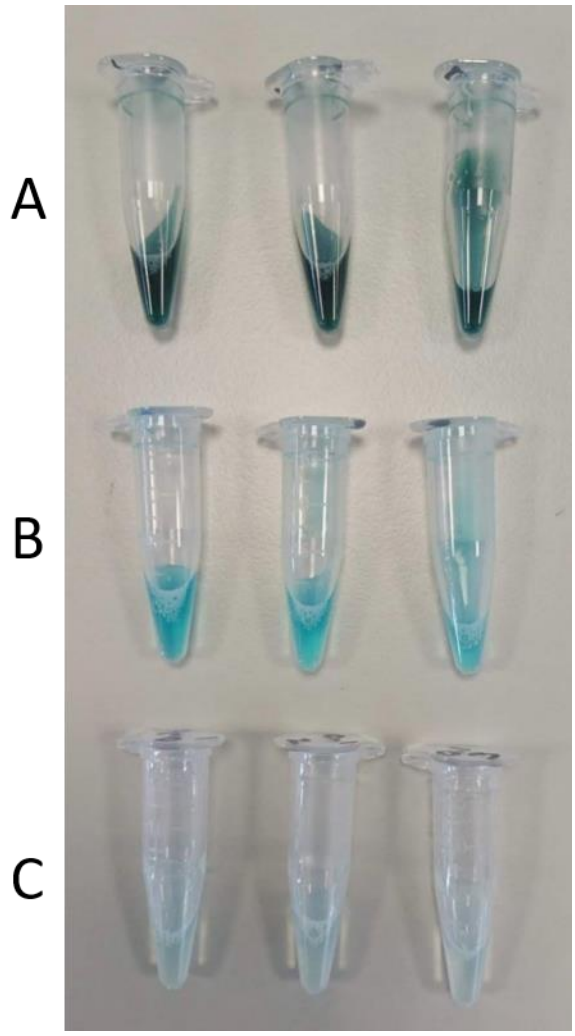


*Figure 5.9: Solutions of various concentrations of glucose oxidase incubated with 1.6 mM glucose, 3,3',5,5'-tetramethylbenzidine and horseradish peroxidase, producing a colorimetric response to the production of hydrogen peroxide. (A) 3.33 µg/mL GOx; (B) 0.33 µg/mL GOx; (C) 0.03 µg/mL GOx.*

There was a clear colorimetric response to the differences in GOx concentration with higher concentrations increasing the rate of Glc reduction and the subsequent oxidation of TMB to a blue charge-transfer complex. The darker blue colour produced showed that a higher concentration of the charge-transfer complex had been produced. This confirmed the production of $H_2O_2$ by the GOx polymer when Glc was present, so investigations could then be made in to the growth of Au NP seeds using this method of GOx production.

Similar to the experiments with TMB and HRP, 1.67 mM Glc was mixed with varying concentrations of GOx polymer (3.33 µg/mL, 0.33 µg/mL, 0.03 µg/mL, and blank control) and 0.6 mM $HAuCl_4$ in the presence of Au NP seeds in pH 5.0 citrate-

phosphate buffer containing 0.1 % v/v Tween 20 and 1 % BSA. Following an hour of incubation at room temperature the samples showed no significant colour change. The samples were left overnight and checked again, at which point a difference in colour could be seen in the samples. (Figure 5.10)

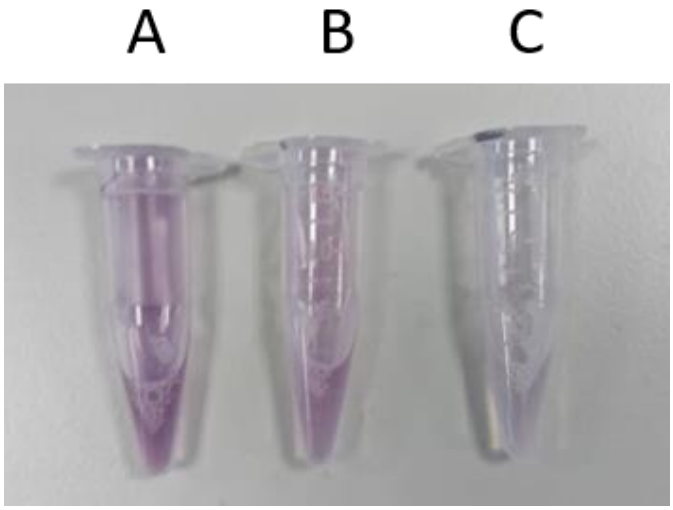


*Figure 5.10: Change in colour of gold nanoparticle seed solutions in the presence of glucose and various concentrations of glucose oxidase: (A) 3.33 µg/mL; (B) 0.33 µg/mL; (C) 0.03 µg/mL.*

The colour change in the samples indicated that the GOx was oxidising the Glc to produce $H_2O_2$, which in turn was reducing the $Au^{3+}$ to $Au^0$ and causing the Au NP seeds to grow. These samples, along with the sample containing no GOx, were analysed using extinction spectroscopy. (Figure 5.11) This showed a clear increase in the extinction of the LSPR peaks of the Au NP seed samples as the concentration of GOx was increased. Therefore, as more $H_2O_2$ was produced, the rate of reduction of $Au^{3+}$ increased and caused the extinction coefficient of the Au NPs to increase. However, the extinction of the blank sample containing no GOx did not follow the trend of the positive samples. The extinction of the Au NP seeds in the blank was between that of the 0.33 µg/mL and 3.33 µg/mL samples. As shown before (Figure 5.6(A)), the Au NP seeds will continue to grow with $Au^{3+}$ cations in solution without the presence of a reducing agent, but in this case the growth rate was faster than that of the samples where $H_2O_2$ was produced. The reason for this lies with the presence of proteins now in solution with the Au NP seeds. Previous experiments did not take in to account how the GOx would interact with the NP surface. It is well-

known that metallic NPs can be functionalised with proteins using non-covalent electrostatic and hydrophobic interactions.[110,174,175] Therefore, it is likely that the GOx polymer would interact with the NPs in solution and hinder the reduction of the $Au^{3+}$ cations on to the NP surface, resulting in a slower growth than observed previously.

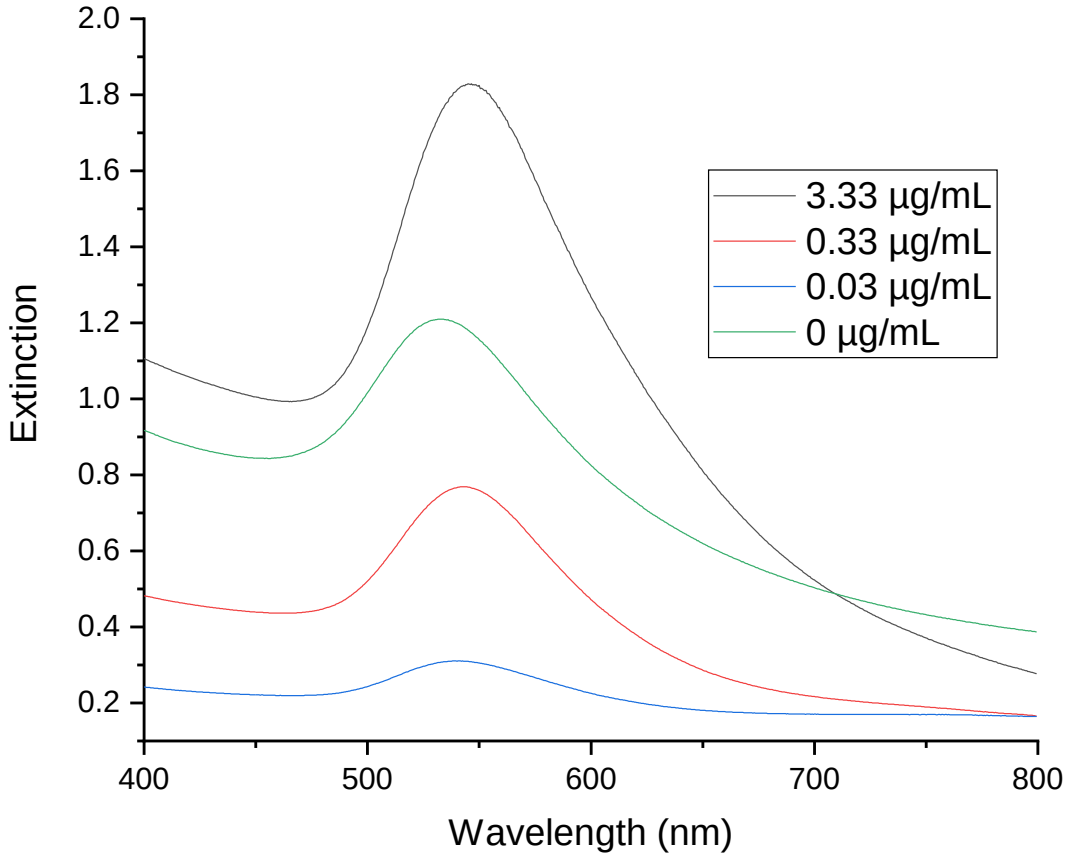


*Figure 5.11: Extinction spectra of the nanoparticle seeds grown using $H_2O_2$ produced by varying concentrations of GOx.*

This interaction between the GOx polymer and the Au NP seeds would influence the final assay. The growth would be much slower and result in an assay that required long incubation times, and potentially give blank samples with higher signals than positive controls. Therefore, different incubation conditions were explored in an attempt to increase the $H_2O_2$ production by the GOx.

## 5.4.2 Varying Growth Conditions

### *5.4.2.1 Room Temperature Conditions*

The GOx was incubated with Glc and the Au NP seeds under different conditions in a series of timed studies to determine whether or not the production of $H_2O_2$ could be improved. This would potentially produce enough reducing agent to overcome the hindrance by the proteins present in solution to give a concentration dependent growth pattern of the NPs, with a low blank signal.

Firstly, the growth was measured with the whole experiment carried out at room temperature. Following the same procedure as in the previous experiment, the extinctions of the growing Au NP solutions were measured every hour overnight (Figure 5.12) This gave a trend which could be used for comparison with other incubation conditions.

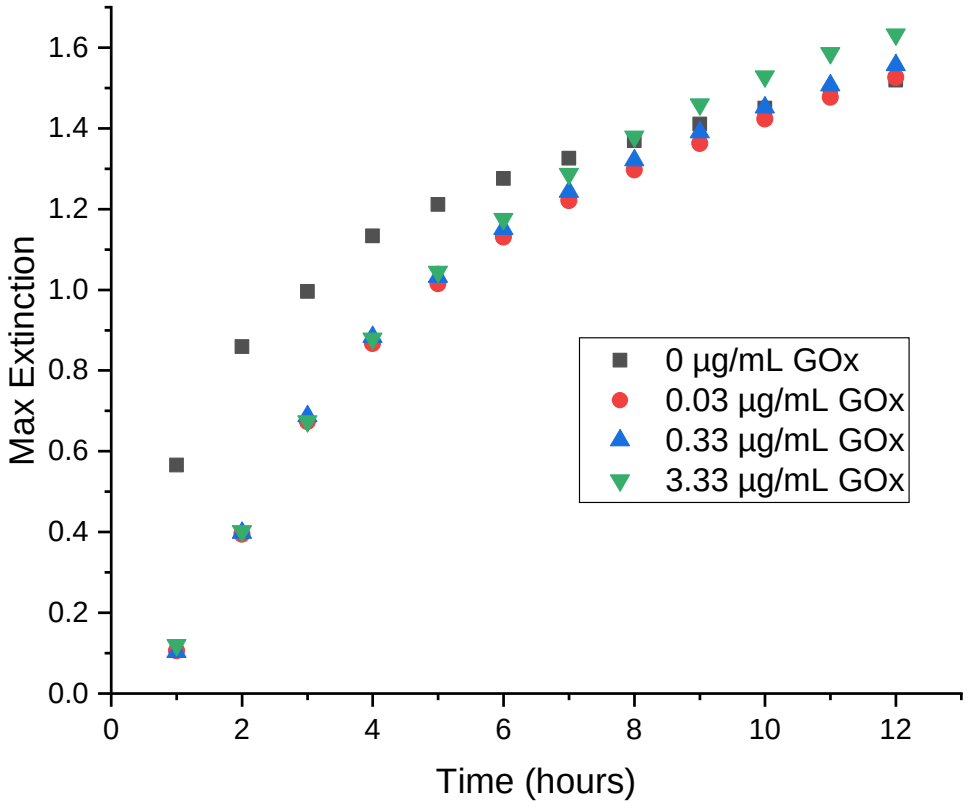


*Figure 5.12: Growth of nanoparticle seeds in the presence of $H_2O_2$ produced by varying concentrations of glucose oxidase at room temperature over a period of 12 hours.*

As expected from the previous experiment, the initial rate of NP growth was fastest for the sample where no protein was present. The samples containing GOx had slow initial growth. This was because the production of $H_2O_2$ was minimal at this point, and the interactions of the proteins with the NP surface were hindering the reduction of $Au^{3+}$ on to the NP crystal faces. It was only after around 9-10 h that the samples containing the GOx produced enough $H_2O_2$ to produce larger NPs than the blank samples. Also, although the sample containing 3.33 μg/mL GOx produced the largest NPs by the end of the 12 h followed by the 0.33 μg/mL and 0.03 μg/mL samples, the discrimination between the samples in term of maximum extinction was minimal. This highlighted the need for increased $H_2O_2$ production to overcome the hindrance of the NP seed growth and to produce a sensitive response to the reducing agent concentration.

#### *5.4.2.2 Glucose Oxidase Incubation with Glucose Before Addition of Gold Nanoparticle Seeds*

Due to the poor discrimination between the growth of NPs from samples with varying GOx concentration, incubation conditions were investigated. There is an exponential relationship between temperature and the reaction rate of an enzyme, whereby for every 10 °C increase the reaction rate will double.[173] Most enzymes will denature at temperatures between 40 °C and 70 °C. However, GOx shows an optimum oxidation rate of Glc at temperatures from 40 °C to 60 °C.[173] Therefore, in order to investigate whether or not temperature could be used to an advantage in NP growth, GOx was incubated at 40 °C in a Glc solution for 1 h before the addition of $HAuCl_4$ and Au NP seeds. The extinction was then measured every 10 min for 1 h. (Figure 5.13(A)) The sample containing no GOx showed a clear exponential increase in the NP extinction, showing an increasing rate of reduction of $Au^{3+}$ on to the NP surface even though there was no reducing agent present. However, as previously shown the reduction of $Au^{3+}$ still takes place in the presence of Au NP seeds, and the rate of this could be expected to increase at higher temperatures. The samples which had GOx present, and therefore should have produced $H_2O_2$ to increase the $Au^{3+}$ reduction rate, also

showed an exponential trend, although much slower than the blank sample. The presence of protein in solution was still an issue in slowing the growth rate by hindering the access of the $Au^{3+}$ to the NP surface. However, the sample containing 3.33 μg/mL GOx did show the greatest growth in comparison to the 0.33 μg/mL and 0.03 μg/mL GOx samples, although the difference in extinction was minimal.

In comparing the trends viewed in Figure 5.12 and Figure 5.13(A), there are clear differences. The incubation of the GOx with Glc at 40 °C seemed to induce an exponential growth in the extinction, whereas this growth decreased over time in previous experiments. This was investigated further by measuring the extinction every hour overnight following 1 h of GOx and Glc incubation. (Figure 5.13(B))

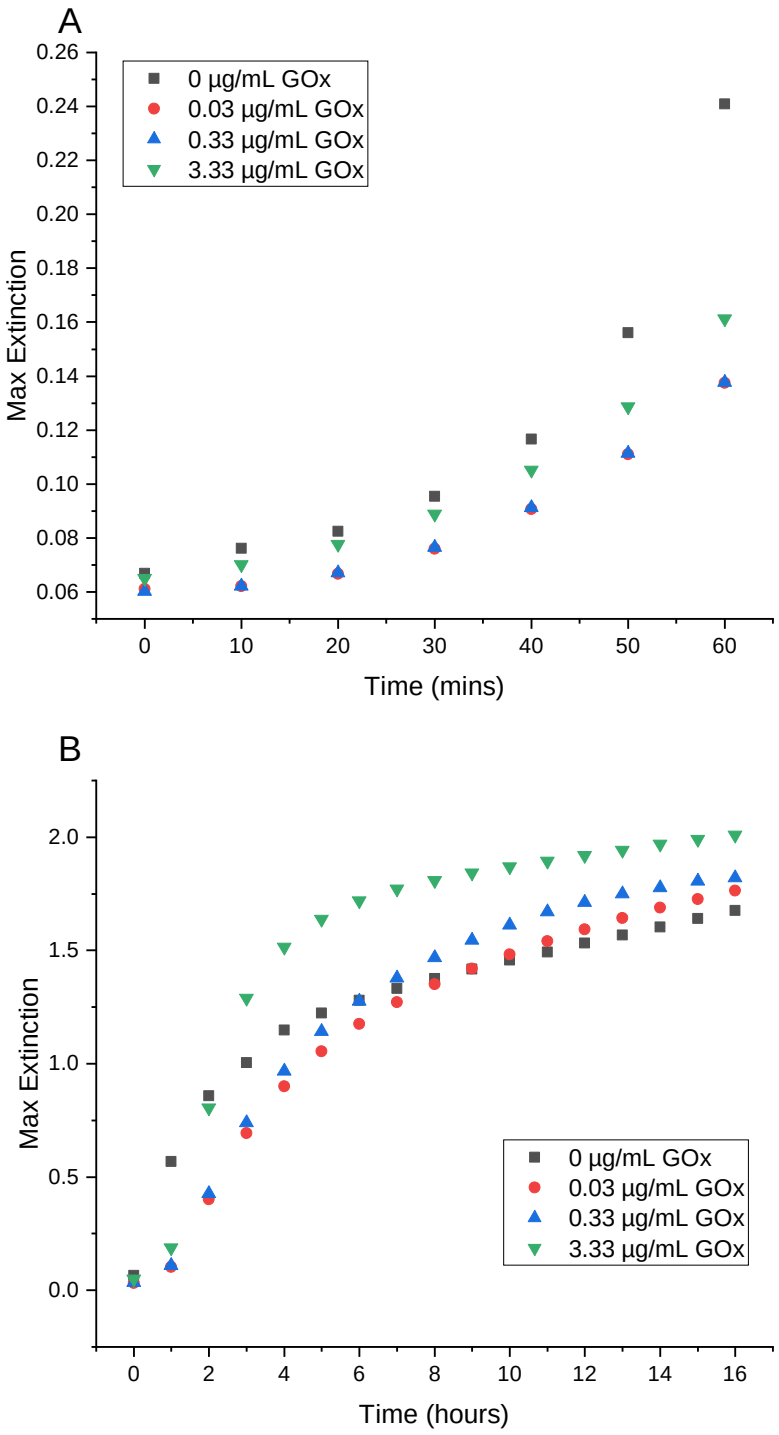


*Figure 5.13: Growth of nanoparticle seeds after being added to a solution of glucose and glucose oxidase which had been incubated at 40 °C for 1 hour. (A) Extinction measurements every 10 minutes for 1 hour. (B) Overnight extinction measurements taken once every hour.*

This showed a trend which contrasted the exponential increase in extinction viewed within the first hour of measurements. (Figure 5.13(A)) This suggested that following around an hour of substrate-enzyme reaction, there was a change in reaction rate.

This was due to Michaelis-Menten enzyme kinetics where the rate of enzymatic conversion of a substrate to a product slows as the maximum number of enzyme sites are filled by substrate moieties.[173] As the GOx and Glc were initially mixed, the substrate sites on the enzyme were filled and $H_2O_2$ was produced quickly. This $H_2O_2$ could then be used to reduce the $Au^{3+}$ on to the NP surface. However, following this initial production, the substrate dissociation rate from the enzyme would affect subsequent product generation, and the rate of $H_2O_2$ production would slow. This then means that initial NP growth would be faster than later growth once the enzyme sites were filled.

The incubation of the GOx and Glc prior to addition of Au NP seeds and $HAuCl_4$ did seem to be effective over the experimental time frame. Making a direct comparison between the samples without prior incubation of GOx and Glc (Figure 5.12) and those incubated at 40 °C (Figure 5.13(B)) the extinction of the samples containing 3.33 µg/mL GOx became greater than that of the blank samples at a much earlier time point. Without incubation, the sample containing 3.33 µg/mL GOx took 8 h to reach the same extinction intensity as the blank sample, whereas in the incubated samples, this happened between 2 and 3 h of measurements. However, the results of the lower GOx concentrations were comparable regardless of whether there was incubation of the GOx and Glc at 40 °C or not. These results suggested that there was a benefit to the incubation step since there was a greater discrimination between the extinction of the Au NPs with the higher GOx concentration and those with the lesser GOx presence. However, the lack of difference between the lower concentrations suggested that the concentration of the enzyme could be an issue in developing a sensitive assay.

#### *5.4.2.3 Constant Incubation of Glucose Oxidase and Glucose in Presence of Gold Nanoparticle Seeds*

The effectiveness of the increased temperature on the enzymatic conversion of Glc to $H_2O_2$ was then investigated further. Here the GOx and Glc were added to Au NP

seeds and $HAuCl_4$ and incubated at 40 °C. The extinction was measured every hour for 5 h, with the samples maintained at 40 °C between measurements. (Figure 5.14)

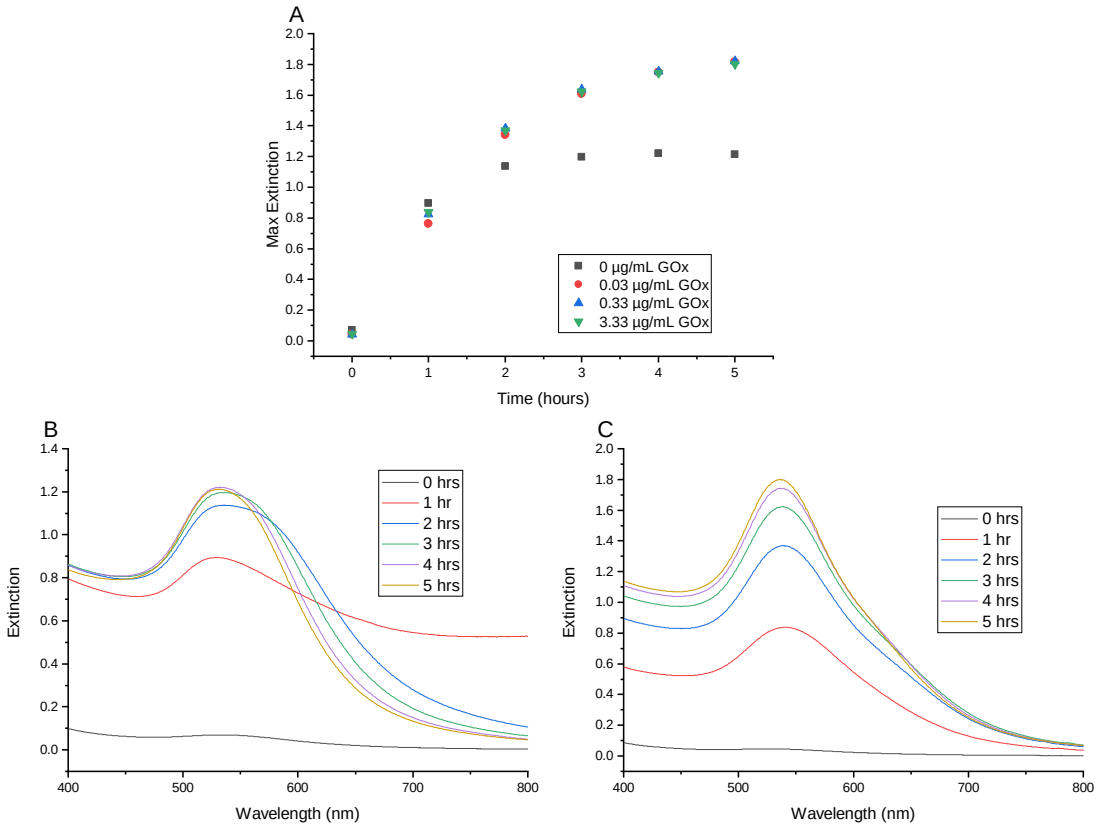


*Figure 5.14: Growth of the Au NP seeds in presence of glucose and glucose oxidase with constant incubation at 40 °C: (A) Maximum extinction of each sample measured every hour; (B) Extinction spectra measured every hour of the blank sample; (C) Extinction spectra measured every hour of the sample containing 3.33 µg/mL glucose oxidase.*

The constant incubation at 40 °C throughout the experimental time frame produced another difference in the Au NP growth pattern. Here, the samples containing GOx surpassed the growth level of the NPs in the blank sample just after 1 h of reaction. (Figure 5.14(A)) This was an improvement over the previous conditions with regards to the blank sample in the final assay. This could potentially allow for a much lower signal when no target glycoprotein is present. However, an interesting and unexpected result was that the maximum growth of the NPs in the blank sample was reached giving a much lower extinction than the samples containing GOx. (Figure 5.14(A)) All samples contained the same concentration of Au NP seeds and $HAuCl_4$. Therefore, in theory all Au NP seeds should eventually grow to the same size, with

the measurable difference coming in the rate in which the samples reached this level. This was not observed in this case. It is not known exactly why this happened, however some clues may be present in the extinction spectra.

The spectra measured for the Au NP seeds in the blank sample (Figure 5.14(B)) did not initially have the characteristic shape of a monodispersed Au colloid. Following 1 h of reaction, the LSPR peak had increased significantly in intensity, due to the NP growth and subsequent increase in extinction coefficient. However, the extinction measured at longer wavelengths was much higher than would be expected for Au NPs of this size. The greater extinction would normally indicate the aggregation of Au colloids, which could mean that the NPs were forming networks of multimers as well as growing. However, as the experiment continued the LSPR peak narrowed, but showed the appearance of a shoulder at around 575 nm. This could indicate the presence of different populations of NP sizes. The peak also continued to narrow as the experiment proceeded. These spectra were very different from the measured spectra in the sample containing 3.33 μg/mL. (Figure 5.14(C)) In those spectra the LSPR peak maintained a similar shape throughout the experiment with the main difference being the increase of the LSPR peak intensity.

Through comparing these spectra, a hypothesis can be presented. The broader and more irregular shape, and the subsequent lower LSPR peak intensity of the blank sample, (Figure 5.14(B)) would suggest that there is irregular growth of the NPs occurring. The broad peak following 1 h of reaction could be due to lack of spherical growth of the NPs. The increased temperature of the sample, as mentioned previously, would increase the rate of reduction of $Au^{3+}$ on to the NP surface, but this could take place in specific areas causing certain crystal faces to grow more rapidly than others. As the reaction proceeds, the remaining $Au^{3+}$ could then be reduced on to the other crystal faces, resulting in a gradually more spherical particle, which would produce a much narrower LSPR peak, with the additional shoulder being due to the presence of more than one aspect ratio of the NPs, as seen in the case of gold nanorods.[176] The consistent narrow LSPR peak when GOx was present (Figure 5.14(C)) could be due to the presence of proteins in solution mediating the NP growth

by controlling the $Au^{3+}$ reduction on to the NP surface. This would result in spherical growth and a much higher LSPR peak intensity, as viewed in the timed experiments.

Aside from this, however, it was clear that there was no significant difference between the samples containing different concentrations of GOx. This suggested that the concentration of GOx would need to be increased significantly to produce the desired response in the NP growth.

## 5.5 Using Magnetic Beads to Maximise Enzyme Activity

It was clear that the concentrations of GOx were not enough to produce concentrations of $H_2O_2$ which were significantly different to induce varying NP growth rates. Therefore, a support was investigated to maximise the presence of GOx per unit of detected glycan. Liu *et al*[166] used NHS-activated magnetic beads in their prostate cancer detection assay for facile attachment of GOx. This resulted in the presence of approximately 76 000 GOx units on each bead, significantly increasing the concentration per unit of target analyte.[166] A similar approach was used here to increase the GOx concentration.

Magnetic beads with a diameter of 1 µm were purchased already functionalised with an NHS ester. The beads (300 µL, 10 mg/mL) were first washed with ice cold HCl (1 mM) and then mixed with GOX polymer, (300 µL, 0.5 mg/ml) allowing for facile binding of the enzyme through a primary amine in the protein structure. (Figure 5.15) The beads could then be purified using a magnet and washed to be used in the NP growth assay.

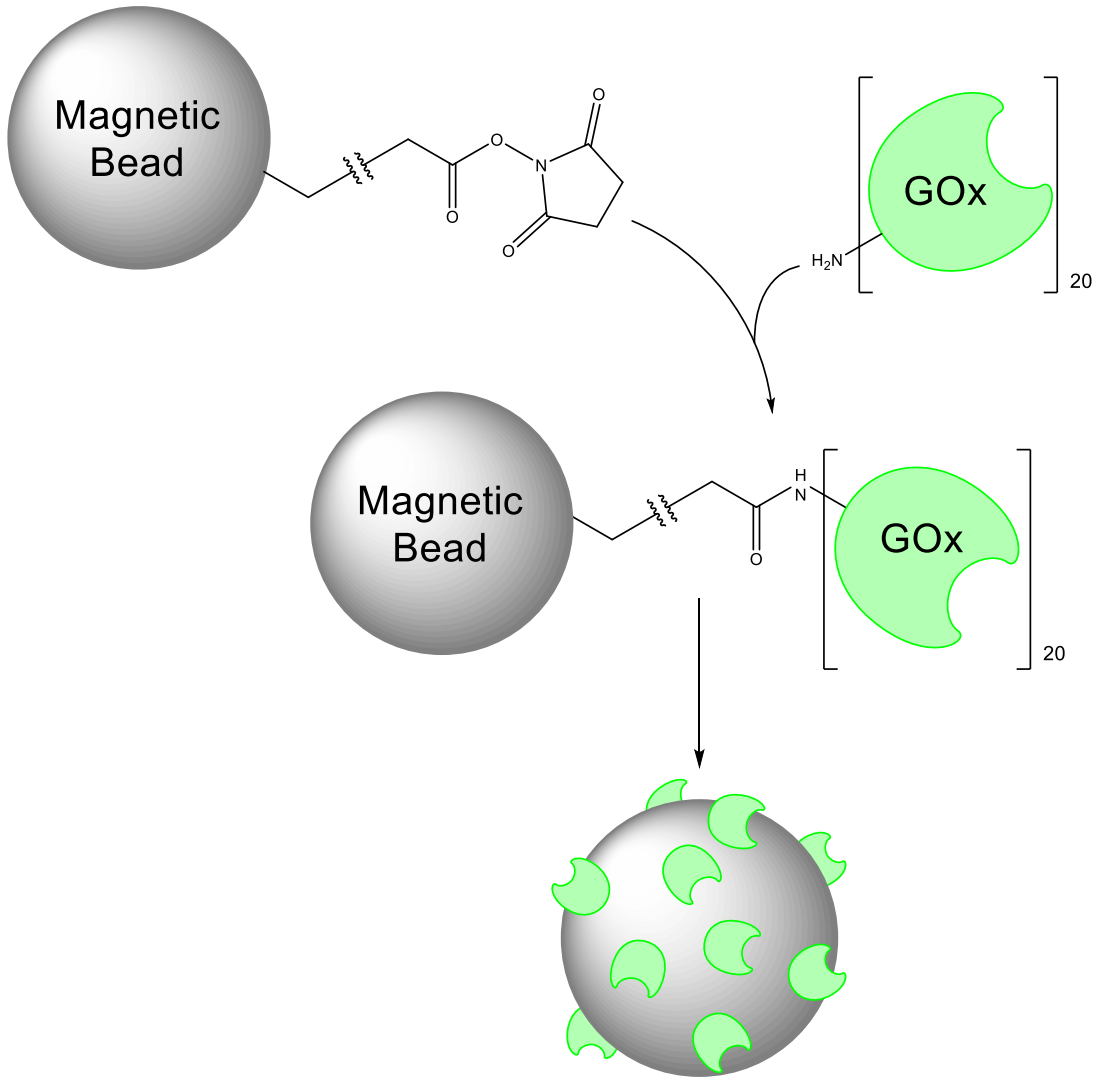


*Figure 5.15: Functionalisation of NHS-activated magnetic beads with a streptavidinated glucose oxidase polymer.*

## 5.5.1 Measuring Protein Binding

Following protein conjugation, the binding of the GOx polymer to the surface of the beads was measured using a bicinchoninic acid (BCA) assay which gives a colorimetric response that can be related to the protein concentration. The BCA assay was first developed by Smith *et al*[177] in 1985, which utilises the biuret-like reaction of polypeptides in reducing $Cu^{2+}$ cations to $Cu^{+}$ in alkaline conditions producing a pale blue colour. This is then followed by chelation of two BCA molecules to the remaining $Cu^{+}$ to produce an intense purple colour. (Figure 5.16)

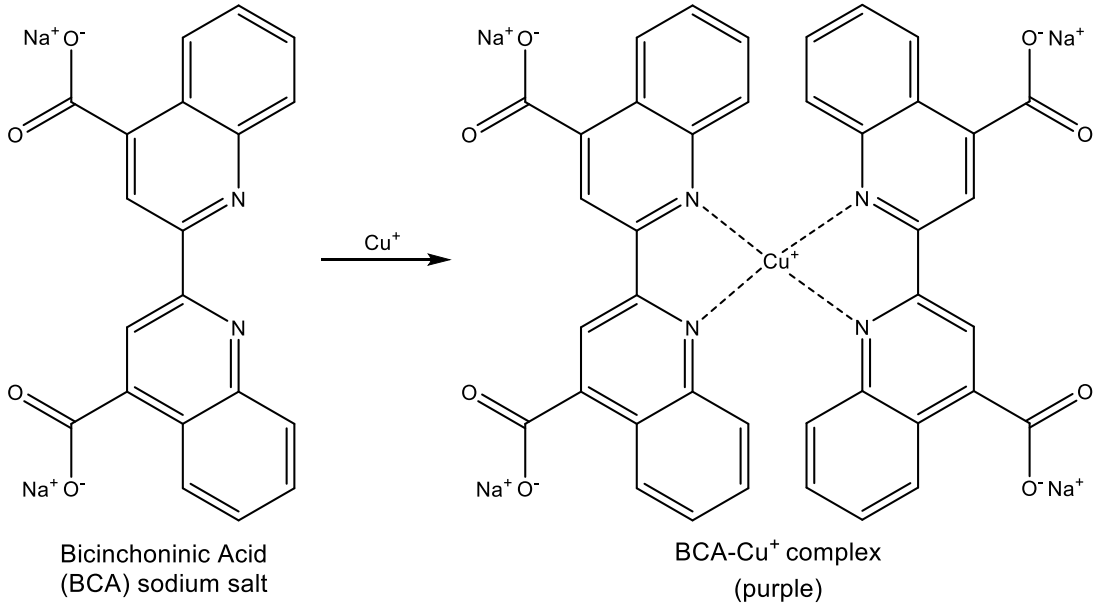


*Figure 5.16: Following reduction of $Cu^{2+}$ to $Cu^{+}$ by a polypeptide, a complex forms between bicinchoninic acid and a $Cu^{+}$ cation which is purple in colour, giving an absorption at 562 nm directly proportional to protein concentration.*

The resulting coloured complex has an absorbance at 562 nm which is directly proportional to the concentration of the protein in solution. This simple assay allows for simple protein quantification, so was ideal for the determination of GOx concentration bound to the magnetic beads.

#### *5.5.1.1 BCA Assay of Magnetic Beads Supernatant*

Following attachment of GOx to the magnetic beads, a magnet was used for purification. The beads were gathered, and the supernatant was tested using a BCA assay to determine the remaining concentration of GOx in solution, which would allow the bound concentration to be calculated.

Firstly, the BCA standards were prepared alongside the supernatant sample dilutions. Each sample (150 µL) was mixed with the BCA working reagent (150 µL) in a 96-well plate and incubated at 37 °C for 2 h. The plates were then cooled to RT and the absorbance was measured at 562 nm. The overall absorbance for each sample was corrected using the values from the blank sample. (Table 5.3)

*Table 5.3: Absorbance values obtained from the BCA assay of the supernatant from the magnetic beads conjugation, with final values following correction using the blank sample.*

| **Concentration** *µg/mL* | **Sample** | **Abs** | **Corrected Abs** | **Ave Corrected Abs** | **Std Dev** |
|---|---|---|---|---|---|
| 200 | A1 | 2.882 | 2.843 | 2.850 | 0.012 |
| | A2 | 2.884 | 2.844 | | |
| | A3 | 2.903 | 2.864 | | |
| 40 | B1 | 0.882 | 0.842 | 0.850 | 0.011 |
| | B2 | 0.884 | 0.844 | | |
| | B3 | 0.902 | 0.863 | | |
| 20 | C1 | 0.517 | 0.478 | 0.468 | 0.024 |
| | C2 | 0.480 | 0.441 | | |
| | C3 | 0.523 | 0.484 | | |
| 10 | D1 | 0.258 | 0.218 | 0.235 | 0.029 |
| | D2 | 0.257 | 0.218 | | |
| | D3 | 0.308 | 0.269 | | |
| 5 | E1 | 0.156 | 0.116 | 0.117 | 0.008 |
| | E2 | 0.165 | 0.125 | | |
| | E3 | 0.149 | 0.110 | | |
| 2.5 | F1 | 0.093 | 0.054 | 0.049 | 0.005 |
| | F2 | 0.083 | 0.044 | | |
| | F3 | 0.088 | 0.049 | | |
| 1 | G1 | 0.058 | 0.018 | 0.018 | 0.002 |
| | G2 | 0.055 | 0.016 | | |
| | G3 | 0.060 | 0.020 | | |
| 0.5 | H1 | 0.047 | 0.008 | 0.013 | 0.009 |
| | H2 | 0.063 | 0.024 | | |
| | H3 | 0.048 | 0.009 | | |
| 0 | I1 | 0.041 | | | |
| | I2 | 0.040 | N/A | N/A | N/A |
| | I3 | 0.037 | | | |
| Unknown GOx concentration in supernatant | U1in25 | 3.121 | 3.082 | N/A | N/A |
| | U1in10 | 3.168 | 3.129 | | |
| | U1in5 | 3.110 | 3.070 | | |
| | U1in50 | 2.575 | 2.535 | | |
| | U1in100 | 1.465 | 1.426 | | |

The average corrected absorbance values for the BCA assay standards gave a linear response with respect to the protein concentration. (Figure 5.17) The micro BCA assay kit used is only linear up to concentrations of 40 µg/mL. Therefore, the supernatant samples were diluted to bring the GOx concentration in to the linear

range. However, the measured absorbance values were much higher than those obtained in the linear range, even when diluted by a factor of 100. (Table 5.3)

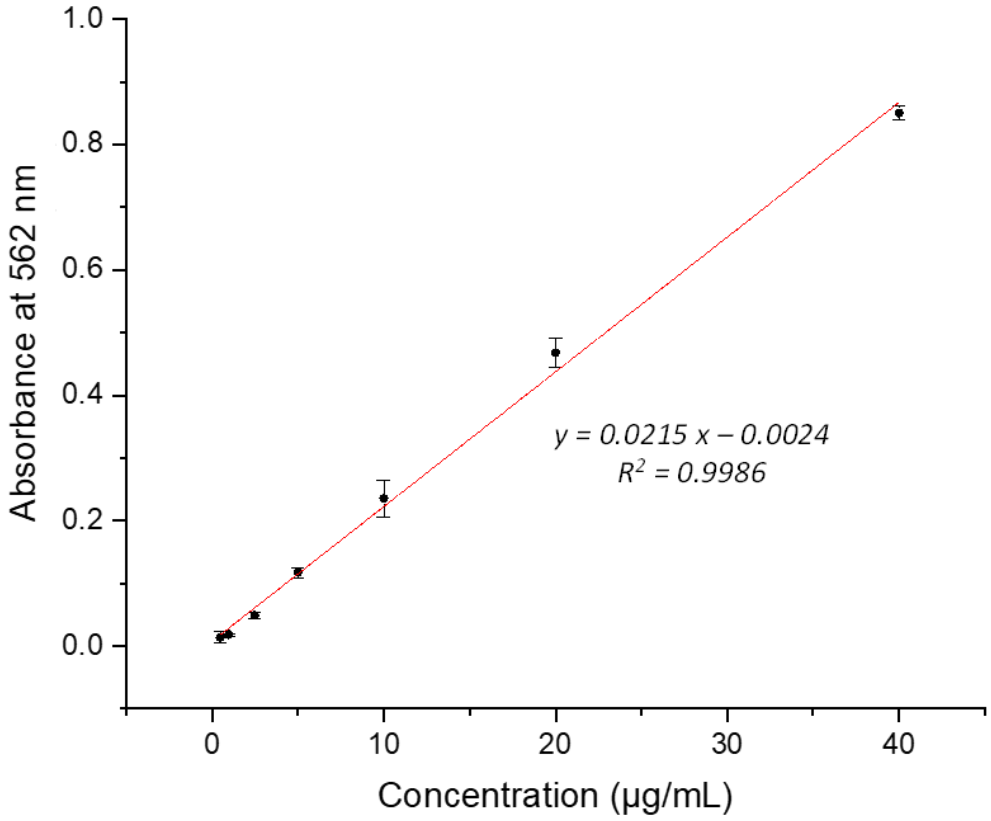


*Figure 5.17: Linear response from the BCA assay calibration graph relating the protein concentration to the measured absorption at 562 nm.*

Using the equation of the line from the calibration graph, the concentration of the most dilute supernatant sample would be calculated at 66.5 µg/mL, assuming the linear range extended beyond 40 µg/mL. This would translate to an initial supernatant protein concentration of 6.65 mg/mL which was much greater than the 0.5 mg/mL GOx solution added. However, in order to obtain a more accurate result, the supernatant sample was further diluted, and compared to the original GOx stock solution.

### 5.5.1.2 Comparison of Glucose Oxidase Stock with Magnetic Beads Supernatant

To obtain an accurate supernatant protein concentration, the sample was diluted by factors of 500 and 1000 to bring the concentration in to the BCA assay linear range. Alongside this, the GOx stock solution was also diluted by a factor of 1000. (Table 5.4)

*Table 5.4: Measured and corrected absorbance values from BCA assay comparing diluted supernatant and gluocse oxidase stock samples.*

| **Concentration** *µg/mL* | **Sample** | **Abs** | **Corrected Abs.** | **Ave Corrected Abs** | **Std. Dev.** |
|---|---|---|---|---|---|
| 200 | A1 | 2.878 | 2.802 | 2.824 | 0.019 |
| | A2 | 2.909 | 2.833 | | |
| | A3 | 2.914 | 2.838 | | |
| 40 | B1 | 0.898 | 0.822 | 0.855 | 0.046 |
| | B2 | 0.913 | 0.837 | | |
| | B3 | 0.984 | 0.907 | | |
| 20 | C1 | 0.527 | 0.451 | 0.459 | 0.021 |
| | C2 | 0.519 | 0.443 | | |
| | C3 | 0.559 | 0.483 | | |
| 10 | D1 | 0.308 | 0.232 | 0.238 | 0.018 |
| | D2 | 0.300 | 0.224 | | |
| | D3 | 0.334 | 0.258 | | |
| 5 | E1 | 0.189 | 0.112 | 0.115 | 0.012 |
| | E2 | 0.180 | 0.103 | | |
| | E3 | 0.204 | 0.128 | | |
| 2.5 | F1 | 0.122 | 0.046 | 0.062 | 0.035 |
| | F2 | 0.113 | 0.037 | | |
| | F3 | 0.178 | 0.102 | | |
| 1 | G1 | 0.085 | 0.009 | 0.012 | 0.004 |
| | G2 | 0.088 | 0.012 | | |
| | G3 | 0.092 | 0.016 | | |
| 0.5 | H1 | 0.107 | 0.031 | 0.014 | 0.016 |
| | H2 | 0.077 | 0.001 | | |
| | H3 | 0.086 | 0.010 | | |
| 0 | I1 | 0.075 | | | |
| | I2 | 0.069 | N/A | N/A | N/A |
| | I3 | 0.084 | | | |
| Unknown | U1in500 | 0.398 | 0.322 | 0.322 | N/A |
| | U1in1000 | 0.243 | 0.167 | 0.167 | N/A |
| GOx | GOx1 | 0.554 | 0.478 | 0.471 | 0.011 |
| | GOx2 | 0.534 | 0.458 | | |
| | GOx3 | 0.553 | 0.476 | | |

In this BCA assay, the absorbance values measured from the supernatant and stock GOx samples did fall within the assay linear range. A graph was then plotted to obtain the unknown concentrations. (Figure 5.18)

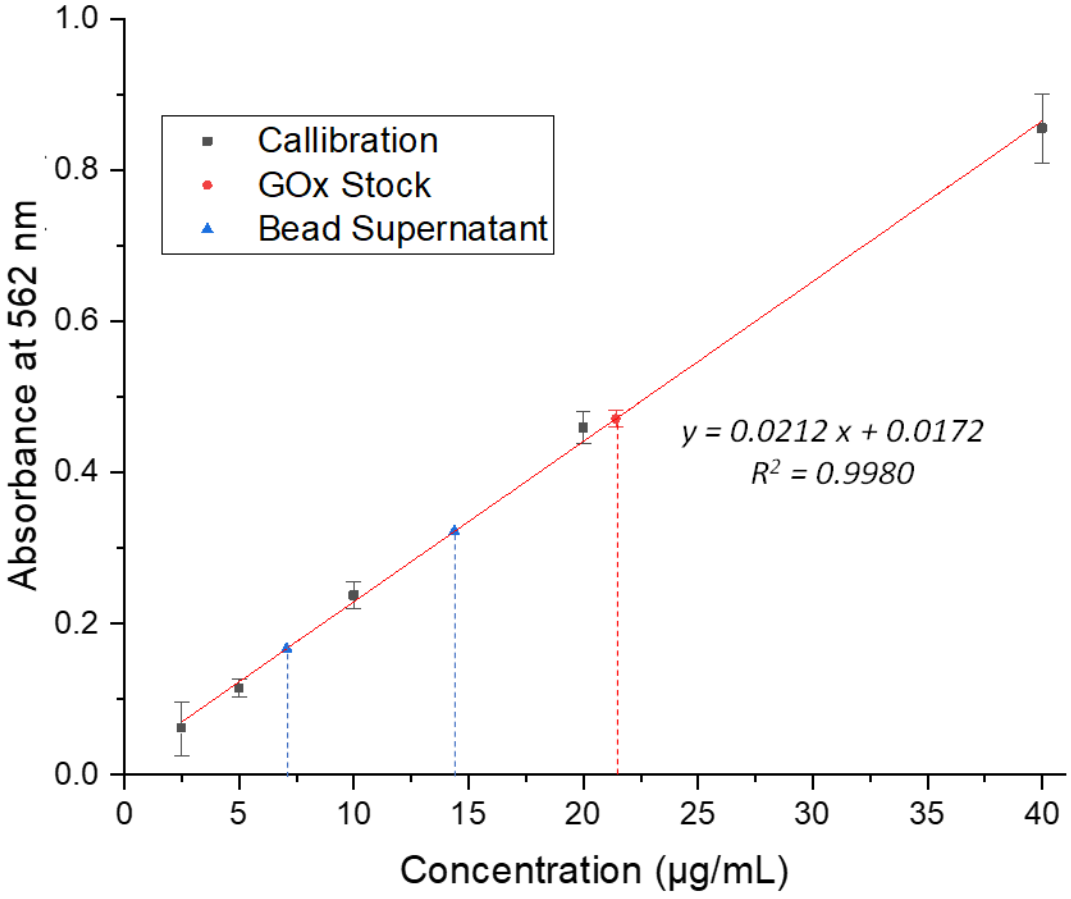


*Figure 5.18: Linear response from the BCA assay standard solutions (black squares) with the recorded absorbance values of the supernatant (blue triangles) and glucose oxidase stock solutions. (red circle)*

Using the equation of the line, the concentrations of the 500 × and 1000 × dilute bead supernatant samples were calculated to be 14.38 µg/ and 7.07 µg/mL, respectively. This equates to an average supernatant concentration of 7.13 mg/mL protein. This was interesting since a 0.5 mg/mL solution of GOx was added to the beads. The stock solution of 1 mg/mL GOx polymer was also tested at a 1000 × dilution and found to contain 21.42 µg/mL protein, meaning that the stock solution contained 21.42 mg/mL protein.

The GOx polymer solution is supplied as a 1 mg/mL solution in 0.1 M potassium phosphate buffer. However, it also contains 1200 ppm of 5-bromo-5-nitro-1,3-

dioxane as a preservative, along with 10 mg/mL ultra-dialysed biotin-free BSA for stability. Therefore, the presence of the BSA in solution accounts for the higher than expected absorbance values. However, the measured concentrations were still much higher than would be expected. The presence of different proteins in solution, however, could potentially affect the accuracy of the assay.

The stock solution of GOx polymer contained 1 mg/mL GOx which was diluted to 0.5 mg/mL before addition to the magnetic beads. Using the stock solution concentration calculated from the BCA assay, (21.42 mg/mL) this would equate to a total protein concentration of 10.71 mg/mL. Therefore, since the supernatant was calculated to contain 7.13 mg/mL protein, it could be assumed that the total final protein concentration on the magnetic beads was 3.58 mg/mL. This would be a mix of BSA and GOx but would still result in an increased concentration of GOx present per detected analyte in solution. The beads were therefore tested for their GOx activity.

### 5.5.2 Measuring Bound Glucose Oxidase Activity

The functionalised magnetic beads were assessed for their glucose oxidase activity using TMB and HRP. The beads were diluted to various concentrations (Table 5.5) and mixed with a solution of 1.67 mM glucose containing ELISA kit TMB and HRP. They were also compared with dilutions of the GOx stock solution. The solutions were incubated at RT for 30 min and the colorimetric responses were viewed. (Figure 5.19)

*Table 5.5: Concentrations of magnetic beads used to assess the catalytic activity of the attached glucose oxidase, in comparison to free polymeric glucose oxidase.*

| | Sample | Concentration |
|---|---|---|
| A | Magnetic beads | 1 mg/mL |
| B | Magnetic beads | 100 µg/mL |
| C | Magnetic beads | 10 µg/mL |
| D | Magnetic beads | 1 µg/mL |
| E | Magnetic beads | 100 ng/mL |
| F | Magnetic beads | 10 ng/mL |
| G | Magnetic beads | 1 ng/mL |
| H | Magnetic beads | 100 pg/mL |
| I | GOx polymer | 10 µg/mL |
| J | GOx polymer | 1 µg/mL |
| K | GOx polymer | 100 ng/mL |

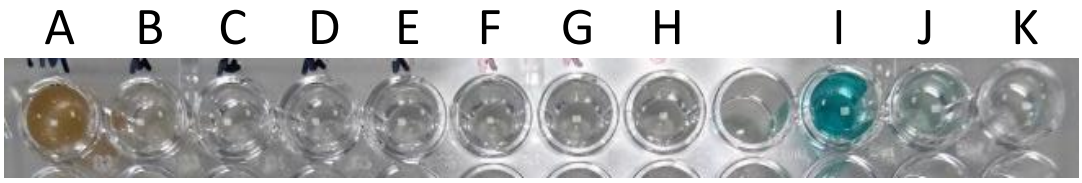


*Figure 5.19: Colorimetric responses of the magnetic beads in comparison to the polymeric glucose oxidase. Concentrations used are shown in Table 5.5.*

As can be seen clearly in Figure 5.19, in the magnetic bead samples there was no oxidation of TMB to form a blue charge transfer complex, indicating that no $H_2O_2$ was present. This suggests that the functionalisation of the magnetic beads was either unsuccessful, perhaps due to NHS hydrolysis, or that the concentration of BSA in the stock solution was too high, such that this completely coated the beads, without sufficient GOx attachment.

Attempts were made to purify the GOx stock solution by using a centrifugal filter unit with a nominal molecular weight limit of 100 kDa. Therefore, the 66.5 kDa BSA should pass through the filter, leaving behind a concentrated solution of GOx polymer, which has a molecular weight of approximately 3500 kDa. However, both fractions were

tested using a BCA assay. This found the BSA fraction to contain 1.8 mg/mL, meaning that there would still be 8.2 mg/mL present in the GOx fraction. The diluted GOx fraction was still outside the linear range of the assay, so would be estimated at 15.96 mg/mL, confirming that the purification was not effective. It was then decided to abandon the use of the magnetic beads in the assay due to time constraints.

## 5.6 Final Glycosylation Detection Assay Attempt

A final attempt was made to carry out the glycosylation detection assay utilising Au NP growth as the measured response. However, an enzyme-linked lectin assay format was followed, in that a capture antibody was not used. This relied on the binding of the glycoprotein, RNase B, directly to the 96-well plate. A biotinylated GNA was then used to detect the high-Man glycan, to which the streptavidinated GOx polymer could bind and provide the catalytic conversion of Glc to gluconic acid. This would produce the $H_2O_2$ required to reduce $Au^{3+}$ cations on to Au NP seeds, causing the NPs to grow. (Figure 5.20)

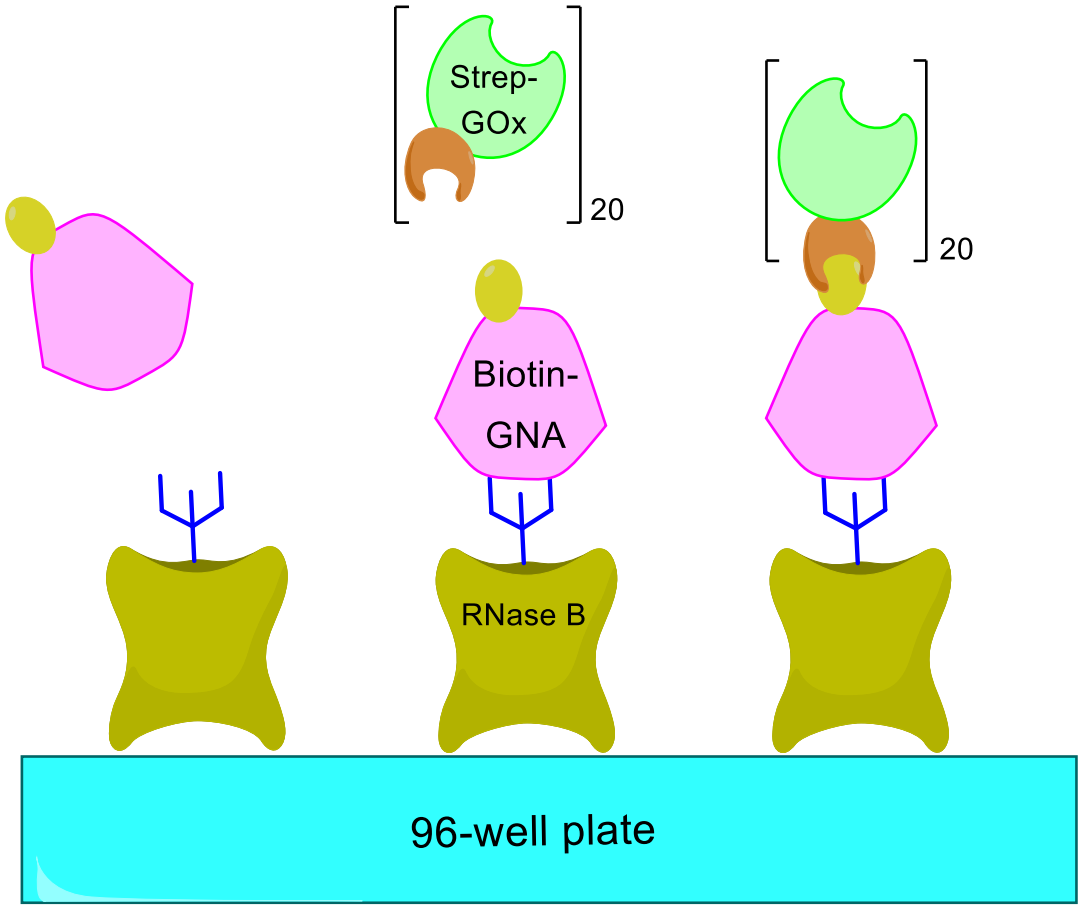


*Figure 5.20: Format of the enzyme linked lectin assay used showing RNase B bound directly to the 96-well plate. This was then detected by a biotinylated lectin, which was subsequently bound by a streptavidinated-glucose oxidase polymer. This would produce $H_2O_2$ in the presence of glucose to promote nanoparticle growth.*

Different concentrations of RNase B were tested, 10 µg/mL (667 nM), 5 µg/mL (333 nM), and 1 µg/mL (67 nM). Following the addition of the Glc, Au NP seeds, and $HAuCl_4$, the assay was incubated for 1 h at 35 °C to allow the NPs to grow in the presence of the produced $H_2O_2$. The samples were then analysed using extinction spectroscopy. (Figure 5.21)

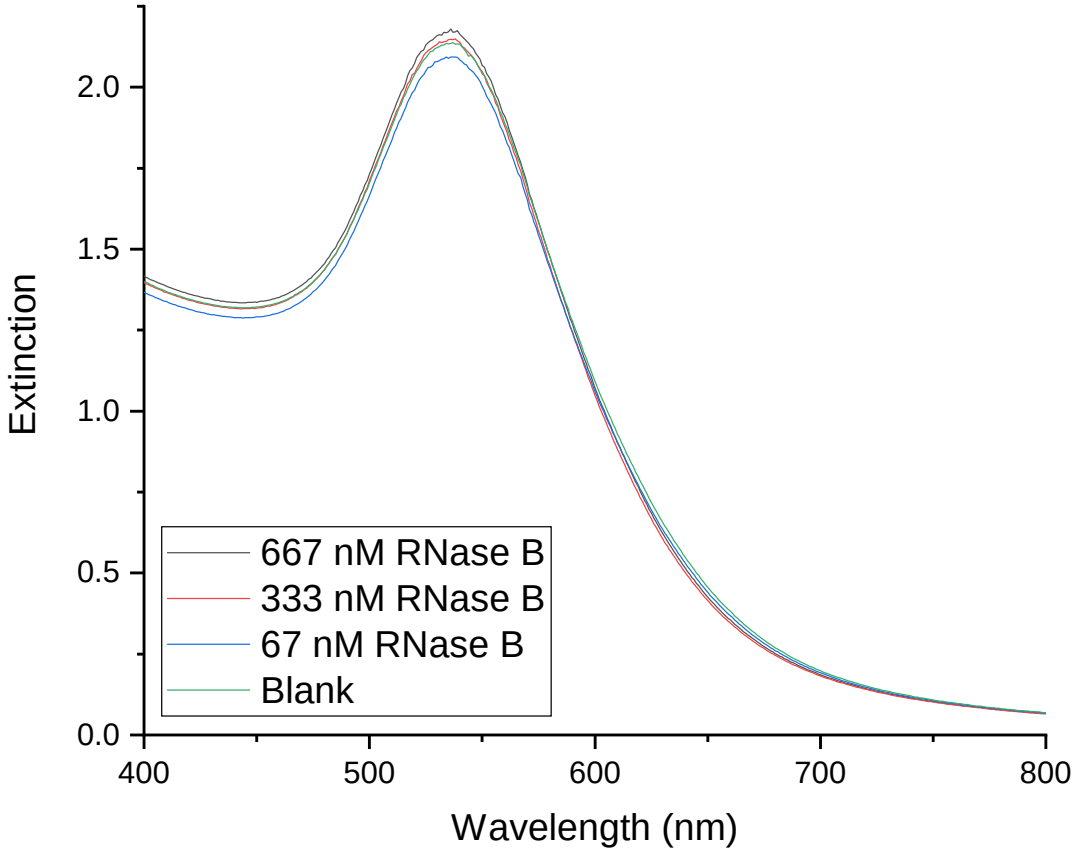


*Figure 5.21: The extinction spectra of the nanoparticle seeds following growth in the glycosylation detection assay.*

The NP seeds had grown over the experimental time frame, but there was no significant difference in maximum extinction between the samples with varying concentrations of RNase B. The intensity of the blank sample was only slightly lower than the positive control samples, which indicates that the initial glycoprotein detection was unsuccessful. Clearly this is a vital flaw in the assay. Likely, the reason for this is the lack of an appropriate antibody to bind the glycoprotein and hold it in position for unhindered detection by the lectin. This would require testing of various antibodies which are, first of all, specific for the glycoprotein, and secondly, binds to the correct epitope and leaves the glycan suitably exposed for detection by the biotinylated lectin. This would maximise chances for the rest of the assay to be successful. As mentioned previously, however, the concentration of GOx needs to be increased to produce significant growth rate differences for the NP seeds. The magnetic beads would be ideal for this purpose, but more work is required in the effective functionalisation of these supports.

## 5.7 Concluding Remarks

The capabilities of $H_2O_2$ as a reducing agent in the growth of Au NP seeds in the presence of $Au^{3+}$ showed great promise as a sensitive detection method for protein glycosylation. The NP growth was shown to be linear with respect to the concentration of $H_2O_2$ in solution. This simple relationship would be ideal in the development of an ELISA-type procedure. This approach has previously been reported in literature in a similar assay with highly sensitive results,[166] so was definitely a viable option for detection.

It was shown that the initial size of the Au NP seeds was important. In using 5 nm seeds, the limit of detection of the $H_2O_2$ was shown to be 4.89 µM, in comparison to limits of 6.08 µM and 8.71 µM for 10 nm and 15 nm seeds, respectively. This was due to the vast increases in extinction coefficient with increasing size of the Au NP seeds, which is more significant with smaller sizes, since a higher concentration of NPs are present for the same extinction value. This contributes to greater increases in extinction as the NPs grow due to the Beer-Lambert law.

Investigations into the growth patterns of the Au NP seeds over time also yielded interesting results. It was clear that at high concentrations of $H_2O_2$ the maximum NP size was reached within 80 min due to the complete reduction of $Au^{3+}$ in solution. After this point there was no more NP growth observed. Solutions with lower $H_2O_2$ concentrations were much slower in their NP growth rates, but would eventually reach the maximum size over a longer period of time, since this is limited by the $Au^{3+}$ concentration. This also found that with these experimental conditions, increasing the assay time period from 20 min to 80 min could maximise the growth of the NPs within this concentration range, and potentially increase the overall assay sensitivity, as was seen by the steeper gradient of the graph comparing the maximum NP extinction to the $H_2O_2$ concentration. (Figure 5.8)

The use of a streptavidinated GOx polymer was then investigated. It was thought that this could be used to generate sufficient $H_2O_2$ from the conversion of Glc to gluconic acid to induce NP seed growth. This was successfully tested using TMB and HRP, whereby TMB formed a blue charge transfer complex in the presence of $H_2O_2$, aided

by HRP. This clear response showed that this could be a viable method of $H_2O_2$ production, and so this was carried forward into the growth of Au NP seeds.

Initial experiments using GOx to control growth of Au NP seeds seemed promising. There was a clear colorimetric difference in the NP solutions with varying GOx concentrations. Spectroscopic measurements confirmed the increases in maximum extinction with increasing GOx concentration as was expected. However, these initial experiments also highlighted an important issue with the assay. The blank signal was significantly higher than the two lower GOx concentrations tested. This showed that the NP growth of the sample without GOx present was faster than those where $H_2O_2$ was being produced. Likely this was due to the presence of proteins in solution, which could interact with the NP surface, and hinder the reduction of $Au^{3+}$ on to the surface, resulting in slower growth rates. The faster growth of the Au NPs in the absence of reducing agents when free from proteins highlighted that steps had to be taken to increase the growth rate of the positive control samples.

Incubation conditions were investigated to improve the efficiency of the catalytic production of $H_2O_2$ from Glc. This showed the need for a continuous increased temperature to increase the enzyme efficiency, but there were still issues with high signals obtained from the blank sample, along with poor discrimination between the GOx samples. This led to the investigation of magnetic beads as an enzyme support to increase the concentration present when glycoprotein detection occurred.

The use of magnetic beads, however, was unsuccessful. This was due to the presence of BSA as a stabilising agent in the GOx solution, which also bound to the surface of the beads. Using BCA assays it was deduced that whilst the magnetic beads were confirmed to be binding to proteins, the exact concentration of bound GOx could not be determined. When used experimentally to produce $H_2O_2$ from Glc, TMB and HRP showed no colorimetric response, showing that there was not a sufficient concentration for significant catalytic activity.

The assay was attempted without the use of magnetic beads or a capture antibody to help orientate the glycoproteins, and was shown to be unsuccessful. The assay still requires a lot of work, mainly with respect to correct antibody choice, whereby it

should bind to an epitope which leaves the glycan exposed for detection, and the enzyme support. The magnetic beads require further investigation to ensure adequate functionalisation with the GOx in the absence of BSA.

Whilst the assay has been so far unsuccessful, this research has demonstrated the potential of $H_2O_2$ controlled growth of Au NPs as a sensitive detection signal output. Similar assays have achieved attomolar levels of detection[166] and once the final assay has been produced, this could significantly aid glycosylation measurements in biopharmaceutical production. ELISAs are commonly used detection procedures, which can be produced as ready to use kits. This removes the requirement of highly skilled personnel and has the potential for automation. Once developed, this could provide rapid, high throughput testing capabilities which could be quicker and less costly than current glycosylation analysis methods, allowing for faster reactions to changes in the product profile from a processing perspective.

# 6. Experimental

## 6.1 Materials

### 6.1.1 Chemicals

$CT(PEG)_{12}$, MGITC, and Pierce magnetic beads were purchased from Thermo Fisher. CALNN was purchased from China Peptides. UEA, MAL, SNA and biotinylated GNA were purchased from Vector Laboratories. All other chemicals were purchased from Sigma Aldrich unless otherwise stated.

### 6.1.2 Buffer Preparation

#### *6.1.2.1 HEPES Buffer*

A stock solution of HEPES buffer (100 mM) was prepared by dissolving 0.47 g HEPES powder in 19 mL $dH_2O$. This was adjusted to pH 7.2 using 1 M NaOH, and then topped up to a final volume 20 mL using $dH_2O$. This was then diluted to 10 mM in $dH_2O$ as required.

#### *6.1.2.2 PB*

A stock solution of PB (50 mM) was prepared by dissolving 171.96 mg PB powder in 20 mL $dH_2O$. This gave a PB buffer solution with pH 7.5. This was diluted to 10 mM in $dH_2O$ as required.

#### *6.1.2.3 PBS*

A solution of PBS was prepared by dissolving one PBS tablet in 200 mL $dH_2O$. (10 mM PB, 2.7 mM KCl, 137 mM NaCl) This gave a PBS buffer with pH 7.4.

#### *6.1.2.4 Citrate-Phosphate Buffer*

A solution of citrate-phosphate buffer (50 mM) was prepared by dissolving 1 tablet in 100 mL $dH_2O$. This have a buffer of pH 5.0.

#### *6.1.2.5 Carbonate Coating Buffer*

A solution of carbonate coating buffer (100 mM) was prepared by dissolving 60.6 mg $Na_2CO_3$ and 120 mg $NaHCO_3$ in 20 mL water. The buffer was adjusted to pH 9.6.

## 6.2 Instrumentation

### 6.2.1 Extinction Spectroscopy

An Agilent Cary 60 UV-visible spectrophotometer was used for all extinction spectroscopic measurements. Before all sample analysis, a baseline of the sample solvent was measured. Samples were scanned with wavelengths from 400 – 800 nm. Measurements were carried out in disposable plastic micro cuvettes with 10 mm path length.

### 6.2.2 Dynamic Light Scattering and Zeta Potential

A Malvern Zetasizer Nano ZS was used for all sizing and zeta potential measurements of NP samples. Dilute NP samples were analysed in plastic cuvettes of 10 mm path length. Scattering intensity percentage distributions were used in sizing analysis. A Malvern dip cell kit was used for zeta potential measurements.

### 6.2.3 Surface Enhanced Resonance Raman Scattering Measurements

To characterise the SERRS response of NPs in solution, a Snowy Range Instruments Sierra 2.0. Samples were interrogated with a 638 nm laser at 100 % laser power (40

mW) with single 1 s acquisitions. Measurements were taken in Supelco 4 mL clear vials.

To measure the SERRS response of paper-based assays, a Renishaw InVia Raman spectrometer with a HeNe laser (633 nm) and a grating of 1800 l/mm was used with a 5× objective (NA = 0.12) to visualise the sample spots, and a 50× objective (NA = 0.75) for SERS measurements.

## 6.3 Nanoparticle Synthesis and Bioconjugation

### 6.3.1 Nanoparticle Synthesis

#### *6.3.1.1 Glassware Preparation*

In order to avoid heterogeneous nucleation from dirt or metallic particles, all glassware to be used in the NP synthesis was washed thoroughly using aqua-regia (3 parts HCl, 1 part $HNO_3$). All glassware was washed for at least 3 hours in aqua-regia to ensure that all metals were removed from the equipment. Each piece of glassware was then rinsed thoroughly with $dH_2O$ to remove all of the acid. The glassware was then used immediately to prepare NPs.

#### *6.3.1.2 Gold Nanoparticle Synthesis*

A modified version of the Lee-Meisel method[93] was used to synthesise citrate reduced Au NPs. In this preparation, $HAuCl_4$ was added to $dH_2O$ (60.5 mg, 500 mL). This was heated with stirring to 98 °C. Then an aqueous solution of sodium citrate (57.5 mg, 7.5 mL) was added to the flask. The solution changed from colourless to black to red. Stirring at 98 °C was maintained for a further 15 minutes before being allowed to cool to room temperature with constant stirring.

## 6.3.2 Nanoparticle Functionalisation

### *6.3.2.1 CALNN Functionalisation*

CALNN is a pentapeptide with a molecular weight of 533.61 g $mol^{-1}$ and a footprint of 0.56 $nm^2$.[107] Using this information, the theoretical concentration of CALNN required for full coverage of any batch of Au NPs can be calculated.

In the experiments detailed in Section 6.3.2.1 and Section 6.3.2.2, a batch of 60 nm Au NPs with a concentration of 43.7 pM was used. For all other conjugation experiments, the batch detailed in Section 3.2.1 was used. The area of each nanoparticle was calculated to be 11 309 $nm^2$, so it follows that 20 195 CALNN molecules would be required to coat each NP. Therefore, using Avogadro's number, it was calculated that 0.88 µM would be required for complete coverage.

To test the stability of CALNN-coated Au NPs, various concentrations of CALNN (1.87 mM stock) were mixed with the NPs to a final volume of 1 mL for 3 h, as shown in Table 6.1. The mixture was then centrifuged (5000 rpm, 20 min) and the supernatant discarded to remove unbound CALNN. The coated NPs were resuspended to 1 mL in $dH_2O$.

*Table 6.1: Volumes of 1.87 mM CALNN used to coat gold nanoparticles.*

| Final [CALNN] / µM | Vol 1.87 mM CALNN / µM |
|---|---|
| 0.75 | 0.40 |
| 1.00 | 0.53 |
| 1.25 | 0.67 |
| 1.50 | 0.80 |
| 1.75 | 0.94 |
| 2.00 | 1.07 |

To test their stability, 275 µL of the CALNN coated NPs was mixed with 120 mM NaCl (100 µL) and analysed using UV-vis spectrophotometry.

### *6.3.2.2 MGITC Study with CALNN*

#### 6.3.2.2.1 Gold Nanoparticle Functionalisation with MGITC and CALNN

The previous stability studies showed that the Au NPs remained stable in the presence of NaCl at all concentrations used. Therefore, 0.75 µM and 1.00 µM CALNN were selected to be taken forward for studies with MGITC. (0.40 µL and 0.53 µL respectively) The volumes of 1 µM MGITC added to AuNPs and their final concentrations are shown below in Table 6.2. The Au NPs and MGITC were mixed first briefly, then the CALNN was added, to a final volume of 1 mL. This was mixed for 3 h. The samples were then centrifuged (5000 rpm, 20 min). The supernatant was discarded, and the coated NP pellets were resuspended to 1 mL in $dH_2O$.

*Table 6.2: Volumes of 1µM MGITC added to CALNN-coated gold nanoparticles and their final concentrations.*

| Volume of 1 µM MGITC / µL | Final [MGITC] / nM |
|---|---|
| 10 | 10 |
| 20 | 20 |
| 30 | 30 |
| 40 | 40 |
| 50 | 50 |

#### 6.3.2.2.2 SERRS Response Measurement of Functionalised Gold Nanoparticles

500 µL AuNPs functionalised with MGITC and CALNN was placed in to a 4 mL vial to analyse the SERRS response. SERRS measurements were taken from the samples alone, and then again following addition of 120 mM NaCl (272 µL, 42.4 mM final concentration) to induce aggregation to simulate detection of an analyte.

#### *6.3.2.3 Bioconjugation of GNA to Gold Nanoparticles by Carbodiimide Coupling*

##### 6.3.2.3.1 MGITC Functionalisation of Gold Nanoparticles

20 µL MGITC (1 µM) was added to 1000 µL Au NPs. The solution was shaken for 30 min and then centrifuged (5000 rpm, 20 mins) and the supernatant discarded to remove any unbound MGITC. The tagged Au NPs were then resuspended to 1 mL in $dH_2O$.

##### 6.3.2.3.2 Ligand Preparation by Carbodiimide Coupling

Lectin bioconjugation was performed by first preparing a ligand off-particle. EDC/sNHS coupling was used to join CALNN/PEG by its carboxylic acid terminus to a lectin by a primary amine group. A ratio of reagents was used to ensure that every linking molecule was attached to a lectin, by keeping every subsequently used reagent in excess. The ratio is shown in Table 6.3.

*Table 6.3: Ratio of reagents used in carbodiimide coupling to prepare functional ligand.*

| **Reagent** | Linker | EDC | sNHS | Lectin |
|---|---|---|---|---|
| **Relative concentration** | 1 | 1.5 | 2 | 4 |

Firstly, 22.5 µM and 30.0 µM solutions of EDC and sNHS respectively were prepared in HEPES (10 mM, pH 7.2). To do this, 10 mM solutions were first prepared (1.917 mg/mL EDC, 2.171 mg/mL sNHS). 22.5 µL EDC and 30 µL sNHS were then both diluted to 1 mL in HEPES (10 mM, pH 7.2) to yield the desired concentrations.

100 µL EDC (22.5 µM) was mixed with CALNN (0.8 µL 1.87 mM), or PEG (2 µL, 1 mM) for 5 min to activate the carboxyl groups. Simultaneously 100 µL sNHS was mixed with lectin (1 mg/mL) to the desired concentration. The mixture of EDC/CALNN was then combined with the mixture of sNHS/GNA and made up to a final volume of 1 mL with HEPES (10 mM, pH 7.2). The solution was left to shake overnight.

#### 6.3.2.3.3 Conjugation of Pre-prepared Ligand to MGITC-tagged Gold Nanoparticles

In duplicate, 500 µL MGITC-tagged Au NPs was added to 500 µL of the pre-prepared ligand and mixed for 3 h. The samples were then centrifuged (5000 rpm, 20 min) and the supernatants were discarded. The conjugated NP pellets were then combined and resuspended to 1 mL with HEPES (10 mM, pH 7.2).

This process could also be scaled up to produce 10 mL Au NP conjugates. Conjugates could then be stored at 5 °C and used when required.

The NP conjugates were characterised using extinction spectrophotometry, DLS, SERRS, and gel electrophoresis.

### *6.3.2.4 Gel Electrophoresis*

Gel electrophoresis was used to assess the success of bioconjugation of lectins to Au NPs. In order to prepare a 1 % gel, 1.1 g agarose was dissolved in 100 mL 1× tris-borate EDTA (TBE) buffer. The mixture was placed in the microwave and heated for 3 min at full power (750 W). The agarose solution was then poured in to a gel mould and a comb inserted to create wells. The gel was allowed to set at room temperature for 30 min.

Whilst the gel was solidifying, the NPs to be analysed were concentrated by centrifugation (5000 rpm, 20 min). The supernatant was removed to leave the concentrated NP pellet.

The mould with the prepared gel was then placed in to a gel chamber and submerged in 1 × TBE buffer. 15 µL NPs were premixed with 5 µL glycerol to increase their viscosity and aid settling in the wells. The NPs were then added in to each well. The chamber was connected to a power supply set at 160 V. The gel was left to run for 1.5 h.

## 6.4 Solution Assays for Glycosylation Detection

### 6.4.1 Initial UV-vis Glycoprotein Detection Experiments

Firstly, 300 µL Au@GNA was diluted with an appropriate volume of HEPES (10 mM, pH 7.2) to give a final volume of 450 µL. RNase B (73.3 µM) was added to produce various final concentrations, as detailed in Table 6.4. The samples were analysed using UV-vis immediately following addition, and again after 10 min. The same procedure was followed for RNase A (73.3 µM), but only with a final concentration of 1.63 µM. A blank sample was prepared by diluting 300 µL Au@GNA with 150 µL HEPES (10 mM, pH 7.2)

*Table 6.4: Volumes of reagents used to assess detection of ribonuclease B by functionalised nanoparticles.*

| Vol Au@GNA / µL | Vol HEPES / µL | Vol RNase B / µL | Final [RNase B] / nM |
|---|---|---|---|
| 300 | 150.0 | 0.0 | 0 |
| 300 | 149.5 | 0.5 | 81 |
| 300 | 149.0 | 1.0 | 163 |
| 300 | 147.5 | 2.5 | 407 |
| 300 | 145.0 | 5.0 | 815 |
| 300 | 140.0 | 10.0 | 1630 |

### 6.4.2 Timed UV-vis Glycoprotein Detection Experiments

The same reaction conditions were used as detailed in Section 6.4.1. However, samples were analysed immediately after addition or RNase B and then every 12 min for 1 h. The same procedure was followed for RNase A/BSA.

The same procedure was used in reactions containing Au@WGA, Au@Con A, Au@UEA, Au@SNA, and Au@MAL in the detection of their specific glycans.

## 6.5 Paper-based Assays

### 6.5.1 Lateral Flow Assays

#### *6.5.1.1 Lateral Flow Assay Materials and Fabrication*

The LFA strips used initially were pre-assembled by collaborators at Universidad de Oviedo by a previously reported method.[126] The backing card was obtained from Kenosha, the sample pads and absorbent pads were purchased from Merck, and the nitrocellulose strips were purchased from Sartorius.

The strips used later were constructed from HiFlow Plus 180 2 mil membranes, cellulose fibre sample pads, and glass fibre diagnostic pads, which were all purchased from Merck Millipore. To assemble the strips, the conjugate (glass fibre) and absorbent (cellulose fibre) pads were stuck to both ends of the nitrocellulose on to the adhesive backing card, with an overlap between each section. This was then cut in to strips around 5 mm in width.

#### *6.5.1.2 Lateral Flow Assay Procedure*

RNase A or B (0.5 µL) was spotted on to the nitrocellulose membrane and allowed to dry for 15 min at room temperature. The running buffer consisted of PB (10 mM, pH 7.5), 1 % BSA, and 0.05 % Tween 20. In a 96-well plate, concentrated Au@GNA (1.88 nM, 10 µL) was added to the running buffer (90 µL). The sample pad of the lateral flow strip was placed upright in to the loading buffer and allowed to run for 15 min. The strip was then washed by placing it in another well of loading buffer (100 µL) for 15 min.

#### *6.5.1.3 SERRS Detection on Lateral Flow Assay Strips*

A SERRS map was taken around the area the analytes were spotted using the mapping function on WiRE with a 100 µm step size. Each point was interrogated at 10 % laser power (0.8 mW), with a single 6 s acquisition. The SERRS heat map was generated by applying an LUT control to the peak at 1614 $cm^{-1}$. The spectra were pre-processed in

WiRE 4.2 software. This included cosmic ray removal, smoothing, and baseline correction. Spectra were then taken from the on and off spot regions and plotted in OriginPro 2018.

#### *6.5.1.4 Colorimetric Analysis of Lateral Flow Assay Strips*

An 8-bit EPSON V370 flatbed scanner was used to scan the lateral flow strips with a resolution of 1200 dpi. The RGB response was then generated from the analyte spots using ImageJ. Since the Au NPs are red in colour, the green channel was the most sensitive, so it was used for quantification. The signal for each sample was subtracted from the maximum RGB value (255) to give a normalised signal.

### 6.5.2 Nitrocellulose Spot Tests

#### *6.5.2.1 Nitrocellulose Spot Test Materials*

Amersham Protran nitrocellulose membrane (0.45 µm pore size) was purchased from GE Healthcare. A Xerox ColorQube 8580 wax printer was used to print the assays. A Graphtec CE6000-40 Plus cutting plotter was used to cut the adhesive sheets.

#### *6.5.2.2 Fabrication and Running of Nitrocellulose Spot Tests*

The assay was wax printed directly on to the nitrocellulose membrane which was taped to a backing sheet of paper to provide stability. The nitrocellulose was then placed in to an oven at 85 °C for 1 min to allow the wax to melt through. If adhesive sheets are being used to assemble the materials, then the pre-cut sheets would now be attached to the back of the nitrocellulose. 5 µL analyte solution at the desired concentration in PB (10 mM, pH 7.5) were then applied to the spots on the nitrocellulose, and placed in an oven to dry at 60 °C for 10 min. Once dry, the nitrocellulose layer would be attached to an absorbent pad using the adhesive sheet. If using an adhesive spray to assemble, at this point the rear of the nitrocellulose and the absorbent pad would both be sprayed briefly with adhesive, and the two layers

would be attached instantly. The assembled assays were then run through a cold laminator to remove any air bubbles and to ensure the nitrocellulose is in complete contact with the absorbent pad. Au NP conjugates (5 µL, 0.2 nM) were then applied to the spots in running buffer (10 mM PB, 1 % BSA, 0.05 % Tween 20) and allowed to flow through the nitrocellulose. Once the assay was complete, it was washed with running buffer.

#### *6.5.2.3 Colorimetric Analysis of Spot Tests*

The same procedure was used as detailed in Section 6.5.1.4.

#### *6.5.2.4 SERRS Detection on Spot Tests*

The sample spot was split in to 4 quadrants, and 6 point spectra were taken from each quadrant. Each point was interrogated at 10 % laser power (0.8 mW), with a single 6 s acquisition. The spectra were pre-processed in WiRE 4.2 software, including cosmic ray removal, smoothing, and baseline correction. Matlab was then used to average the spectra. The final averaged spectra were plotted in Origin Pro 2018.

## 6.6 Enzyme-linked Nanoparticle Growth for Glycosylation Detection

### 6.6.1 Nanoparticle Seed Synthesis

To produce 5 nm Au NP seeds, a method detailed by Ieong *et al*[164] was used. To a 240 mL solution containing $HAuCl_4$ (0.21 mM) and trisodium citrate (0.21 mM), ice cold $NaBH_4$ (5 mL, 0.1 M) was added. The solution rapidly changed from colourless to red. This was stirred overnight at room temperature.

To produce 10 nm and 15 nm seeds, a method detailed by Ghosh *et al*[167] was used. A solution of $HAuCl_4$ (50 mL, 0.29 mM) was heated to boiling with stirring. Sodium citrate (0.81 mM for 10 nm, 0.67 mM for 15 nm) was then added. The solution turned

from colourless to black to red. Stirring was continued with heat for 15 min, after which it was cooled to room temperature with stirring.

### 6.6.2 Nanoparticle Growth with $H_2O_2$

In a 96-well plate, $HAuCl_4$ (90 µL, 2 mM), Au NP seeds (30 µL, 66.7 nM for 5 nm, 8.4 nM for 10 nm, and 1.3 nM for 15 nm), and varying volumes of $H_2O_2$ (2 mM) were mixed to give different final concentrations. (Table 6.5) Water was added to a total volume of 300 µL.

*Table 6.5: Volumes of 2 mM $H_2O_2$ added to give different final concentrations in 300 µL reaction.*

| **Volume $H_2O_2$ / µL** | **Concentration $H_2O_2$ / µM** |
|---|---|
| 0 | 0 |
| 1.5 | 10 |
| 3 | 20 |
| 7.5 | 50 |
| 15 | 100 |
| 30 | 200 |
| 75 | 500 |
| 150 | 1000 |

For individual measurements, samples were left for 20 min and then the extinction spectra were collected. For growth kinetics investigations, extinction measurements were collected every 20 min overnight.

### 6.6.3 TMB/HRP Detection of $H_2O_2$ Produced by Glucose Oxidase

In citrate-phosphate buffer (50 mM, pH 5.0) with 0.1 % Tween 20© and 1 % BSA, samples were prepared containing Glc (1.67 mM), different concentrations of GOx polymer (3.33 µg/mL, 0.33 µg/mL, and 0.03 µg/mL) and TMB (1mM). To this HRP (1 µL) from an ELISA kit was added, and the samples were incubated for 1 h.

### 6.6.4 Nanoparticle Growth Detection of $H_2O_2$ Produced by Glucose Oxidase

#### *6.6.4.1 Nanoparticle Growth at Room Temperature*

In citrate-phosphate buffer (50 mM, pH 5.0) containing 0.1 % Tween 20© and 1 % BSA, samples were prepared containing Glc (1.67 mM), different concentrations of GOx polymer (3.33 µg/mL, 0.33 µg/mL, and 0.03 µg/mL), and $HAuCl_4$ (0.6 mM). 5 nm Au NP seeds (6.67 nM) were added and the samples were incubated for 20 h at room temperature. The extinction spectra were collected from samples every hour for 12 h.

#### *6.6.4.2 Incubation of Glucose Oxidase and Glucose Before Nanoparticle Seed Addition*

In citrate-phosphate buffer (50 mM, pH 5.0) containing 0.1 % Tween 20© and 1 % BSA, samples were prepared containing Glc (1.67 mM), different concentrations of GOx polymer (3.33 µg/mL, 0.33 µg/mL, and 0.03 µg/mL), and $HAuCl_4$ (0.6 mM). The samles were left to incubate for 1 h at 40 °C before 5 nm Au NP seeds (6.67 nM) were added. Extinction spectra were then collected every 10 min for 1 h, and then every hour for 16 h.

#### *6.6.4.3 Constant Incubation of Glucose Oxidase and Glucose in Presence of Gold Nanoparticle Seeds*

In citrate-phosphate buffer (50 mM, pH 5.0) containing 0.1 % Tween 20© and 1 % BSA, samples were prepared containing Glc (1.67 mM), different concentrations of GOx polymer (3.33 µg/mL, 0.33 µg/mL, and 0.03 µg/mL), and $HAuCl_4$ (0.6 mM). 5 nm Au NP seeds (6.67 nM) were added and the samples were incubated constantly at 40 °C. Extinction spectra were collected every hour for 5 h.

### 6.6.5 Magnetic Beads Conjugation to Glucose Oxidase

Pierce magnetic beads with a diameter of 1 µm with NHS groups on a blocked superparamagnetic surface were purchased from Thermo Fisher. The beads (300 µL, 10 mg/mL) were added to a 1.5 mL centrifuge tube. The beads were collected using a magnet and the supernatant was discarded. Ice cold HCl (1 mL, 1 mM) was added and vortexed for 15 s. The beads were collected with a magnet and the supernatant was discarded. Immediately, the GOX polymer solution in phosphate buffered saline (PBS) (300 µL, 0.5 mg/mL, pH 7.4) was added and the solution was vortexed for 15 s. The beads and GOx solution were then incubated for 1 h at room temperature on a shaker. For the first 30 min the beads were vortexed for 15 s every 5 min. For the second 30 min, the beads were vortexed for 15 s every 15 min. The beads were collected with a magnet and the supernatant was extracted. This was retained for BCA assays to assess bound protein. Glycine (1 mL, 0.1 M, pH 2.0) was added to remove unbound proteins and the beads were vortexed for 15 s. The beads were collected with a magnet and the supernatant was discarded. Washing with glycine was repeated once more. Water (1 mL) was added and the beads were vortexed for 15 s. The beads were collected with a magnet and the supernatant was discarded. Ethanolamine (1 mL, 3 M, pH 9.0) was added to quench the beads by hydrolysing the remaining NHS groups and the beads were vortexed for 30 s and then mixed for 2 h on a shaker at room temperature. The beads were collected with a magnet and the supernatant was discarded. Water (1 mL) was added and mixed well. The beads were then collected with a magnet and the supernatant was discarded. PBS (1 mL) containing 0.05 % sodium azide was added and mixed well. The beads were collected with a magnet and the supernatant was discarded. Washing with PBS was repeated a further two times. The beads were then resuspended in PBS (300 µL) with 0.05 % sodium azide as a preservative and stored at 4 °C until ready for use.

### 6.6.6 BCA Assay Procedure

A Thermo Scientific Pierce Micro BCA Protein Assay Kit was used to assess concentration of bound protein to the magnetic beads. In this kit 3 reagents were

supplied to produce the BCA working reagent. (WR) The three reagents (MA, MB, MC) were mixed in a ratio of 25:24:1 MA:MB:MC before addition to the BSA standards and solutions of unknown concentration.

Standard solutions of BSA were prepared in PBS at various concentrations. (0.5, 1.0, 2.5, 5.0, 10, 20, 40, and 200 μg/mL) Each standard or unknown solution (150 μL) was added in to a microplate well. WR (150 μL) was added to each well and the solutions were mixed thoroughly on a shaker for 30 s. The microplate was covered and incubated at 37 °C for 2 h. The plate was cooled to room temperature and the absorbance was measured at 562 nm.

### 6.6.7 Measuring Bound Glucose Oxidase Activity

Solutions were prepared containing Glc (1.67 mM) and various concentrations of magnetic beads, detailed in Table 5.5. TMB (1 mM) and ELISA kit HRP were added and the solutions were incubated at room temperature for 30 min.

### 6.6.8 Final Glycosylation Detection Assay Attempt

In a microplate, wells were coated with RNase B (667 nM, 333 nM, and 67 nM) in carbonate coating buffer. (100 μL, 100 mM, pH 9.6) The plates were incubated overnight at 4 °C. The RNase B solution was removed and washed 3 times with PBS (200 μL) containing 0.1 % Tween 20©. The wells were blocked with polyvinylalcohol (PVA) (200 μL, 0.5 %) in PBS. (10 mM) The plate was then incubated at room temperature for 1 h. The blocking solution was removed and the wells were washed 3 times with PBS (200 μL, 10 mM) containing 0.1 % Tween 20©. Biotinylated GNA (100 μL, 10 μg/mL) was then added in PBS (10 mM, 0.5 % PVA) GOx-streptavidin (×20) polymer (100 μL, 10 μg/mL) was added in blocking buffer and incubated at room temperature for 1 h. The GOx was removed and the wells were washed 3 times with PBS (200 μL, 10 mM) containing 0.1 % Tween 20©. Glc (100 μL, 5 mM) in citrate phosphate buffer (50 mM, pH 5.0) was added and the plate was incubated at 35 °C for 10 min. $HAuCl_4$ (60 μL, 2 mM), Au NP seeds (20 μL, 8.67 nM) and citrate phosphate

buffer (20 µL, 50 mM, pH 5.0) were added and the plate was incubated at 35 °C for 20 min. The extinction spectra of each sample were then collected.

# 7. Conclusions

In the biopharmaceutical industry glycosylation characterisation of therapeutic proteins is vital to ensure the efficacy and safety of the final drug product. Current research methods, whilst effective, are expensive, time consuming, and require highly trained analysts to conduct measurements. Therefore, this research was conducted with the aim of developing assays which could detect protein glycosylation whilst maintaining a rapid, cheap, and user-friendly format.

Au NPs were selected as sensing beacons due to their extensive optical properties, ease of functionalisation, and commonplace use in biochemical detection assays. Three different assay formats were investigated: a solution assay relying on LSPR measurements, a 2D µPAD utilising colorimetric analysis and SERRS, and an ELISA-style format taking advantage of the reductive properties of $H_2O_2$ to induce Au NP growth.

Firstly, the synthesis and functionalisation of Au NPs was shown to be successful and versatile. Mixed monolayer NP coverage was achieved using MGITC as a Raman reporter, and a heterobifunctional linker tethered to a lectin for sensing. Versatility was achieved in the interchangeable use of linkers, between CALNN and PEG, and the attachment of various lectins through EDC-NHS coupling. These functional NPs could then be used in both the solution assays and in the 2D µPADs.

It was shown that the presence of RNase B in solution with Au@GNA induced a shift in the LSPR peak position of the functionalised Au NPs. This was a result of the change in the dielectric surrounding the NP upon binding to the Man residues in the RNase B glycan. This was shown to be specific to the presence of the glycan, since no change in the extinction spectrum was observed in the presence of non-glycosylated BSA. Through timed concentration studies, it was found that the LSPR peak shift was linear with respect to the concentration of glycoprotein, allowing for a limit of detection of 29.2 nM to be achieved. This was higher than current commercial glycoprotein quantification assays, but had the added advantage of being specific for Man, rather than the glycoprotein as a whole. The assay was diversified to show that various

lectins could be used in the detection of Man and GlcNAc, the components of the high-Man N-glycan. The detection of Fuc, and SA was attempted with poor results. The detection of Fuc was minimal, although shifts were observed in the negative control, meaning that detection could not be confirmed. SA detection, however, was unsuccessful, perhaps due to the low concentrations of lectin used.

In order to utilise the sensitive detection capabilities of SERRS, a support platform was investigated to allow for side-by-side NP conjugate assembly upon detection of a glycoprotein. LFAs were first used with Au@GNA, and were shown to be successful at higher concentrations of RNase B. However, sensitivity was poor due to the format of the assay allowing for NPs to travel around the analyte spot. Therefore, a new 2D µPAD was investigated, where hydrophobic barriers were created to control regions of NP flow. These printed assays had the benefit of being colorimetric, so quantitative results could be obtained using a simple flatbed scanner, creating a relatively sensitive assay at low cost, with a LOD of 197.2 nM. In order to improve the sensitivity, SERRS was used, but was found to be problematic due to the depth penetration of the laser causing collection of scattered photons from NP conjugates in the absorbent pad below. Therefore, a change in objective to reduce the longitudinal focussing spot size produced much more coherent results, showing that this assay format had the possibility of facilitating rapid and sensitive glycan profiling.

Finally, initial experiments were conducted in the development of an ELISA for glycan detection. This involved the use biotinylated lectins for detection of the glycoprotein, to which a streptavidin-conjugated GOx polymer would bind. The presence of GOx would then cause the conversion of Glc to gluconic acid with the liberation of $H_2O_2$. The production of $H_2O_2$ would enable the reduction of $Au^{3+}$ on to the surface of Au NP seeds causing growth which could be tracked using extinction spectroscopy. This relied on the increase in the extinction coefficient with the growth of Au NPs, which presented in an increase in intensity of the extinction peak, as described by the Beer-Lambert Law. The development of this assay was still in the early stages, but highlighted the possibility for the production of a sensitive ELISA based on controlled NP synthesis. Similar assays have achieved attomolar levels of detection, showing

that this could significantly aid glycosylation measurements in biopharmaceutical production.

Overall, it has been shown that NP-based assays can provide sensitive and specific detection of protein glycosylation. The versatility and ease of NP functionalisation allows for the production of libraries of lectin-conjugated Au NPs for the detection of a diverse range of glycans. Solution assays based on LSPR detection can produce sensitive results by simply mixing reagents and using extinction spectroscopy, giving rapid and quantifiable information about glycan composition. Paper-based 2D µPADs allow for high-throughput and rapid detection of protein glycosylation with two different detection methods. A user-friendly and low cost option of colorimetric detection is available, as well as potentially highly sensitive detection using SERRS. Finally, an ELISA format could be particularly advantageous. These assays are commonly available as kits for biochemical detection, so require little training for use, and can provide low LODs for analyte quantification. All three methods investigated here are still in the early research stages. However, with further optimisation, they could provide attractive alternatives to current glycosylation characterisation methods, due to their simple, low cost, and user-friendly formats, whilst maintaining sensitivity in glycan detection

# 8. Future Work

This research has shown that NP-based assays have the potential to provide sensitive detection of protein glycosylation. However, more work is required to make these viable assays for biopharmaceutical glycan characterisation. Firstly, whilst the solution assays were simple and effective in assessing the presence of glycan components, the reproducibility of these assays must be improved by reducing the batch-to-batch variability in the NP conjugation process to ensure a consistent lectin concentration on the NP surface. This quality control could be carried out using fluorescence studies to ensure that the conjugated lectin concentration is reproducible. Further to this, the library of lectins used must be expanded to widen the scope of the assay for the potential of further glycan characterisation. This would involve investigation of a wide panel of lectins to ensure that strong binding interactions can be observed with each individual glycan component. Coupled with microplate readers, this assay has the potential to be a simple, yet rapid, technique for the elucidation of glycan components.

In the 2D µPADs, the assay format must be made more robust to ensure that the test runs consistently every time. The materials used in the construction, namely the adhesive layers, should be investigated to reduce the variability in the flow properties of the assay, and potentially allow for removal of the detection layer for separate analysis. Further studies must also be carried out with the SERRS-based detection to ensure that reproducible and strong signals are achieved over different control samples. This could be achieved by the investigation of different RRMs and concentrations on the NP surface. Similar to the solution based LSPR assays, the library of lectin-NP conjugates must be diversified. This would allow for high-throughput assays to be performed where different glycan components can be tested for in a single test sheet. Further to this, SERRS has the advantage of multiplexing capabilities. LFAs have shown already shown promise for SERS multiplexing.[127] This could prove particularly useful in biopharmaceutical glycan characterisation where multiple glycan components could be detected within a single test spot, reducing materials required and significantly increasing throughput.

Finally, the NP growth ELISA is still in its infancy. For this research to progress the use of GOx to induce nanoparticle growth must be optimised. This would first involve investigating the optimum reaction conditions with regards to temperature and concentration to produce sufficient $H_2O_2$ to reduce $Au^{3+}$ to $Au^0$. As demonstrated in this research, having sufficient presence of enzyme to produce $H_2O_2$ is vastly important. Therefore, more work is required to provide a support for GOx to increase $H_2O_2$ production upon glycan detection. In purchased GOx polymer solutions any stabilising BSA must be removed to allow for attachment of only the enzyme to a magnetic bead surface. This could be carried out by size exclusion chromatography. The resulting presence of multiple GOx groups per detected glycan would maximise the difference in $H_2O_2$ production at different carbohydrate concentrations, in turn increasing the sensitivity of the overall assay. Further to this, in producing a final working assay, suitable antibodies must be investigated to bind the glycoproteins at specific epitopes so that their glycans are oriented away from the plate surface and are exposed for detection by a lectin.

.

# References


1 B. Leader, Q. J. Baca and D. E. Golan, *Nat. Rev. Drug Discov.*, 2008, **7**, 21–39.

2 N. Lingg, P. Zhang, Z. Song and M. Bardor, *Biotechnol. J.*, 2012, **7**, 1462–1472.

3 S. A. Berkowitz, J. R. Engen, J. R. Mazzeo and G. B. Jones, *Nat. Rev. Drug Discov.*, 2012, **11**, 527–540.

4 S. Kozlowski, Testimony - Potential Need for Measurement Standards to Facilitate R&D of Biologic Drugs, http://www.fda.gov/NewsEvents/Testimony/ucm183596.htm, (accessed 25 May 2018).

5 N. Kawasaki, S. Itoh, N. Hashii, D. Takakura, Y. Qin, X. Huang and T. Yamaguchi, *Biol. Pharm. Bull.*, 2009, **32**, 796–800.

6 A. Garrod, *Lancet*, 1902, **160**, 1616–1620.

7 J. Haemmerling, *Annu. Rev. Plant Physiol.*, 1963, **14**, 65–92.

8 J. Brachet and H. Chantrenne, *Cold Spring Harb. Symp. Quant. Biol.* , 1956, **21**, 329–337.

9 S. Brenner, F. Jacob and M. Meselson, *Nature*, 1961, **190**, 576.

10 J. M. Berg, J. L. Tymoczko and L. Stryer, *Biochemistry*, W. H. Freeman and Company, New York, 7th edn., 2006.

11 E. Buxbaum, *Fundamentals of Protein Structure and Function*, Springer US, Portsmouth, Dominica, 2007.

12 S. A. Berkowitz and D. J. Houde, *The Complexity of Protein Structure and the Challenges it Poses in Developing Biopharmaceuticals*, Elsevier B.V., 2014.

13 C. T. Walsh, S. Garneau-Tsodikova and G. J. Gatto, *Angew. Chemie - Int. Ed.*, 2005, **44**, 7342–7372.

14 E. A. Eklund and H. H. Freeze, *Semin. Pediatr. Neurol.*, 2005, **12**, 134–143.

15 R. G. Spiro, *Glycobiology*, 2002, **12**, 43R–56R.

16 E. Higgins, *Glycoconj. J.*, 2010, **27**, 211–225.

17 M. A. Tarp and H. Clausen, *Biochim. Biophys. Acta - Gen. Subj.*, 2008, **1780**, 546–563.

18 Y. Shaaltiel, D. Bartfeld, S. Hashmueli, G. Baum, E. Brill-Almon, G. Galili, O. Dym, S. A. Boldin-Adamsky, I. Silman, J. L. Sussman, A. H. Futerman and D. Aviezer, *Plant Biotechnol. J.*, 2007, **5**, 579–590.

19 N. Sharon and H. Lis, *Glycobiology*, 2004, **14**, 53–62.

20 J. Kocourek, eds. I. E. Liener, N. Sharon and I. J. B. T.-T. L. Goldstein, Academic Press, 1986, pp. 1–32.

21 J. B. Sumner and S. F. Howell, *J. Bacteriol.*, 1936, **32**, 227–37.

22 W. C. Boyd and E. Shapleigh, *Science*, 1954, **119**, 419–419.

23 K. Anderson, D. Evers and K. G. Rice, *Structure and Function of Mammalian Carbohydrate-Lectin Interactions*, Springer, Berlin, 2008.

24 S. S. Komath, M. Kavitha and M. J. Swamy, *Org. Biomol. Chem.*, 2006, **4**, 973.

25 D. Craig, S. McAughtrie, J. Simpson, C. McCraw, K. Faulds and D. Graham, *Anal. Chem.*, 2014, **86**, 4775–4782.

26 Y. Qiu, T. H. Patwa, L. Xu, K. Shedden, D. E. Misek, M. Tuck, G. Jin, M. T. Ruffin, D. K. Turgeon, S. Synal, R. Bresalier, N. Marcon, D. E. Brenner and D. M. Lubman, *J. Proteome Res.*, 2008, **7**, 1693–1703.

27 A. Bond, A. Alavi, J. S. Axford, B. E. Bourke, F. E. Bruckner, M. A. Kerr, J. D. Maxwell, K. J. Tweed, M. J. Weldon, P. Youinou and F. C. Hay, *J. Autoimmun.*, 1997, **10**, 77–85.

28 Z. Yang and W. S. Hancock, *J. Chromatogr. A*, 2004, **1053**, 79–88.

29 G. Sánchez-Pomales, T. A. Morris, J. B. Falabella, M. J. Tarlov and R. A. Zangmeister, *Biotechnol. Bioeng.*, 2012, **109**, 2240–2249.

30 A. Barre, Y. Bourne, E. J. M. Van Damme, W. J. Peumans and P. Rougé, *Biochimie*, 2001, **83**, 645–651.

31 S. Eustis and M. A. El-Sayed, *Chem. Soc. Rev.*, 2006, **35**, 209–217.

32 L. L. Kiessling, T. Young, T. D. Gruber and K. H. Mortell, *Multivalency in Protein-Carbohydrate Recognition*, Springer, Berlin, 2008.

33 J. R. Birch and A. J. Racher, *Adv. Drug Deliv. Rev.*, 2006, **58**, 671–685.

34 F. M. Ausubel, R. Brent, R. E. Kingston, D. D. Moore, J. G. Seidman, J. A. Smith and K. Struhl, *Current Protocols in Molecular Biology*, Wiley, New York, 2001.

35 D. N. Nesbeth, M. A. Perez-Pardo, S. Ali, J. Ward and E. Keshavarz-Moore, *Biotechnol. Bioeng.*, 2012, **109**, 517–527.

36 H. J. P. Marvin, M. B. A. Terbeest and B. Witholt, *J. Bacteriol.*, 1989, **171**, 5262–5267.

37 A. Berrill, S. V. Ho and D. G. Bracewell, *Biotechnol. Prog.*, 2008, **24**, 426–431.

38 S. McNulty, S. Kong, E. C. Lau, M. Hoare, C. Entwisle, A. Mcilgorm and K. A. Dalton, *Biotechnol. Bioeng.*, 2013, **110**, 1973–1983.

39 D. Fernandes, *BioPharm Int.*, 2011, **24**, 44.

40 ICH Topic Q 6 B - Specifications: Test Procedures and Acceptance Criteria for Biotechnological/Biological Products, http://www.ema.europa.eu/docs/en_GB/document_library/Scientific_guideline/2009/09/WC500002824.pdf, (accessed 1 May 2015).

41 A. J. Chirino and A. Mire-Sluis, *Nat. Biotechnol.*, 2004, **22**, 1383–1391.

42 M. Schiestl, T. Stangler, C. Torella, T. Čepeljnik, H. Toll and R. Grau, *Nat. Biotechnol.*, 2011, **29**, 310–312.

43 C. Q. Reid, A. Tait, H. Baldascini, A. Mohindra, A. Racher, S. Bilsborough, C. M. Smales and M. Hoare, *Biotechnol. Bioeng.*, 2010, **107**, 85–95.

44 F. M. Greer, *Eur. Biopharm. Rev.*, 2004, **1**, 64–67.

45 A. Dell and H. R. Morris, *Science*, 2001, **291**, 2351–2356.

46 F. Greer, A. Reason and M. Rogers, *Eur. Biopharm. Rev.*, 2002, **1**, 106–111.

47 N. L. Rosi and C. A. Mirkin, *Chem. Rev.*, 2005, **105**, 1547–1562.

48 S. F. Vert, M., Doi, Y., Hellwich, K.H., Hess, M., Hodge, P., Kubisa, P., Rinaudo, M., *Pure Appl. Chem.*, 2012, **84**, 377–408.

49 D. J. Barber and I. C. Freestone, *Archaeometry*, 1990, **32**, 33–45.

50 D. Graham, R. Stevenson, D. G. Thompson, L. Barrett, C. Dalton and K. Faulds, *Faraday Discuss.*, 2011, **149**, 291–299.

51 Z. Wang, R. Lévy, D. G. Fernig and M. Brust, *Bioconjug. Chem.*, 2005, **16**, 497–500.

52 F. Gonzàlez de Rivera, I. Angurell, O. Rossell, M. Seco and J. Llorca, *J. Organomet. Chem.*, 2012, **715**, 13–18.

53 M. C. M. Daniel and D. Astruc, *Chem. Rev.*, 2004, **104**, 293–346.

54 R. Narayanan and M. A. El-Sayed, *J. Phys. Chem. B*, 2005, **109**, 12663–12676.

55 L. Guerrini and D. Graham, *Chem. Soc. Rev.*, 2012, **41**, 7085.

56 M. H. N. Famili, H. Janani and M. S. Enayati, *J. Appl. Polym. Sci.*, 2011, **119**, 2847–2856.

57 R.-J. Zhou and T. Burkhart, *J. Mater. Sci.*, 2011, **46**, 2281–2287.

58 P. K. Jain, K. S. Lee, I. H. El-Sayed and M. A. El-Sayed, *J. Phys. Chem. B*, 2006, **110**, 7238–7248.

59 T. Klar, M. Perner, S. Grosse, G. Von Plessen, W. Spirkl and J. Feldmann, *Phys. Rev. Lett.*, 1998, **80**, 4249–4252.

60 E. Smith and G. Dent, *Modern Raman Spectrocopy: A Practical Approach*, Wiley, Chichester, 2005.

61 T. R. Jensen, M. L. Duval, K. L. Kelly, A. A. Lazarides, G. C. Schatz and R. P. Van

Duyne, *J. Phys. Chem. B*, 1999, **103**, 9846–9853.

62 S. Link and M. A. El-Sayed, *J. Phys. Chem. B*, 1999, **103**, 8410–8426.

63 G. Mie, *Ann. Phys.*, 1908, **330**, 377–445.

64 K. A. Willets and R. P. Van Duyne, *Annu. Rev. Phys. Chem.*, 2007, **58**, 267–297.

65 C. R. Yonzon, E. Jeoung, S. Zou, G. C. Schatz, M. Mrksich and R. P. Van Duyne, *J. Am. Chem. Soc.*, 2004, **126**, 12669–12676.

66 C. Yonzon and R. P. Van Duyne, *Mater. Res. Soc. Symp. Proc.*, 2005, **876**, 3–8.

67 R. Elghanian, J. J. Storhorf, R. C. Mucic, R. L. Letsinger and C. A. Mirkin, *Science*, 1997, **277**, 1078–1081.

68 H. Li and L. Rothberg, *Proc. Natl. Acad. Sci. U. S. A.*, 2004, **101**, 14036–14039.

69 G. J. Wegner, H. J. Lee, G. Marriott and R. M. Corn, *Anal. Chem.*, 2003, **75**, 4740–4746.

70 D. Craig, J. Simpson, K. Faulds and D. Graham, *Chem. Commun.*, 2013, **49**, 30–32.

71 C. V Raman and K. S. Krishnan, *Nature*, 1928, **121**, 501–502.

72 A. Smekal, *Naturwissenschaften*, 1923, **11**, 873–875.

73 S. McAughtrie, K. Faulds and D. Graham, *J. Photochem. Photobiol. C Photochem. Rev.*, 2014, **21**, 40–53.

74 M. Fleischmann, P. J. Hendra and A. J. McQuillan, *Chem. Phys. Lett.*, 1974, **26**, 163–166.

75 D. L. Jeanmaire and R. P. Van Duyne, *J. Electroanal. Chem. Interfacial Electrochem.*, 1977, **84**, 1–20.

76 M. G. Albrecht and J. A. Creighton, *J. Am. Chem. Soc.*, 1977, **99**, 5215–5217.

77 M. Moskovits, *Rev. Mod. Phys.*, 1985, **57**, 783–826.

78 A. Otto, I. Mrozek, H. Grabhorn and W. Akemann, *J. Phys. Condens. Matter*,

1992, **4**, 1143–1212.

79 A. Stephenson-Brown, A. L. Acton, J. A. Preece, J. S. Fossey and P. M. Mendes, *Chem. Sci.*, 2015, **6**, 5114–5119.

80 X. Zhang, X. Du, X. Huang and Z. Lv, *J. Am. Chem. Soc.*, 2013, **135**, 9248–9251.

81 Z. Bie, Y. Chen, J. Ye, S. Wang and Z. Liu, *Angew. Chemie - Int. Ed.*, 2015, **54**, 10211–10215.

82 V. L. Brewster, L. Ashton and R. Goodacre, *Anal. Chem.*, 2011, **83**, 6074–6081.

83 L. Ashton, V. L. Brewster, E. Correa and R. Goodacre, *Analyst*, 2017, **142**, 808–814.

84 Z. Wen, *J. Pharm. Sci.*, 2007, **96**, 2861–2878.

85 D. P. Cowcher, T. Deckert-Gaudig, V. L. Brewster, L. Ashton, V. Deckert and R. Goodacre, *Anal. Chem.*, 2016, **88**, 2105–2112.

86 S. Chen, T. LaRoche, D. Hamelinck, D. Bergsma, D. Brenner, D. Simeone, R. E. Brand and B. B. Haab, *Nat. Methods*, 2007, **4**, 437–444.

87 L. Zhang, S. Luo and B. Zhang, *MAbs*, 2016, **8**, 524–535.

88 H. Tsutsumi, H. Ohkusa, H. Park, T. Takahashi, H. Yuasa and H. Mihara, *Bioorg. Med. Chem. Lett.*, 2012, **22**, 6825–6827.

89 Y. Chen, L. Ding, W. Song, M. Yang and H. Ju, *Chem. Sci.*, 2016, **7**, 569–574.

90 J. Wang, T. Duan, L. Sun, D. Liu and Z. Wang, *Anal. Biochem.*, 2009, **392**, 77–82.

91 J. Turkevich, P. C. Stevenson and J. Hillier, *Trans. Faraday Soc.*, 1951, **11**, 55–75.

92 G. Frens, *Nat. Phys. Sci.*, 1973, **241**, 20–22.

93 P. C. Lee and D. Meisel, *J. Phys. Chem.*, 1982, **86**, 3391–3395.

94 M. Wuithschick, A. Birnbaum, S. Witte, M. Sztucki, U. Vainio, N. Pinna, K. Rademann, F. Emmerling, R. Kraehnert and J. Polte, *ACS Nano*, 2015, **9**, 7052–

7071.

95 W. Haiss, N. T. K. Thanh, J. Aveyard and D. G. Fernig, *Anal. Chem.*, 2007, **79**, 4215–4221.

96 M. R. Ivanov, H. R. Bednar and A. J. Haes, *ACS Nano*, 2010, **3**, 386–394.

97 Nanocomposix, *Zeta Potential Analysis of Nanoparticles*, Nanocomposix, San Diego, 2012.

98 R. Pamies, J. G. H. Cifre, V. F. Espín, M. Collado-González, F. G. D. Baños and J. G. De La Torre, *J. Nanoparticle Res.*, 2014, **16**, 2376–2387.

99 H. Hinterwirth, S. Kappel, T. Waitz, T. Prohaska, W. Lindner and M. Lämmerhofer, *ACS Nano*, 2013, **7**, 1129–1136.

100 E. Pensa, E. Cortés, G. Corthey, P. Carro, C. Vericat, M. H. Fonticelli, G. Benítez, A. A. Rubert and R. C. Salvarezza, *Acc. Chem. Res.*, 2012, **45**, 1183–1192.

101 M.-C. Bourg, A. Badia and R. B. Lennox, *J. Phys. Chem. B*, 2000, **104**, 6562–6567.

102 H. Otsuka, Y. Nagasaki and K. Kataoka, *Adv. Drug Deliv. Rev.*, 2012, **64**, 246–255.

103 P. Ghosh, G. Han, M. De, C. K. Kim and V. M. Rotello, *Adv. Drug Deliv. Rev.*, 2008, **60**, 1307–1315.

104 C. C. You, M. De and V. M. Rotello, *Curr. Opin. Chem. Biol.*, 2005, **9**, 639–646.

105 J. Simpson, D. Craig, K. Faulds and D. Graham, *Nanoscale Horiz.*, 2016, **1**, 60–63.

106 G. Zhou, Y. Liu, M. Luo, Q. Xu, X. Ji and Z. He, *ACS Appl. Mater. Interfaces*, 2012, **4**, 5010–5015.

107 R. Lévy, N. T. K. Thanh, R. Christopher Doty, I. Hussain, R. J. Nichols, D. J. Schiffrin, M. Brust and D. G. Fernig, *J. Am. Chem. Soc.*, 2004, **126**, 10076–10084.

108 R. Lévy, *ChemBioChem*, 2006, **7**, 1141–1145.

109 X. Qian, S. R. Emory and S. Nie, *J. Am. Chem. Soc.*, 2012, **134**, 2000–2003.

110 G. T. Hermanson, in *Bioconjugate Techniques (Third Edition)*, ed. G. T. Hermanson, Academic Press, Boston, Third Edit., 2013, pp. 549–587.

111 M. E. Taylor and K. Drickamer, *Introduction to Glycobiology*, Oxford University Press, Oxford, 2nd edn., 2006.

112 J. Olson, S. Dominguez-Medina, A. Hoggard, L. Y. Wang, W. S. Chang and S. Link, *Chem. Soc. Rev.*, 2015, **44**, 40–57.

113 Y. L. Jeyachandran, E. Mielczarski, B. Rai and J. A. Mielczarski, *Langmuir*, 2009, **25**, 11614–11620.

114 P. E. Magnelli, A. M. Bielik and E. P. Guthrie, *J. Vis. Exp.*, 2011, 1–5.

115 R. L. Shields, J. Lai, R. Keck, L. Y. O'Connell, K. Hong, Y. Gloria Meng, S. H. A. Weikert and L. G. Presta, *J. Biol. Chem.*, 2002, **277**, 26733–26740.

116 R. Abès and J. L. Teillaud, *Pharmaceuticals*, 2010, **3**, 146–157.

117 M. Dalziel, M. Crispin, C. N. Scanlan, N. Zitzmann and R. A. Dwek, *Science*, 2014, **343**, 37–44.

118 L. Zhang, S. Luo and B. Zhang, *MAbs*, 2016, **8**, 205–215.

119 L. Valtola, A. Rahikkala, J. Raula, E. I. Kauppinen, H. Tenhu and S. Hietala, *Eur. Polym. J.*, 2014, **59**, 282–289.

120 Y. Shang, Y. Zeng and Y. Zeng, *Sci. Rep.*, 2016, **6**, 1–11.

121 K. D. Smith, J. Behan, G. Matthews-Smith and A. M. Magliocco, in *Glycosylation*, ed. S. Petrescu, IntechOpen, 2012, pp. 201–222.

122 E. B. Bahadır and M. K. Sezgintürk, *Trends Anal. Chem.*, 2016, **82**, 286–306.

123 C. Parolo, A. de la Escosura-Muñiz and A. Merkoçi, *Biosens. Bioelectron.*, 2013, **40**, 412–416.

124 X. Ge, A. M. Asiri, D. Du, W. Wen, S. Wang and L. Yuehe, *Trends Anal. Chem.*, 2014, **58**, 31–39.

125 D. Kim, Y. Kim, S. Hong, J. Kim, N. Heo, M.-K. Lee, S. Lee, B. Kim, I. Kim, Y. Huh and B. Choi, *Sensors*, 2016, **16**, 2154.

126 L. Blanco-Covián, V. Montes-García, A. Girard, M. T. Fernández-Abedul, J. Pérez-Juste, I. Pastoriza-Santos, K. Faulds, D. Graham and M. C. Blanco-López, *Nanoscale*, 2017, **9**, 2051–2058.

127 X. Wang, N. Choi, Z. Cheng, J. Ko, L. Chen and J. Choo, *Anal. Chem.*, 2017, **89**, 1163–1169.

128 Y. Yang, E. Noviana, M. P. Nguyen, B. J. Geiss, D. S. Dandy and C. S. Henry, *Anal. Chem.*, 2017, **89**, 71–91.

129 X. Fu, Z. Cheng, J. Yu, P. Choo, L. Chen and J. Choo, *Biosens. Bioelectron.*, 2016, **78**, 530–537.

130 T. M. G. Cardoso, P. T. Garcia and W. K. T. Coltro, *Anal. Methods*, 2015, **7**, 7311–7317.

131 W. Chen, X. Fang, H. Li, H. Cao and J. Kong, *Sci. Rep.*, 2016, **6**, 31948.

132 Y. Chen, Y. Zilberman, P. Mostafalu and S. R. Sonkusale, *Biosens. Bioelectron.*, 2015, **67**, 477–484.

133 K. L. Peters, I. Corbin, L. M. Kaufman, K. Zreibe, L. Blanes and B. R. McCord, *Anal. Methods*, 2015, **7**, 63–70.

134 J. Hu, S. Wang, L. Wang, F. Li, B. Pingguan-Murphy, T. J. Lu and F. Xu, *Biosens. Bioelectron.*, 2014, **54**, 585–597.

135 R. Thompson, A. Creavin, M. O'Connell, B. O'Connor and P. Clarke, *Anal. Biochem.*, 2011, **413**, 114–122.

136 D. D. Liana, B. Raguse, J. Justin Gooding and E. Chow, *Sensors*, 2012, **12**, 11505–11526.

137 L. Anfossi, C. Baggiani, C. Giovannoli, G. D'Arco and G. Giraudi, *Anal. Bioanal. Chem.*, 2013, **405**, 467–480.

138 K. F. Domke, D. Zhang and B. Pettinger, *J. Phys. Chem. C*, 2007, **111**, 8611–8616.

139 S. Schneider, G. Brehm and P. Freunscht, *Phys. Status Solidi*, 1995, **189**, 37–42.

140 A. Kamińska, I. Dzięcielewski, J. L. Weyher, J. Waluk, S. Gawinkowski, V. Sashuk, M. Fiałkowski, M. Sawicka, T. Suski, S. Porowski and R. Hołyst, *J. Mater. Chem.*, 2011, **21**, 8662.

141 W. Wang, Y. Yin, Z. Tan and J. Liu, *Nanoscale*, 2014, **6**, 9588–9593.

142 A. W. Martinez, S. T. Phillips, M. J. Butte and G. M. Whitesides, *Angew. Chemie - Int. Ed.*, 2007, **46**, 1318–1320.

143 A. W. Martinez, S. T. Phillips and G. M. Whitesides, *Proc. Natl. Acad. Sci. U. S. A.*, 2008, **105**, 19606–19611.

144 N. S. Dechiara, D. J. Wilson and C. R. Mace, *Sci. Rep.*, 2017, **7**, 1–8.

145 J. E. Schonhorn, S. C. Fernandes, A. Rajaratnam, R. N. Deraney, J. P. Rollanda and C. R. Mace, *Lab Chip*, 2014, **14**, 4653–4658.

146 P. Damborský, K. M. Koczula, A. Gallotta and J. Katrlík, *Analyst*, 2016, **141**, 6444–6448.

147 G. G. Lewis, M. J. Ditucci, M. S. Baker and S. T. Phillips, *Lab Chip*, 2012, **12**, 2630–2633.

148 Y. He, Y. Wu, J. Z. Fu and W. Bin Wu, *RSC Adv.*, 2015, **5**, 78109–78127.

149 R. B. Channon, M. Srisa-Art, K. Boehle and C. Henry, *Critical Components and Innovations in Paper-Based Analytical Devices BT - Paper-based Diagnostics: Current Status and Future Applications*, Springer International Publishing, New York, 2019.

150 S. C. Fernandes, D. J. Wilson and C. R. Mace, *J. Vis. Exp.*, 2017, **17**, 1–10.

151 E. Hecht, *Optics*, Addison-Wesley, Boston, 2002.

152 N. A. Owens, A. Pinter and M. D. Porter, *J. Raman Spectrosc.*, 2019, **50**, 15–25.

153 S. B. Rosalyn Yalow, *J. Clin. Invest.*, 1960, **39**, 11–13.

154 R. M. Lequin, *Clin. Chem.*, 2005, **51**, 2415–2418.

155 J. R. Cowther, in *The ELISA Guidebook*, Humana Press, Totowa, NJ, 2009, pp. 1–8.

156 S. Aydin, *Peptides*, 2015, **72**, 4–15.

157 F. M. Fesmire, W. W. Decker, D. B. Diercks, C. A. Ghaemmaghami, D. Nazarian, W. J. Brady, S. Hahn and A. S. Jagoda, *Ann. Emerg. Med.*, 2006, **48**, 270–301.

158 Y. Kumada, Y. Ohigashi, Y. Emori, K. Imamura, Y. Omura and M. Kishimoto, *J. Immunol. Methods*, 2012, **385**, 15–22.

159 L. Saso, G. Valentini, A. M. Giardino, A. Spadaro, V. Riccieri, A. Zoppini and B. Silvestrini, *Biochem. Mol. Biol. Int.*, 1998, **46**, 867–875.

160 A. Fotinopoulou, T. Meyers, P. Varley and G. Turner, *Biotechnol. Appl. Biochem.*, 2003, **37**, 1–7.

161 P. D. Josephy, T. Eling and R. P. Mason, *J. Biol. Chem.*, 1982, **257**, 3669–4675.

162 L. Tang and J. Li, *ACS Sensors*, 2017, **2**, 857–875.

163 M. Brust, M. Walker, D. Bethell, D. J. Schiffrin and R. Whyman, *J. Chem. Soc. Chem. Commun.*, 1994, 801–802.

164 N. S. Ieong, K. Brebis, L. E. Daniel, R. K. O. Reilly and M. I. Gibson, *Chem. Commun.*, 2011, **47**, 11627–11629.

165 R. De La Rica and M. M. Stevens, *Nat. Nanotechnol.*, 2012, **7**, 821–824.

166 D. Liu, J. Yang, H. F. Wang, Z. Wang, X. Huang, Z. Wang, G. Niu, A. R. Hight Walker and X. Chen, *Anal. Chem.*, 2014, **86**, 5800–5806.

167 D. Ghosh, D. Sarkar, A. Girigoswami and N. Chattopadhyay, *J. Nanosci. Nanotechnol.*, 2011, **11**, 1141–1146.

168 X. Liu, H. Xu, H. Xia and D. Wang, *Langmuir*, 2012, **28**, 13720–13726.

169 G. Wohlfahrt, S. Trivić, J. Zeremski, D. Peričin and V. Leskovac, *Mol. Cell. Biochem.*, 2004, **260**, 69–83.

170 J. Yang, D. Liu, W. Wang, Y. Xiong, P. Rong and Y. Zhang, *Nanoscale*, 2015, **7**, 15584–15588.

171 J. Li, J. Yan, L. Lin, L. Tang, L. Wang and Y. Liu, *Biosens. Bioelectron.*, 2015, **70**, 404–410.

172 J. H. Pazur and K. Kleppe, *Biochemistry*, 1964, **3**, 578–583.

173 S. B. Bankar, M. V. Bule, R. S. Singhal and L. Ananthanarayan, *Biotechnol. Adv.*, 2009, **27**, 489–501.

174 E. Omanovic-Miklicanin, I. Manfield and T. Wilkins, *J. Therm. Anal. Calorim.*, 2017, **127**, 605–613.

175 J. Liu and Q. Peng, *Acta Biomater.*, 2017, **55**, 13–27.

176 J. G. Hinman, A. J. Stork, J. A. Varnell, A. A. Gewirth and C. J. Murphy, *Faraday Discuss.*, 2016, **191**, 9–33.

177 P. K. Smith, R. I. Krohn, G. T. Hermanson, A. K. Mallia, F. H. Gartner, M. D. Provenzano, E. K. Fujimoto, N. M. Goeke, B. J. Olson and D. C. Klenk, *Anal. Biochem.*, 1985, **150**, 76–85.